1. Ultrasonic Studies of Binary Liquid Structure in the Critical Region. Theory and Experiment for the 2,6-Lutidine/ Water System.

2. Hartree-Fock Calculations of Electric Polarizabilities of Some Simple Atoms and Molecules, and Their Practicality.

3. Calculation of Vibrational Transition Probabilities in Collinear Atom-Diatom and Diatom-Diatom Collisions with Lennard-Jones Interaction.

Thesis by

Vincent P. Gutschick

In partial fulfillment of the requirements

for the degree of

Doctor of Philosophy

California Institute of Technology

Pasadena, California

1972

(submitted September 8, 1971)

Dedication

This thesis is dedicated to the people who contributed to my present predicament...to my parents in Chicago, for every manner of help--and my sisters and their families...to my cousin Mae in Huntington Beach, for much hospitality...to my advisors Neil Pings and Vincent McKoy, for a free hand in research, the tools of the trade, the cross-fertile research interests in their groups, and help with employment--and to G. Wilse Robinson, W. A. Goddard, III, Harry Gray, and Angelo Lamola (Bell Labs) for the latter...to the two research groups I was in, for a general, mutual increase in scientific knowledge, for a social life, and for moral support in the face of shared frustrations with computers, experimental apparatus, and other perverse items...to Profs. Robinson and Kuppermann, for stimulating my interest in other directions through their courses on photosynthesis and scattering, respectively...to Dennis Diestler, for some direction in scattering theory research and much entertainment...to the NSF, for financial support past and future, with no strings attached...to the Morrisons Paul and Sandy and the Wagners Al and Arlene, my best friends...with some notable and mostly very visible exceptions, to the people of California, for entry into the promised land after living in Chicago...to past teachers, formal and informal: Drs. Hofman, Freeman, and Klawiter at Notre Dame; Tollestrup, Feynman (damn the hacks, full speed

ahead), and Peck here; and Robinson and Holzer of my high school days...to the buggers who thought up candidacy exams and propositions--traumatic but useful...to departmental staffs, who usually provided dependable and unbureaucratic help...not to University Microfilms, for their damn thesis margins...to boring seminar givers, authors, and assorted bigwigs, for steering me away from science as cult or even tool, to science as culture and simple world-enjoyment; on the positive side of same, to R. P. Feynman, Stalkie, and even the authors of Time-Life and Scientific American...to IBM, for not changing computers every year, bless their $oul...to the keepers of mountains, desert, and sea, for recreation...to the city of Pasadena and its neighbors, for shutting down at 10 P.M. and trying to keep me out of trouble...to my draft board, for a II-S, but not for participating in the loss of my Miller Fellowship...but I wouldn't do it over again; there must be an easier, mellower way to live.

Abstract

Part 1. Many interesting visual and mechanical phenomena occur in the critical region of fluids, both for the gas-liquid and liquid-liquid transitions. The precise thermodynamic and transport behavior here has some broad consequences for the molecular theory of liquids. Previous studies in this laboratory on a liquid-liquid critical mixture via ultrasonics supported a basically classical analysis of fluid behavior by M. Fixman (e. g., the free energy is assumed analytic in intensive variables in the thermodynamics)--at least when the fluid is not too close to critical. A breakdown in classical concepts is evidenced close to critical, in some well-defined ways. We have studied herein a liquid-liquid critical system of complementary nature (possessing a lower critical mixing or consolute temperature) to all previous mixtures, to look for new qualitative critical behavior. We did not find such new behavior in the ultrasonic absorption ascribable to the critical fluctuations, but we did find extra absorption due to chemical processes (yet these are related to the mixing behavior generating the lower consolute point). We rederived, corrected, and extended Fixman's analysis to interpret our experimental results in these more complex circumstances. The entire account of theory and experiment is prefaced by an extensive introduction recounting the general status of liquid state theory. The introduction provides a

context for our present work, and also points out problems deserving attention. Interest in these problems was stimulated by this work but also by work in Part 3.

Part 2. Among variational theories of electronic structure, the Hartree-Fock theory has proved particularly valuable for a practical understanding of such properties as chemical binding, electric multipole moments, and X-ray scattering intensity. It also provides the most tractable method of calculating first-order properties under external or internal one-electron perturbations, either developed explicitly in orders of perturbation theory or in the fully self-consistent method. The accuracy and consistency of first-order properties are poorer than those of zero-order properties, but this is most often due to the use of explicit approximations in solving the perturbed equations, or to inadequacy of the variational basis in size or composition. We have calculated the electric polarizabilities of H_2, He, Li, Be, LiH, and N_2 by Hartree-Fock theory, using exact perturbation theory or the fully self-consistent method, as dictated by convenience. By careful studies on total basis set composition, we obtained good approximations to limiting Hartree-Fock values of polarizabilities with bases of reasonable size. The values for all species, and for each direction in the molecular cases, are within 8% of experiment, or of best theoretical values in the absence of the former. Our results support the use of unadorned Hartree-

Fock theory for static polarizabilities needed in interpreting electron-molecule scattering data, collision-induced light scattering experiments, and other phenomena involving experimentally inaccessible polarizabilities.

Part 3. Numerical integration of the close-coupled scattering equations has been carried out to obtain vibrational transition probabilities for some models of the electronically adiabatic H_2-H_2 collision. All the models use a Lennard-Jones interaction potential between nearest atoms in the collision partners. We have analyzed the results for some insight into the vibrational excitation process in its dependence on the energy of collision, the nature of the vibrational binding potential, and other factors. We conclude also that replacement of earlier, simpler models of the interaction potential by the Lennard-Jones form adds very little realism for all the complication it introduces. A brief introduction precedes the presentation of our work and places it in the context of attempts to understand the collisional activation process in chemical reactions as well as some other chemical dynamics.

Table of Contents

Part 1

I. Introduction

We have recently completed an experimental study of the velocity and linear attenuation or absorption coefficient of ultrasonic waves in 2,6-lutidine: water mixtures. We concentrated on the behavior near the lower consolute or critical mixing point of temperature and composition. Our intent was learning more of the statics and dynamics of the large, correlated fluctuations in order parameter--here, the local composition--occurring at critical points. Among probes of such phenomena, ultrasonics is convenient for its simplicity and for the directness of its relation to the dynamics. The raw ultrasonic data were carefully corrected for systematic experimental errors and statistically analyzed. Results were reduced to molecular parameters (persistence length, friction constant) using Fixman's[1] theory for the critical fluctuations and their coupling to the sound waves. We selected this theory over rival theories[2,3] principally for its good balance of tractability and rigor. The formalism was rederived with some correction and reinterpretation, in order to extend it to the mixed behavior of our system.

The present studies cover but one aspect of liquid state theory, and employ but one experimental probe of structure and dynamics. We review below the present status of theories for fluids of complexity ranging from simple

monatomic fluids through pure and mixed systems possessing rotational, vibrational, and chemical degrees of freedom. The context of our research, which is summarized in the two journal preprints following, should become clear in the process.

Various levels of microscopic structure and dynamics develop through the progression of fluid types under study: simple fluids and their mixtures, fluids with well-defined internal degrees of freedom as rotation or vibration, fluids where the molecules self-associate in large aggregates, and mixtures of an associated liquid with a species it solvates chemically. These four classes are not inclusive: for example, we have excluded dilute solutions of reactive species, electrolytes, or polymers. In such solutions the fluid acts as a carrier phase, a dielectric or solvating medium, or a large reservoir of one reactive species, rather than being of central interest.

Simple fluids are under the most intensive study. Their thermodynamic and transport properties have been correlated with model solid- and gas-like structures by approximate theories. More rigorously, one can correlate their properties with the basic molecular parameters, the mass $\underline{m}$ and the intermolecular potential $\underline{V(r)}$. One does not assume a small set of basic structures; rather, one employs full statistical mechanical theory and describes the fluid with very general distributions containing complete infor-

mation. Critical phenomena are still beyond fully successful quantitative description by rigorous or even approximate theories, as the critical region's thermodynamic instability is reflected strongly in its microscopic structure. In the second class of fluids, the members are necessarily polyatomic and nonspherical. Equilibrium properties are modified either by the strong coupling of rotation and translation, or (in the dimerization case) by the strong coupling of all internal degrees of freedom in two molecules. Repartitioning of phase space allows adequate treatment by rigorous statistical mechanics or thermodynamics. Transport in dilute fluids of this type involves more complex (angle-dependent) distributions and some new mechanisms, and is difficult to describe. Dense phases pose a virtually insoluble problem to date. The associated liquids forming the third class possess extensive spatial and motional structure, built from a great modification of the degrees of freedom of the isolated molecules through an n-body interaction potential deviating strongly from pairwise additivity. So much of the framework of rigorous molecular statistical mechanics on the few-body level is inapplicable, that only phenomenological descriptions are possible, based on a few large and fixed structures or on a set of linked chemical reactions. The behavior of a mixture of another liquid with an associated one is even more difficult to explain with molecular or other microscopic units of structure. More

narrow empirical relations of bulk properties are required, except for critical mixing phenomena, which are qualitatively similar to all other critical systems.

A. Simple Dense Fluids

These fluids show no evidence of internal structure, meaning they are generally monatomic. We exclude from consideration the liquid metals, whose cohesive forces are qualitatively different from those of insulating liquids; a recent conference[4] has summarized what is known of liquid metal structure and dynamics. We also exclude quantum effects[5a,6a] as manifested by the light atoms He and Ne even to "high" temperatures. The properties typically of interest are, for equilibrium, the PVT data or equation of state, the heat capacity C_p or C_v, the chemical potential μ, and the surface tension σ; and for transport, the shear and bulk viscosities η_s and η_v, the thermal conductivity λ, and the diffusion coefficient D, as they depend on the equilibrium state and possibly on the transport process angular frequency ω. The dynamic responses of the fluid to nonthermal, mechanical perturbations or probes such as elastic and inelastic light and neutron scattering are also of interest, on independent grounds as well as for further confirmation of our understanding of related bulk transport coefficients.

Experimental techniques for equilibrium and transport properties are many and varied. PVT data have been compiled extensively by straightforward pressure bomb measurements[7] on confined samples. Ultrasonic studies yield the velocity β, which provides a simple and accurate additional determination of the adiabatic compressibility $K_S = (\rho\beta^2)^{-1}$,

which otherwise requires extensive numerical analysis of the straight PVT data. The critical region equation of state is also probed on special cuts in the thermodynamic plane by such unseemly means as NMR[8]. Heat capacities C_v or C_p are taken by direct calorimetry,[7] by and large. The ultrasonic value for K_s is also used to check the critical region divergence of $C_v = C_p K_s / K_T$ from the better-known behavior of C_p and K_T[9]. Surface tension σ is primarily measured by capillary rise[10]. Among transport coefficients, the best-studied are η_s and λ , the former by capillary flow or rotating disk viscometers[11,12a] and the latter by heat flux measurements across parallel plates or concentric cylinders[11,12a]. The self-diffusion constant D requires some ingenuity (though for mixed fluids mutual diffusion also exists and is straightforward to determine). Radioisotope diffusion[13], NMR spin echoes[12b], and light scattering[14,15] are in use, the latter two particularly near criticality. Ultrasonics provides the only measure of the bulk viscosity η_v[16-20] through its proportionality to the absorption coefficient $\alpha = \omega^2 \eta_v / 2\rho\beta^3$. Additional fluid properties which touch more or less directly on the microscopic structure we seek to understand include pair distribution functions g(r) from x-ray[21a,22] or neutron scattering[23a]. The validity of the g(r) concept and calculations as well as the form of the intermolecular potential is investigated. The long-range structure of g(r) near the critical point is probed by

light scattering[7,12c]. Other light-scattering information includes the velocity and attenuation of hypersonic thermal waves (Rayleigh and Brillouin scattering[15]), also investigated ultrasonically[18a,19a], depolarization spectra[24], and induced Raman[25]. Further afield are such properties as second-order transport coefficients, of which thermal diffusivity[5b] is an example.

The bulk properties of the liquid phase pose the greatest theoretical problems. They reflect the properties of the solid and of the gas to which the liquid is related by the first-order transitions of melting and evaporation; in addition there is the dramatic connection to the gas through or above the second-order critical transition. Similarly to the gas, the liquid has high fluidity η_s^{-1}; an entropy S much higher than the solid; diffusion constant $\underline{D}$ and dilational viscosity η_v of similar magnitude to those of the gas; and modes of bulk motion described by the Navier-Stokes equations[18b]. In common with the solid, the liquid has a heat capacity $\underline{C_v}$, internal energy $\underline{E}$, and enthalpy $\underline{H}$ reflecting strong molecular interactions; a compressibility K and a molar volume $\underline{\overline{V}}$ showing similar packing and mean forces; and a heat conductivity λ indicating similar mechanisms of energy transport[23b]. Of course, the similarities or differences are often more quantitative than qualitative and depend upon which thermodynamic cut one chooses. There is also the more microscopic structure such as equilibrium

pair distribution functions $g(r)$ to compare among phases. We wish to explain the properties above, in their dependence on the thermodynamic state within the liquid or dense gas phases as well as across the transitions. Correlations with the solid or gaseous phases are useful, but a more basic explanation should derive primarily from the molecular parameters of mass m and potential $V(r)$, which also ground the properties of the other two phases. The critical region connection of gas and liquid poses a special challenge by its anomalous rate of change of properties (C_v, η_s, light scattering power = opalescence, e.g.[12,26]) and its violation of classical thermodynamics based on the analytic nature[27a] of the free energy G. The cooperative phenomena here are apparently in basic analogy[27b,28] to many other thermal many-body phenomena in highly dissimilar systems such as ferromagnets and superfluids, or in the more closely related consolute binary liquids.

B. Equilibrium Theory

The earliest success in explaining dense gas non-ideality and in correlating the same to the existence of a gas-liquid phase transition was achieved by van der Waals in the equation[29] bearing his name. He postulated an excluded volume $\underline{b}$ in the total volume due to finite molecular size, as well as a pressure term $\underline{a}/\underline{V}^2$ proportional to the inverse square volume due to the attractive portion of the pair potentials. The parameters can be set from the critical parameters of the fluid to yield a reasonably good gas description. There arises a principle of corresponding states[5,29] among all gases when $\underline{P}$, $\underline{V}$, and $\underline{T}$ are all reduced to their ratio with the corresponding critical values $\underline{P}_c$, $\underline{V}_c$, and $\underline{T}_c$. Experiments bear out the principle rather well. In the true liquid region the van der Waals equation describes fictitous states, but the ad hoc Maxwell construction[29a] locates the liquid-gas phase boundary. The shape of the coexistence curve in the critical region is now known to be qualitatively incorrect[30], but this defect is shared with every theory based on classical thermodynamics assuming the analyticity of the free energy in the intensive variables. Basically, we assess that the van der Waals theory takes a gas to be structureless: within the excluded volume the molecules are entirely random in time-average placement. However, both the repulsive core and the attractive tails in the pair potential induce structure[5c,31a] in the pair

distribution, directly between two bodies and indirectly through third bodies. Statistical mechanics notes that the momentum-averaged probability of occurrence of a spatial configuration $(\vec{r}_1,\vec{r}_2,\ldots,\vec{r}_N)$ of $\underline{N}$ molecules is proportional to $\exp-U(\vec{r}_1,\vec{r}_2,\ldots,\vec{r}_N)$, where U is the total potential energy.

The search for a better equation of state, particularly for the liquid state and preferrably a less empirical one based more on the intimate molecular mechanics, yielded no essential advance until the 1930's. At this time, the x-ray diffraction patterns of liquids were measured[32] and found to show remarkable short-range order reminiscent of the solid state. Quasi-crystalline models of liquids sprung up in number, all partitioning the configuration of the liquid into effective single-particle distributions for one particle moving in the averaged field from a lattice of the other particles. Originally, these cell theories[5,6b,33] postulated a complete lattice structure and uncorrelated one particle motions under hard-sphere or Lennard-Jones potentials. They considerably underestimated the entropy by overestimating the structure, particularly by not allowing the interchange of particles among cells, much less multiple cell occupancy. The equation of state is quite poor, while the internal energy is quite acceptable. Lennard-Jones and Devonshire accounted for the extra potential from two further 'coordination shells' in the lattice in establishing both free volume and total lattice energy. They also corrected

the 'communal entropy' from particle exchange fully toward the gas value. Double occupancy of lattice sites was proposed later, introducing the communal entropy more gradually through the liquid range and giving better critical constants and overall liquid properties. Allowance for vacant sites in the lattice, to an extent dependent on temperature, marks the hole theories, with the best accounting for the entropy. The net equation of state is little better than the three-shell straightforward cell theory. A tunnel theory proposed by Barker incorporated effective linear channels in the lattice for freer motion but only partially corrected the entropy errors. Eyring and coworkers[33] ad-

mechanical partition function or, equivalently, the configuration integral. They start from hole theory and reject all but the 'significant structures' in the N-particle distribution, meeting with modest success.

These solid-like models can give reasonable properties in limited ranges. They fail near the gas region, of course, and will ever be insensitive to the features of the intermolecular potential. They still provide empirical correlations for engineering usage, particularly for mixtures, and do incorporate enough of the proper energetics to ground reasonable transport theory. The first steps toward an a' priori equilibrium theory were taken in the same era by Ursell[34] and especially by Mayer and coworkers[35], work-

ing from the definition of the configuration integral and expanding it in orders of the density--the so-called virial or cluster expansions. One chooses a parameterized pair potential and then carries out successively higher-order integrations of $\underline{\exp -U_N/kT}$ involving larger and larger clusters of $\underline{n}$ molecules. The required time and effort limit the approach to the lowest orders of virial coeffiecients (of $\underline{P/kT}$), less than six for the Lennard-Jones potential[36]. Convergence difficulties appear[36a,37] to defeat any application to real liquids in any case. The chief use of virial theory now is production of exact virial coefficients for a given potential, to compare to the effective coefficients from equations of state yielded by promising approximate theories.

Yvon[38] and Born and Green[39] in the late '30's and '40's proposed a description of fluids by $\underline{n}$-particle distribution functions $\underline{g}^{(n)}(\vec{r}_1,\ldots,\vec{r}_n)$, which are integrals over $(\underline{N}-\underline{n})$ other particles of the configuration probability $\underline{\exp -U_N/kT}$, times a combinatorial factor for the ways $\underline{n}$ particles can be chosen among $\underline{N}$. The pair function $\underline{g}^{(2)}(\vec{r}_1,\vec{r}_2) = \underline{g(r_{12})}$ is central for all properties (but total entropy[21b]) of our type of fluids. One may derive a coupled set of inhomogeneous integro-differential equations for the heirarchy of the $\underline{g}^{(n)}$ from the Liouville equation in total phase space or its equivalents. The resulting Born-Green-Yvon (BGY) equations are unclosed, in that the $\underline{g}^{(n)}$ equation in-

volves an integral with $\underline{g}^{(n+1)}$. Closure can be obtained by approximating $\underline{g}^{(3)}$ as a product of $\underline{g}^{(2)}$'s--the superposition approximation of Kirkwood[40]--or a little more flexibly as in Cole's[41] or Fisher's[42] approximations. Bogolyubov[43] also postulated similar equations without practical extensions. Kirkwood[40] proposed an alternate set of equations to go with the closure scheme, using a coupling parameter for a test particle and obtaining slightly different results in the superposition approximation.

The pair distribution approach is desirable for several reasons. Its prime quantity $\underline{g}^{(2)}(\underline{r})$ has a direct integral relation to the macroscopic equilibrium properties[21c] and to the Fourier components (in the space of $\underline{s} = 4\pi \sin\theta/\lambda$) of the x-ray scattering intensity. By reason of this second relation (an analogous one exists for neutron scattering), the theory's output $\underline{g}(\underline{r})$ can be checked in point-by-point detail, over and above as a weighted average with potential operators for bulk properties. X-ray experiments are not currently accurate enough to be a prime source for $\underline{g}(\underline{r})$, since the computed properties, especially the pressure[44], are rather sensitive to errors in $g(r)$. A third 'advantage' of the distribution theory is that the equations are readily truncated by an approximation (superposition) with some intuitive physical interpretation. Unfortunately, alternate approximations more appropriate for true liquids are not possible and the theory is presently

bogged down. Critical phenomena remain outside the competence of the theory by any foreseeable extension, as they are true many-body instabilities.

The superpositon technique has been tested extensively[36a] up through liquid densities and temperatures, where it fails badly in predicting the equation of state. Rushbrooke and Scoins[45] looked at the effective 'direct' correlation function $c(r)$ which determines $g(r)$ by the Ornstein-Zernicke integral equation[46] and advanced a simplification called the netted-chain(NC) equation. This was quickly replaced by the better hypernetted chain (HNC) which gave encouraging results in dense systems. Near this time, Percus and Yevick[47] derived a related approximation (PY) and justified it on the basis of arguments in many-body theory for collective motion of the Fourier density components. PY theory is the most successful distribution approach, as it even shows a phase transition in appropriate conditions. It has been improved (the PY2 form[48]) and also adapted for nonspherical systems[49] and for the presence of three-body potentials[50]. Further advances are still needed for the densest liquids near the melting transition and for the critical region, but they are not foreseen as extensions of present forms. There exists the direct expansion of $g(r)$ in cluster integrals[51] that can be systematically extended to any order in density, amounting to stopping at the next-to-last stage in virial theory. However, the theory is at

least as difficult as the latter and has mostly formal utility in searching for new approximate theories.

Several groups, beginning with Zwanzig[52], have developed theories for the equation of state starting from the free energy, and perturbing it from the hard-core reference result to change the configuration integral and the pair distribution function. A limited class of systems are treated successfully by this approach in a straightforward application.

Two 'brute force' approaches to fluids are applicable with all pair potentials and all thermodynamic states. They provide reference values for other theories to measure up to, essentially giving the experimental behavior of ideal fluids uncomplicated by any trace of triplet potentials or experimental errors. The Monte Carlo theory[21,53a] generates the configuration integral by assembling random points or N-particle configurations for the integrand. The latest practical versions select configurations with a probability proportional to $\exp -U_N/kT$ to gather the largest contributions with the least work. Properties are excellent when referred to real substances such as argon. They are accurate enough to relate deviations from experiment to triplet potentials and other complications. The limited size of systems of N particles that can be handled leaves a little doubt on some properties, certainly near criticality where the long-range correlations cannot be represented. The

second approach, molecular dynamics[53b], consists in numerically integrating the equations of motion for N particles over a representative time span, in two or three dimensions. This technique is also very accurate and is packed with information including transport coefficients (autocorrelation function theory[54] relates macroscopic gradient dissipation to that of spontaneous microscopic gradients). It is restricted to even smaller systems than MC for the same effort or computing time. Neither theory can be considered an everyday working theory for investigating liquids, particularly as the quantitative results are not readily broken down into a limited number of qualitative concepts for a physical understanding.

Critical phenomena are in a territory of true many-body instabilities untouched by all the microscopic theories. The vanishing of the derivative $(\partial P/\partial V)_T$ and of the gas-liquid density difference (and hence, the meniscus) makes for dramatic mechanical and visual effects[26]. Several cuts in the PVT plane are of interest--the isotherms, the isochores, and particularly the coexistence curve. Anomalous--even diverging--specific heats are present[12d]. The microscopic parameters of correlation, as the total correlation length κ^{-1} in the asymptotic part of $g(r) \sim e^{-\kappa r}/r$, become macroscopic and show up in strong light scattering or opalescence[7,26]. Transport also shows significant anomalies, though we are presently considering only equilibrium aspects.

The original phenomenological theory of van der Waals did touch on critical phenomena. Its principal predictions[7,55,56] are a parabolic shape for the coexistence curve in $(\underline{T-T_c})$ versus $(\rho-\rho_c)$, a simple discontinuity in specific heat across the critical point on the isochore, and an inverse linear divergence of the isothermal compressibility K_T with $(\underline{T-T_c})$. We may use the shorthand of Fisher's[27c] critical exponents to express these results. The exponents are power laws relating two intensive variables' differences from their critical values. The van der Waals' exponents corresponding to the three predictions above are $\beta=\frac{1}{2}$, $\alpha=\alpha'=0$, and $\gamma=1$, the same for <u>all</u> fluids. The critical point in van der Waals theory appears to originate in cooperative motion from long-range forces[12e], while the quantum theory of intermolecular forces[57] by London and others showed the forces to be of short range, varying as r^{-6} asymptotically. Ornstein and Zernicke[46] proposed an alternate microscopic theory to calculate the long-range total correlation function $\underline{g(r)}$ from a short-range direct correlation function $\underline{c(r)}$. They focused on the critical opalescence intensity and on the related divergence of K_T, both tied to the behavior of the correlation length κ^{-1}. Their results for K_T agree with van der Waals theory, despite the assumed different nature of the forces. A more detailed microscopic theory originally applied to ferromagnetic systems, Landau theory[58], clarified the connection. All the theories to

that time were mean field theories, in which the order parameter for the transition ($\rho - \rho_c$ for fluids) is not allowed to fluctuate spatially while computing the free energy, but the form of the free energy allows the spectrum of fluctuations to diverge at the same time. Any assumption of the analyticity of the free energy in $\underline{T}$ and $\underline{V}$ brings these conclusions.

Experimentally, the coexistence curve was shown[30] in time to be flatter than parabolic, consistent with a β closer to 1/3 than $\frac{1}{2}$ and contrary to classical theories. The Ising model[58a,59] for the analogous ferromagnetic transition predicts a β of nearly 5/16, however, and this is encouraging. The Ising model can be converted[60] to a model of the gas-liquid critical point called the lattice gas by redefining variables and interactions. The fluid molecules are restricted to lattice sites which may be singly occupied or unoccupied. Nearest neighbors interact with a single fixed strength. It is essentially a hole or free volume description with exact correlation of the particles and holes, though the Hamiltonian is oversimple. The other critical exponents it predicts are quite good. An important result is $\alpha = 0$, in the sense that the isochoric specific heat $\underline{C}_V$ diverges logarithmically. This definitely quashes hopes for applying classical thermodynamics to the model. Experimental verification of the $\underline{C}_V$ anomaly was slower in coming, due to the difficulty of doing calorimetry in the critical

region. The ultrasonic value for K_s was and is used to confirm the anomaly through the known divergences of C_p and K_T and the relation $C_v/K_s = C_p/K_T$ [9].

A total of nine critical exponents are now defined and more or less accurately known[27] from classic PVT data as well as from more exotic and direct probes such as refractive index differences[61] and NMR line splittings[8]. Their universal disagreement with classical predictions has stimulated the development of a nonclassical thermodynamic scheme known as the static scaling laws[58b,62], which relate the exponents to each other. The basis is a universal equation of state in the reduced intensive variables, in turn based on the analyticity of the chemical potential through the critical transition. It is by no means a complete explanation, for it does not yield enough relations to predict all the exponents; it does not give the coefficients in the power law relations; and it cannot locate the critical parameters P_c, V_c, and T_c on any basis, much less a molecular one. It is useful in displaying the essential analogy[28,60] among all fluid transitions and even among all critical transitions. (We exploit this analogy in our work here, as we study the experimentally convenient binary liquid-liquid transition in lieu of the harder gas-liquid one.) More microscopic theoretical leads have come from Fixman and from Kawasaki and several others for the behavior of K^{-1}, under investigation by light scattering[63,64] and also ultrasonic absorption[1,2], although the latter has a

strong connection to the dynamics to cloud the issue. Other problems faced by critical thermodynamic theory include slight variations[58c] of exponents among systems, possibly from quantum corrections or residual sensitivity of exponents to the exact form of the intermolecular potential.

Many investigators continue to look at the critical region with greater precision and more sophisticated techniques. It is important to qualitatively and quantitatively refine our understanding of this gas-liquid connection, for its basic many-body character reflects on our general ability to describe fluids. The dynamic aspects are similarly important and will be discussed under transport theory.

C. Transport Theory

A fluid subjected to external stresses (such as shear or dilational forces from forced flow or sound wave passage, or heat stress from a temperature gradient on its boundaries) reacts against the stresses to dissipate them. Outside the Knudsen regime[5d,64x] of extremely low density, and excluding gradients over distances comparable to molecular separations, the bulk fluid may be treated as a continuum described[5e] by local mass density ρ , temperature $\underline{T}$, and velocity $\vec{v}$ for these nonequilibrium conditions. Gradients in these quantities are dissipated by corresponding fluxes of mass, energy, and momentum. The empirical equations of motion for these five local variables have been formulated thoroughly as continuum mechanics or hydrodynamics, beginning with the work of Newton, of Euler, and others[65,66]. The equations express the conservation[67a] of mass, momentum, and energy (the respective densities of which are ρ , $\rho \underline{v}$, and $\frac{1}{2}\rho v^2 + \rho\epsilon(T,\rho)$, where ϵ =internal energy per unit mass for the same $\underline{T}$ and ρ at equilibrium) and introduce the phenomenological coefficients of transport η_s, η_v, and λ :

Mass flux $\quad \frac{\partial \rho}{\partial t} + \nabla\cdot(\rho\vec{v}) = 0 \quad$ continuity (1)

Momentum flux $\quad \frac{\partial(\rho\vec{v})}{\partial t} + \nabla\cdot\underset{\sim}{\Pi} = 0$,

$$\Pi_{ij} = \begin{cases} \underbrace{\rho v_i v_j}_{\text{circulation}} + \underbrace{P\delta_{ij}}_{\text{source}} & \text{Euler,} \quad (2a) \\ \text{OR} & \\ \rho v_i v_j + P\delta_{ij} + \sigma'_{ij} & \text{Navier-Stokes,}^{68} \text{ for viscous fluids,} \quad (2b) \end{cases}$$

$$\sigma'_{ij} = \eta_s \left(\frac{\partial v_i}{\partial x_j} + \frac{\partial v_j}{\partial x_i} - \frac{2}{3}\delta_{ij} \nabla\cdot\vec{v} \right) + \eta_v \delta_{ij} \nabla\cdot\vec{v} . \quad (2c)$$

Energy flux

$$\frac{\partial}{\partial t}\left(\tfrac{1}{2}\rho v^2 + \rho\epsilon\right) + \nabla\cdot\left[\vec{v}\left(\tfrac{1}{2}\rho v^2 + \rho h\right)\right] = 0, \quad (3a)$$

$h = h(T, \rho)$ = enthalpy per unit mass,

OR

$$\rho T\left(\frac{\partial s}{\partial t} + \vec{v}\cdot\nabla s\right) = 0 \quad \text{linearized adiabatic equation.} \quad (3b)$$

For viscous, heat-conducting fluids, add to (3a) the extra terms (ref. 67b):

$$-\nabla\cdot\left[\vec{v}\cdot\underset{\sim}{\sigma}' - \lambda\nabla T\right].$$

(Pure heat conduction follows the empirical law:

$\vec{q}$ = heat flux = $-\lambda\nabla T$ $(\vec{v} = 0)$,

or equivalently,

$$\frac{\partial T}{\partial t} + \frac{\lambda}{C_p}\nabla^2 T = 0 , \quad \text{Fourier's law.)}$$

These equations describe an enormous range of possible bulk flow patterns, depending upon the boundary conditions and the magnitudes of the transport coefficients. The whole of hydrodynamics is not of immediate interest to us in this review (but see ref. 66). We are concerned with the eventual explanation of the transport coefficients in terms of molecular parameters---and also with the bulk

response to special boundary conditions such as the time-dependent periodic motion in sound waves, that allows us to measure the coefficients. To develop this last point: it suffices here to linearize[18c,69] all the equations, i.e., to retain terms only of first order in the small fluctuations $\delta\rho$, $\delta\underline{P}$, $\delta\underline{T}$, and $\vec{\underline{v}}$. In this event, the energy equation (3) to first order expresses the adiabatic equation of state $dS = 0$. Internal dissipative processes give second-order perturbations, and thus an entropy production or energy loss restricted to quadratic or higher order in the gradients[19b,67c], as required for stable equilibrium and a propagative mode. Heat conduction and shear viscosity are two dissipative processes that have a reasonably direct intuitive picture. Bulk viscosity is more of a catch-all for all other dynamic additions to the equation of state, from the finite-time relaxation of internal degrees of freedom (relative concentration in a mixture, chemical equilibria in an associated liquid, e.g.). We must find additional empirical rate laws for these degrees of freedom, or relaxation equations[19c]. In conclusion, the energy loss from the combined effects of η_s, η_v, and λ manifests itself as a linear attenuation[18d,19d] $\left(\frac{d\,\delta P}{\delta P} = \alpha\, dx\right)$ of the travelling sound wave,

$$\alpha = \frac{\omega^2}{2\rho\beta^3}\Big[\underbrace{\tfrac{4}{3}\eta_s + \lambda\left(\frac{1}{C_v} - \frac{1}{C_p}\right)}_{\text{'classical'}} + \underbrace{\eta_v}_{\text{'excess'}}\Big].$$

We may identify η_s with momentum transport, λ with energy transport, and η_v with a mixture. The self-diffusion

constant $\underline{D}$ clearly concerns mass transport, but in a special sense, as ρ is unchanged by self-diffusion unless the experimental probe can distinguish molecular labels such as spin (NMR)[12b] or isotopic mass differences[13]. The empirical equation in which $\underline{D}$ appears relates the labelled mass flux $\vec{\underline{i}}$ and the gradient in concentration $\underline{c}$[67d],

$$\vec{i} = -\rho D \underbrace{\nabla c} - \beta \nabla T$$

$$\text{or } \nabla c \to (\partial \mu / \partial c)^{-1} \nabla \mu \text{ in complex cases;}$$

$$\Rightarrow \quad \frac{\partial c}{\partial t} = D \nabla^2 c \quad \text{isothermally; Fick's law.}$$

The molecular-mechanical explanation of these transport coefficients lies ultimately in the parameters $\underline{m}$ and $\underline{V(r)}$ and in the classical mechanical equations of motion for the $\underline{N}$ identical particles. (Quantum equations of motion for transport make only small corrections for simple liquids and have been put together very piecemeal, in any event,[5f, 6c,70,71a,72a] after von Neumann[73] laid the basics.) For $\underline{N}$ particles, the Hamiltonian equations of motion are most compactly expressed as the single Liouville equation[5,74a,75a] for a trajectory of the system (or flow, for a statistical average or distribution[5,36b,74a,75a,76] of initial conditions) in the $6\underline{N}$-dimensional space of positions and momenta. On an ensemble average for $\underline{N}$ very large, the system exhibits (irreversible) continuum hydrodynamic behavior at times much longer than individual collision times. Before we can solve for the motion and numerically evaluate the transport coef-

ficients, we face the great conceptual and practical problems of (a) reducing the Liouville equation and N-particle distribution functions to the level of few-body collisions and distributions, rigorously or approximately, and (b) resolving the dilemma posed by the time-reversibility[11a, 36b,74b,75b,77] of the Liouville equation in contrast to the irreversibility of the long-time phenomena it describes. Rice, et al.[11b] break down the molecular theory of transport into three major areas: (1) analysis of the essential mechanical nature of irreversibility, (2) derivation of a suitable kinetic equation for the long-time evolution (much beyond individual collision transients) of some few-body distribution, and (3) solution of the equation for the transport coefficients in terms of the molecular parameters plus ρ and T. The first two problems are not simply annoying obstacles to the final numerical calculations; rather, they lead to rich and useful concepts in statistical condensation of the intricate molecular motions down to the level of observation in real systems, all of which are extremely complex many-body systems.

On the first level, important work was furthered by Kirkwood[11c,36c,71b,77a] on coarse-graining the detailed molecular distributions down to the level of crudity of real observations, and by Prigogine and coworkers[11d,36d,74b,78a] on the destruction of motional invariants (=mechanical order) by the collisions. It is now understood that for

systems of macroscopic size reversibility manifests itself only at times so long as to be cosmologically meaningless[36e]. In autocorrelation function theory[54a,71c,77b,78b], the practical irreversibility of the bulk equations of motion and of the low-order molecular distributions is postulated, and then used to declare the identity of the regression laws for fluctuations in both cases. Generally, the formal studies on the first problem of irreversible behavior have been peripheral to the more intensive work on the second problem of constructing actual few-body kinetic equations. The third step, numerical testing of the equations, follows the second quite rapidly and establishes the limits of applicability. We'll recount below the general history of kinetic equations as a way of summing up transport theory.

The first kinetic equations were limited to dilute gases, where the collision phenomena are easiest to sort out. The N-body motion can be reduced to considering only binary collisions occurring in a completely random fashion. Early free-path models for hard-sphere gases were proposed by Maxwell and others[72b,79,80a,78c] in the nineteenth century and made almost fully quantitative by the time of Jeans[80]. While providing adequate fits to data and a very good intuitive picture of transport, the free-path models depend upon some undetermined coefficients which must be estimated, and they also apply only to hard spheres[71d]. Boltzmann's[81] work culminating in his famous equation solved

these problems, but some work did continue on these lines: Eucken[5g,72] developed corrections for nonspherical molecules which can carry extra momentum and energy in rotation; and Bhatrager, Gross, and Krook[75] constructed a complementary approach based on the distribution of collision times rather than free paths, leaning on some of Boltzmann's formalism.

In 1872 Boltzmann postulated a fully determinate equation for the time-dependence of the singlet distribution function, which is the time-dependent generalization of the $\underline{f}^{(1)}$ of equilibrium theory, and the carrier of the hydrodynamic information. (1) $\underline{f}^{(1)}$ is presumed to be a functional of the initial gradients which relaxes by isolated binary collisions occurring under the influence of arbitrary but short-ranged intermolecular potentials. Ternary and higher collisions are taken as negligible. (2) The equation for $\underline{f}^{(1)}$, $\dot{\underline{f}}^{(1)}$ is made closed by factoring the pair distribution occurring in the collisional driving term into a product of singlet distributions. This is the same as assuming that pair and higher correlations do not build up for successive collisions. (3) The gradients and time-dependence of the distribution functions on the molecular collision time and distance scales are assumed negligible. All these conditions hold for dilute gases[36f,71e], with (2) being most difficult to justify. Condition (2), called the molecular chaos assumption, short-circuits the infinite heirarchy of time-dependent BGY equations in the exact but impossible $\underline{N}$-body

treatment, and it introduces the irreversibility. Its analysis as a coarse-graining of the distribution functions remained the primary, if not fully satisfactory, explanation of irreversibility until the time of Prigogine and his school.

Jeans[80] and others used the Boltzmann theory for qualitative and formal studies. Enskog, with others[5h,82], gave the explicit solution for the transport coefficients in terms of collision integrals, starting in 1922. Final numerical solutions[5i] for a series of model potentials, including the Lennard-Jones, came in the 1940's. The results were good enough for a quantitative understanding of transport in dilute gases. The analogous equation for truly quantum-mechanical systems like the lighter atoms and plasma electrons was shown in 1928 by Pauli[83]. Grad[84] extended the Boltzmann approach to very low densities and other conditions where the continuum nature of the fluid begins to disappear. Grad also notes[85] that the Boltzmann equation is even more important for strong-gradient pnenomena (shock waves, ultrahigh frequency sound) than for standard stationary transport. An extension to polyatomic systems in a realistic description of internal motion has been made by Wang-Chang, Uhlenbeck, and deBoer[86].

The initial work for the dense gas region was done by Enskog[87], who accounted for finite molecular separation during collision (hard-sphere) in calculating the collision

integrals. The Boltzmann theory thus corrected works down to liquid densities and explains[5j,71f] qualitatively the observed minimum in viscosity as a function of density. However, a hard-sphere model with fixed parameter σ is inadequate through the liquid range, as new mean forces and structure develop; Enskog's theory cannot be made quantitative over any extended density range. Bogolyubov[88] proposed a heirarchy of Boltzmann-like equations as an expansion in powers of density, to be used with realistic non-impulsive intermolecular forces, hopefully for all densities. While the numerical results are good for moderately dense gases, the series does not converge. It has been discovered in consequence that the density expansion of transport coefficients is non-analytic[89], due to the subtle growth of high-order correlations among collisions. The formal, exact theories that can handle this problem have come only recently and suffer from great complexity and other inadequacies; they will be discussed shortly.

More phenomenological approaches gloss over the details of the individual binary collisions, all coupled strongly to one another in dense gases and liquids. At the same time, they make more tenuous the connection of molecular parameters with numerical values for transport coefficients. The principle of corresponding states[5k] for non-equilibrium states was developed early, and continuously, on dimensional analyses of model kinetic equations. The

principle as applied far into the liquid region seems to work well for the rare gases. However, some discrepancies occur with polyatomics, even those so nearly spherical as CH_4. The simple two-parameter models for the intermolecular potentials smooth over small features that differ between rare gases and polyatomics, while transport seems to be much more sensitive to such features than equilibrium properties.

A second approach is that of Eyring's[90] rate process theory, first advanced in 1936. Here it is presumed that every transport process has some rate-limiting step, of the character of a unimolecular passage over a barrier in an appropriate space. Quasi-molecular parameters for a relaxation time and an energy of activation are needed. Reasonably consistent connections can be made to simple equilibrium properties for all kinds of molecules, if one avoids the dilute gas region. The shear viscosity is well accounted for in its $\underline{P}$- and $\underline{T}$-dependence; $\underline{D}$ is poorly given: and λ is given well, except in its $\underline{P}$-dependence.

Kirkwood[40b,71g] started a third approach, using a Brownian motion model for the evolution of singlet and pair distributions. The Markovian nature of the time-evolution (a generalization of Fokker-Planck form[91]) ensures irreversibility. The pair function $\underline{f}^{(2)}$ or $\underline{g}$ is required, since liquids with nonimpulsive interactions have special[71h] potential contributions to transport, in addition to the

kinetic or 'piggyback' part considered in Boltzmann-like theories. The new phenomenological parameter is the molecular friction constant ζ, of uncertain relation[36g,71i] to the molecular parameters and equilibrium distribution functions; this is the method's weakness. Kirkwood's theories give us fair numerical results, but quite sensitive to the friction constant value and not mutually consistent even with ζ adjusted[71j]. Insofar as the theory is correct quantitatively, it gives us some insight into the nature of collisional correlations and new mean forces in liquids. However, molecular dynamics data on model systems have recently provided[92] evidence against Kirkwood's picture of velocity autocorrelation decays. The principal defect is the lack of validity of Markovian equations for the strong collisions[71k] which are responsible for much of the transport, in contrast to their validity for the more common weak collisions in the 'cage' of neighbor molecules. Rice and Allnatt[93] attempted to correct this defect in large part by introducing 'hard' and 'soft' friction constants at the expense of greater empiricism. Their results for realistic systems, especially for pressure and temperature dependence, are encouraging but may never be adequate--even if only due to the need for gross approximations in equilibrium g(r) and other input data[11f]. As a final note, many workers[94] have extended Brownian theories for mixtures, principally to provide good engineering correlations of data.

Cell models are a fourth empirical approach. Cohen and Turnbull[95] proposed a dynamic version of the hole or free volume theory. A molecule may move only if a void of some critical size opens next to it, by the random coalescence of the free volume. It requires the hard-sphere diameter σ as an additional empirical parameter and can fit transport data quite well in temperature, except for $\underline{D}^{11g}$. It fails to represent the intermolecular potential flexibly enough, apparently.

Of recent origin are the rigorous formal theories of transport which provide an analysis of the fluid response to a perturbation of any nature or frequency. They begin with an operator resolution of the Liouville equation or of the quantum density matrix and delve into the many-body phenomena to define the most meaningful collision events. Particularly, they show how correlations are destroyed to generate irreversibility; they further provide, as by the partial summation techniques of many-body theory, approximate kinetic equations on the few-body level. Their value lies in their facility with all kinds of transport for any state of the system (in principle only, at present), their utility in developing concepts about the collisional nature of irreversible processes, and their position to start and to assess different model knietic equations. Really adequate theories for liquids may derive from these soon.

The early BGY or BBGKY heirarchy[38,39,40,43] of

equations for the time-dependent reduced distribution functions is rigorous in principle but shows no systematic way to analyze irreversibility and then to generate new kinetic equations. (Born and Green[39] did use a superposition approximation in transport to get fair results for dense gases.) Kirkwood[40b] suggested a many-body operator technique be used before reducing the Liouville equation to the few-body level. vanHove[96] later succeeded in treating weakly-coupled (weak potentials) systems, stirring much enthusiasm. Essentially, he obtains a master equation for the time-dependent populations of the unperturbed N-body states, by disregarding phase-coherence and interference of the successive sets of collisions, in quantum terms. Brout and Prigogine[97] derived a similar classical master equation on rather intuitive grounds (classically, one works with similar N -body eigenstates of the Liouville equation, defined in phase space). Finally, Prigogine[74] developed an operator resolution of the classical Liouville equation (looking very much like quantum mechanics in form) and showed how a simple master equation resulted from summing certain classes of the perturbation expressions to infinite order. The formalism displayed an explanation of irreversibility without extra, ad hoc statistical postulates: the collisions destroy motional or mechanical invariants of the system on the hydrodynamic time scale to give increasing disorder; correlations built up by success-

-ive binary collisions flow[77c] into higher-order correlation functions whose detailed structure is unimportant for observed properties. It also shows, in the structure of the master equation, that the short-time evolution of the system is non-Markovian[11h,74c], degenerating to Markovian (random, Brownian) only for longer times. Transport and relaxation in weakly-coupled gases and weakly-anharmonic solids were understood quantitatively[74] with Prigogine's theory, but strongly-coupled systems like real liquids are still too complicated to treat. A more approximate form suitable for liquids on the pair distribution level was derived[98] and tested[11f] recently, but found lacking.

The other principal formal theory concerns itself with autocorrelation functions.[54a,71c,77b,78b] These are time correlation functions for simple dynamic variables such as ρ or $\underline{\vec{v}}$, e.g.,

$$C_{vv}(t) = \langle \vec{v}(t)\vec{v}(0) \rangle .$$

The brackets indicate that an equilibrium ensemble average is to be taken, and imply that the autocorrelation functions are implicitly dependent on the equilibrium intensive variables ρ, $\underline{T}$, etc. The ACF's or their Fourier transforms contain all the basic dynamic data. This remarkable discovery of transport information in equilibrium fluctuations has been known quite a while in diverse systems such as electrical resistors[99]. The application to transport in dense neutral (molecular) systems is more recent[100].

The usual transport coefficients are just zero-frequency components[54a] of a few autocorrelation functions times definite numerical factors.

The ACF's can be represented as the linear or first-order response of the system to the appropriate adiabatically-applied perturbation, either mechanical---electromagnetic radiation, a moving boundary, e.g., or thermal--temperature gradient, pressure gradient, etc. However, explicit solution for the perturbed (N-body) phase-space distribution involves solution of the complete N-body problem. We must depend upon further leads within or outside the theory to compute ACF's using only few-body dynamics. Some approximate kinetic equations for the ACF itself directly are being tested[54a]. Also, the numerical results of molecular dynamics calculations can be reduced to numerical values for transport coefficients, using the basic discovery noted initially[100].

The ACF approach is extremely difficult in principle and in practice now, but it holds much promise. Certainly, it has the advantage of using the entire frequency spectrum of transport to understand and check the model kinetic equations. It also interrelates data from ordinary transport and relaxation (such as the dielectric relaxation spectrum derived from the ACF for one molecule's electric dipole $\langle \vec{u}(0)\cdot\vec{u}(t)\rangle$) with data from special probes from more complex perturbations (such as fluorescence

depolarization: $\langle \frac{3}{2}\left[\vec{u}(0)\cdot\vec{u}(t)\right]^2 - 1\rangle$).

Critical region anomalies in transport were slow to be recognized and studied experimentally[12g], so the corresponding theory is relatively new and undeveloped. The earliest, and qualitative, theories were directed toward the excess ultrasonic attenuation[101,102] in critical liquid mixtures. These theories claimed that other wave propagation phenomena (shear viscosity in special flow patterns around fluctuations[101], or Rayleigh scattering by same[102]) were masquerading as anomalous changes in the bulk viscosity. They ignored the possibility that near the critical point there were changes in the nature of mutual diffusion, which is the principal mode of relaxation of the fluctuations in concentration. These theories were wrong, for diffusion is altered from its standard form[19e]; Fixman's ideas on this line[1] gave the first quantitative success for the anomaly in bulk viscosity. His related theories for shear viscosity[103] and for static heat capacity[104] also worked fairly well. Kawasaki[2] advanced another microscopic approach to critical sound absorption. It was based on ACF theory and is much less transparent, but only slightly different--in fact, he uses Fixman's modification[103] of the diffusion law, though in a more rigorous way (as we do, in paper I). Kadanoff and Swift[3] have recently presented very general theories for <u>all</u> transport coefficients in both gas-liquid and liquid-liquid (mixture) critical regions. The K & S

perturbation approach to the master equation is very complex. However, it is of the same strain as Fixman's and Kawasaki's, in that it describes dissipative processes as the breakdown of one transport mode into several others. As such, it is called 'mode-mode coupling'. Unfortunately, it is less successful[105] with experimental data than the other two theories.

The final generalization for critical region transport is a type of corresponding states theory, called the dynamic scaling laws[3,106], very similar in form to the static scaling laws of Widom and others for equilibrium. Kadanoff[107] reviews their experimental support, which is incomplete in itself, and not very encouraging.

(paper I gives detailed comparisons of sound absorption data with the various theories.)

D. Fluids with Well-Defined Internal Degrees of Freedom

The first level of complication above simple fluids is represented by non-associated polyatomic molecules, which possess permanent multipole interactions (esp. dipoles) and the new internal motions of rotation, vibration, internal rotation (rotational isomerism, when rotation is restricted), or simple dimerization equilibrium. These extra internal motions and the multipole interactions coupling them allow the molecules to structurally store and to transport additional energy and momentum. The coupling of these motions, particularly to the external translational motion---sometimes so strongly as to merge identity with the latter, alters the nature of collisions and of static structural correlations. Quantitative changes from simple fluid behavior are found in the equation of state (particularly in the location of phase boundaries), heat capacities, and transport coefficients; qualitative trends with pressure, temperature (and frequency, for transport) are sometimes altered, especially in polar fluids. Rotational reorientation or rotational diffusion[108] arises in dense fluids as a new transport process. In consequence, the electromechanical response becomes interesting: dielectric relaxation[109] in (di)polar fluids, or in nonpolar fluids the lineshapes for microwave,[110d] IR, Raman[110b], visible, UV[110a], and NMR[111]. Static dielectric constant and strength and

materialism[111a] are equilibrium aspects. Rotational relaxation[16-20,112,113] (as well as vibration, internal rotation, and dimerization) also makes a dominating contribution to the old transport coefficient, the bulk viscosity.

We exclude from consideration very large polymers or macromolecules, with yet more drastically different properties. For example, their transport even at modest frequencies is governed by v scoelastic equations[114,115] rather than Navier-Stokes equations. We leave untouched the large field of rheology.

To be sure, much of the interest in properties of such polyatomic fluids as we consider is still outside our scope: color, reflectivity, and other electromagnetic properties which are more utilitarian; chemical stability and kinetics of degradatinn or reaction; and all manner of chemical and physical behavior in complex, possibly multiphase, mixtures. Still other interesting aspects are only in part related to the simple equilibrium and transport behavior we'll study, and may be touched on briefly, e.g., relaxation of artificially inverted vibrational populations in chemical lasers[116]. We justify our artificial limitations of interest on pure convenience, as well as on the opinion that qualitative and quantitative understanding of these simple properties is the major work in understanding all the properties of these fluids---and by extension those of the associated liquids, in particular the compound of

greatest chemical and biological interest, water.

We have previously mentioned some new transport behavior. We should now like to elaborate on some more qualitative effects in properties, beginning with equilibrium. Dipolar forces and orientation in the fluids, especially dense fluids, cause imperfectly understood but significant additions[51] to heat capacities and to the equation of state. The melting and boiling transitions are raised in temperature, and the critical constants' interrelations are changed[5m]. Empirical equations of state like van der Waals or approximate virial still apply with more error; more parameters are now desirable. In the corresponding states treatment[5m], the reduced dipole moment is a necessary new parameter. Even in polyatomics which are not dipolar, there are new small terms in the heat capacity[117] and the virial coefficients[5n] or other representation of the equation of state. The well in the spherical-average pair potential is also generally deeper in polyatomics[118], from stronger dispersion forces, more densely-packed excited electronic states. The liquid ranges are also higher in temperature and the specific heats higher in value[119] than those of simple fluids, in consequence. The exact treatment of the equilibrium properties must include the new mutual-orientation dependence in the fluid structure. For example, in the distribution function approach one uses a host of coupled pair distribution functions[49]. These are a type of

harmonic expansion of the pair function as used for simple fluids, and are quite difficult to use. (This is a proper description of combined translation and rotation. Vibration remains essentially separable even in dense fluids; some subtle changes show up spectroscopically[120] to give evidence of the fluid structure and interactions.) The dimerization equilibrium causes the grossest changes in equilibrium properties. Its sensitivity to temperature increases the heat capacity, to 4-5 times the expected value[121a] in the case of NO_2. The volume change in forming the dimer modifies the PVT behavior as well. The energy storage in the internal motion, especially vibration, manifests itself in yet more ways, even for gases. The restriction to quantized levels may become evident at low temperatures. For example, the molar vibrational heat capacity begins to 'freeze out'[122a, 5o] from its high-temperature value of R per vibration mode as the temperature is lowered, but still well above room temperature. Rotation freezes out well below room temperature. Quantum symmetry[122b] restricts the pairing of vibrational with rotation levels in cases as H_2, causing further divergences in heat capacities. Free internal rotation [123] partially freezes to become few-state hindered rotation or (for asymmetrical barrier) rotational isomerism[19f,124] before it disappears.

The nature of molecular collisions is also new. Momentum and energy are transported internally by the

molecules--quite dramatically in the case of dimerizing species; NO_2 has 4-5 times the thermal conductivity[121b] expected. Collision dynamics are quite definitely quantum mechanical, particularly for vibrational excitation, as shown by interpretation of ultrasonic data. The nature of trajectories is also affected by the initial orientation correlations imposed by the static structure. In dense gases, rotational relaxation or reorientation degenerates to small, diffusive steps described by a new transport coefficient, the rotational diffusion constant $\underline{D}_{rot}$[108]. Dipolar molecules show strongest correlation and are probed easily by dielectric relaxation[109]. This rotational diffusion persists even in solids[125]. Ordinary transport--viscosity, conductivity, diffusion--is also presumably affected by the new orientation-dependent packing and the anisotropy of the interactions. "Piggyback" and potential contributions are both altered. The changes in magnitudes of the transport coefficients η_s, λ, and $\underline{D}$ from simple fluid values are not large[119b,121,126] and the theory[86] is difficult, so this aspect has not seen much work. On the other hand, the bulk viscosity is greatly increased and otherwise affected by the new internal relaxations possible. The extra energy in the internal motions is traded around or exchanged with translational energy at finite rates[18e,19g]. Time lags in energy adjustment in response to temperature (or sometimes pressure) fluctuations cause dissipation of the energy in

paasing sound waves[18f,19h]. The study of this relaxation--vibrational, rotational, rotational isomeric, and chemical--is a well-developed and dominant part of ultrasonics. Time-dependent order parameters (say, effective temperatures[18e, 19g] of internal motions) are needed to formulate the relaxation laws in the new 'dynamic' equation of state. Each kind of relaxation has its characteristic dependence upon ω, $\underline{P}$, and $\underline{T}$, which is helpful in qualitative identification. Detailed molecular models using quantum scattering theory are needed to explain the parameters of the empirical relaxation equations (or η_v directly). Among the first successes of molecular collision theory[18g,127] and the first uses of ultrasonics were studies of relaxation in gases.

Chemical reaction, specifically the dimerization we consider here, is an extreme limit of the interaction of the degrees of freedom of two (or more) molecules. The statistical mechanical description of structure in a reactive fluid merits some discussion. A pair interaction defined in a relative coordinate is an insufficient description of binding. The rotations, the vibrations, and even the relative translation are totally recast with new energy levels. The new quantization and new phase space alters the partition function[128] and hence the thermodynamic properties rather intricately compared to the simply interacting molecules. The interaction of the dimerized pair with a third molecule is now given by a second effective pair potential.

Overall, reaction is too complex to be described in detailed phase- space distributions as were simple fluids. More phenomenological groupings into all the monomer states and all the dimer states are used, with thermodynamic parameters and gross rate constants[18h,19i,129].

The overall magnitudes of transport coefficients for non-simple fluids are not greatly different from those of simple fluids in analogous states of packing and temperature,[119b,121,126] but for the bulk viscosity and the new $\underline{D}_{rot}$ and in isolated cases of other transport (λ for NO_2). Both the equation of state and transport properties can often be 'explained' in the framework of simple fluid theories by using effective spherical pair potentials. However, the resultant state-dependence of the effective simple fluid parameters, especially trying to reproduce contrary trends with $\underline{P}$, $\underline{T}$, or ω , is unsatisfactory. More elaborate theoretical frameworks are then justifiable. Certainly we will need them on the way to understanding associated liquids like water.

New probes are available for the new features of non-simple fluids. All the common gases have been studied by ultrasonics[16-20,112,113] for their rotational and vibrational relaxation (actually coupled into one vibrational-rotational-translational --VRT--relaxation set). Initially the studies were prompted by shock and combustion phenomena, since bulk viscosity is unimportant in ordinary conditions.

After initial triumphs of crude quantum explanations[18g,127], ultrasonics and VRT relaxation were kept as a proving ground for scattering theory, including classical and semi-classical modifications[130], and as an adjunct to molecular beam and other experiments for determining intermolecular potentials[113]. At low temperatures the relaxation times between distinct quantum levels have been pinned down[18i, 19j,132; 18j,19k,133a], though in general multiple relaxation[18k,19l,134] occurs and complicates analysis--even worse in liquids. The dimerization kinetics of NO_2 were also studied early[133b] and adequate interpretation of other properties was made. Dimerization by H-bonding in acetic and propionic acids has been studied in liquids[19m]. Similarly, liquids have been probed for vibrational relaxation, as in CS_2[18l]--though the new nature of collisions makes definition of basic collision rates ambiguous[18m,19n]. Pure rotational isomeric transitions[18n,19o,135] are studied primarily by ultrasonics, though the presence of isomerism was first demonstrated[136] by spectroscopy, electron diffraction, calorimetry, and dielectric behavior. Liquids are, in fact, classified[18o] as simple (no relaxation or excess sound absorption from η_v), Kneser (distinct thermal relaxation from a well-defined internal degree of freedom), and associated (modest excess absorption, nearly T-independent, etc.). The characteristic ω,P, and T-dependence of different relaxation processes makes ultrasonics a good tool, rich in

information. Dramatic cross-relaxation[19p] of one species by another in mixtures has seen some work. Equilibrium properties, especially in mixtures, are often taken[137] from ultrasonic measurements.

NMR[111] is another probe for rotational relaxation or diffusion, at the Larmor frequency ω_L. IR, UV, and Raman lineshapes[110] inform us of vibrational or rotational relaxation at the vibrational relaxation itself. Dielectric relaxation[109] lineshapes probe rotational relaxation. X-ray scattering[138] may conceivably be developed for studying orientational effects in liquid structure. Relaxation of nonthermal vibrational populations inverted by light absorption[139], laser scattering[140], or chemical laser action[116] is more precise for level-by-level studies.

E. Equilibrium Theory

Our coverage of theory for non-simple fluids will be more sketchy than for simple fluids. Some general observations have been included in the previous section. Many of the theories of § B can be simply extended. van der Waals theory and other few-parameter empirical equations give about as good agreement with small non-polar non-simple fluids as for simple fluids. Larger molecules such as hydrocarbons require a greater number of parameters[141], as do polar species. Corresponding states treatments[5m] are good for small molecules and can be explicitly adjusted to three-parameter form for dipole forces. Cell theories are similarly used for polyatomic species with somewhat less success[5p] than for simple fluids.

Virial cluster theories and distribution function theories, including PY and HNC approximate forms, are less often used for polyatomics, for they do more in the role of exhaustive testing as quite accurate, rigorous equilibrium theory. The proper extension is to include multipole forces and harmonically expand the pair function in orientation angles. Pople and Buckingham[142] have used cluster theory with dipole and quadrupole forces added. Levine and McQuarrie[143] and Stogryn[144] have included higher multipoles and proceeded to the third virial, for both ordinary and dielectric coefficients in the first case. Frisch and Lebowitz[145] have done a scaled particle theory extension.

Gibbons and Steele[146] and also Buckingham[147] have done some less quantitative work at liquid densities. Steele and Chen[49] have used angle-dependent PY theory through liquid densities with encouraging results. Perturbation theories[52,117] based on the free energy function with a hard-sphere zero-order model are by and large inapplicable, as the angle dependent forces so complicate the perturbation expansion as to eliminate the advantage over more direct approaches. Molecular dynamics[54] and Monte Carlo[148] calculations have been done for a few moderately nonspherical potentials including dipoles.

Dimerization, and solvation in mixtures, are too complex for present a' priori theories. Phenomenological theories are in use[149a], at least for the deviations from additivity of thermodynamic functions for mixtures in which one component either self-associates or solvates the other. Pure species' gas imperfection from dimerization is calculable[149b], but there is no treatment for dense gas or liquid.

In all, much more work has been done on empirical representation of data on real systems than on a' priori approaches. The latter must be greatly improved within the simple fluid domain before moving up to more complex fluids.

Critical phenomena occur at higher temperatures and pressures than in simple species, reflecting stronger pair potentials. The critical compressibility factor P_cV_c/R_cT_c is altered from the general simple fluid value of 0.292

by polar forces in particular.[5m] The critical exponents are not detectably altered for the moderately nonshperical molecules[7] commonly studied. This indicates once more that the critical region equation of state is not sensitive to the exact nature of the intermolecular potential. Critical exponents for dipolar gases, on the other hand, could be very interesting. The generally stronger molecular interactions, within or between species, can lead to strongly nonadditive thermodynamic behavior in mixtures. Regions of liquid[149,150a] (or even gaseous[150b]) immiscibility and new liquid-liquid critical mixing points occur. Here we have a whole new field for critical investigations, often at more convenient conditions of temperature and pressure. These systems seem to behave analogously to gas-liquid critical systems, with the appropriate transcription of intensive variables[12h,105a]. The few equilibrium exponents known appear to be the same[7,12h] as for gas-liquid transitions. Liquid-liquid critical mixtures are more commonly used for transport studies than for equilibrium.

F. Transport Theory

As for equilibrium, transport in non-simple fluids is often handled by simple extension of simple fluid theories. Now, it is often easiest to use effective spherical models, except for η_v and $\underline{D_{rot}}$. In light of the unspectacular differences among all manner of fluids in ordinary transport, this is justifiable in large part. It is also necessary in generating semi-empirical forms for transport in mixtures[5i,11i,94], quite a large field. When one does explicitly consider the internal motions, there are more or less evident corrections or generalizations of simple fluid theory. The Eucken correction[5g,72] for rotation can be appended to the early free-path models for gases with some success, especially at elevated temperatures[5g]. It may also be used with the Boltzmann equation solution[5q] of Chapman and Enskog. A more rigorous treatment is given by Wang-Chang, Uhlenbeck, and deBoer[86] for all separable degrees of freedom as we are considering. There are also many models of loaded spheres and other rigid bodies[151] for which the Boltzmann equation has been solved, in an attempt to include nonspherical interactions in the repulsive core. The dense gas and liquid are less amenable to such models, as the necessary Enskog correction[87] involves a difficult pair distribution; molecular dynamics calculations are more suitable. More phenomenological models have little difficulty with polyatomics. Corresponding states[5k], rate

process[90], and cell[95] theories gloss over so much detail and are so heavily empirical that the qualitative subtleties are lost. They give often acceptable fits to data, as discussed in § C, and are useful for semi-empirical calculation of transport in mixtures[11i]. Reactions such as dimerization are a complication tending to invalidate all but Eyring's rate process model. Brownian models[40b,71g,93] are too inaccurate and undeveloped to warrant worries about the anisotropy of interaction, though they are also used semi-empirically for mixtures[94].

The rigorous formalisms which might incorporate non-spherical molecules are principally Prigogine's[74] and ACF[54a,71c,77b,78b] theory. The minor effort[39] on the gradient-dependent BGY pair distribution in the superposition approximation has not been continued for either simple or polyatomic fluids. It is inevitably inaccurate at true liquid densities and is not a notable advance over competing dense gas theories. Prigogine's theory has not been explicitly developed for nonspherical molecules, again because simple fluids (with their strong coupling) still are waiting. Internal degrees of freedom are quite a complication for the theory and apparently will make it a complete master equation[78d] formalism (internal quantum states are resolved), while their inherently weak coupling makes them better suited for study, given quantum scattering calculations for excitation cross sections. The ACF theory, on

the other hand, has been used at least once[54a], in conjunction with molecular dynamics, on nonspherical and even dipolar molecules. $\underline{D_{rot}}$ can be derived from the results, along with more detailed information, principally on the electromechanical response.

The two transport properties which really show the new features of unassociated polyatomic fluids are η_v and $\underline{D_{rot}}$, as we have said in the previous section. In consequence, most theoretical effort has been expended on them, including specialized theories outside the realm of the other transport modes. Rotational diffusion is the subject of several phenomenological theories. A mechanism of small diffusive steps was proposed early by Debye[108] and others and seems to be confirmed for larger molecules, while finite random reorientations are proposed for smaller molecules[152]. The internal relaxations responsible for the large bulk viscosity η_v are usually approached by calculating the inelastic binary collision cross-sections, which are then plugged into elementary free-path theories. As a result, the relaxation time is the inverse of a simple Boltzmann average[19q] of probability of excitation per collision. Multi-level relaxation is given inadequately; coupled relaxation equations[18k,191,134] for all the levels can be formed, again in the free-path approxi tion for collisions. While the more detailed relaxation process in dense gases and liquids deserves much attention in statistical mechanics, most of

the recent work in relaxation phenomena tries to improve the realism and scope of binary scattering theory calculations. Much of this effort, in turn, is expended on bimolecular reactive collisions[153], particularly simple exchange reactions. The advent of better molecular beam[154] and other[116, 139,140] techniques for direct observation of partial cross-sections has much to do with the resurgent interest in a' priori kinetics.

The anomalous increase of η_v from slowed diffusive decay of increasingly large fluctuations in critical fluids gets the lion's share of the attention, both theoretically and experimentally. This is primarily because it is most straightforward. The experiments for η_v, which are fairly numerous (esp. in liquid-liquid cases) and are reviewed in paper II, are readily done with ultrasonics. Fixman[1], Kawasaki[2], and Kadanoff and Swift[3] give quantitative theoretical explanations, which are discussed at the end of § C. The dynamical scaling theory[3,106], an outgrowth primarily of the last theory, touches upon the other transport coefficients but is not very successful even for η_v.[105] Fixman has adapted his ideas for the shear viscosity[103]. Otherwise, critical transport theory is unexplored. The experiments on η_s, by standard[11,12a] or torsional crystal[155] viscometers, on λ again by standard apparatus[11,12a], and on $\underline{D}$ by NMR[12b] or light scattering[14,15] cover both gas-liquid and liquid-liquid phenomena. In aggregate the work is not definitive[12a]

in establishing the existence and nature of anomalies in these three transport modes.

G. Associated Liquids

Some polyatomic species can hydrogen-bond into extensive arrays in the liquid (and solid). Water is the most famous example, while others are low-molecular weight alcohols and polyols (e.g., glycerol), HF, and HCN. H-bonding is weak[156a] by the standards of chemical bonds, but strong compared to the van der Waals forces binding the types of fluids discussed previously. As a result, associated liquids have anomalously high melting and boiling points, heats of transition, and surface tension. Water, which bonds to as many as four neighbors, boils 162 degrees above its congener H_2S. The strongly directional character of chemical H-bonds also shows in bulk properties. The strong molecular alignment causes high dielectric constants in these liquids[119b]. Water also has to great extent a distinct, extensive three-dimensional network[156b]. This contributes to its melting and boiling anomalies, high molar volume, and high viscosity. Its thermal breakdown is responsible for a large heat capacity and for its density increase on melting and on slight further warming of the melt. Thermal conductivity is large through the semi-rigid solid-like lattice, and compressibility is low. The lattice structure is also broken down by pressure, leading to an anomalous decrease in viscosity[156c]. It is labile on a short time scale so that molecules do rotate and flow rather independently. Self-diffusion, most reliably measured by

NMR, is normal[156,126].

The other associated fluids usually show less dramatic anomalies. Most alcohols to modest size are somewhat higher-boiling and the polyols in particular are quite viscous. Glycerol is so extensively bonded as to have a huge viscosity which relaxes much like bulk viscosity does at modest frequencies[19r]; relaxation is so slow at low temperatures that it acts glassy. All associated liquids show a modest bulk viscosity which is in near constant ratio to shear viscosity over the temperature range[19s,18p].

In water, HF, and HCN the protons are very mobile, unbonding and rebonding to travel, aided by their lightness. Noticeable electrical conductivity[156d] is found in the pure liquids, and it is greatly enhanced by solvation ionic compounds normally conductive themselves only as melts. Water in particular shows great solvating power for a wide range of substances. Great chemical and biochemical importance accrues to water for its abilities to solvate so many species and to promote reactions, particularly those with ionic intermediates. Solvation is accompanied by lattice breakdown to smaller units, and by strong electrical forces. Isotopic substitution of deuterium or tritium for normal hydrogen makes noticeable changes in properties[156], principally by altering the H-bond strength. In the vapor phase, association is weakened essentially to dimerization, causing lesser anomalies[156e] in the gas imperfection.

Associated liquids are certainly very difficult to describe theoretically because they show cooperative motion of very many molecules. The intermolecular potential is well-established[156f] as non-pairwise-additive, involving three-body and possibly higher distortions. The short range and directional nature of the H-bond aggravates the problem of describing transport a' priori. There are some new tools for help in qualtiatively understanding the added structural and dynamic features. X-ray[156b] and neutron scattering give us pictures of inter- and intra-molecular structure. Water shows such definite orientational effects that the lattice-like structure found in the 1930's prompted the cell models of all liquids. The proton magnetic resonance[156g] is strong and readily resolved into chemical chift and linewidth information on various environments and rates of motion. Vibrational spectroscopy[156h] is at its most informative for associated liquids. While properties under normal conditions are heavily studied, the critical phenomena of associated fluids remain unknown, partly because of their high critical temperatures and pressures (water: 373 C., 218 atm. methanol: 240 C., 79 atm.).

The rather spotty equilibrium and transport theory will be briefly recounted in this one section. We will concentrate on the story of water, with occasional comments on other species. Most of the equilibrium theories for water are heavily phenomenological and can be classified as

mixture models. A finite set of distinct chemical structures is presumed in equilibrium. Each structure is assigned an enthalpy and specific volume (in interstitial models, the smaller species--monomers--can hide in the free volume of major structures). Eucken[157] and Hall[158] postulated mass-action (straight chemical) models, based primarily on the ultrasonic bulk viscosity. Both temperature and pressure dependence of η_v and K_s are acceptably given in Eucken's form. Application of Hall's theory to alcohols' ultrasonic behavior has been attempted with slight success [159]; since there is no density minimum, the thermal driving term neglected by Hall is no longer small compared to the pressure driving term in the dynamic equation of state. A number of other workers[156i] have used similar chemical models for water, obtaining the molecular parameters from molar volumes, compressibilities, or radial distribution functions.

Getting away from mass-action equilibria models, Pauling and others[156i] advanced simpler interstitial forms with one major structure. They have difficulty explaining the high configurational heat capacity of water. Recently, Eyring and others[156i] have given multiple-species models for the partition function directly, sometimes including vacancies, and all using extensive thermodynamic data. The large number of variational parameters tends to make these theories simply empirical fits, hard to test for reasonable-

-ness of the parameter values. The general problem with mixture models is the variability they imply for the environments of individual molecules, contraindicated by the narrow spread of dielectric relaxation times[156j]. They also fail to explain the strong molecular alignment leading to the high dielectric constant.

Pople[156k] proposed distortion of a complete network of H-bonds to explain the observed radial distribution functions, assigning a bending force constant for each bond. The dielectric constant and volume decrease on melting seem to come naturally from the model, while the viscosity from such a model would be too high. The very characterization of intact--perhaps bent-- and broken H-bonds is difficult either macroscopically or microscopically[156l] within any model, however.

There are two recent a' priori approaches employing effective pair potentials. Ben-Naim[160] performed a PY calculation on water, having directly approximated the potential of mean force. His results reproduce features in the pair distribution but he does not compute properties. Barker and Watts[148] did a Monte Carlo study on water, taken to have a spherical potential plus a strong dipole. The vapor has been the subject of virial cluster theory[156e] in which it is characterized by a pair multipole potential or by a dimerization equilibrium. Neither alternative is consistently good for the temperature dependence, particularly

for the third virial coefficient.

In summary, there is no consistent and successful nonempirical theory through an extended domain in the thermodynamic plane. Eisenberg and Kauzmann[156] have collected a great mass of experimental data and theoretical correlations for water, from which one might make more detailed judgments.

Transport is more fragmented than equilibrium theory, as most transport theories correlate only one such property with some equilibrium or distribution data, and do not cross-correlate transport data. Again, Eisenberg and Kauzmann have assembled the data on water. Dielectric relaxation in water[156j] is interesting for its very small spread of relaxation times, implying near uniform molecular environments on a quite short time scale (but not so short as a vibration time, where a spread of environments shows up spectroscopically[156m]). It also possesses a large high-frequency limit ϵ_∞, indicating persistent rapid motions, probably rotations. Generally, qualitative models are employed to explain its behavior. Haggis, et al.[161] used their complicated mixture model of equilibrium among zero- through four-bonded molecules plus postulates on simple reorientational motions available to these species. This theory also covers equilibrium and other transport, notably, though it is highly parameterized. Rotational diffusion apparently occurs at a slightly faster rate[156n] with a

similarly low spread in ω-dependence of the obviously related relaxation it represents. Eyring's rate process theory is used[156o] to obtain an energy of activation for dielectric reorientations, which energy happens to match that for self-diffusion and viscosity, tying them to some common mechanism too.

Self-diffusion has been the subject of rate process theory[156o] only, to date. Neutron-scattering data[156o] on the ω-dependence of $\underline{D}$ may soon be helpful in generating better detailed models. Shear viscosity[156p] is also given only in a rate process analysis. Its decrease with pressure at low temperatures supports the qualitative equilibrium picture of network breakdown, with shear flow sustained primarily in the free (monomer) phase. Rate process theory reflects this feature.

Bulk viscosity is curious in all the associated liquids in that it has a ratio[19s,18p] to η_s largely independent of $\underline{T}$ and $\underline{P}$. Some underlying identity of mechanism is apparent, while the only theoretical treatments cover only η_v and equilibrium. Eucken's[157] and Hall's[158] models, developed originally for ultrasonics, are rather successful in correlating the bulk viscous behavior with the bulk compressibility and molar volume as functions of pressure and temperature. For the very viscous fluids as glycerol, both shear and bulk viscosity appear to relax together[19t] in frequency and temperature. Shear and bulk 'fluidities' or

moduli are used in the largely empirical viscoelastic description[19u,114], as they are now the additive quantities. A considerable spread in relaxation times is evident[19u].

H. Mixtures Containing an Associated Liquid

Fluid mixtures quite commonly show nonadditive thermodynamic and transport properties. Some of the largest of such effects are shown by solutions in associated liquids of unassociated species which are solvated by new H-bonding. Aqueous solutions of organic amines or of higher alcohols are examples. Some important features are large heats and volumes of mixing $\underline{E}^e$ and $\underline{V}^e$, as well as partial liquid immiscibility[149c,162a] leading in particular to lower consolute points. The anomalous properties of the associated liquid may be much reduced in mixing, due to the structural breakdown needed to accomplish solvation. The dielectric behavior, thermal expansion[163], and molar volume become more normal. On the other hand, the heat capacity and bulk viscosity have new contributions from the solvation equilibria, with the latter being greatly increased[19t,163,164]. The compressibility anomaly is increased[163], which may be unexpected at first glance; the shear viscosity is likewise increased (see paper II, e.g.). Mutual diffusion is interesting, especially near the critical consolute point where it vanishes.

Many simple fluid equilibrium theories have been generalized to treat the odd forces in polyatomic and even associated fluids, and also to treat mixtures. Cell theories[165] and distribution function theories[166] come to mind,

but in any event these generalizations are largely formal. They are mostly unexplored and very much more difficult than the parent theories. Few, then, are up to the task of handling both association and mixture behavior at the same time. More often the work falls to more empirical theories from physical chemistry, seeking solely to explain nonadditive thermodynamic behavior in terms of the pure component parameters. This separate handling of the association and mixing problems gives a more reasonable return for the effort involved. The physicochemical approaches to nonelectrolyte solubilities also gets much attention because of the direct technological application of solution thermodynamics, solute partition between two solvents, etc. Prausnitz' [149] book on solutions recounts in detail the physical bases for the major theories. Again, few of these theories are adequate for associated liquids, due principally to their assumptions of simple-fluid equations of state for both components. Many of them also require that volume changes or entropy changes $\underline{V}^e$ or $\underline{S}^e$ vanish, making them extremely doubtful for associated solvents. Several of them (Guggenheim's quasi-chemical[149d,167] method; Flory-Huggins polymer[149e,162] theory; two-liquid theory[149f,168]) attempt a crude treatment of the nonrandom mixing of the two components, the preferred molecular aggregations in the process of solvation.

The most satisfying empirical tack begins with the chemical theory of solutions[149g]. Here explicit association

chains ($A + A_{n-1} \rightleftharpoons A_n$) and solvation ($A_n + B \rightleftharpoons BA_n$) equilibria are proposed, with quite simple progressions of equilibrium constants and of $\Delta \underline{H}$, $\Delta \underline{V}$ values for each step. The activity coefficients, hence thermodynamics, of solvent A and solute B are calculated from their true mole fractions as free monomers. Many thermal and volumetric properties are given reasonably well, However, the solutions of the postulated species must actually be nonideal from additional 'physical' forces (difficult to divide from stronger 'chemical' forces) to give any immiscibility[150c]. Renon[169] has given the most comprehensive theory in this regard, one which is fairly heavily empirical. Of course, the usual objections to mixture models for associated liquids do imply the inadequacy of Renon's and other theories for some properties, such as dielectric behavior, especially at low mole fractions of the unassociated component. Andreae, et al.[163] tested the simpler chemical theories on the thermodynamics and ultrasonic absorption behavior (see next paragraph) of aqueous amine and alcohol solutions, but achieved poor results and extracted only qualitative indications of the real structure and dynamic processes. To close the discussion, we note that Rowlinson[150d] regards aqueous nonelectrolyte solutions as the hardest, least understood aspect of equilibrium phenomena, though a mass of data and empirical correlations has been obtained, as seen in the book by Hildebrand and Scott[162].

Dynamics are again a great problem. The ultrasonic bulk viscosity is handled in the chemical theory of solutions. Over and above the equilibrium constants and thermodynamic changes for each partial reaction, rate constants[19t,163,164] are fitted to the absorption and perhaps some equilibrium data. Andreae, et al.[163] achieved only partial success. Qualitatively it is quite clear that the relaxing solvation equilibria are responsible for the large bulk viscosity; the relaxation times can even be resolved in some cases. However, any adequate treatment should dynamically generalize Renon's theory. To justify the effort in obtaining the latter, one would require very precise ultrasonic and thermodynamic data and would achieve only a rather unwieldy semiempirical correlation. Advances in associated liquid theory are highly desirable beforehand.

For the other transport phenomena, particularly η_s, λ, and $\underline{D}$ (dielectric relaxation and $\underline{D_{rot}}$ are generally ignored), there are again formal generalizations of simple fluid models. The generalizations of corresponding states[170], rate process[90], and Brownian[94] theories have been given, at least for mixtures of normal liquids. None is particularly suited to mixtures containing an associated component: pure associated liquids and normal fluids do not have corresponding states; Brownian models have not been used for associated liquids pure or otherwise, with their complex potentials and hard-to-represent structure. Only

rate process is sufficiently empirical, and it does not do well for thermal conductivity[171], for example.

The liquid-liquid critical phenomena are qualitatively different in origin from those in simple fluids as discussed in §§ D-F. The immiscibility and critical consolute behavior in the latter arise from largely athermal mixing which is nonetheless non-random (cf. the success of Flory-Huggins polymer theory even for simple molecular mixtures[172] ---this may be fortuitous, however); upper consolute behavior is the rule, with complete miscibility at higher temperatures from the wiping out of the nonrandom structure. On the contrary, the strong H-bonding in solvation by associated liquids most commonly[149h] leads to lower consolute behavior. In many systems, the phase diagram is quite skewed toward low mole fraction of the unassociated component[173]. The obvious occurrence of solvation equilibria points to a large chemical contribution to the free energy of mixing, hence the phase behavior. However, the analysis of our own experiments on 2,6-lutidine/water in paper II shows that the phase phenomena are hard to explain with chemical theory augmented by any simple physical (nonideality) corrections.

As for the liquid-gas transition, the critical region equation of state in liquid-liquid transitions is not given by classical, analytic thermodynamics. After transcription of the intensive variables, the two kinds of

critical points appear similar, as noted in §§ D-F. For example, the shape of the phase diagram (now in the $\underline{X}$-$\underline{T}$ plane, $\underline{X}$= mole fraction) is cubic rather than parabolic. There is less detailed information deep in the critical region than for the gas-liquid transition, however, so very few analyses have been made for critical exponents. Only α for the $\underline{C}_p$ divergence and β for the coexistence curve shape are reasonably well established[12h]. In transport, η_v receives the most attention, from the theories of Fixman[1], Kawasaki[2], and Kadanoff and Swift[3]. As noted in § F, these gave the first quantitative explanations of the anomalous critical region absorption. The anomaly in the diffusive decay of the fluctuations is now in mutual diffusive decay of relative composition fluctuations at constant density. Some recent work, as that in our following two papers, has attempted to show the identity in nature of liquid-liquid critical phenomena at upper and lower consolute points. Paper II indicates this is not clear, for at the lower consolute point the ultrasonic absorption from the critical processes is partly obscured by non-anomalous but large thermal relaxation (this has not been generally recognized in investigations of other lower consolutes[102,174] which did not include the composition-dependence of absorption). Furthermore, the separation of the critical and thermal ultrasonic effects once recognized is still difficult, due to the implicitly classical and wrong thermodynamics of

the coexistence curve--hence also of the $\underline{X}$-dependence of ---in all three absorption theories. In general, we expect that the dynamic critical exponents will be hard to pin down and to compare among systems.

More realistic irreversible thermodynamics should be worked into Fixman's and other theories of transport to analyze critical phenomena, complemented by better equilibrium thermodynamics combining chemical and physical models of the solutions. The pressure dependence of the consolute temperature is also interesting. The excess volume of mixing gives a $\underline{P}$-sensitivity to $\underline{T_c}$, through the $\underline{X}$-dependent free energy of mixing $\underline{G^e}$ acquiring a term $\underline{PV^e}$. (See paper II for a treatment of the extra ultrasonic absorption from the harmonic variation of $\underline{T_c}$ with the sound wave's $\delta \underline{P}$.)[149i] For the air-saturated (hence ternary) solutions commonly used, the nature of the consolute point as a true critical point deserves some attention[175].

I. Concluding Remarks

We have reviewed the status of theory and experiment aimed at understanding basic equilibrium and transport properties of fluids, particularly in terms of the few most basic molecular parameters and the classical equations of motion. We have seen many shortcomings in our understanding, particularly in theory. In this final section, we should like to speculate as to what advances are most needed for describing liquids and dense gases.

In equilibrium theory, a list of 'reasonable' expectations might read as follows: 1) use of a small basic set of 'structures' to compose pair distribution functions, as if in variational theory; or a more direct description of liquid structure in a transformed phase space, not necessarily reduced uniformly to the two-body level--less sensitive to errors in small regions of phase space; 2) better representation of molecular interaction than $V(r)$, one with capabilities for nonadiabatic encounters; complementing an improved choice of zero-order degrees of freedom and (quantum phase space) states; and lending itself to flexible yet simple mixing rules for unlike-molecule interactions; 3) more semiempirical entries into fluid theory; tractable variational approaches to $g(r)-1$, and/or truncation of the infinite heirarchy of BGY equations by use of simple, experimental, directly physical parameters describing the medium

of other particles; 4) overhaul of water structure description--also aqueous nonelectrolytes; involving an overhaul of mass action principles (cf. Renon's[169] work) by an appeal to a simply-parameterized partition function still distinguishing chemical species on some few-body level; also involving a rigorous few-body description of structures, yet with room to describe cooperative effects as in dielectric alignment; 5) a coherent explanation of structural, largely chemical, relaxation in aqueous solutions and of phase behavior (duly noting its nonanalytic nature); 6) in elementary fluid reactions, an overhaul of the net representation of degrees of freedom upon reaction; one which allows chemical species distinction, and also remedies inadequacies of the pair potential description; 7) more detail on critical many-body phenomena--on the location of T_c, on explaining exponent differences among systems; real use of the liquid-gas connection, in a comprehensive theory for the dilute gas through the liquid region; (b) better semiempirical, nonanalytic thermodynamics for critical phase behavior, as for use in Fixman theory; 8) developing spectroscopy in mixed/dense media (with their increased number of degrees of freedom and states) for details of internal motion interactions; including linewidth information for 'state' lifetimes.

In transport: 1) modelling of correlation decays in the few-body space parametrically; alternative perturbation summations from many-body theory, for new quasi-

particle descriptions generalizing Prigogine's[74] approach; more studies on the functionality of $\underline{f}^{(N)}$ in terms of $\underline{f}^{(1)}$, and of $\underline{f}^{(1)}$ in terms of gradients; formalisms for nonthermal processes; 2) less artificial connection of the various time scales of evolution (collisional, kinetic, hydrodynamic); multiple parametric representation of non-Markovian time evolution; 3) clarification of the problem in density-expanding transport coefficients; rational function representations; 4) developing concepts of the nature of collisions in liquids, especially involving polyatomic species; probing the utility of quasi-particle descriptions or of interrupted binary-collision formalisms; analyzing the boundary conditions and other aspects of getting a general form for two-body motion in a medium; learning to average over neglected degrees of freedom by adiabatic, stochastic, or intermediate postulates--possibly in a uniform semiclassical approximation[131]; clarifying piggyback and potential contributions; handling multiple relaxation, local nonequilibrium effects; utilizing the best resolution of elementary flow patterns in phase space, perhaps reducing from autocorrelation theory[54]; 5)handling the nature of collisions and fluxes in water and aqueous solutions in particular; remedying the inadequacies of pair potential descriptions; pinning down the role of physical interactions and of the recasting of degrees of freedom upon association; 6) developing spectroscopy as a tool for details of nonadiabatic

encounters, extending the equilibrium applications; 7) utilization of the ω-dependence in transport (even in $\underline{D}$, as from neutron scattering[156o]) for full inversion from thermal and mechanical responses to the complete several-body dynamical features--a reversal of the ordinary procedure of testing theories by predictive numerical calculations of the response from the theory.

Our ultrasonic experiments and their analysis have brought us up against several of the stumbling blocks noted above, especially (4), (5), and (7b) under equilibrium, and less directly (4) and (7) under transport. The following two papers outline our findings in these regards. The appendices after them give the details of the apparatus, operating procedure, calibrations, data reduction, and theoretical fittings. We achieve limited advances in our qualitative understanding of liquid-liquid phase behavior and structural relaxation from these investigations. These are reviewed at the end of paper II. To proceed further requires more comprehensive experiment and theory. Specifically, we recommend more isotherms for absorption and velocity measurements, including at least one quite far removed from critical, and perhaps one in the two-phase region (separate measurements in each phase, of course). Thermodynamic data on the phase diagram and vapor pressure should be obtained, to numerically evaluate the derivatives $\partial^2 \mu_1 / \partial \underline{n}_2 \partial \underline{T}$ to plug into Fixman theory in place of ad hoc, classical analytic approximations.

This remedies the defects of classical thermodynamics, particularly for the $\underline{X}$-dependence of the absorption. It allows essential testing of Fixman's mode-coupling, and removes one obstacle to separating CR and TR effects in α. To remove the other obstacle, the TR theory should be made quantitatively accurate and consonant with the phase behavior (free energy of mixing) by generalizing Renon's[169] theory of associated solutions to relaxation phenomena. Detailed excess volume and heat of mixing data will be necessary to fix the $\Delta \underline{H}$ and $\Delta \underline{V}$ values for reaction steps in the expanded model. The composition dependence for α in at least one other lower consolute system--say, triethylamine/water--should be observed (only the relatively crude level of the present work is necessary) to see the uniformity in relative magnitudes of CR and TR relaxations in lower consolute systems. All of this extra work is probably within the scope of one more doctoral research effort.

References

1. M. Fixman, J. Chem. Phys. 36,1961(1962).

2. K. Kawasaki: a)Proc. Phys. Soc. 90,791(1967); Phys. Rev. 150,291(1966); b) ibid.,A1,1750(1970).

3. L. P. Kadanoff and J. Swift, ibid., 165,310(1968); 166, 89(1968); J. Swift, ibid., 173,257(1968).

4. P. D. Adams, H. A. Davies, and S. G. Epstein, eds., The Properties of Liquid Metals (Taylor and Francis, London, 1967); reprinted from Adv. Phys. 16, parts 62-64(1967).

5. J. O. Hirschfelder, C. F. Curtiss, and R. B. Bird, Molecular Theory of Gases and Liquids (Wiley, N.Y., 1954): a) Chs. 6,10; b) 541 ff., 582 ff.; c) 321 ff.; d) 695; e) 468; also 492; f) Ch. 10; g) 498 ff.; h) §7.3;i) Ch. 8; j) 647 ff.; k) §9.1; l) §§3.10,3.B; m) 248 ff.; n) §§3.8,3.9; o) 114 ff. p) 304 ff.; q) 534.

6. J. deBoer and G. E. Uhlenbeck, eds., Studies in Statistical Mechanics (North-Holland, Amsterdam, 1962): a) Vol. 3; b) Vol. 2; c) Vol. 1.

7. P. Heller, Rep. Prog. Phys.30,731(1967).

8. L. M. Stacey, B. Pass, and H. Y. Carr, Phys. Rev. Lett. 23,1424(1969).

9. V. F. Nozdrev, Applications of Ultrasonics in Molecular Physics (Gordon and Breach, N.Y., 1963), 265 ff.

10. F. P. Buff and R. A. Lovett, in Simple Dense Fluids, eds. H. L. Frisch and Z. W. Salsburg (Academic, N.Y., 1968), 17ff.

11. S. A. Rice, J. P. Boon, and H. T. Davis, ibid., 252 ff. a) 262 ff.; b) 259; c) 260 ff.; d) 278 ff.; e) 326-328; f) §3.2; g) 329-332; h) 279 ff.; i) §2.5.

12. M. S. Green and J. V. Sengers, eds., Critical Phenomena (N. B. S. Misc. Publ. 273, 1966): a) 165 ff.; b) 178 ff.; c) 116 ff., and 123 ff.; d) 86 ff.; e) 4; f) 110; g) Sec. "Transport and Relaxation Phenomena"; h) 9 ff.

13. R. P. Mills and L. A. Woolf, The Diaphragm Cell (Australian National U. Press, Canberrs, 1968).

14. R. D. Mountain and J. M. Deutch, J. Chem. Phys. 50,1103 (1969).

15. B. Chu, Ann. Rev. Phys. Chem. 21,145(1970).

16. T. A. Litovitz and C. M. Davis, in Physical Acoustics, ed. Warren P. Mason (Academic, N. Y., 1965), Vol. IIA, 293.

17. General accounts of ultrasonics as a probe of transport or relaxation are infrequently presented as a formal bulk viscosity; see he remainder of the volume in ref. 16; also all of refs. 18-20.

18. K. F. Herzfeld and T. A. Litovitz, Absorption and Dispersion of Ultrasonic Waves (Academic, N. Y., 1959): a) 361 ff.; b) 38 ff.; c) Ch. 1; d) §§7,8; e) §§10,11; f) §31; g) §66; h) §§27-29; i) §§49, 69; j) §§50-51; Ch. 7; k) §§20-25; Chs. 6,11; l) §97; m) §95; n) §98; o) §73; p) Tables 73-2, 73-3.

19. A. B. Bhatia, Ultrasonic Absorption (Oxford, London, 1967): a) 259 ff.; b) Ch. 4; c) Ch. 9; d) §4.6; e) §14.3; f) 205 ff.; g) Ch. 5; h) §9.1; cf. §5.1, thermal response only; i) §§9.4,9.5; j) §§6.5,6.6, 7.8; k) §§6.2-6.4, Ch. 7; l) §§5.9,5.10,5.13, Chs. 6, 10; m) §10.3; n) §10.1; o) §10.2; p) 199 ff.; q) 137 ff., 152; r) §10.6; s) §8.1; t) 232 ff.

20. S. Flügge, ed., Handbuch der Physik (Springer-Verlag, Berlin, 1961), Vol. 11/1.

21. I. Z. Fisher, Statistical Theory of Liquids (U. Chicago Press, 1964): a) 64 ff., plus recent references by many authors too numerous to mention; b) 54 ff.; c) 46 ff.

22. R. W. James, The Optical Principles of the Diffraction of X-Rays (Cornell.U. Press, Ithaca, N. Y., 1948), Ch. 9.

23. P. A. Egelstaff, An Introduction to the Liquid State (Academic, London, 1967): a) 66 ff.; b) 4.

24. For chemical reactions: B. J. Berne and R. Pecora, J. Chem. Phys. 50,783(1969); for rotational diffusion: H. Z. Cummins, F. D. Carlson, T. J. Herbert, and G. Woods, Biophys. J. 9,518(1969).

25. J. P. McTague, P. A. Fleury, and D. B. DuPre, Phys. Rev. 188,303(1968).

26. J. V. Sengers and A. Levelt-Sengers, Chem. Eng. News 46,104(1968).

27. M. E. Fisher, Rep. Prog. Phys. 30,615(1967): a) 659 ff. b) 624 ff; c) 623 ff.

28. R. B. Griffiths, Phys. Rev. 158,176(1967).

29. J. A. Pryde, The Liquid State (Hutchinson U. Library, London, 1966), 15.

30. E. A. Guggenheim, J. Chem. Phys. 13,253(1945).

31. J. S. Rowlinson, Rep. Prog. Phys. 28,169(1965): a) 174 ff.; b) see §5.3, 185.

32. F. Zernicke and J. Prins, Z. Phys. 41,184(1927); P. Debye and H. Menke, Ergeb. d. Tech. Röntg. 2(1931).

33. H. Eyring and M. S. Jhon, Significant Liquid Structures (Wiley, N. Y., 1940).

34. H. D. Ursell, Proc. Camb. Phil. Soc. 23,685(1927).

35. J. E. Mayer, J. Chem. Phys. 5,67(1937); with M. G. Mayer, Statistical Mechanics (Wiley, N. Y., 1940).

36. S. A. Rice and P. Gray, The Statistical Mechanics of Simple Liquids (Wiley, N. Y., 1965): a) end of Ch. 2; b) Ch. 3; c) §3.3; d) 486 ff.; e) 200; f) 270; g) 462.

37. J. E. Lebowitz and O. Penrose, J. Math. Phys. 5,84 (1964).

38. J. Yvon, Actualités Scientifiques et Industriel (Herman et Cie, Paris, 1935); La Théorie Statistique des Fluides et l'Equation d'Etat (Herman et Cie, Paris, 1935).

39. M. Born and H. S. Green, Proc. Roy. Soc. (London) A188, 10(1946); A General Kinetic Theory of Liquids (Cambridge U. Press, N. Y., 1949); H. S. Green, Molecular Theory of Fluids (North-Holland, Amsterdam, 1952).

40. J. G. Kirkwood: a) J. Chem. Phys. 3,300(1935); b) 14, 180(1946); c) 15,72(1947).

41. G. H. A. Cole, Adv. Phys. 8,225(1959).

42. I. Z. Fisher, Soviet Phys. Usp. (Engl. transl.) 5, 239 (1962).

43. N. N. Bogolyubov, Problems of Dynamical Theory in Statistical Physics (State Tech. Press, Gostekhizdat, 1946).

44. Rice, Boon, and Davis, op. cit., 336; P. Egelstaff, op. cit., 86.

45. G. S. Rushbrooke and H. I. Scoins, Phil. Mag. 42,582 (1951); Proc. Roy. Soc. A216,203(1953).

46. L. S. Ornstein and F. Zernicke, Proc. Acad. Sci. Amst. 17,793(1914).

47. J. K. Percus, Phys. Rev. Lett. 8,462(1962); with G. J. Yevick, Phys. Rev. 110,1(1958).

48. L. Verlet, Physica 30,95(1964).

49. Yi-Der Chen, thesis, Penn. State. U., March, 1970 (unpubl.); with W. A. Steele, J. Chem. Phys. 52,5284 (1970); 54,703(1971).

50. G. S. Rushbrooke and M. Silbert, Mol. Phys. 12,505(1967) J. S. Rowlinson, ibid., 12,513(1967).

51. J. E. Mayer and E. W. Montroll, J. Chem. Phys. 9,2,626 (1941); J. deBoer, Rep. Prog. Phys. 12,305(1949); with A. Michels, Physica 6,97(1939).

52. R. W. Zwanzig, J. Chem. Phys. 22,1420(1954); J. A. Barker and D. Henderson, ibid., 47,4714(1967); with W. R. Smith, ibid., 53,508(1970); D. Levesque and L. Verlet, Phys. Rev. 182,307(1969).

53. G. A. Neece and B. Widom, Ann. Rev. Phys. Chem. 20,167 (1969): a) refs. 45-52; b) refs. 40-44.

54. a) B. J. Berne and G. D. Harp, Adv. Chem. Phys. 17,63 (1970); b) B. J. Alder, D. M. Gass, and T. E. Wainwright, J. Chem. Phys. 53,3813(1970).

55. M. E. Fisher, J. Math. Phys. 5,944(1964).

56. L. P. Kadanoff, et al., Rev. Mod. Phys. 39,395(1967), 417.

57. F. London, Z. f. Physik 63,245(1930). Modern account:

J. O. Hirschfelder, ed., Adv. Chem. Phys. 12(1967).

58. H. E. Stanley, Introduction to Phase Transitions and Critical Phenomena (Oxford, London, 1971): a) part 4; b) Chs. 11,12; c) §3.3.

59. C. Domb, Phil. Mag. Suppl. 9,151(1960).

60. T. D. Lee and C. N. Yang, Phys. Rev. 87,410(1952); R. B. Griffiths, ibid., 158,176(1967).

61. C. J. Pings and R. K. Teague, Phys. Lett. 26A,496(1968); J. Chem. Phys. 48,4973(1968).

62. B. Widom, ibid., 43,3898(1965).

63. W. Botch and M. Fixman, ibid., 36,3100(1962); 42,199 (1965).

64. K. Kawasaki, Ann. Phys. (N. Y.), 1970 (in press).

64X. M. H. C. Knudsen, Kinetic Theory of Gases (Methuen, 1946); W. Crookes, Phil. Trans. 172,387(1882).

65. L. Euler, Principes Géneraux du Mouvement des Fluides (Hist. de l'Acad. de Berlin, 1755); D. Bernoulli, Hydrodynamica (Argentorati, 1738); I. Newton, Principia (Le Seur et Jacquier, 1686).

66. H. Lamb, Hydrodynamics (Dover, N. Y., 1932).

67. L. D. Landau and E. M. Lifshitz, Fluid Mechanics (Pergamon, London, 1959): a) §§1,2,6,7,15,49; b) §49; c) §§49,77; d) 224.

68. C. L. M. H. Navier, Mém. de l'Acad. des Sceinces 6,389 (1822); G. Stokes, Trans. Camb. Phil. Soc. 8,287 (1845).

69. P. M. Morse, in Handbuch der Physik, ed. S. Flügge (Springer-Verlag, Berlin, 1961), Vol. 11/1.

70. S. Fujita, Introduction to Non-Equilibrium Quantum Statistical Mechanics (W. B. Saunders, Philadelphia, 1966).

71. R. M. Mazo, Statistical Mechanical Theories of Transport Processes (Pergamon, Oxford, 1967): a) 28 ff. b) 53 ff.; c) Ch. 10; d) 61, 66-7; e) Ch. 5; f) 66 g) Chs. 7-9; h) Chs. 8,9; i) 119 ff.; j) 118; k) 91.

72. S. Chapman and T. G. Cowling, The Mathematical Theory

of Non-Uniform Gases (Cambridge U. Press, 1952); a) Ch. 17; b) Chs. 5, 6.

73. J. von Neumann, Nachr. Ges. Wiss., Göttingen 1,245,273 (1927); Mathematische Grundlagen der Quantenmechanik (Springer-Verlag, Berlin, 1932).

74. I. Prigogine, Non-Equilibrium Statistical Mechanics (Interscience, N. Y., 1962): a) Ch. 1; b) Chs. 12, 14; c) Ch. 11.

75. R. L. Liboff, Introduction to the Theory of Kinetic Equations (Wiley, N. Y., 1969): a) Ch. 2; b) 180.

76. J. W. Gibbs, Elementary Principles of Statistical Mechanics, Vol. 2 of Collected Works... (Yale U. Press, New Haven, Conn., 1948).

77. S. A. Rice and H. L. Frisch, Ann. Rev. Phys. Chem. 11, 187(1960): a) II.3; b) 215 ff.; c) 203.

78. G. V. Chester, Rep. Prog. Phys. 26,411(1963): a) 433 ff. b) 445 ff.; c) 415; d) 417.

79. F. Reif, Fundamentals of Statistical and Thermal Physics (McGraw-Hill, N. Y., 1965), Ch. 12.

80. J. H. Jeans, The Dynamical Theory of Gases (Dover, N.Y., 1954), Ch. 11.

81. L. Boltzmann, Vorlesungen über Gastheorie (2 vols; Barth, Leipzig, 1912); Engl. Transl. by S. G. Brush, Lectures in Gas Theory (U. C. Press, Berkeley, 1964); also, S. B. Akad. Wiss. Wien (II) 58, 517(1872).

82. D. Enskog, Archiv för Matematik, Astronomi, och Fysik 16,16(1922); in German.

83. W. Pauli, in Probleme der Moderne Physik, ed. P. Debye (Hirzel, Leipzig, 1928), 30.

84. H. Grad, Communication in Pure and Applied Mathematics 2,331(1949).

85. H. Grad, in Handbuch der Physik, ed. S. Flügge (Springer-Verlag, Berlin, 1958), Vol. 12.

86. C. S. Wang-Chang and G. E. Uhlenbeck, Transport Phenomena in Polyatomic Molecules (U. Michigan Publ. CM-681, 1951); with J. deBoer, in Studies in Statistical Mechanics 2,243(1964).

87. D. Enskog, Kgl. Svenska Vetenskap. akad. Handl. 63, no. 4(1922).

88. N. N. Bogolyubov, J. Phys. U. S. S. R. 10,256,265(1946).

89. J. D. Dorfman and E. G. D. Cohen, Phys. Lett. 16,124 (1965); J. V. Sengers, Phys. Rev. Lett. 15,515 (1965); J. Weinstock, ibid., 140,A461(1965); K. Kawasaki and I. Oppenheim, ibid., 139,A1763(1965).

90. H. Eyring, J. Chem. Phys. 4,283(1936); with J. H. Kincaid and A. E. Stearn, Chem. Revs. 28,301(1941); with S. Glasstone and K. J. Laidler, The Theory of Rate Processes (McGraw-Hill, N. Y., 1941).

91. S. Chandrasekhar, Rev. Mod. Phys. 15,1(1943).

92. R. A. Fisher and R. O. Watts, J. Chem. Phys. (subm. for publ., 1971).

93. S. A. Rice and H. R. Allnatt, ibid., 34,2144,2156(1961).

94. refs. 63-74 and 88 of Rice, Boon, and Davis, op. cit.

95. M. H. Cohen and D. Turnbull, ibid., 31,1164(1959).

96. L. van Hove, Physica 21,517(1955); 23,441(1957).

97. R. Brout and I. Prigogine, ibid., 22,621(1956).

98. I. Prigogine, G. Nicolis, and J. Misguich, J. CHem. Phys. 45,4516(1965).

99. H. Nyquist, Phys. Rev. 32,110(1928); H. B. Callen and T. A. Welton,ibid., 83,34(1951).

100. M. S. Green, J. Chem. Phys. 20,1281(1952); 22,398(1954); and others more recent--see refs. 9-12 of Mazo, ref. 71 here.

101. R. Lucas, J. Phys. Rad. 8,41(1937).

102. A. E. Brown and E. G. Richardson, Phil. Mag. 4,705 (1959); A. E. Brown, Acustica 18,169(1967).

103. M. Fixman, J. Chem. Phys. 36,310(1962).

104. M. Fixman, ibid., 36,1957(1962).

105. M. P. Puls, thesis, McMaster U., May, 1970, 126, 137-8; K. Kawasaki, Prog. Theor. Phys. 40,930(1968).

106. R. A. Ferrel, et al., Phys. Rev. Lett. 18,891(1967).

107. L. P. Kadanoff, J. Phys. Soc. Japan 26,S122(1969).

108. P. Debye, Polare Molekulen (Hirzel, Leipzig, 1929).

109. V. V. Daniel, Dielectric Relaxation (Academic, London, 1967).

110. a) Y. Toyazawa, Prog. Theor. Phys. (Kyoto) 20,53 (1958); b) J. van Kranendonk, thesis, Univ. of Amsterdam, Holland, Dec. 17, 1952; d) G. Birnbaum, Adv. Chem. Phys. 12,487(1967).

111. A. Abragam, The Principles of Magnetic Resonance (Oxford, London, 1961).

111a. T. B. Bottomore, Early Writings of Karl Marx (McGraw-Hill, N. Y.).

112. K. Takayanagi, Porg. Theor. Phys. 25,1S(1963).

113. R. Gordon, W. Klemperer, and J. I. Steinfeld, Ann. Rev. Phys. Chem. 19,215(1969).

114. D. Sette, in Handbuch der Physik, ed. S. Flügge (Springer-Verlag, Berlin, 1961), Ch. A.III.

115. F. W. Billmeyer, Jr., Textbook of Polymer Science (Interscience, N. Y., 1962), Ch. 6; P. Meares, Polymers: Structure and Bulk Properties (D. van Nostrand, London, 1968), Chs. 6-9.

116. J. V. V. Kasper and G. C. Pimentel, Phys. Rev. Lett. 14 (1965); Appl. Phys. Lett. 5,231(1964); K. L. Kompa and G. C. Pimentel, J. Chem. Phys. 47,857 (1967); R. E. Honig and J. R. Woolston, Appl. Phys. Lett. 2,138(1963); A. deMaria and C. J. Ultee, ibid., 9,67(1966).

117. J. A. Pople, Disc. Far. Soc. 15,35(1953).

118. See, for example, Table I-A of ref. 5.

119. See tables in the Handbook of Chemistry and Physics (Chem. Rubber Publ. Co., Cleveland, Ohio); note that the organics cluster about the same value of specific heat, implying a heat capacity proportional to mass or size.

120. D. Eisenberg and W. Kauzmann, The Structure and Properties of Water (Oxford, London, 1969), §§3.5,

4.4, 4.7; H. L. Strauss, Ann. Rev. Phys. Chem. 19, 419(1968).

121. International Critical Tables (McGraw-Hill, N. Y., 1929), Vol. 5; a) 81; b) 213-4.

122. D. F. Eggers, Jr., N. W. Gregory, G. D. Halsey, Jr., and B. S. Rabinovitch, Physical Chemistry (Wiley, N. Y., 1964): a) § 6.4; b) 662 ff.

123. G. N. Lewis and M. Randall (rev. K. S. Pitzer and L. Brewer), Thermodynamics (McGraw-Hill, N. Y.,1961), 438 ff.

124. J. Lamb, in Physical Acoustics, ed. W. P. Mason (academic, N. Y., 1965), Vol. IIA, 227 ff.

125. E. R. Andrew, Nuclear Magnetic Resonance (Cambridge U. Press, 1955).

126. For D in cryogenic liquids: G. T. Preston, T. W. Chapman and J. M. Prausnitz, Cryogenics 7,274(1967); in normal liquids: P. A. Johnson and A. L. Babb, Chem. Rev. 56,387(1965); D. W. McCall, D. C. Douglass and E. W. Anderson, J. Chem. Phys. 31,1555 (1959).

127. Herzfeld and Litovitz, op. cit.,328.

128. S. Golden, Quantum Statistical Foundations of Chemical Kinetics (Oxford, London, 1969).

129. D. Sette, in Handbuch der Physik, ed. S. Flügge (Springer-Verlag, Berlin, 1961), Vol. 11/1, 287 ff.

130. D. Rapp and T. Kassal, Grumann Res. Dept. Rept.RE-345.

131. W. H. Miller, J. Chem. Phys. 53,1949,3587(1970).

132. C. Sluitjer, in Dispersion and Absorption of Sound by Molecular Processes, ed. D. Sette (Academic, N. Y., 1963), 338 ff.

133. H. O. Kneser, in Physical Acoustics, ed. W. P. Mason (Academic, N. Y., 1965), Vol. IIA: a) §II.B; b) 193 ff.

134. M. Eigen and L. deMayer, in Techniques of Organic Chemistry, ed. Weissberger, et al. (Wiley, N. Y., 1962), Vol. 8, Part 2; see esp. Eq. (II.3.90b).

135. J. Lamb, op. cit., §§3,4.

136. S. Mizushima, Structure of Molecules (Academic, N. Y., 1954).

137. D. Sette, op. cit., 339 ff.

138. W. Steele and R. Pecora, J. Chem. Phys. 42,1863(1965).

139. R. C Millikan and L. A. Osburg, ibid., 41,2196(1964).

140. F. deMartini and L. Ducuing, Phys. Rev. Lett. 17, 117 (1966).

141. J. J. Martin, Ind. Eng. Chem. 59,34(1967).

142. A. D. Buckingham and J. A. Pople, Trans. Far. Soc. 51, 1173(1955).

143. H. B. Levine and D. R. McQuarrie, Physica 31,749(1965); J. Chem. Phys. 44,3500(1966).

144. D. E. Stogryn, ibid., 50,4967(1969).

145. H. Reiss, H. L. Frisch, and J. L. Lebowitz, ibid., 31, 3699(1959).

146. R. M. Gibbons, J. Mol. Phys. 17,81(1968); with W. A. Steele, ibid., 15,567(1968).

147. A. D. Buckingham, Disc. Far. Soc. 43,205(1967).

148. J. A. Barker and R. O. Watts, Chem. Phys. Lett. 3,144 (1969).

149. J. M. Prausnitz, Molecular Thermodynamics of Fluid Phase Equilibria (Prentice-Hall, Englewood Cliffs, N. J., 1969): a) Chs. 5-7; b) §5.10; c) §6.15; d) §7.6; e) §7.7; f) §7.10; g) §7.11; h) 239; i) §10.8

150. J. S. Rowlinson, Liquids and Liquid Mixtures (Butterworths, London, 1959): a) Ch. 5; b) 230; c) 181; d) 183.

151. Hirschfelder, Curtiss, and Bird, op. cit., §7.6d; and numerous recent articles.

152. R. G. Gordon, J. Chem. Phys. 44,1830(1966).

153. J. C. Light, Adv. Chem. Phys. 19,1(1971); M. Karplus,

R, N. Porter, and R. D. Sharma, J. Chem. Phys. 43, 3259(1965).

154. R. R. Herschbach, Adv. Chem. Phys. 10,319(1966); R. J. Beuhler, Jr. and R. B. Bernstein, Chem. Phys. Lett. 2,166(1968); Y. T. Lee, et. al., J. Chem. Phys. 51,455(1969); 53,3385(1970); F. P. Tully, Y. T. Lee, and R. S. Berry, Chem. Phys. Lett. 9,80(1971); J. Geddes, H. F. Krause, and W. L. Fite, J. Chem. Phys. 52,3296(1970); C. Maltz, Chem. Phys. Lett. 9,251(1971), refs. 1-3.

155. W. P. Mason, Trans. Amer. Soc. Mech. Eng. 69,359(1947); Piezoelectric Crystals and Their Application to Ultrasonics (D. van Nostrand, Princeton, N. J., 1950); the first actual use in the critical region is under way in the laboratory of C. J. Pings at this institution.

156. D. Eisenberg and W. Kauzmann, The Structure and Properties of Water (Oxford, London, 1969): a) 148, and Tables 3.18, 4.2; b) §4.2; c) 222; d) §4.6e; e) §2.1b; f) 56, 257, 190ff.; g) §§4.4b,4.6b; h) §4.7; i) §5.2; j) §4.6a; k) §5.3; l) §4.8a; m) §4.7, esp. 240; n) 112; o) 219 ff.; p) §4.6d

157. A. Eucken, Nachr. Ges. Wiss. Göttingen, Math. Phys. Kl. 38(1946); 1(1949); Z. Electrochem. 52,255 (1948).

158. L. Hall, Phys. Rev. 73,775(1948).

159. D. Sette, Phys. Rev. 78, 476(1950); E. H. Carnevale and T. A. Litovitz, J. Acoust. Soc. Am. 27,547 (1955).

160. A. Ben-Naim, J. Chem. Phys. 52,5531(1970).

161. G. H. Haggis, J. B. Hasted, and T. J. Buchanan, ibid. 20,1452(1952).

162. J. H. Hildebrand and R. L. Scott, The Solubility of Nonelectrolytes (Dover, N. Y., 1964), 41, and Ch. 16.

163. J. H. Andreae, P. D. Edmonds, and J. F. McKellar, Acustica 15,74(1965).

164. D. Sette, op. cit., §27.

165. T. L. Hill, An Introduction to Statistical Thermodynamics (Addison-Wesley, Reading, Mass., 1960),§20.2.

166. J. L. Lebowitz, Phys. Rev. 133A,895(1964); with J. S. Rowlinson, J. Chem. Phys. 41,133(1964).

167. E. A. Guggenheim, Mixtures (Oxford, London, 1952); Applications of Statistical Mechanics (Oxford, London, 1966).

168. R. L. Scott, J. Chem. Phys. 25,193(1956).

169. H. Renon and J. M. Prausnitz, Chem. Eng. Sci. 22,299, errata 1891(1967).

170. G. Thomaes and J. van Itterbeek, Mol. Phys. 2,372 (1959); J. P. Boon and G. Thomaes, Physica 28,1074 (1962); 29,208(1963).

171. E. McLaughlin, Chem. Rev. 64,389(1964).

172. A. V. Anantaraman, A. B. Walters, P. D. Edmonds, and C. J. Pings, J. Chem. Phys. 44,2651(1966); M. P. Puls, op. cit.

173. J. D. Cox and E. F. G. Herington, Trans. Far. Soc. 52, 926(1956).

174. M. Cevolani and S. Petralia, Atti Accad. Naz. Lincei 2,674(1952).

175. R. B. Griffiths and J. C. Wheeler, Phys. Rev. A2,1047 (1970).

Rederivation and Analysis of Fixman's Theory of Excess Sound Absorption Near Fluid Critical Points*

Vincent P. Gutschick† and C. J. Pings

Division of Chemistry and Chemical Engineering
California Institute of Technology
Pasadena, California 91109

We retrace the thermodynamic and hydrodynamic analysis used by M. Fixman (J. Chem. Phys. 36, 1961 (1962)) in the first quantitative explanation of the anomalously large sound absorption near fluid critical points. With some oversights and ambiguities corrected, the basic theory is seen to be firmly based in classical thermodynamics and hydrodynamics. The use of the Ornstein-Zernike, Debye, and Flory-Huggins models for reduction of key quantities appears necessary for thermodynamic consistency. For analysis of experimental data, Fixman's theory is preferred over alternative theories, though no one theory is truly satisfactory. With a view toward interpreting our data presented in the following paper (J. Chem. Phys. xx, xxxx, (1971)), we argue the applicability of Fixman theory in systems having a strong background of additional (thermal) relaxation.

* Research sponsored by AFOSR (SRC)-OAR, USAF Grant No. AFOSR-68-1382.

† National Science Foundation Predoctoral Fellow, 1966-1970.

Introduction

As a probe of energy exchange, especially in simple fluid systems, measurement of the ultrasonic pressure amplitude attenuation or absorption coefficient α and of the sound velocity β has shown much utility. 'Thermal' relaxation of internal degrees of freedom, such as vibrational, or of local structure, as in chemical association, causes absorption and dispersion behavior whose details of magnitude, temperature- and composition-dependence can often be correlated closely with kinetic and thermodynamic parameters of the system.[1] Near critical points - and here we speak specifically of gas-liquid and binary liquid-critical points - additional strong absorption arises,[2] somehow tied to the presence of strong fluctuations in density or composition, up to macroscopic size. Early attempts at an explanation included Lucas'[3] proposal that the fluctuations undergo differential acceleration relative to the bulk fluid because of their different density, thus causing excess viscous losses; and work by Richardson and Brown[4] ascribing it in at least one system to an <u>apparent</u> loss of energy by Rayleigh scattering. Both models fail quantitatively, for both give too small a magnitude for the absorption, and dependences on frequency not generally observed.

Using irreversible thermodynamics as a framework unifying our treatment with that of ordinary thermal relaxation, we shall retrace the approach of M. Fixman,[5] which proved the first successful model. The primary thermodynamic quantity to relate to absorption and dispersion is the effective complex compressibility (adiabatic) $\underline{K_s}^{\omega}$ giving the volume response of the system to the periodic pressure perturbation of the sound wave, hence the measure of reversible and irreversible work done. Substituting a complex compressibility in the wave equation for the pressure variation δp,

$$\frac{\partial^2 \delta p}{\partial t^2} - \frac{1}{\rho K} \nabla^2 \delta p = 0 \ , \tag{1}$$

where $$(\rho K)^{-1} = \beta^2 = \text{squared sound velocity}, \tag{2}$$

gives a solution

$$\delta p = \delta p_o e^{-\alpha x} e^{i(kx-wt)} \tag{3}$$

with $$\alpha = \frac{\omega \rho \beta}{2} \ \text{Im } K. \tag{4}$$

To calculate $\underline{K}$, it is generally sufficient to assume expansions of the volume and entropy differentials $\underline{\delta V}$ and $\underline{\delta S}$ in the state variables[6] (also sound wave progress variables)

$\delta\underline{T}$, $\delta\underline{p}$, and $\delta\xi$; the latter is some order parameter for the internal degrees of freedom:

$$\delta S = \frac{C_p^{\infty}}{T}\,\delta T - V\theta^{\infty}\,\delta p + \frac{H'}{T}\,\delta\xi \tag{5}$$

$$\delta V = V\theta^{\infty}\,\delta T - VK_T^{\infty}\,\delta p + V'\,\delta\xi. \tag{6}$$

The superscript '∞' refers to processes in the limit of infinite frequency, where the internal degree of freedom is frozen. The quantities $\underline{C_p}$, θ, $\underline{H'}$, $\underline{K_T}$, and $\underline{V'}$ are respectively isobaric heat capacity, thermal expansivity, an internal enthalpy, isothermal compressibility, and an internal volume change. The first equation is used in the form $\delta\underline{S}=0$ to eliminate one variable and to express the lack of spatial heat transfer to first order during sound passage. A simple $\underline{\delta V} \leftrightarrow \underline{\delta p}$ relation to obtain $\underline{K_S^{\omega}}$ is obtained with the addition of kinetic equation for $\delta\xi$, assumed to be

$$\frac{d}{dT}\,\delta\xi \equiv \delta\dot{\xi} = -L\delta Z. \tag{7}$$

Here $\underline{Z}$ is some ordering force associated with $\delta\xi$,

$$\delta Z = -\frac{H'}{T}\,\delta T + V'\delta p + \phi\delta\xi\ , \tag{8}$$

and ϕ is defined by the above equation. The total solution is then

$$K_s^{\omega} = K_s^{\infty} + \left\{ \frac{[V' - V\theta^{\infty}H']^2}{V\phi[1 + (H')^2/TC_p^{\infty}\phi]} \right\} \frac{1}{1 + i\omega\tau}, \qquad (9)$$

with $$\tau = (L\phi)^{-1}. \qquad (10)$$

This yields

$$\text{Im } K_s^{\omega} = -\left\{ \quad \right\} \frac{\omega\tau}{1 + \omega^2\tau^2} \qquad (11)$$

and thus a typical relaxation curve for α, proportional to $\frac{\omega^2\tau}{1 + \omega^2\tau^2}$. We have throughout neglected the extra shear viscous and thermal conduction losses, which require extra terms in Eq. (1), since these are always additive for our uses.[7]

For our purposes, the internal degree of freedom is the local density or concentration. Treating binary systems more specifically, this is the local concentration (by mass, volume, or mole fraction, as is convenient) c_2 of component 2. Its kinetic equation (Eqs. 7 and 8 combined) is a dissipative diffusive equation whose form outside the critical region is taken as[8]

$$\rho \dot{c}_2 = \alpha \left(\frac{\partial \mu}{\partial c_2}\right) \nabla^2 c_2 + \left[\alpha\left(\frac{\partial \mu}{\partial T}\right) + \varepsilon\right]\nabla^2 T + \alpha\left(\frac{\partial \mu}{\partial p}\right)\nabla^2 \delta p. \qquad (12)$$

Here μ is a chemical potential $\mu_1 - \mu_2$, with μ_1, μ_2 the chemical potential per unit concentration, and α, ε are constants; also $\frac{\partial \mu}{\partial p} = \underline{V}'$ and $\frac{\partial \mu}{\partial c_2} = \phi$ in the terminology of Eq.(8). This choice of kinetic equation describes the baro-diffusion ($\delta \underline{T} \equiv 0$) or thermal diffusion ($\delta \underline{p} \equiv 0$) mechanisms. The former yields a response of

$$\delta c_2 = \frac{\alpha V' k^2}{\rho(i\omega + D_{12}k^2)} \delta p \quad , \qquad (13)$$

where $\underline{k}$ is the propagation vector magnitude as in Eq. (3), and an absorption

$$\alpha = \frac{\rho\beta}{2} \frac{(V')^2}{V\phi} \frac{\omega^2\tau}{1 + \omega^2\tau^2} \quad , \qquad (14a)$$

$$\tau = \alpha\phi/\rho\beta^2 \equiv D_{12}/\beta^2 \quad . \qquad (14b)$$

While ϕ vanishes at the critical point, so does $\underline{D_{12}}$ and the absorption is not only finite but negligibly small.

Fixman's Development

Clearly the diffusion of c_2 follows a modified equation in the critical region. The thermodynamic equations (5) and (6) may also need to be taken to higher order. Fixman[9] realized that the differential of the local Gibbs energy density δG from which (5) and (6) are derived must include a quadratic term in $(\delta c_2)^2$, since the linear term is vanishing. Taking c_2 as n_2, the molecular or molar density, he obtains

$$dG\Big|_{p,T} = \mu_1 dn_1 + \mu_2 dn_2$$

$$= [\mu_1^{\circ} + \left(\frac{\partial \mu_1}{\partial n_2}\right) \delta n_2]\, dn_1 + [\mu_2^{\circ} + \left(\frac{\partial \mu_2}{\partial n_2}\right) \delta n_2]\, dn_2, \quad (15)$$

where μ_1° is the bulk or average value of μ_1. The Gibbs-Duhem relation $n_1 d\mu_1 + n_2\, d\mu_2$ yields

$$dG = \mu_1^{\circ} dn_1 + \mu_2^{\circ} dn_2 + \left(\frac{\partial \mu_1}{\partial n_2}\right) \left[dn_1\, \delta n_2 - \frac{n_1}{n_2}\, dn_2\, \delta n_2\right] . \quad (16)$$

The relation of dn_1 and dn_2 in the fluctuation is taken as preserving the molar volume,

$$dV = \frac{\partial V}{\partial n_1}\, dn_1 + \frac{\partial V}{\partial n_2}\, dn_2 \equiv \bar{V}_1\, dn_1 + \bar{V}_2\, dn_2 \longrightarrow 0, \quad (17)$$

corresponding to isochoric propagation conditions which can be related later to the proper adiabatic conditions. Integration over the fluctuation volume yields

$$\delta G = \int dG = - \frac{1}{2n_2} \bar{V}_1 \left(\frac{\partial \mu_1}{\partial n_2}\right)_{p,T,n_1} (\delta n_2)^2 \qquad (18)$$

for the anomaly-containing quadratic term. Additionally, Fixman notes that we should make the replacement,

$$(\delta n_2)^2 \longrightarrow (\delta n_2)^2 + \kappa^{-2} |\nabla \delta n_2|^2 , \qquad (19)$$

where κ is the inverse correlation length of the critical region pair distribution function $\underline{g(R)}$ in Ornstein-Zernike[10] form,

$$G(R) = g(R) - 1 \underset{R\to\infty}{\longrightarrow} \frac{a}{R} e^{-\kappa R}. \qquad (20)$$

κ is very temperature-sensitive but $\left(\frac{\partial \mu_1}{\partial n_2}\right)$ in Eq. (18) is proportional to κ^2 so this extra term in $\underline{\delta G}$ is as a whole negligible. Now make the good approximation

$$\delta S = \frac{\partial}{\partial T} \delta G\Big|_{p,T}$$

$$\approx - \frac{1}{2n_2\bar{V}_1} \left(\frac{\partial^2 \mu_1}{\partial n_2 \partial T}\right)_{p,n_1} (\delta n_2)^2 . \qquad (21)$$

We take some liberties with Fixman's original presentation from here on, as by keeping n_2 as the concentration variable rather than going over to the volume fraction ϕ_2; our final result is unchanged.

The dynamic response of $(\delta n_2)^2$ must now be computed from the diffusion equation with critical region corrections. Now, $(\delta n_2)^2$ is not the square of the sound-driven fluctuation, which can be made arbitrarily small by reducing the sound intensity. Rather, $(\delta n_2)^2$ has a finite equilibrium average related to the 2-2 pair distribution function $G^{22}(R) \equiv G(R)$:
consider

$$< \delta n_2 (\vec{R}_1)\ \delta n_2 (\vec{R}_2) > \equiv \frac{n_2}{V}\, \delta(\vec{R}_{12}) + n_2^2\, G(\vec{R}_{12}). \tag{22}$$

Assuming Fourier decompositions of $\delta n_2 (\vec{R})$ and of $G(\vec{R})$ as

$$\delta n_2 (\vec{R}) = \int d\vec{k}\ \ n_{\vec{k}}\, e^{i\vec{k}\cdot\vec{R}} \tag{23a}$$

$$G(\vec{R}) = \int d\vec{k}\ G_{\vec{k}}\, e^{i\vec{k}\cdot\vec{R}}\ , \tag{23b}$$

a few manipulations yield

$$<\delta n_2(\vec{R})^2> = \frac{n_2}{V} \int d\vec{k} + n_2^2 \int d\vec{k}\ G_{\vec{k}}\ . \tag{24}$$

The first term is dropped if we are considering a volume considerably larger than the fluctuation.

The periodic temperature excursion $\delta\underline{T}$ due to the sound wave alters the dynamics of the spontaneous fluctuations, adding a correction to $(\delta n_2)^2$ that is correlated to the sound wave. The resulting energy exchange with the sound wave has a phase lag and causes a loss or absorption of energy. The dynamics of the decay of spontaneous fluctuations in the singlet distribution c_2 are given by Fixman's modified diffusion equation[11] (less the non-anomalous direct driving terms in $\delta\underline{p}$, $\delta\underline{T}$ of the sound wave),

$$\rho\dot{c}_2 = -\frac{h\rho}{2}\kappa^2\left[\nabla^2 c_2 - \kappa^{-2}\nabla^2\nabla^2 c_2\right] . \tag{25}$$

The diffusion constant product $\alpha\phi$ of Eq. (12) has been written in the new variables $\underline{h}$ and κ^2, from the thermodynamic expression for κ^2 in terms of $\partial\mu_1/\partial\underline{n_2}$ in the Ornstein-Zernike model,

$$\frac{4\pi a}{\kappa^2} = -\frac{\bar{V}_1}{n_2}\left[\frac{kT}{(\partial\mu_1/\partial n_2)} + \frac{1}{\bar{V}_1}\right] . \tag{26}$$

The relation $\underline{d\mu} = (\rho/\underline{n_2 m_1 m_2})\ \underline{d\mu_1}$ is also used to express $\underline{h}$ as [13]

$$h = \frac{\alpha \bar{V}_1^{\,2}\, \bar{V}_2\, kT\rho}{m_1^{\,2} m_2 c_2 2\pi a \phi_2} \quad , \tag{27}$$

where $\bar{V}_i$, m_i , c_i, and ϕ_i are respectively partial molar volume, molecular mass, weight- and volume-fraction concentrations, and a is as in Eq. (26). The second or correction term in Eq. (25) has been derived by Fixman[11] and justified as consistent with the critical-region form of the free-energy density in a fluctuation.

The dynamic response of $(\delta n_2)^2$ to the sound wave perturbation δT is more readily expressed in terms of the response of $G(R)$. Intuitively, Fixman adapts the diffusion equation (25) for the pair density $G(R)$ simply by doubling the diffusion constant $h/2$,

$$\dot{G} = h\kappa^2 \left[\nabla^2 G - \kappa^{-2} \nabla^2 \nabla^2 G\right] . \tag{28}$$

The equilibrium solution to Eq. (28) is the proper Ornstein-Zernike form,

$$G(R) \underset{R\to\infty}{\longrightarrow} \frac{a}{R} e^{-\kappa R} . \tag{29}$$

The primary temperature sensitivity is in κ^2, such that Fixman[14] adds the term

$$h \left(\frac{\partial \kappa^2}{\partial T}\right) \delta T \, \nabla^2 G \tag{30}$$

to Eq. (28). There is no way to treat a spatial dependence of $\delta\underline{T}$, so the implicit assumption is that the sound wavelength is very large relative to the fluctuation size, or

$$\lambda_{\text{sound}} >> \kappa^{-1} \; ; \tag{31}$$

this is consistent with dropping the first term in Eq. (24). A perturbation solution in Fourier space yields a correction $\delta G_{\underline{k}}$ to the component $G^{\circ}_{\underline{k}} = \underline{a/(2\pi^2\,[k^2+\kappa^2])}$, given by

$$\delta\dot{G}_k = i\omega\delta G_{\vec{k}} = -\,h\,k^2(k^2+\kappa^2)\,\delta G_{\vec{k}} - hk^2\left(\frac{\partial\kappa^2}{\partial T}\right)\delta T\; G^{\circ}_{\vec{k}} \; . \tag{32}$$

The fluctuating excess entropy $\delta\underline{S}$ of Eq. (21) is, using Eqs. (21), (26) and (32),

$$\delta S = \delta T \frac{kT\,h}{4\pi^2}\left(\frac{\partial\kappa^2}{\partial T}\right)^2 \int dk\, \frac{k^4}{(k^2+\kappa^2)\,[i\omega + hk^2(k^2+\kappa^2)]} \; . \tag{33}$$

This is equivalent to an excess heat capacity Δ_M per mole,

$$\Delta_M = T_c \frac{\delta S}{\delta T}\,\frac{N_0}{(n_1+n_2)} \tag{34}$$

$$N_0 = \text{Avogadro's number}$$

which is clearly complex. The compressibility is then computed from Eqs. (5) and (6) by altering $C^{\infty}_{\underline{p}}$ to $C^{\infty}_{\underline{p}} + \Delta_M$ and neglecting the small direct driving terms in $\delta\underline{p}$ and

$\delta\xi=\delta n_2$, $(H'/T)\delta n_2$ and $\bar{V}_2\delta n_2$. We have, dropping superscripts,

$$\delta V = V\theta\delta T - VK_T\delta P, \tag{35}$$

and from $\delta S=0$,

$$\delta V = \left[T\frac{(V\theta)^2}{(C_p + \Delta_M)} - VK_T\right] \delta p. \tag{36}$$

Expanding $(C_p + \Delta_M)^{-1}$ with Δ_M assumed small and using

$$\frac{TV\theta^2}{C_p^2} \approx K_T \frac{(C_p - C_V)}{C_p^2}, \tag{37}$$

(equality holds for C_p replaced by the net $C_p + \Delta$), we obtain an absorption

$$\alpha = \frac{\omega}{2\beta} \frac{(\gamma-1)}{C_p} \text{ Im } \Delta_M, \tag{38}$$

where $\gamma = C_p/C_V$ as usual. This is Fixman's result. More rigorous attention to the mathematics, esp. in Eq. (37), would show small differences for the true adiabatic propagation conditions.

Discussion and Redevelopment

In principle, Fixman's theory contains no adjustable parameters. The two central microscopic parameters κ and $\underline{h}$ may be derived from some light-scattering data[15]; also, thermodynamic data could be used for κ through its relation to $(\partial\mu_1/\partial n_2)$ in Eq. (26). Practically, the theory has always been used with $\underline{h}$ and κ as two adjustable parameters to be set from a least-squares fit of the absorption α or $\alpha/\underline{f}^2$ as a function of frequency $\underline{f}$ and temperature $\underline{T}$ at the critical composition. (Extension of the theory for the composition dependence of α has also been done.) To reduce κ, which varies with temperature, to a fixed parameter, the Debye[11] relation is used,

$$\kappa^2 = \frac{6}{\ell^2} \frac{|T-T_c|}{T_c} \quad , \tag{39}$$

$\underline{\ell}$ being the Debye persistence length. This last step fixes the theory squarely in classical critical thermodynamics, as the compressibility then diverges as $|T-T_c|^{-1}$. Similarly, a Flory-Huggins type[11,16] model for the chemical potential μ_1,

$$\mu_1 = kT \left[\ell n\, \phi_1 + a\phi_2 + b\phi_2^2 \right] \tag{40}$$

is used to set the constant $\underline{a}$ of Eq. (26), since the

diffusion constant $\underline{h}$ can be expressed through an involved reduction[13] in terms of equivalent ideal diffusion constants in the form

$$h = H/a\zeta \ , \tag{41}$$

where ζ is a molecular friction constant of more intuitive value.

Overall then, Fixman theory as used in analyzing experimental data incorporates several classical thermodynamic models--the two above, plus the Ornstein-Zernike model for $\underline{G(R)}$ which can be made partially non-classical by letting κ^2 have its true order of zero at $\underline{T_c}$. None of this compromises the theory, which is necessarily classical from the point where an integer order (second) expansion of $\delta\underline{G}$ in terms of $\delta\underline{n_2}$ is taken. The restriction is more apparent in the final expression for α, proportional to $(\partial\kappa^2/\partial\underline{T})$ - the classical relation Eq. (39) gives an α neither divergent nor vanishing at $\underline{T_c}$, while the true critical behavior of κ^2 has a higher than linear relation to $\underline{|T-T_c|}$ and would yield $\alpha=0$ at the critical point. At modest distances from the critical point at the mere onset of the anomaly, the deviation from classicality should be tolerable and the theory valid. In its usage to date on data quite near critical, Fixman theory yields more

questionable parameters. We return to this point after discussing the relative success of the theory as well as competing theories.

In application to various sets of experimental data on binary consolute points, Fixman's theory has been qualitatively upheld in most respects. The early data of Chynoweth and Schneider[17] on aniline/n-hexane at one frequency was analyzed by Fixman in his original paper, finding the predicted temperature dependence. The temperature derivative of the velocity, $d\beta/dT$, was positive and half as large as predicted. Anantaraman, et al.[18] found good f- and T-dependence, but $d\beta/dT < 0$ contrary to expectations in nitrobenzene/isooctane. D'Arrigo and Sette[19] found adequate T-dependence and again $d\beta/dT < 0$ in nitrobenzene/n-hexane. They also give a form for the composition or X-dependence of α/f^2 based on keeping the $\bar{V}_2/\bar{V}_1$ term in Eq. (26). This yields a peak in α/f^2 in composition that was far too narrow, due to the need to use the Flory-Huggins model for $(\partial\mu_1/\partial n_2)$ with its inherent limitation to a quadratic coexistence curve rather than the flatter, cubic true curve. Limited work on nitroethane/isooctane by Shakhparonov, et al.[20] showed an f-dependence fitting a power law like $\alpha/f^2 \sim f^{-(p+1)}$, with p in the range (0,1), roughly consistent with the $f^{-5/4}$ dependence predicted for small $|T-T_c|$. Puls[22] studied the liquid metal

system Ga/Bi as one of the simplest binaries, finding fair f- and T-dependence and $d\beta/dT \approx 0$. The X-dependence was fair but still too narrow. Interestingly, α/f^2 predicted with the persistence length ℓ set from the least-squares fit and ζ calculated from an estimate of the ideal diffusion constant, was 6.5 times too large, again reflecting the defects of classical thermodynamics, this time for the fluctuation spectrum δn_2^2.

Attempts have been made to avoid the defects of Fixman theory regarding mathematical rigor or thermodynamics in the rival theories of Kawasaki[23] and of Kadanoff and Swift.[24] Kawasaki[23a] originally gave a treatment based on the autocorrelation function expression for the combination of (frequency-dependent) shear and bulk viscosities,

$$\theta = \frac{4}{3}\eta_S + \eta_B \,. \tag{42}$$

The anomalous absorption from the shear viscosity anomaly is automatically included, unlike Fixman's treatment. The fluxes in the autocorrelation function are expanded to second order in the concentration fluctuations, and for the equation of motion of the latter Fixman's form Eq. (25) is used, as also the Ornstein-Zernike form for the equilibrium average fluctuations. Kawasaki's result is substantially that of Fixman but for the change from isobaric to

adiabatic propagation conditions, which is minor. It is similarly restricted to classical thermodynamics, again due to the quadratic expansion of quantities (here, the fluxes) of thermodynamic significance. The theory of Kadanoff and Swift[24] incorporates a perturbation solution of the master equation, using the so-called dynamic scaling laws. Though the derivation is quite involved, their result for the critical region behavior of the quantity θ, hence of α, is that it diverges as $|T-T_c|^{-2+A}$—where $\underline{A}$ is the critical exponent of the heat capacity C_p—and is independent of frequency. Kawasaki's[23b] extended theory is also a dynamic scaling theory that extends to the non-hydrodynamic region of sound frequency where the condition (31) is reversed. He also incorporates a quadratic expansion for the fluxes, which is classical thermodynamics. His results are the frequency and temperature exponents for absorption divergence, similar to Kadanoff and Swift.

As Kawasaki's original theory is essentially a corroboration of Fixman's, and as the form

$$\frac{\alpha}{f^2} \sim |T-T_c|^{-p} \text{ (times } f^{-q}\text{, possibly)} \qquad (43)$$

predicted by Kadanoff and Swift or by Kawasaki in his extended theory is not observed and in addition the dynamic

scaling laws are unproven,[25] we may take Fixman theory as the one of primary utility in analyzing experimental results. Its defects are only partly remediable. One that can be fixed is the expression of the dynamic response of $(\delta n_2)^2 = n_2^2 \int d\vec{k}\ G_{\vec{k}}$ to the perturbation δT. Here $\delta G_{\vec{k}}$ can be computed *after* solution of the proper singlet diffusion equation. Assuming the Fourier decomposition (23a) for the *undriven* fluctuation plus a decomposition for the driven portion $\delta n_2^{\,d}$,

$$\delta n_2^{\,d} = \int n_{\vec{k}}^{d}\, e^{i\vec{k}\cdot\vec{R}}\, d\vec{k}\ , \tag{44}$$

the perturbation solution is

$$[i\omega + \frac{h}{2} k^2\ (k^2 + \kappa^2)]\ n_k^d = \frac{h}{2} k^2\ \frac{\partial \kappa^2}{\partial T}\ \delta T\ n_{\vec{k}}^{o}\ .$$

Then

$$n_2^2\ \delta G_{\vec{k}} = \langle n_k^o\ \ n_{\vec{k}}^{d} \rangle + \langle n_{\vec{k}}^{d}\ n_{\vec{k}}^{o} \rangle = 2\ \langle n_{\vec{k}}^{o}\ n_{\vec{k}}^{d}\ \rangle \tag{45}$$

and

$$\int dk\ G_{\vec{k}} = \delta T\ h \left(\frac{\partial \kappa^2}{\partial T}\right)\ \int d\vec{k}\ \frac{k^2 G_{\vec{k}}^{o}}{[i\omega + \frac{h}{2} k^2\ (k^2 + \kappa^2)]}, \tag{46}$$

and $\delta \underline{S}$ has the form of Eq. (33) but for the replacement of $\underline{h}$ in the denominator of the integral over $\underline{k}$ by $\underline{h/2}$. According to this correction, values of the parameters $\underline{\ell}$ and ζ derived from the original theory should be multiplied by $2^{-7/3} = 0.20$ and $2^{1/3} = 1.26$, respectively. As the parameters $\underline{\ell}$, $\underline{a}$, ζ backed out of the data by Fixman theory are generally order-of-magnitude, this is not a dramatic change, and certainly not a change of philosophy.

Another point of rigor that can be resolved is Fixman's choice of the term in Eq. (30) as the dominant perturbation. We know that the new driving term must be linear in the ultrasonic progress variables $\delta \underline{p}$, $\delta \underline{T}$, and also that the separate linear terms in $\nabla^2 \underline{T}$ and $\nabla^2 \underline{p}$ cause no anomaly. Therefore, we require a perturbation to the coefficients of $\underline{c_2}$ in the diffusion equation. Here the main sensitivity to $\delta \underline{T}$ or $\delta \underline{P}$ is in κ^2. In a recent thesis, Puls[26] notes that a term in $\delta \underline{p}$ analogous to term (30) is neglected by Fixman yet may be significant. Now the $\delta \underline{T}$ term originated in the derivative

$$\left(\frac{\partial \kappa^2}{\partial T}\right) \delta T \sim \frac{\partial^2 \mu_1}{\partial T \partial c_2} \delta T = \frac{\partial^3 G_{mix}}{\partial N_1 \partial T \partial c_2} \delta T, \qquad (47)$$

where $\underline{G_{mix}}$ is the Gibbs energy of mixing of an arbitrary mass and the derivative with respect to N_2 is at constant

N_1. The analogous pressure term is

$$\frac{\partial^2}{\partial N_1 \partial c_2}\left(\frac{\partial G_{mix}}{\partial p}\right)\delta p = \frac{\partial^2}{\partial N_1 \partial c_2}\,\Delta V_{mix}\;\delta p, \qquad (48)$$

where $\underline{V_{mix}}$ is the volume change on mixing. The ratio of (48) to (47) is

$$\frac{\left(\frac{\partial^2 \Delta V_{mix}}{\partial N_1 \partial c_2}\right)}{\left(\frac{\partial^2 \mu_1}{\partial T \partial c_2}\right)}\;\frac{\delta p}{\delta T} = \frac{\left(\frac{\partial^2 \Delta V_{mix}}{\partial N_1 \partial c_2}\right)}{\left(\frac{\partial^2 \mu_1}{\partial T \partial c_2}\right)}\;\frac{C_p}{TV\theta}\;. \qquad (49)$$

Using the Flory-Huggins model for $(\partial^2 \mu_1/\partial c_2 \partial T)$ and experimental density data for $(\partial^2 \underline{\Delta V_{mix}}/\partial N_1 \partial c_2)$, we have evaluated this ratio for the system 2,6-lutidine/water reported in the following paper[27] and have found it to be roughly -7.9%. In general the $\delta \underline{p}$ term should be negligible.

In light of the previous discussion, the defects of the theory as valid classical thermodynamics and hydrodynamics are resolved. The inherent deficiency of classical thermodynamics is difficult to remedy and we can see no path for improvement at present, with or without incorporating features of the other mode-coupling theories commented upon. One final point actually extrinsic to the theory is whether or not ordinary thermal relaxation involving

driving of the same concentration variable $\underline{c_2}$ is truly additive to the Fixman mechanism. Intuitively, it appears so, as the two mechanisms involve vastly different spatial scales or $\underline{n_{\vec{k}}}$ components: the former involves structure on the order of one or two molecular diameters, the latter, structure on the order of hundreds of Angstroms. On a more rigorous basis, the two mechanisms are seen to drive distinct linear terms in the $\delta\underline{S}$ and $\delta\underline{V}$ expressions, Fixman's driving an added heat capacity in the first term in Eq. (5) and (6). As Eqs. (5) and (6) are combined to calculate the effective complex compressibility, the terms of the two types occur linearly and thus additively. This additivity of thermal relaxation is commonly employed in analyzing experimental data, and it is found particularly important for the lutidine/water system we have studied.

References

1. A. B. Bhatia, Ultrasonic Absorption (Clarendon Press: Oxford, 1967); K. F. Herzfeld and T. A. Litovitz, Absorption and Dispersion of Ultrasonic Waves (Academic Press: New York, 1959); W. P. Mason, ed., Physical Acoustics (Academic Press: New York, continuing series); S. Flügge, ed., Handbuch der Physik, Vol. XI/1 (Springer-Verlag: Berlin, 1961).

2. Early indications are in references 1-8 of M. Fixman, J. Chem. Phys. 33, 1363 (1960).

3. R. Lucas, J. Phys. Rad. 8, 41 (1937).

4. A. E. Brown and E. G. Richardson, Phil. Mag. 4, 705 (1959); A. E. Brown, Acustica 18, 169 (1967).

5. M. Fixman, J. Chem. Phys. 36, 1961 (1962).

6. We follow the notation and development of Bhatia (ref. 1), pp. 174 ff.

7. R. M. Mazo, J. Chem. Phys. 28, 1223 (1958).

8. L. D. Landau and E. M. Lifshitz, Fluid Mechanics (Addison-Wesley Publ. Co.: Reading, Mass., 1959), Chapter VI.

9. M. Fixman, J. Chem. Phys. 36, 1957 (1962).

10. L. S. Ornstein and F. Zernike, physik. Z. 19, 134 (1918); a more recent discussion is given by M. E. Fisher, J. Math. Phys. 5, 944 (1964).

11. M. Fixman, J. Chem. Phys. 36, 310 (1962); actual derivation by P. Debye, ibid. 31, 680 (1959), and by M. Fixman, ibid. 33, 1357, (1960).

12. M. Fixman, J. Chem. Phys. 36, 310 (1962), Section A.

13. Ibid., Eqs. (22), (23), and Section VIII.

14. ref. 5, Eq. (6).

15. R. D. Mountain, J. Chem. Phys. 38, 205 (1966); with J. M. Deutch, ibid, 50, 1103 (1969).

16. J. H. Hildebrand and R. L. Scott, Solubility of Non-electrolytes (Reinhold Publ. Corp.: New York, 1950).

17. A. G. Chynoweth and W. G. Schneider, J. Chem. Phys. 19, 1566 (1951); 20, 760 (1952).

18. A. V. Anantaraman, A. B. Walters, P. D. Edmonds, and C. J. Pings, J. Chem. Phys. 44, 2651 (1966).

19. G. D'Arrigo and D. Sette, J. Chem. Phys. 48, 691 (1968).

20. M. I. Shakhparonov, Yu. G. Shoroshev, S. S. Aliev, P. K. Khabibullaev, and L. V. Lanshina, Sov. Phys. - JETP Letters 7, 315 (1968).

21. R. P. Singh and G. S. Verma, Proc. Phys. Soc. 1, 1476 (1968).

22. M. P. Puls, thesis, McMaster Univ., May, 1970.

23. K. Kawasaki: a) Proc. Phys. Soc. 90, 791 (1967); Phys. Rev. 150, 291 (1966); b) ibid., A1, 1750 (1970).

24. L. P. Kadanoff and J. Swift, Phys. Rev. 165, 310 (1968); 166, 89 (1968); J. Swift, ibid. 173, 257 (1968).

25. L. P. Kadanoff, J. Phys. Soc. Japan Suppl. 26, 122 (1969).

26. Puls, op. cit., p. 136.

27. V. Gutschick and C. J. Pings, J. Chem. Phys. xx, xxxx (1971); following paper.

Ultrasonic Investigation of the Lower Consolute Point of the 2,6-Lutidine: Water System*

Vincent P. Gutschick† and C. J. Pings

Division of Chemistry and Chemical Engineering
California Institute of Technology,
Pasadena, California 91109

Sound absorption coefficients and velocities have been measured over ranges in frequency, temperature, and composition for 2,6-lutidine/water near its critical mixing point. Large excess absorption coupled to critical fluctuation dynamics is found, as in other binary mixtures. A strong background of ordinary thermal relaxation is also apparent. Interpretation of the details of the absorption and velocity, as well as of auxiliary data on the shear viscosity and density, in terms of the Fixman mechanism of critical region absorption combined with a chemical association model cannot be attempted quantitatively. The reason lies in defects in Fixman theory for the composition dependence of the critical absorption, and

* Research sponsored by AFOSR (SRC)-OAR, USAF Grant No. AFOSR-68-1382.

† National Science Foundation Predoctoral Fellow, 1966-1970.

in the inherent inability of the chemical association model to account for phase separation behavior. Nevertheless, Fixman's form for the absorption as a function of frequency and temperature at the critical composition is satisfactory, and some important qualitative aspects of binary fluid structure come to light, including inherent differences of upper and lower consolute points.

Introduction

Binary liquid mixtures commonly exhibit nonadditive thermodynamic and kinetic behavior, many of the details of which are manifested in the ultrasonic absorption coefficient α and velocity β. In some cases, chemical association of small numbers of the two basic species in a linked set of chemical reactions causes enthalpy, volume, and excess entropy changes on mixing. Values of these three parameters for each reaction, as well as relaxation times related to the forward or backward rate constants, can sometimes be extracted for the principal reactions by analyzing the ultrasonic data as a function of mixture composition and temperature and of sound frequency.[1] The periodic temperature and pressure perturbation alters the microscopic dynamics in a well-defined manner and causes a sound energy loss or absorption. Additionally, the chemical and physical associations may generate a free energy of mixing of such form as to cause a region of imperfect miscibility and a corresponding critical mixing (consolute) point of incipient phase separation. Large thermodynamic composition fluctuations or changes in large-scale association occur here, and these are also susceptible to the sonic

perturbation. Added absorption and velocity dispersion arise, describable readily by a theory of Fixman[2] in terms of the Ornstein-Zernike correlation length κ or the Debye persistence length ℓ, plus a friction constant ζ.

Numerous investigations have been made on both the chemical relaxation loss mechanism, which we denote as thermal relaxation (TR) and the latter mechanism, which we call critical relaxation (CR). In most studies the system, composition, and temperature have been chosen to make one or the other mechanism dominant, especially in the absorption behavior. Our present work on the 2,6-lutidine/water system focuses on the critical losses, although a comparably large background of TR accompanies the CR. Our system was chosen because it has a lower consolute point, or phase separation above a critical temperature, rather than the typical upper consolute point. The critical point is conveniently close to room temperature. For the description of the CR portion of the absorption, we use Fixman's theory as presented in the preceding paper[3] (I), as it was shown there that CR and TR may be considered additive and that Fixman's CR theory has been reasonably successful in the past. A chemical association model for TR and equilibrium properties is also attempted. The original goal of our study was the

quantitative understanding of the ultrasonic and equilibrium properties using these two models. While this has failed, we can pinpoint the precise difficulties in such an approach and also draw some significant qualitative conclusions on binary mixture structure, differences of upper and lower consolute points, and the adequacy of Fixman theory.

Experimental

The absorption α and the velocity β were measured at fourteen compositions over the whole range, at four frequencies, nominally 4.5, 7.5, 10.5, and 13.5 MHz, and at least two temperatures of $\underline{T_c}$ - 0.92 $\underline{C}$ and $\underline{T_c}$ - 0.12 $\underline{C}$, plus a third temperature for most compositions as close to the phase separation temperature as practical but not exceeding $\underline{T_c}$ + 1.08 $\underline{C}$. Supplementary data on the shear viscosity and density were also taken. The phase diagram of Cox and Herington[4] was used to help locate the critical composition and temperature.

The basic ultrasonic apparatus is a pulsed variable-path single pass cell, a modification of the typical design of Andreae, et al.[5a] Equipment used in previous investigations in our laboratory[5b] has been adapted, but with better temperature control and electronic stability.

The temperature is controlled with a circulating water jacket supplied from an external bath, and also a heated Lucite enclosure for the total apparatus. The sample is mixed, and its composition identified by density measured in a thermostatted pycnometer. It is introduced into the sample cell, which is immediately reassembled. An upper silica and a lower Duralumin delay rod carry the ultrasonic pulse to the liquid gap. After equilibration, measurements of the absorption coefficient α and the velocity β are made at all frequencies, the temperature is changed and the measurements repeated. In all ultrasonic measurement, pulses of 8 μsec. duration and one kHz repetition rate from a Chesapeake U-100 signal generator drive an X-cut transducer at low power. For path length variations, a Gaertner micrometer carries the upper delay rod through a Teflon seal. Horizontal and vertical alignment between the two rods is insured by several independent techniques. Both rods were initially finished to 0.1 mil or better, though the lower rod's surface deteriorated without noticeable bad effects. Absolute liquid path lengths are occasionally checked, for use in establishing diffraction corrections. Signal frequency is measured by visual beating against the calibrated reference signal generator. The received signal is preamplified in an

Arenberg PA-620L and displayed on a Tektronix 547 CRO, along with the reference signal from the Hewlett-Packard HP-606A. The reference signal is attenuated in calibrated steps of one db nominally by a Hewlett-Packard HP-355C attenuator and the liquid path changed to keep the two signal displays superposed. A least-squares fit of path length versus attenuation directly yields the absorption coefficient. Signal quality is good except that some mode conversion in the delay rods causes spurious signal envelope fluctuations, for which an empirical correction to the raw absorption coefficients is applied at the two lowest frequencies. Velocity measurements are made by varying the path length and restoring signal superposition with the calibrated variable delay of the CRO.

Raw path-length/decibel data were corrected for diffraction by calculations on the method of Bass.[6] They were then reduced to an attenuation coefficient by a least-squares fit, weighted by estimated visual matching and amplitude stability errors, and augmented by a students' t-test. A similar reduction averaged the repeated runs made, generally three to five. Finally, error estimates were rescaled to give a unity chi-squared. Accuracies of α values are typically 0.5% near peak α, on up to 5% for the lowest absorptions at $\underline{f}$ = 4.5 MHz.

Velocity accuracy is of the order of 0.3%. A total calibration run on reagent benzene titrating as 0.02% water produced the result $\alpha/f^2 = 962 \times 10^{-17}$ Np. $cm.^{-1}$ $sec.^2$ (Np. = neper = 8.686 db.), near the literature value[7] of 960 ± 15 in these units.

99% lutidine was used after refluxing over BaO and distilling; water content was typically 0.1 mole percent by titration. Laboratory distilled water was used. Initial density ↔ mole fraction identifications were established by making solutions by weight on an analytical balance. Temperatures of pycnometers in the thermostat and of samples in the cell were ordinarily read to ± 0.01 C. with glass thermometers calibrated against a Leeds and Northrup platinum resistance thermometer certified by the NBS. The latter was also used to establish the critical temperature and composition by visual observations of phase separation as T_c = 33.57 C. and mole fraction X_c = 0.065 ± 0.001 lutidine, respectively, versus T_c = 34.06 C. and X_c = 0.0665 of reference 4. Sample composition in the ultrasonic cell was stabilized by an evaporation buffer in the line to the atmosphere, and cell corrosion was prevented by silver plating. Mixtures were ring-stirred in the cell (not during actual measurements). All temperatures were controlled to within the 0.03 C.

stability of the external bath. Independent thermocouple measurements indicated a drop of 0.01 C. between the external bath and the sample.

Auxiliary determinations of shear viscosity were made on separate samples with a Cannon-Fenske viscometer calibrated with distilled water and with reagent acetone. Corrections were made to the raw kinematic viscosities according to NBS monograph No. 55 to yield final accuracies of 1%.

Results

The corrected absorption coefficients are presented[8] in Figs. 1-3. They are presented in the form α/f^2, f being the sound frequency. Furthermore, the so-called classical[9] contribution α_{cl}/f^2 from ordinary viscous losses,

$$\frac{\alpha_{cl}}{f^2} = \frac{8\pi^2\eta_s}{3\,\rho\beta^3} \qquad (1)$$

with η_s the shear viscosity, have been subtracted to leave the excess quantity α_{ex}/f^2 which is to be interpreted in terms of relaxation (or, formally, in terms of a bulk viscosity $\eta_v = \rho\beta^3\alpha_{ex}/2\pi^2f^2$). Thermal conduction also causes a classical loss but is negligible in binary

liquids. Typically α_{cl}/f^2 is of the order of 5% of α_{ex}/f^2, showing relaxation as the dominant loss mechanism. Fig. 1 presents α_{ex}/f^2 as a function of composition X = mole fraction lutidine for the temperature $T = T_c - 0.92$ C., with one curve for each of the four frequencies used. Figs. 2, 3 present similar results for temperatures T_c - 0.12 C., T_c + 1.08 C. Much structure in X- and f-dependence is evident; the T-dependence of α_{ex}/f^2 is also strong but less obvious.

The magnitude and frequency-dependence of α_{ex}/f^2 allows us to dismiss two loss mechanisms and to retain the CR-plus-TR explanation we have mentioned earlier. The first loss mechanism is scattering of sound[10] by the inhomogeneous acoustical impedance $\rho\beta$, ρ = density, in the presence of fluctuation. The frequency-dependence associated with such a mechanism is

$$\frac{\alpha_{ex}}{f^2} \sim f^p \quad , \quad 0 < p < 2 \, , \tag{2}$$

certainly not seen here although strong critical opalescence was seen in several of the states investigated. The small variation of $\rho\beta$ with macroscopic composition adds support to the conclusion. The second mechanism is the persistence of the excess absorption of the pure

liquids, possibly as

$$\frac{\alpha_{ex}}{f^2} = X \left(\frac{\alpha_{ex}}{f^2} \right)_{\text{lutidine}} + (1-X) \left(\frac{\alpha_{ex}}{f^2} \right)_{\text{water}} \qquad (3)$$

$$\simeq [70\ X + 18(1-X)] \times 10^{-17}\ \text{Np. cm. sec.}^{-2}$$

Our measured absorptions are considerably larger than this, and in addition, the contributions are less than additive due to cross-relaxation.[11]

Presumably all our data can be well represented as the sum of the CR and TR contributions,

$$\frac{\alpha_{ex}}{f^2} = Af^{-5/4}\, I(d) + B \quad , \qquad (4)$$

where

$$d = Cf^{-1/2}\, \kappa^2 \quad (=C' f^{-1/2}\, |T-T_c| \text{ at } X=X_c) \qquad (5)$$

(see Ref. 18). The second term is actually composite,[12]

$$B \simeq \sum_i \frac{Bi}{1 + (f/f_{ci})^2}$$

but all of the chemical relaxation times f_{ci} are almost surely higher than any frequencies we have used. B is primarily a strong function of composition X; it is also

expected to have a modest and probably negative linear temperature dependence. It should peak at the composition of strongest chemical association. The first or CR term is translated from Fixman[2] form, with $\underline{A}$, $\underline{C}$ known functions of $\underline{X}$ with weak dependence on $\underline{T}$, and with $\underline{\mathcal{I}(d)}$ a dimensionless monotonically decreasing function of $\underline{d}$ related to an excess dynamic heat capacity presented to the sound wave. The parameters $\underline{A}$ and $\underline{C}$ can be simply reduced to the parameters ζ and ℓ^2 or κ^2 of Fixman theory.

The TR absorption is quite extensive in composition, while its peak is strongly skewed, peaking near $\underline{X} = 0.1$. It shows little $\underline{f}$-dependence. The CR absorption peaks strongly at $\underline{X} = \underline{X_c}$ with strong $\underline{f}$- and $\underline{T}$-dependence. It is also quite extensive in $\underline{X}$, as $\alpha/\underline{f}^2$ has significant $\underline{f}$-dependence far from $\underline{X_c}$, and its strong $\underline{T}$-dependence extends to the TR peak, the base of which lifts with temperature as a result. Quantitative analysis of the results will be attempted below. Additional insight into the internal structure and dynamics is also provided by examining the sound velocity β at $f = 4.5$ MHz (its dispersion or $\underline{f}$-dependence is low) and the sign of its temperature derivative, in Fig. 4; also the volume change on mixing, $\underline{V_{mix}}$, in the same figure; the shear viscosity η_s as a function of composition at a typical temperature

$\underline{T_c}$ - 0.4 $\underline{C}$. in Fig. 5; and the logarithmic temperature derivative $d\ell n\ \eta_s/dT$ also in Figure 4. Of these four quantities, only $d\ell n\ \eta_s/dT$ and to a lesser extent β show marked evidence of critical phenomena. All four show major 'structure' at intermediate compositions $\underline{X} \simeq 0.2\text{-}0.5$ from the chemical association behavior.

Discussion

A quantitative formulation of the chemical model for the TR portion of the absorption and for equilibrium properties begins with the choice of a chain association model for water,[13]

$$A + A_{n-1} \rightleftharpoons A_n \quad , \quad K_n = \frac{\delta_n}{\delta_{n-1}\delta_A} \quad , \tag{7}$$

where δ_n is the true mole fraction of the species $A_n = (H_2O)_n$,

$$\delta_n = \frac{N_n}{\sum_i N_i} \tag{8}$$

The progression of K_n must follow a simple series to be tractable; K_n = constant = K, or $K_n = K_o r^n$, r = constant are possibilities. The H-bonding of lutidine to water may

be described as

$$B + A_n \rightleftharpoons BA_n \ , \ K'_n = \frac{\delta_{Bn}}{\delta_n \delta_B} \ . \qquad (9)$$

Refinements with direct association of two chains and with formation of associations A_nB_m are generally intractable. By postulating the average complexation of lutidine to be with many water molecules, we assure that the relaxation or absorption peaks at a high water/lutidine ratio, as observed. One can solve Eqs. (7) and (9) for the equilibrium concentrations N_α. After assigning volume and enthalpy changes per step, the net $\Delta\underline{V}$ and $\Delta\underline{H}$ of mixing can be computed from these concentrations. These two properties and their temperature dependence are useful criteria for the model. The contribution $\underline{G_{chem}}$ of the reactions to the free energy of mixing $\underline{G_{mix}}$ can be calculated simply as[14]

$$G_{chem} = -RT \ [X_A \ \ell n \ \delta_A + X_B \ \ell n \ \delta_B] \ , \qquad (10)$$

where $\underline{X_A}$, $\underline{X_B}$ are the macroscopic or apparent mole fractions. The condition $\partial^2 \underline{G_{mix}}/\partial x_A^2 > 0$ for miscibility maps out the region of phase separation. An extra term $\underline{G_{phys}}$ from 'physical' interactions is necessary[15] to get

$\partial^2 G_{mix}/\partial x_A^2 < 0$, but G_{chem} helps the separation occur and partly determines its location in mole fraction; also, its temperature dependence is crucial to the nature of the consolute point as being upper or lower. Finally, one may assign the forward rate constants k_n, k'_n for reactions (7) and (9) and solve an eigenvalue equation[12] for the relaxation frequencies f_{ci} and relaxation strengths B_i of the 'normal moles' of reaction. This last step is quite difficult in general, especially as a numerical solution must be obtained. The infinite chain of reactions and its analytic form of solution must be retracted.

The CR mechanism contributes to some degree to the static specific heat and compressibility (hence sound velocity) and much to the sound absorption. It has been formulated by Fixman,[2] whose theory is re-examined[3] in paper I. In practice, the forms Eqs. (4) and (5) are used in analyzing absorption data. To represent the data in its composition dependence, the explicit X-dependence of the 'constants' A and C must be known. A and C are known functions of macroscopic quantities as specific heat and density - whose X-dependence is known experimentally to sufficient accuracy - and of the two microscopic parameters ζ and κ^2. ζ is presumably composition-independent, while κ^2 is given by Eq. (26) of paper I,

$$\frac{4\pi a}{\kappa^2} = -\frac{\bar{V}_1}{n_2}\left[\frac{kT}{(\partial\mu_1/\partial n_2)} + \frac{1}{\bar{V}_1}\right] . \qquad (11)$$

The $\underline{X}$-dependence on the right is principally in $(\partial\mu_1/\partial\underline{n_2})$, for which a Flory-Huggins[16] model may be taken using $(\partial\mu_1/\partial\underline{n_2}) = (\partial\mu_1/\partial\phi_2)\ (\partial\phi_2/\partial\underline{n_2})$. D'Arrigo and Sette[17] in particular have developed this technique, though they made the oversight of taking a factor in the absorption α_{CR} as $(\partial\kappa^2/\partial\underline{T})^2$ valid at $\underline{X} = \underline{X_c}$, rather than as $(\partial^2\mu_1/\partial\underline{n_2}\ \partial\underline{T})$ $(\partial\kappa^2/\partial\underline{T})$. In any event, the total $\underline{X}$-, $\underline{T}$-, and $\underline{f}$-dependence of $\alpha/\underline{f}^2$ can presumably be modeled now by Eq. (4) with judicious choice of parameters.

Least squares adjustment of the CR and the TR or chemical parameters to match observed absorptions and equilibrium (including phase diagram) properties is a reasonable expectation. Of course, it is a nonlinear fit requiring iteration, but Andreae, et al.[13] have had modest success in treating a pure TR mechanism in aqueous solutions of nonelectrolytes. In our preliminary work, the qualitative magnitude and $\underline{X}$-dependence of α_{TR} were visually estimated from our $\alpha_{ex}/\underline{f}^2$ data and several chemical models were tested for plausibility. We became dissatisfied on realizing that phase separation behavior

always requires an extra term G_{phys} in G_{mix},[15] making the connection of the α_{TR} and the critical region chemical potential or its relative G_{mix} a very tenuous one. Much of the value of tying the two mechanisms together to analyze all properties is lost. However, we did obtain useful qualitative insight by proceeding to add G_{phys} terms of the form $Ax_B^n x_A$ to force $\partial^2 G_{mix}/\partial x_A^2$ to vanish. Temperature dependence in G_{chem} alone then explains the existence of a lower consolute point at intermediate mole fraction for small exponents n in G_{phys}, or of an upper point at low concentrations forced by a large exponent n. This failure points to deficiencies in the form of G_{chem}, in our understanding of the structure of water and its solutions. To be sure, large H-bonded structures of water and large complexes of water and lutidine exist and such strong H-bonding association seems a general requirement for a lower consolute point. However, the arbitrary distinction of chemical and physical interactions is faulty. Even if elaborate interlocking chemical equilibria are used to describe the former, the ideality of the solution of true chemical species is implicit in the equilibrium constant formulas as in Eqs. (7) and (9). Physical interactions make a continuous transition to chemical bonding and a continuous perturbation from

ideality that is difficult to describe in mass action terms. The chemical simplification of the many-body problem fails badly here. This difficulty has not been cited by investigators[18] of other critical systems, since most of these are upper consolutes in which the phase diagram is grounded principally in G_{phys} and little TR contribution to α occurs. G_{phys} describes an entropy of mixing effect and has an adequate empirical form in the Flory-Huggins[16] theory.

A final and practical barrier to using superposed CR and TR mechanisms to explain the absorption also came to our attention in the generally poor results from use of the composition-dependent Fixman theory. To date, investigators[17,19] have found the theory to predict absorption peaks which are too narrow, at times grossly so, as functions of X. The necessity of 'classical' thermodynamics of the critical phase diagram and of κ^2 causes the problem. The least-squares fit of Eq. (4), weighting α_{ex}/f^2 at all compositions equally, would be invalidated. We settle for the lesser information in a least-squares fit to Fixman's parameters from the eight pieces of absorption data at $X = X_c$, consisting of measurements at four frequencies and at two temperatures, T_c - 0.92 C. and T_c - 0.12 C. We obtain the values

$$A = 2.2\times10^{-6}\ \text{cm.}^{-1}\ \text{sec.}^{3/4}$$
$$B = 201\times10^{-17}\ \text{Np. cm.}^{-1}\ \text{sec.}^{2} \qquad (12)$$
$$C = 2.0\times10^{2}\ \text{sec.}^{-1/2}\ \text{deg.}^{-1}$$

for the best fit as in Table I. Note that Fixman theory is moderately good but gives too sharp an $\underline{f}$-dependence and about the right $\underline{T}$-dependence. Separate fits for the two temperatures use three parameters for four points, but serve to show that the theory is strained, as the $\underline{B}$ values become large and unphysically negative. The $\underline{B}$ value for the eight-point fit, on the other hand, is very reasonable in light of the size of the TR peak at $\underline{X} \approx 0.1$. Final reduction of the $\underline{A}$, $\underline{C}$ values to estimates of the Debye persistence length ℓ and the friction constant ζ was made with the correction noted after Eq. (46) in paper (I), and it yields

$$\ell = 9.0\ \text{Å}$$
$$\zeta = 0.32 \times 10^{13}\text{sec.}^{-1}\ , \qquad (13)$$

in the same range as for other systems similarly corrected. The value of the correlation length κ^{-1} at $\underline{T_c}$ - 0.5 $\underline{C}$. is, from Eq. (39) of paper I,

$$\kappa^{-1} \approx 91\ \text{Å} \qquad (14)$$

compared to an estimated 100-200 Å from light scattering data in our laboratory.[20] Our final quantitative work with Fixman theory is calculating the ratio of the excess absorptions from the temperature and pressure perturbations of the sound wave. Only the former is included in the theory as originally developed. The second pressure term was suggested by Puls[19] and is formulated in our paper I. The result, a pressure contribution only 0.4% of the temperature term, supports Fixman's choice of the dominant perturbation.

We can extract more information of a qualitative nature from $\alpha_{ex}/\underline{f}^2$. Earlier we noted that the $\underline{f}$-dependence is expected to lie principally in the CR mechanism. The appearance of significant $\underline{f}$-dependence to $\underline{X} \approx \frac{1}{2} \underline{X_c}$ and to $X \approx 2\underline{X_c}$ indicates a fair extent for CR. The $\underline{T}$-dependence of $\alpha_{ex}/\underline{f}^2$ has more detail. Near $\underline{X} = 1.0$, it is positive as expected for internal vibrational relaxation of pure lutidine.[21a] At the intermediate composition $\underline{X} = 0.3042$, it dips slightly negative, as expected[21b] for thermal relaxation of lutidine/water associations. It is large and positive for the remainder of the composition range. The magnitude is the same at both peaks in $\alpha_{ex}/\underline{f}^2$, indicating either a larger extent for CR than hinted by the $\underline{f}$-dependence, or a change to positive $\underline{T}$-dependence for

TR in this range. Now the 'definition' of the CR peak at $\underline{X} = \underline{X_c}$ is good only at $\underline{f}$ = 4.5 MHz for $\underline{T} = \underline{T_c} - 0.92\ \underline{C}$. This suggests the CR mechanism is at least as restricted as the $\underline{f}$-dependence indicates. Thus the TR temperature coefficient seems to undergo a sign reversal not very far down its shoulder in a composition profile, which points once again to complexity in the chemical behavior.

The sound velocity β showed no clear dispersion with frequency in our most reliable measurements. The 4.5 MHz values show nontrivial composition dependence. At low lutidine concentrations β rises rapidly with $\underline{X}$, due to breaking down of water structure (chain-length) that causes a decrease in compressibility.[13] Around $\underline{X}$ = 0.15 and just beyond the composition of peak TR absorption, β turns downward. The trend is not smooth, for the region near $\underline{X} = \underline{X_c}$ forms a step of increased velocity. Everywhere the temperature derivative is slightly negative or vanishing. This corresponds in the critical region to the expected increase in compressibility on nearing the critical state. In regions dominated by the chemical phenomena, the positive temperature coefficient of compressibility shows that the simple reduction of water structure breaking (by the decrease of chemical association) more than counteracts the decrease in the chemical

contribution to the compressibility (from the same cause).

The excess volume $\Delta\underline{V}$ shows a broad minimum near $\underline{X} = 0.5$. This is probably due to peaking here of the chemical association as measured by greatest reduction in water chain length. Similarly, the shear viscosity peaks near $\underline{X} = 0.3$, and by Eyring's[22] theory of viscosity this is roughly the peak of the heat of vaporization. Another measure of complexation, involving the enthalpy changes $\Delta\underline{H_i}$ of the chemical steps, must be largest here. The temperature coefficient of the shear viscosity, $d\ell n\ \eta_s/dT$, has been estimated from a fit of the η_s data to the form

$$\eta = Ae^{-E/T} \left(+ \frac{B}{|T-T_c|^{1/2}} \text{ in critical region}\right). \qquad (15)$$

It is uniformly negative except for a sharp positive-going peak at $\underline{X} = \underline{X_c}$. Critical phenomena contributions appear as well-localized and as strong here as in absorption.

Table I. Comparison of experimental absorption data with best fit from Fixman theory at the critical composition $X = X_c$.

	f(MHz.)	$\alpha_{ex}/f^2 \times 10^{17}$, Np. cm.$^{-1}$sec.^{2}	
		Experimental	Best theoretical fit
$T=T_c-0.92$ C.	4.5	557	573
	7.5	465	406
	10.5	327	338
	13.5	262	303
$T=T_c-0.12$ C.	4.5	613	641
	7.5	498	435
	10.5	358	355
	13.5	285	314

Acknowledgments

We would like to thank William C. Hocker for helping with the experimental measurements. We are grateful to George Griffith and his staff for expert design and construction of sections of the apparatus, and to John Yehle for help with electronics problems. Hollis Reamer is due thanks for many suggestions on experimental technique.

References

1. K. F. Herzfeld and T. A. Litovitz, Absorption and Dispersion of Ultrasonic Waves (Academic Press: New York, 1959), Sections 27-29; A. B. Bhatia, Ultrasonic Absorption (Clarendon Press: Oxford, 1967), Sections 9.4, 9.5.

2. M. Fixman, J. Chem. Phys. 36, 1961 (1962).

3. V. Gutschick and C. J. Pings, J. Chem. Phys. xx, xxxx (1971).

4. J. D. Cox and E. F. G. Herington, Trans. Faraday Soc. 52, 926 (1956).

5. a) J. H. Andreae, R. Bass, E. L. Heasell, and J. Lamb, Acustica 8, 131 (1958);
   b) A. V. Anantaraman, A. B. Walters, P. D. Edmonds, and C. J. Pings, J. Chem. Phys. 44, 2651 (1966).

6. R. Bass, J. Acoust. Soc. Am. 30, 602 (1958). There is some experimental evidence and qualitative theoretical argument that Bass' corrections are not adequate when they reach 25-50% or more of the total apparent absorption. See E. F. Carome, J. M. Witting, and P. A. Fleury, J. Acoust. Soc. Am. 33, 1417 (1961). Our data were never corrected more than 20% even at the lowest frequencies and lowest-absorbing compositions. Typically, our corrections were of the order of 1%, and not more than 5% at the lowest frequency in the critical region. Our empirical correction for mode conversion at the two lowest frequencies is about as large as for diffraction, at the lowest frequency. No assessment of its adequacy is available.

7. D. Sette, Nuovo Cimento Suppl. 6, 1 (1949).

8. Full numerical tables of the absorption coefficients may be obtained from ADI Auxiliary Publication Project, Photoduplication Service, Library of Congress, Washington, D.C., by requesting Document No. XXXXX and remitting in advance $X.XX for photoprints or $X.XX for 35-mm microfilm. Make checks or money orders payable to Chief, Photoduplication Service, Library of Congress.

9. See, for example, Bhatia, op. cit., Secs. 4.3, 4.4; note that his α is $\alpha\lambda$ in our terms, the absorption per wavelength.

10. A. E. Brown and E. G. Richardson, Phil. Mag. 4, 705 (1959); A. E. Brown, Acustica 18, 169 (1967).

11. Herzfeld and Litovitz, op. cit., Secs. 99, 117.

12. The generalization of relaxation of chemical equilibrium as in Ref. 1 to cases of more than one reaction is treated by M. Eigen and L. de Maeyer, Techniques of Organic Chemistry, ed. Weissberger, et al. (J. Wiley and Sons, Inc.: New York, 1962), Vol. VIII, Part 2; see esp. Eq. (II. 3. 90b) in the section on sound absorption.

13. J. H. Andreae, P. D. Edmonds, and J. F. McKellar, Acustica 15, 74 (1965).

14. J. M. Prausnitz, Molecular Thermodynamics of Fluid-Phase Equilibria (Prentice-Hall, Inc.: Englewood Cliffs, N. J., 1969), Eq. (7.15-13); γ_i chosen as δ_i for ideal solution.

15. J. S. Rowlinson, Liquids and Liquid Mixtures (Butterworths Publ.: London, 1959) p. 181; I. Prigogine and R. Defay (transl. D. H. Everett), Chemical Thermo dynamics (Longmans, Green and Co., Ltd.; London, 1954), Ch. XXVI, Sec. 8.

16. J. H. Hildebrand and R. L. Scott, Solubility of Nonelectrolytes (Reinhold Publ. Corp.: New York, 1950).

17. G. D'Arrigo and D. Sette, J. Chem. Phys. 48, 691 (1968).

18. See the 'Discussion and Redevelopment' section of Ref. 3 for a recounting of earlier experiments as analyzed by Fixman theory plus a Flory-Huggins form for the phase behavior.

19. M. P. Puls, Thesis, McMaster Univ., May, 1970.

20. E. Gulari, unpublished work.

21. a) Herzfeld and Litovitz, op. cit., p.356; b) p.510.

22. J. O. Hirschfelder, C. F. Curtiss, and R. B. Bird, Molecular Theory of Gases and Liquids (J. Wiley and Sons, Inc.: New York, 1954), Ch. 9, Sec. 2a.

Figure Captions

Fig. 1 - Excess absorption of sound at $T = T_c - 0.92$ C. for four frequencies.

Fig. 2 - Excess absorption of sound at $T = T_c - 0.12$ C.

Fig. 3 - Excess absorption of sound at $T = T_c + 1.08$ C. ($T_c + 0.28$ C. for solid points).

Fig. 4 - Sound velocity and excess volume of mixing. Velocity is averaged over two or three temperatures near T_c and qualitative trend with temperature $d\beta/dT$ is indicated by +, -, or 0 under data point. Excess volume is measured at $T = 32$ C. $= T_c - 1.57$ C.

Fig. 5 - Shear viscosity η_s and its logarithmic temperature derivative, both at $T = T_c - 0.37$ C. See Eq. (15).

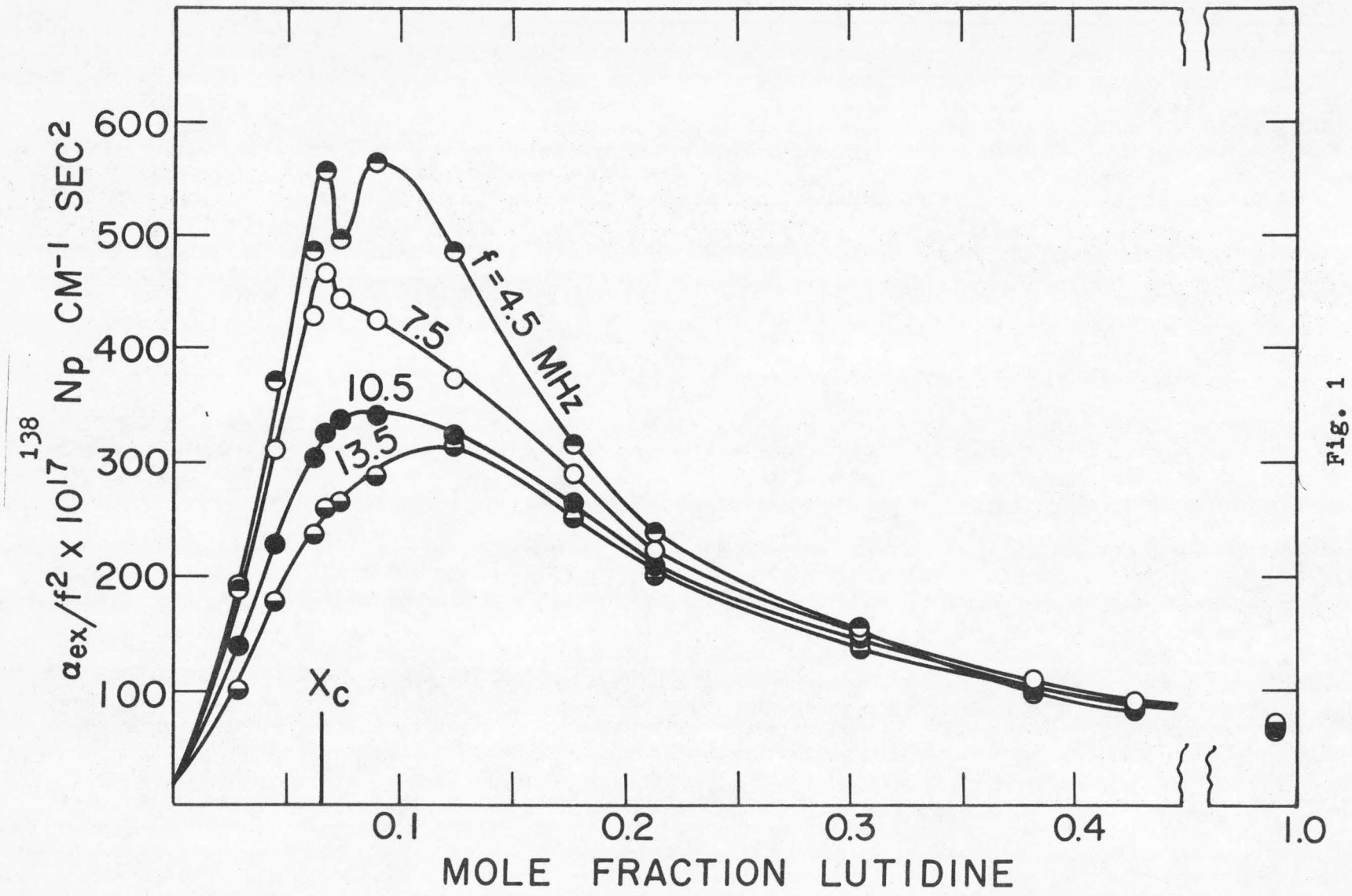
$\alpha_{ex}/f^2 \times 10^{17}$ Np CM^{-1} SEC^2
600
500
400
300
200
100
f=4.5 MHz
7.5
10.5
13.5
X_c
0.1
0.2
0.3
0.4
1.0
MOLE FRACTION LUTIDINE

Fig. 1

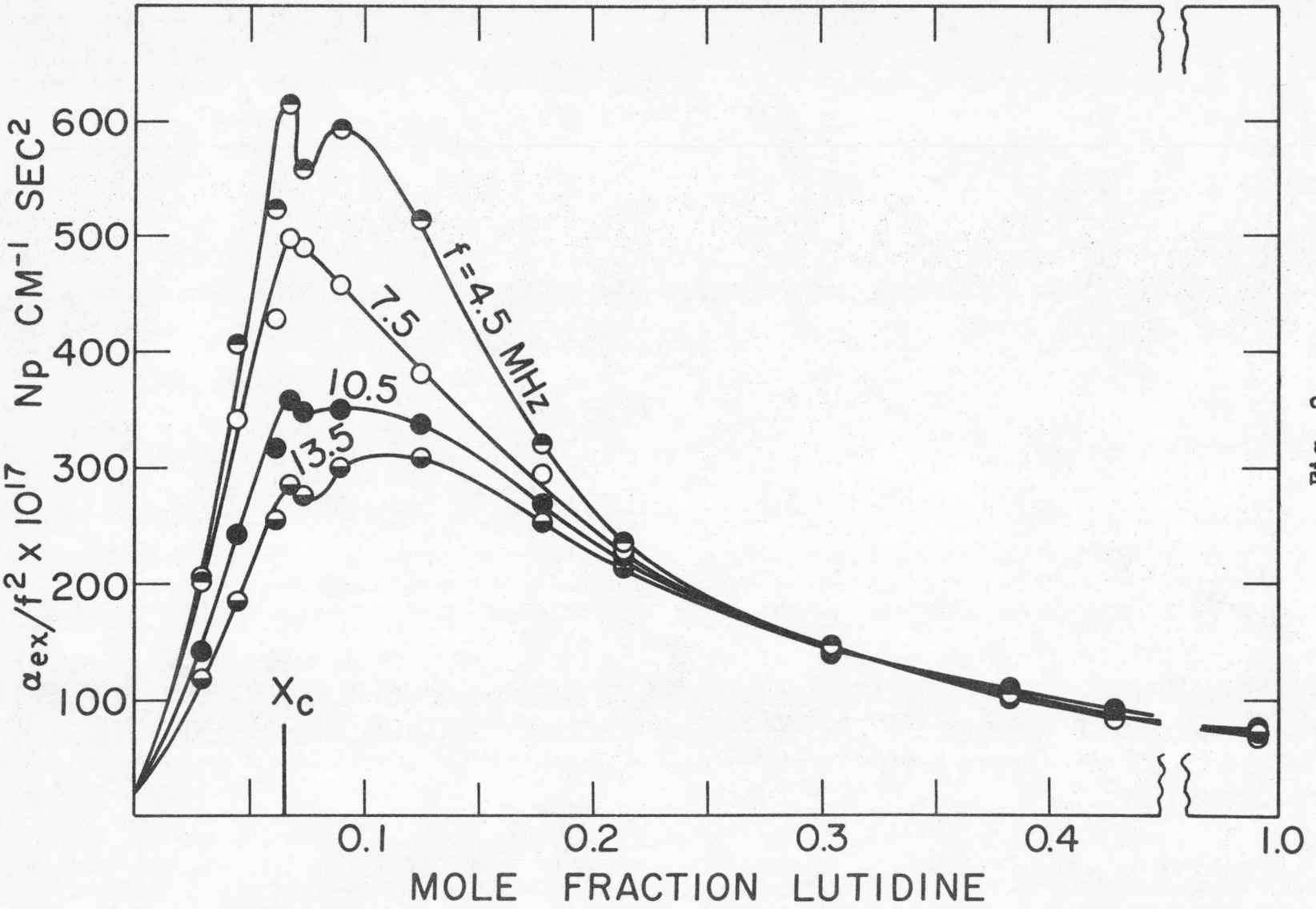
$\alpha_{ex}/f^2 \times 10^{17}$ Np CM^{-1} SEC^2
600
500
400
300
200
100
f=4.5 MHz
7.5
10.5
13.5
X_c
0.1
0.2
0.3
0.4
1.0
MOLE FRACTION LUTIDINE

Fig. 2

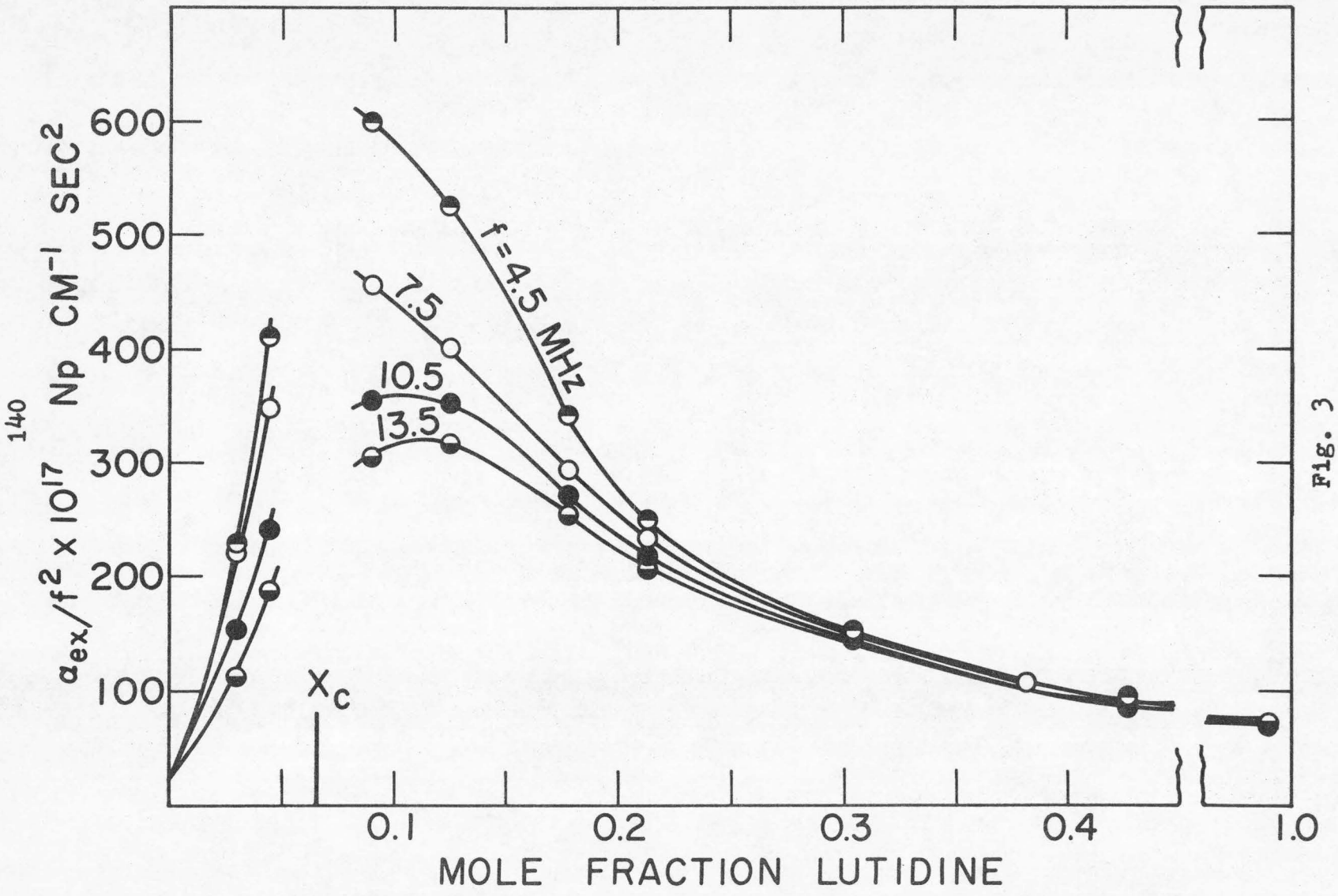
$\alpha_{ex}/f^2 \times 10^{17}$ Np CM^{-1} SEC^2
600
500
400
300
200
100
f=4.5 MHz
7.5
10.5
13.5
X_c
0.1
0.2
0.3
0.4
1.0
MOLE FRACTION LUTIDINE

Fig. 3

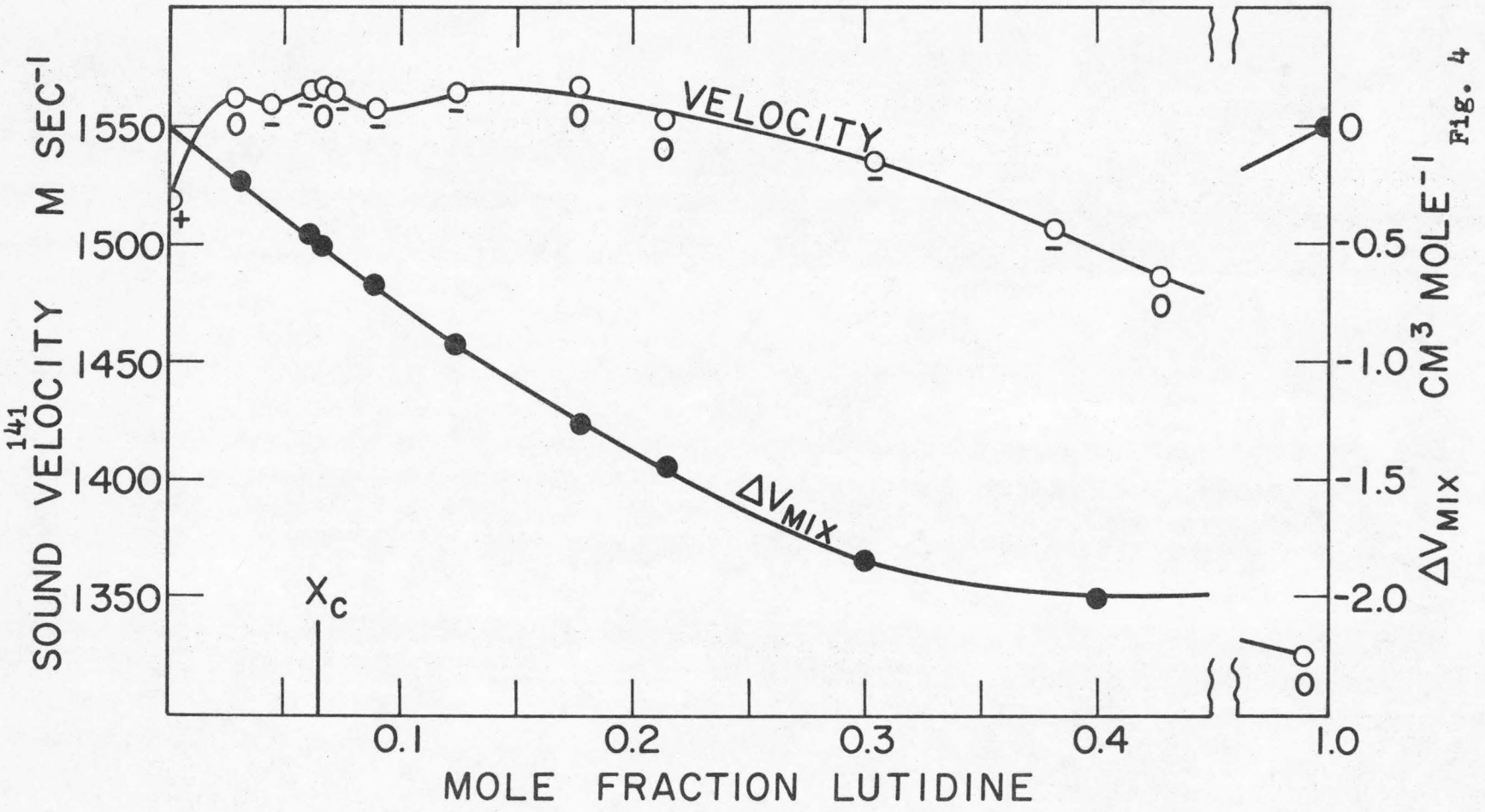
SOUND VELOCITY M SEC⁻¹
1550
1500
1450
1400
1350
VELOCITY
ΔVMIX
Xc
0.1
0.2
0.3
0.4
1.0
MOLE FRACTION LUTIDINE
0
-0.5
-1.0
-1.5
-2.0
ΔVMIX CM³ MOLE⁻¹

Fig. 4

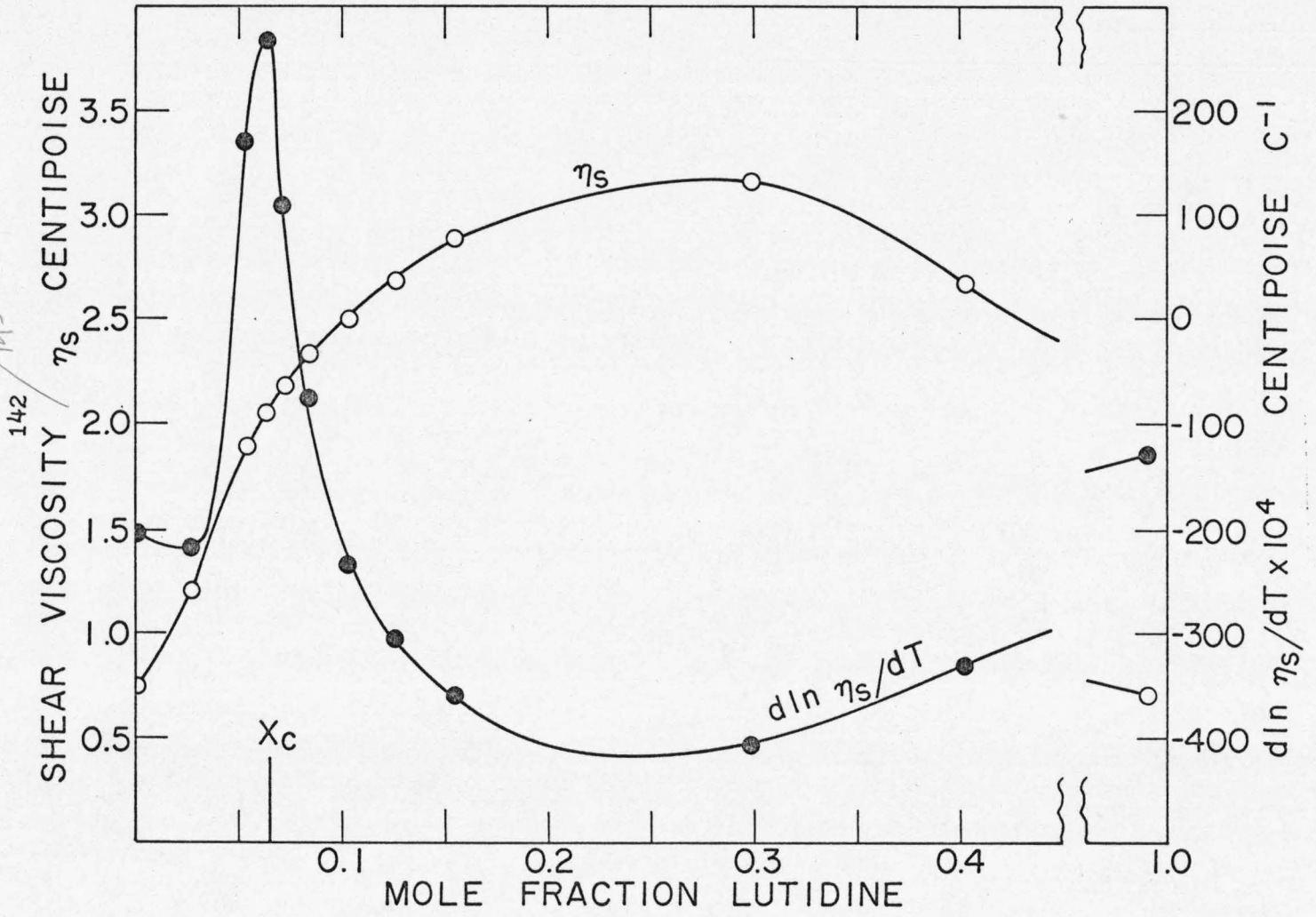
SHEAR VISCOSITY η_s CENTIPOISE
3.5
3.0
2.5
2.0
1.5
1.0
0.5
η_s
X_c
d ln η_s/dT
200
100
0
-100
-200
-300
-400
d ln η_s/dT x 10^4 CENTIPOISE C^{-1}
0.1
0.2
0.3
0.4
1.0
MOLE FRACTION LUTIDINE

Fig. 5

Appendix I. Experimental Apparatus

Our ultrasonic cell is a slight modification of that of Andreae, et al.[1] It was constructed principally by P. D. Edmonds and A. V. Anantaraman for earlier binary liquid studies in this laboratory[2], with special care in design for the close temperature control required near critical states. We have further modified it for better temperature control and homogeneity, prevention of bulk composition changes from air contact, and improved electronic stability. The basic sample cell is a 300 ml. thin-walled copper cylinder brazed to a brass base and surrounded by a circulating water jacket on the same base providing temperature control. The sample liquid has a free surface and is covered on top by a screw-on plate similar to the base. Coaxial upper and lower ultrasonic delay rods, of low fixed losses, project into the liquid through holes in the base and cover to conduct the sound from transducers to the liquid gap. This arrangement keeps the transducers out of the corrosive and somewhat conductive solution. Extra fittings on the cell provide for stirring and for vapor venting (through a buffer solution). In manner of sound propagation, the apparatus is described as a pulsed, variable path, single pass cell. Short sound pulses, converted from RF pulses by a transducer, traverse the acoustical path in the liquid between the delay rods. The attenuated pulses are reconverted to

electrical signals by a similar transducer at the end of the lower rod, amplified (in a tuned preamp for lower noise), and displayed on a CRO screen. The path is varied by moving the upper rod up or down, and the change in received signal amplitude is observed and eventually reduced to a linear attenuation α. Similarly, the change in received signal delay is converted to a sound velocity β.

The pulse technique contrasts with the interferometric methods employing continuous standing waves and either electromechanical (transducer) or optical detection[3]. Continuous wave methods heat the sample more and are therefore less desirable in the critical region. Our method also contrasts with the pulsed double pass, where a reflector returns the attentuated pulse to the same transducer which generated it. While this guarantees a transducer match, it requires sophisticated fast switching between electrical transmitting and receiving circuitry and has trouble with moderately long pulse trains at short acoustical paths. Fixed path pulsed methods[2] are also in use for samples confined under unusual conditions where sealing of the moveable delay rod or the disturbances induced by its motion cause difficulties. Absolute signal levels must be measured, which is difficult. Pinkerton[4] discusses the best implementation of the pulse methods.

We used pycnometers and an auxiliary temperature bath to measure densities of solutions at representative

compositions, and the bath with a viscometer to measure shear viscosities. The densities were used to compute excess volumes of mixing and also to establish a $\rho \longleftrightarrow \underline{X}$ curve for identifying solutions by density, after making them up quickly by volume. The exact locus of the critical point $(\underline{X}_c, \underline{T}_c)$ was examined in more detail to ensure that the states we investigated for ultrasonic and viscous behavior were accurately located relative to the critical point, irrespective of absolute errors in $\underline{X}_c$ and $\underline{T}_c$. The ultrasonic cell and auxiliary equipment were extensively calibrated and tested for operating problems, and reliable operating procedures were set up. We recount below the detailed construction of the apparatus and the underlying design considerations. At the end we tabulate the equipment specifications and list the suppliers. Later appendices describe the test and calibrations, and finally the results.

CELL: Figure 1 is a sketch of the important mechanical parts of our apparatus. To give scale, we note that the delay rods are 1" in diameter and 6" long. The walls of the cell are of 23 gauge copper formed into a cylinder of $3\frac{1}{2}$" inside diameter by 2-3/4" tall. The general dimensions are dictated by the magnitude of the absorptions expected and the usable frequencies. A range of about 10-12 db in attenuation is conveniently measured by our comparison pulse technique (discussed shortly) using a precision attenuator in the comparison pulse circuit along with visual matching.

A frequency range of a factor of four or so is desirable, to test the frequency dependence of absorption predicted by various theories. To minimize diffraction losses, the lowest frequency should have a wavelength (in the sample material) less than around 0.04 of the diameter of the transducer. At the same time, the transducer should be moderately thick for mechanical strength, while it should be used near its fundamental frequency which is inversely proportional to its thickness. At a modest diameter of 1½" (larger than the delay rod), a thickness of 0.075" is reasonable, giving it a fundamental of 1.5 MHz. Odd harmonics are easily excited, so that a range of 4.5-13.5 MHz is practical for both the transducer and the pulse generator; at 1.5 MHz. we have too great a diffraction loss. This f-range is in the lower range of thermal relaxation frequencies for mixtures[5], so that we might touch on these interesting phenomena as well as critical relaxation. The expected α/f^2 values are of the order of 10^{-14} Neper $cm.^{-1}$ $sec.^2$, several tens or hundreds of times the classical losses. One Neper, abbreviated Np., is equivalent to an attenuation of amplitude by a factor of e, and hence to 8.686 db of power. Thus α values of 0.2-2 db per cm. are expected and a delay rod travel of 5-6 cm. is desirable.

Given the acoustical path dimensions, the remaining design considerations for the cell center on making the cell walls sufficiently distant from the beam to prevent

echoes, achieving good sample temperature control, homogeneity and purity, and insuring accurate and stable mechanical alignment of the delay rods. Drawings 50023-1,-2, and -3 on file in the Chemical Engineering drafting lay out the original design. A cell diameter several times the delay rod's loses the echoes yet leaves possible good thermal contact (with stirring) of sample with circulating jacket. Corrosion protection was afforded in the original design by nickel plating, which is sufficient in the nitrobenzene-isooctane system but not for lutidine/water. Lutidine, a nitrogen heterocycle, is a powerful copper complexing agent. It presented us with severe corrosion problems (notebook 5072: 50,98,102ff.,127; 5090: 114) until gold and later silver platings were applied (see notebook 5072: 127; 5090: 79,116-23,124-5, es½. 130-36).

Temperature-control water for the circulating jacket is drawn from a large-capacity (30 liter) bath thermostatted by a Sargent S-84805 controller. Control within 0.03 C. is achieved in both bath and cell (notebook 5072: 8, 19), with a loss of 0.01 C. in temperature on the way to the cell via thick rubber tubing. A small submersible 1/30 hp. centrifugal pump does the lifting job. The outer circulating jacket is of no critical dimensions. Originally, it did not encompass the cell bottom--only the sides, while heat losses from the bottom set up convection currents upsetting signal stability (notebook 5072; 104 ff.). We added a false

bottom (notebook 5072: 109) and connected it to the rest of the jacket with a number of large drill holes. Even this was not sufficient (notebook 5090: 79) and we eventually enclosed the whole apparatus in a Lucite box (notebook 5090: 80-82). Cables, the micrometer handle, the stirrer string, and two air temperature thermometers entered through ports; jacket hoses entered through the bottom (the apparatus cabinet) as before. A small heater-blower controlled by one of the thermometers maintained a preset air temperature within 0.2 C. Snap-out Lucite panels with aluminum borders for screw fastening allowed easy manual access to the cell.

The cell is made to seal on the lower rod simply by resting upon the rod's taper. Both rod and hole must be precisely machined (drawing 50012). In addition, a thin plastic sleeve or shim must be used between rod and cell; we eventually settled on a Teflon cone made by the shop. The cell must not be too heavy to be supported by the delay rod without damage or a bending misalignment.

The last main part of the cell is the upper plate (drawing 50023-1) which serves to contain the pressurized circulating water in the outer jacket and also to shield the sample from the ambient air in large part. To accomplish the former task, the cover plate is grooved and fitted with a large nylon O-ring ($\frac{1}{2}$" wide, 1/16" thick) of median diameter equal to the cell proper diameter. This seals by compression, aided by a disposable ring of Teflon tape

draped over the cell walls, upon screwing the plate to the outer flange of the jacket. To shield the liquid from the air, the plate's center hole must be only minimally larger than the upper delay rod. The original design left an annulus of about ¼" around the rod, large enough to allow a lot of evaporation, and also incorporated an ineffective 8-vaned coaxial stirrer. These two defects are corrected by the auxiliary fittings discussed shortly.

DELAY RODS AND TRANSDUCERS are the other main concern. The rods must have low absorption loss at the highest frequencies, and be strong and elastic. Fused silica is excellent, at least for the upper rod, as it has an absorption $\alpha = (3\times10^{-10}f + 1.9\times10^{-17}f^2)$ db cm.$^{-1}$ (ref. 6a). Silica was also used in the lower rod originally, but it chips too easily under stress. Duralumin alloy, of similar low loss[6b], are a better choice. The upper rod must be carried on a micrometer-mounted arm (drawing 50013-1) and thus it and its transducer assembly must be light. The rod must be long enough beyond the transducer housing and arm clamp to project through the thickness of the cell cover plate and through the vapor space into the liquid 6-8 cm. A length of 6" is sufficient. The edges of the rod are beveled to reduce the chipping hazard in handling. The faces have a finish of about 1/20 th of the shortest wavelength (in the liquid) to be used, to prevent surface scattering of the signal at the rod-liquid interface, and to assure good

acoustical contact at the transducer end. The face should also be perpendicular to the axis within an angle θ such that R sin θ is again about 1/20 th the wavelength, to minimize refraction errors. The supplier, Englehard Industries, automatically finishes the rods to one wavelength of light and an alignment of 1" of arc, which is adequate up to 200 MHz. in ultrasonics. Somewhat larger diameter irregularities are tolerable. The final design is given in drawings 50012,-1 (Edmonds) and 60037 (our work), also on file. The lower rod must be held securely in a wide base attached to the micrometer. A collet design is given in drawings 50013, -1, and -2, with trimming screws to to align the planes of the two delay rods. The main micrometer assembly pivots on a vertical post from its base to bring the rods into coaxiality. A lower rod length of 6" is also sufficient. A Gaertner micrometer model M342 was chosen to carry the tubular arm which clamps onto the upper rod (drawing 50013 -1). The required micrometer travel accuracies and precision must restrict to a few tenths of a percent the error over the shortest distance in which one db attenuation occurs. The Gaertner's implicit specifications of better than 0.005 mm. satisfy this readily.

X-cut quartz transducers are excellent[3,6] for their high signal purity and low loss (high Q-value, though this also means low conversion efficiency), and atmospheric stability. They must be matched to within about one-quarter

of their frequency bandwidth in circuit. Gold platings on both sides form the electrodes for applying the RF signal. Transducer housings (drawings 50012,50013-2) position each transducer against the delay rods for acoustical and electrical contact. Electrical contact to the upper side of the transducer is made through a copper leaf pressed onto the face by a spring inside the housing. The spring also helps the acoustical contact, which is completed by a film of silicone grease between rod and transducer not covering the entire surface. The ungreased annulus forms an electrical contact of the lower transducer face and delay rod (in the case of the silica rod, there is a Cr-Ni or Ag plating over the face and one inch down the rod sides, maximum resistance 10Ω between any two points). The delay rod in turn contacts the grounded transducer housing. In use the delay rods are pressed into their housings far enough to lift the oversize (1¼") transducers a fraction of an inch from their resting positons over the rod holes in the housings. A collet fitting on each housing grips the delay rod and maintains the pressure. Standard coaxial cables with low-loss polymer dielectric carry the signals in and out to the external electronics.

OTHER CELL ACCESORIES: There are three auxiliary fittings on the cell. First is an evaporation buffer (notebook 5072: 62) added for our work, mounted on the cover plate. It is needed because the vapor volume above the

sample changes as the delay rod moves. Makeup air flow is routed (bubbled) through a smaller sample of liquid, about 5 ml., which undergoes sacrificial composition changes by evaporation and water pickup, protecting the bulk sample composition. The tubing from the buffer volume enters the cell volume through the second accessory, a short length of threaded pipe brazed to the cover plate and encircling the upper delay rod. A thick Teflon ring fits in a collar screwing onto the pipe, to seal closely but without binding against the delay rod. The third fitting is our ring stirrer, replacing the old vaned stirrer of the original design. A horizontal, flat, 16 gauge stainless steel ring 3" O.D. by 2¼" I.D. travels up and down in the sample to provide fast and efficient mixing.(notebook 5072: 107). Its vertical pushrod emerges from the cover plate through a bushing. It ties to a string, the other end of which attaches to a flywheel on a small 57 RPM motor to provide reciprocating motion; the stirrer falls by gravity.

ELECTRONICS: Figure 2 gives the electronic configuration needed for the pulse technique. A Chesapeake U-100 RF generator puts out a continuous series of shaped 8 μsec. pulses to the upper transducer, through a transformer (impedance matching box; notebook 5031: 17, 20, P. D. Edmonds) for improved signal transfer. After passing through the sample and being reconverted to an electrical signal at the lower transducer, the received pulse passes through a tuned

preamp (Arenberg PA-620L) powered by a regulated HV supply (HP 712B), and is displayed on a CRO (Tektronix 547, with 1A1 dual-trace plug-in). The sample's attenuation of the signal as a function of liquid path length is observed visually on the CRO and measured by reference to a comparison signal which can be attenuated in precise steps. At some initial path length or micrometer height, the received signal and the comparison signal are displayed superposed on the CRO with their amplitudes adjusted to match at the peaks of their envelopes. The comparison signal is attenuated or deattenuated one fixed step (one db, with our attenuator) and the path length is changed to bring the pulses into superposition again. This is repeated until one runs out of micrometer travel or attenuator steps. The data points of relative attenuation as a function of height, $\alpha(h)$, are least-squares fit to the form $\alpha = \alpha x + b$ to get the linear absorption coefficient α. In practice, theoretical diffraction losses are first subtracted from $\alpha(h)$. The lower half of the electronics schematic is concerned with the display of the comparison pulse. Part of the initiating pulse shaping the RF output pulse of the Chesapeake is taken off as a trigger signal. This is subsequently reshaped into a square wave of very stable height and adjustable duration by the Tektronix 162 and 163 units. This square wave modulates the RF output of the highly stable reference signal generator, an HP 606A. The precision, frequency-compensated

0-12 db attenuator (HP 355 C) passes the signal out to the second channel of the CRO. The use of separate CRO channels for received and comparison pulses eliminates the problems of impedance changes and mixing nonlinearity. It also facilitates use of the variable time delay on the second channel to bring the signals into superposition--especially for velocity measurements discussed shortly. The only critical parameters in the setup not related to stability are the 50 ohm impedances which must be presented to the input and output of the attenuator for it to give calibrated attenuations. The HP 606A has an output impedance of 50Ω ; the scope channel input must be terminated by a frequency-compensated 50Ω dummy load (Tektronix part no. 011-0049-00); and the generator-attenuator-dummy load interconnections must be made with 50Ω cable. These considerations were overlooked in the original electronic design.

Of course, the preamp in the received channel must be linear and noise free. The overall signal levels are chosen as the smallest for an acceptable signal-to-noise ratio at the CRO (say, 10 db) at the highest attenuation at the preamp's frequency of least gain. For our system, a 300V peak-to-peak signal at the upper transducer is satisfactory. A pulse duty of less than one percent insures low sample heating; the 8 μsec. pulses repeat on the average every msec. The pulses must be long enough to contain about 50 RF cycles minimum to insure good spectral purity, and

they must similarly be well-shaped and smooth.

Sound velocities are measured from the received signal delay as a function of liquid path. Initially the received signal's leading edge is aligned with one fiduciary line on the CRO screen (the peak is flat and hard to locate). As the path length is changed, the variable delay on the CRO necessary to restore the display is observed. A least-squares fit of delay to height yields the sonic velocity directly. There are some difficulties with the technique, as the signal amplitude varies with liquid path and hence in discernible shape. Limited careful checks in which one particular RF cycle was tediously followed rather than the envelope edge indicate that only the least-absorbed 4.5 MHz. signal is suitable for the simpler leading-edge type of measurement.

AUXILIARY EQUIPMENT: As mentioned above, we require an apparatus to determine densities of solutions, either for establishing initial $\rho \leftrightarrow \underline{X}$ correlations or for identifying compositions of aliquots taken from samples being used in ultrasonic or viscosity measurements. We use glass pycnometers hand-blown from marked small-bore tubing. As a result of the marking, they have calibrated divisions on the neck for reading and interpolating the liquid volumes. They also have caps for stopping evaporation. The caps must be placed on carefully to avoid slightly pressurizing the contents, as the thin pycnometer bottoms bulge

easily. They are filled using ground-glass syringes fitted with long 17 gauge or finer stainless steel needles.

The pycnometers are thermostatted in a Tamson TV40 water bath of 40 liter controlled volume. The bath controls within 0.005 C. over an hour with a variation over the volume of 0.005 C. To achieve this accuracy, the bath requires a regulated flow of cooling water of fairly stable temperature, with flow rate and temperature adjusted to induce the proper cooling/heating cycle. Cooling water is supplied by a Tamson T3 water circulator, itself cooled by either tap water or the probe of a Tamson PBC-5 portable refrigeration unit.

Temperatures were commonly observed visually on Princo -10 to +100 C. or -10 to +50 C. glass thermometers. Readings could be interpolated and reproduced to a little worse than 0.01 C. A platinum resistance thermometer (Leeds and Northrup ser. 676711; notebook 5090: 145 ff.) was used in conjunction with a potentiometer to observe the bath fluctuations, to calibrate the glass thermometers, and to closely resolve the critical point. These tests and calibrations are described in a later Appendix.

The pycnometer masses, dry and filled, were measured on an analytical chain balance (Weston Bros. type BB, ser. 35973; weights: Ch. E. no. 20187) to o.1 mg. after cleaning and drying their exterior surfaces with reagent acetone. Reagent acetone was also used to clean and dry

their interiors, along with dry air blown in through stainless steel needles. The balance was also used in making up flasks of solutions by weight for the initial $\gtrless \leftrightarrow \underline{X}$ studies.

Shear viscosities were determined in an Ostwald-Cannon-Fenske viscometer, of the bent-U design with two calibrated bulbs on the capillary arm of the U separated by a neck marked with a reference line. Viscometer operation and calibration is discussed in NBS Monograph no. 55. The viscometer was held in the Tamson bath by an array of clamps and aligned visually with a plumb line. For proper temperature control the viscometer must be almost fully submerged. Then to impeded water vapor and/or air from circulating in the viscometer vapor space, we led plastic tubing from the arm ends to the outside air. Flow times were recorded with a synchronous electric timer resolving to 0.01 sec. operated by a snap switch. The viscometer was cleaned originally with chromic acid cleaning solution briefly, and routinely with reagent acetone.

CHEMICALS: 100 gm. bottles of Matheson, Coleman, and Bell 99% purity lutidine were combined into 500-1000 ml. lots, dried by refluxing over BaO, and distilled (notebook 5072: 19,68,104,113; 5090: 28,115). Occasional water determinations in the stored, distilled lutidine by titration with Karl Fischer reagent showed contents of 0.04% typically. Better purification could be obtained by gas chromatography, fractional crystallization, or zone-refining the

solid, but these are too difficult. Laboratory distilled water was the other component of the critical mixtures and also served as one of the viscometer calibrating fluids. Metal ion assays performed incidental to cell corrosion tests showed traces of Sn ions but no other common metal contaminants. Baker reagent acetone was used in cleaning and also for viscometer calibration. A total ultrasonic calibration, to be described later, was run on Mallinckrodt thiophene-free analytical reagent benzene, titrating as less than 0.12 mole 5 water (notebook 5096: 20,34).

Lutidine/water samples for viscosity, $\rho \leftrightarrow X$ studies, and ultrasonics were all disjoint. The large amount of lutidine used in any one ultrasonics sample necessitated several consecutive reuses of the same sample, diluted appropriately each time. Upon long storage the solutions tended to discolor but critical properties--at least T_c--seem unaffected.

SUPPLIERS

Chesapeake Instrument Co.
Shadyside, Md.

U-100 signal generator (ser. 118)

- -500 W instantaneous peak into 100Ω resistive load; adjustable.
- -0.9-200MHz. with 12 plug-in coils
- -rise time 0.5 μsec.
- -pulse width 1,1.5, or 6 μsec. nominal
- -internally or externally triggered; 100V
- -pulse repetition rate, internal trigger: 50-7000 Hz.

Arenberg Ultrasonic Laboratory, Inc.
94 Green Street
Jamaica Plain, Mass. 02130

PA-620L preamp (ser. SN 241)

-gain: dependent on freq. and bandwidth; approx. 35 db min.
-Input impedance 93-15,000Ω; output 2.7kΩ, capacitatively coupled
-0.1-17 MHz.
-has instruction manual on file

Hewlett-Packard
275 Page Mill Road
Palo Alto, Calif.

712B regulated DC power supply (ser. 002-04783)

-0-500 out, 200 ma. max. load; also -300V, 50 ma.; 6.3V AC CT, 10 A. (unreg.); etc.
-less than 50 mv. change on 500V line, no load to full load
-less than ±100 mv. change for ± 10% line in.
-less than 500 μv ripple
-internal impedance at full load 0.1Ω in series with 25 μH
-current metering; overload protection

606A signal generator (ser. 038-03448)

-(extensive spec sheet)
-50kHz.-65 MHz. in 6 bands; freg. acc. within 1%
-calibration within 0.01% (BFO), 0-50 C.
-RF output 0.1 μv-3V continuously adjustable, into 50 resistive load
-output accuracy with change of vernier ±1 db
-freq. response ± 1 db over the entire freq. band range at any setting of output
-output impedance 50Ω; SWR 1.1 on 3V range; less than 1.1 on 1 and 3V ranges to 20 MHz.
-spurious harmonic output < 3%
-continuously adjustable amplitude modulation 0-100%, constant within ±½ db over full range of carrier freq. and output level; DC to 20 kHz. bandwidth
-envelope distortion < 1% at 30% modulation
-incidental FM < 0.0025% or 100 Hz. (larger) on 1V and lower ranges
-spurious FM < 0.001% or ± 20 Hz.
-spurious AM: hum and noise -70 db

-freq. drift: 1V and lower ranges, < 0.005% or 5 Hz. for 10 min. period after warmup or restabilization at freq. of use

355 C attenuator (ser. 219-00194)

-0-12 db in 1 db steps, ± 0.05 db
-0-1000 MHz. compensation
-0.5 W max. dissipation
-50Ω in and out

Tektronix, Inc.
S. W. Millikan Way
P.O. Box 500
Beaverton, Oregon

547 oscilloscope (ser. 006668)

-(extensive spec sheet and manual)
-sweep rates 0.1 μsec./cm. to 5 sec./cm. in 24 calibrated steps, ± 2%; uncalibrated vernier to 0.4 of rate
-sweep magnification 2X, 5X, and 10X, ± 5%
-trigger source, coupling, level all adjust.
-time-delay on sweep 0.1 μsec. to 50 sec., ± 1% of indicated delay, ± 2 minor divisions of multiplier 50 μsec.-50 sec.; incremental delay accuracy ± 2 minor divisions; jitter < 0.005%
-horizontal deflection continuously variable 0.1 V/cm. to 10 V/cm.; DC-400 kHz. (3 db)
-input 1 MΩ, shunted by 55 pF.
-has internal amplitude calibrator; output trigger, gate, sweep signals
-tolerates ± 10% line voltage variations

calibration service; local representative

1A1 dual-trace plug-in (ser. 014214)

-50 mv./cm. -20 V/cm.; DC-50 MHz.; rise time 7 nsec., 15 pF. input
-5 mv./cm/; DC-28 MHz.; rise time 12.5 nsec., 47 pF. input

011-0049-00 50Ω termination

-freq.-compensated over wide range

162 waveform generator (ser. 007495)

-pulse, gate, or sawtooth of adjustable

duration and repetition
-externally or manually triggered
-pos. pulse: + 0-50 V; 10 μsec. to 0.05 sec.; rise time ~1 μsec.; repetition 0.1 Hz.-10 kHz.
-neg. sawtooth: amplitude decreases uniformly from 150 V to 20 V; duration 100 μsec.-10 sec.; repetition 0.1 Hz.-10 kHz.
-output ~1000Ω
-trigger: any pulse, into ~1 MΩ, pulse 15 V, 5 msec. or less rise time

161 pulse generator(ser. 006421)

-to supply calibrated rectangular output or pos. gating pulse; variable delay on sawtooth input
- + 50 V gate, not adjustable
-output impedance 1 kΩ max.
-trigger sensitivity 3 V p-p min.; max. repetition rate 50 kHz.

163 pulse generator (ser. 1123)

-to supply rectangular pulses of adjustable duration and amplitude; triggered by pos. pulse or sawtooth; variable delay on sawtooth
-0-25 V p-p pulse
-pulse output impedance 500Ω; varies with amplitude setting; min. load 3.5 kΩ

C-12 oscilloscope camera

E. H. Sargent and Co.
4647 W. Foster Ave.
Chicago, Ill.

S-84805 constant temperature water bath; circ. pump and heaters with separate controller (excl. contact thermometer)

-heaters: 400 W fixed booster; 300 W adjustable uncontrolled; 250 W adjustable, controlled by saturable reactor; all switchable
-regulation ± 0.01 C. and uniformity ± 0.01 C. to 70 C.; ±0.005 C. in vicinity of 25 C.

S-84810 water bath; Pyrex 16" dia. by 10" high

S-81840 mercurial thermoregulator (contact thermometer)

ASTM Ostwald-Cannon-Fenske viscometer

-inherent accuracy discussed for general type in NBS Monograph no. 55

The Gaertner Scientific Corp.
1201 Wrightwood Ave.
Chicago 14, Ill.

M342 micrometer slide (ser. 2352P)

-accurately ground and corrected lead screw and lap-fitted nut
-threaded carriage for mounting
-100 mm. (certificate 100.000 @ 20 C.), reading to 0.001 mm. with 10 part vernier; lead screw pitch 1 mm.

P. M. Tamson
Zoeltermeer, Holland

local: Neslab Instruments, Inc.
P. O. Box Y
Durham, N. H. 03824

TV40 viscometer bath (ser. 660239)

-0-230 C., ± 0.005 C. (0-100 C.)
-40 liters capacity, most inside controlled volume (baffled)

T3 circulation thermostat (ser. 0003635)

- ± 0.06 C. to 250 C.
-capacity 3.5 liters
-pump head 10', 130 gal./hr.

PBC-5 portable bath cooler (ser. 75043J)

-temperature control allowed to -15 C.

Englehard Industries, Inc.
Amersil Quartz Division
685 Ramsey Ave.
Hillside 5, N. J.

delay rods

-Amersil Optical Quality #2 , fabricated from specs on drawing 60037 (earlier 50012-1)

Keim Precision Mirrors Corp.
124 E. Angeleno Ave.
Burbank, Calif. 91502

silvering of delay rod ends (C.I.T. P. O. 25L-50364)

-on one face and 1" down adjacent sides
-10 max. resistance between any two points

Leeds and Northrup Co.
4901 Stenton Ave.
Philadelphia 44, Penn.

7556-1 guarded six-dial potentiometer (K-6) (ser. 1631257)

-high range 0-1.6 V in steps of 1.0 μv, $\pm$ (0.0005% + 1 μv)
-plus accessory standard resistors, adjustable DC resistors
-used for temperature measurements in conjunction with Pt thermometer below; cf. note by H. Strumpf to C. J. Pings on use of potentiometer for temperature measurements.

Platinum resistance thermometer (ser. 676711)

-calibrated by NBS, Nov. 18, 1949; certificate on file in Ch. E.; test no. 122106
-polynomial coefficients of resistance in temperature are in bounds

There is no record in any reports or notebooks by previous investigators, of the sources for the X-cut quartz transducers, or of the glass tubing blown into pycnometers, except for the cryptic notation about the transducers, "ex I.C.I." Transducers which are at least similar in performance can probably be obtained from Valpey-Fisher Corp., 1015 First Street, Holliston, Mass. 01746.

Other useful equipment, noted only by manufacturer or supplier:

Coaxial cables, BNC connectors: Belden; widely available
Submersible circ. pump: Little Giant Corp., Okla. City; distributed by Fisher Scientific
Syringes and needles: Becton, Dickinson and Co. "Yale" series with Leur-Lok needles; available readily through Bio. Dept.
Silicone grease: Halocarbon Products Corp., Hackensack, N. J.; does not tarnish platings

Remaining equipment: either standard items from stock or common fixed equipment, or fabricated from same according

to mechanical drawings as noted in preceding text.

REFERENCES

1. J. H. Andreae, R. Bass, E. L. Heasell, and J. Lamb, Acustica 8,131(1958).

2. A. V. Anantaraman, A. B. Walters, P. D. Edmonds, and C. J. Pings, J. Chem. Phys. 44,2651(1966).

3. V. F. Nozdrev, Applications of Ultrasonics in Molecular Physics (Gordon and Breach, N. Y., 1963).

4. J. M. M. Pinkerton, Proc. Phys. Soc. B62,286(1949).

5. J. H. Andreae, P. D. Edmonds, and J. F. McKellar, Acustica 15,74(1965).

6. W. P. Mason, ed., Physical Acoustics (Academic, N. Y., 1964), Vol IA: a) 488; b) 364-5.

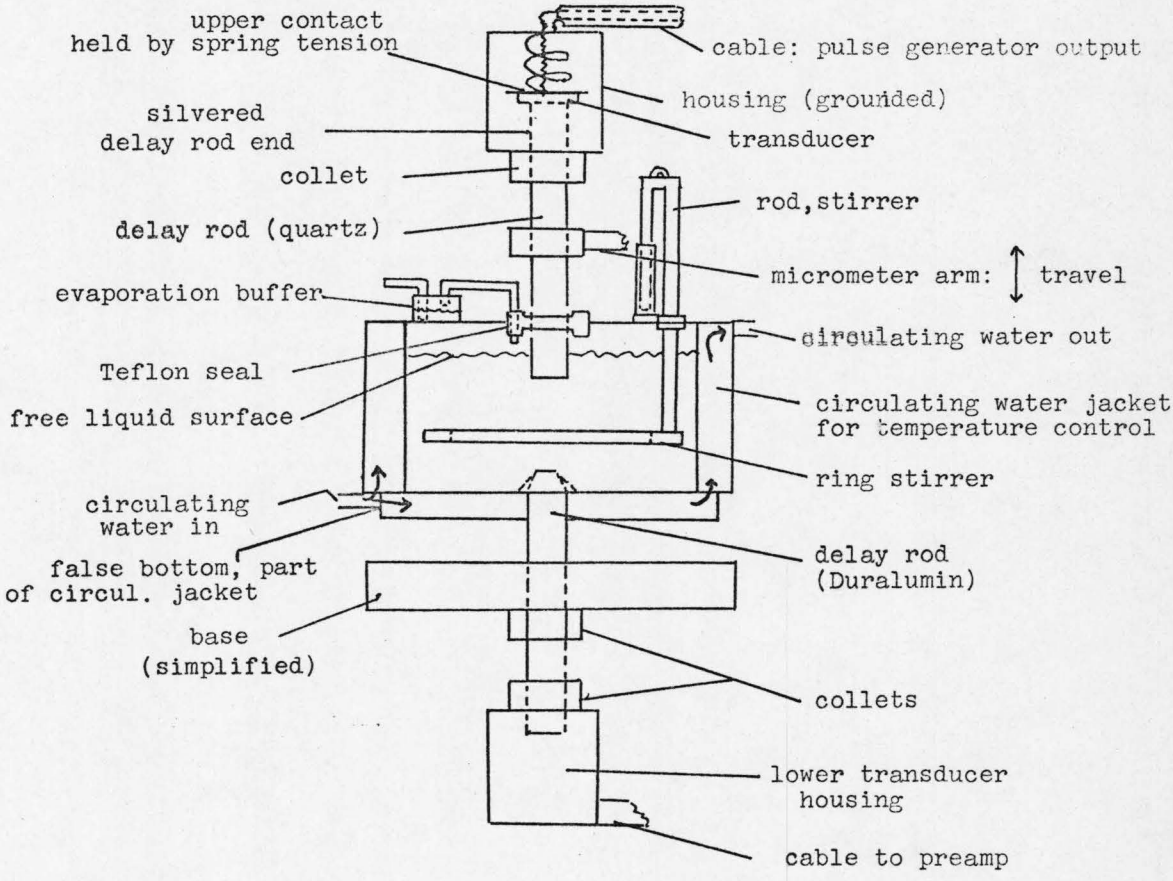

Fig. 1. The Ultrasonic Cell

~~The electronics configuration is presented without explanation:~~

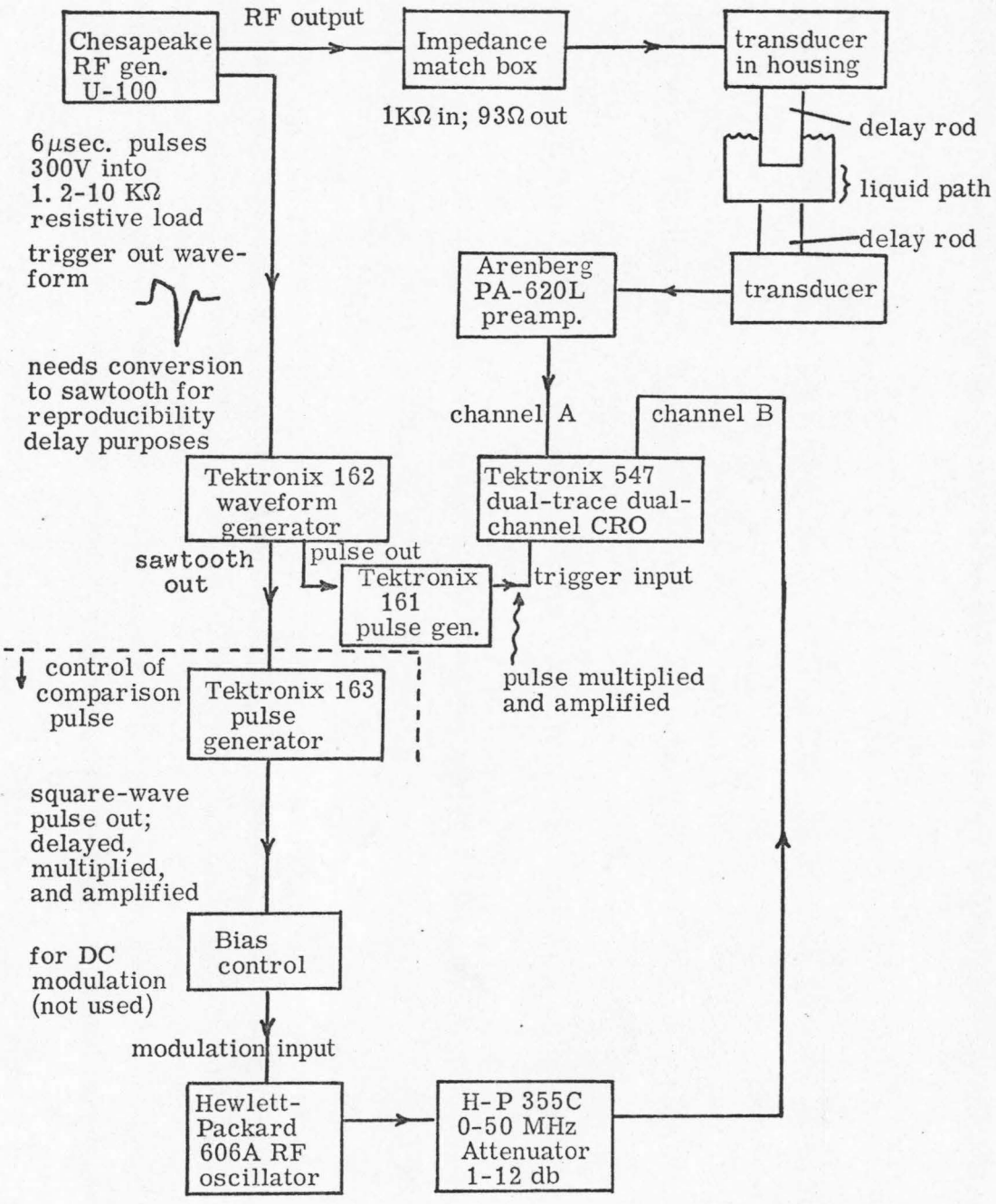

Fig. 2. Pulse Method Electronics

Appendix II. Operating Procedure

Our experiments lie in three groupings. First, a set of mixtures spanning the full range of mole fractions were carefully prepared and their densities measured on several isotherms. The data were used to compute excess volumes of mixing but more importantly to construct $\rho \leftrightarrow \underline{X}$ calibration curves for pinpointing by density the compositions of samples made volumetrically for ultrasonics or viscosity measurements. The original data reported in notebook 5072: 43-61 and the more carefully taken later data recorded in notebook 5096: 11-13 are reduced to final density values in 5096: 11-13 and to excess volumes in 5096:56. Table I presents the results from the accurate later data. Second, a similar series of mixtures were prepared and the shear viscosities measured on three or four isotherms. The raw data are recorded in 5072: 43-61; 113 ff. and transcribed in 5096: 48-9. Values of η_s are computed at 5096: 54-5 and these in turn are fitted for temperature dependence to theoretical forms in 5096: 75-80. These results, which were used to construct figure 5 of paper II, are tabulated in Table II. Third, a similar series of compositions were prepared for ultrasonic absorption and velocity measurements. Actually, all the experiments were run several times with various improvements in the ultrasonic cell and procedure, before a satisfactory full set of data was

obtained. Each mixture was prepared volumetrically, identified by density, entered into the sample cell, measured for α and β at four isotherms (when possible) accessed successively at four frequencies (4.5,7.5,10.5, and 13.5 MHz.) each time, rechecked for composition by density, and stored. Succeeding mixtures were prepared by enriching or diluting the previous mixture with lutidine. About every three compositions, fresh lutidine and distilled water were used, usually drawing from the same lutidine distillation batch as the previous set. The raw data require some discussion, particularly about diffraction and mode conversion corrections and error bounds, so we defer this presentation to Appendix IV. All equipment, chemicals, and procedures were thoroughly tested and calibrated as reported in Appendix III following.

Our specific procedure for accumulating the $\rho \leftrightarrow \underline{X}$ density calibration data is straightforward. The Tamson bath is warmed up while the pycnometers, weighing flask, and syringes are cleaned. The Tamson is trimmed to the first isotherm and the sample is made up by weight: the flask is weighed empty; one syringes out the approximate volume of lutidine into the narrow-neck weighing flask, then trims the weight drop-by-drop (quickly, to avoid evaporation and water pickup errors). The flask is stoppered and weighed. The procedure is repeated with the water portion, using a new or cleaned syringe. A sample is entered into the pycnometer

with a small syringe and fine needle, with care to avoid forming bubbles in the pycnometer bulb or neck or to remove those that form. The pycnometer is equilibrated until 10 minutes after the liquid level stops visibly rising in the neck. After tapping loose any new bubbles, the volume is read and the Tamson reset for the next isotherm. After all four isotherms have been taken, the pycnometer is removed, its exterior and cap are dried with reagent acetone, and it is weighed, and finally cleaned.

The viscosity technique is similar. The Tamson is warmed up and the viscometer and syringes cleaned. The sample is made up approximately by volume in a 50 cc. flask and identified by density in a pycnometer much as above, at a reference temperature of 33.32 C. Two lengths of plastic tubing (one with suction bulb) are attached to the viscometer, which is then inserted in the bath and aligned vertically by a plumb line. One syringes as close as possible to 10 cc. of the sample into the viscometer, corks the tubing ends, and equilibrates the setup at the first isotherm for 15 minutes. The corks are removed and the suction bulb used to lift the sample to the proper level in the capillary arm. The time of flow between the fiduciary lines (around the upper bulb in our work, while this is not recommended in the NBS Monograph no. 55) is recorded. The timing is repeated twice more and then a new isotherm selected. Again, 15 minutes equilibration time is allowed

before running. The composition was sometimes rechecked by density after the viscosity runs. The viscometer is then removed and cleaned with acetone.

Ultrasonic measurements are somewhat more involved, partly because of the complication of cell assembly. The Tamson and Sargent baths are warmed up. The alignment of the upper with the lower delay rod is checked by running them both into a close-tolerance Lucite tube made by the shop. Occasionally, we measured the additive constant for converting micrometer readings to absolute delay rod spacings. These must be known for diffraction corrections to the measured absorptions. Next the upper rod is removed and the cell proper is cleaned with acetone and seated on the lower rod. The upper plate and its stirrer are cleaned and fastened to the cell, with a strip of Teflon tape run around the cell lip for extra sealing. The stirrer drive is assembled. Circulation to the jacket is begun and one then checks for leaks to the inner cell. The Lucite box is assembled and its temperature control warmed up. Then about 350 ml. of sample is made up volumetrically. An aliquot is put into a pycnometer for identification by density. If the composition is too far from the desired one, the bulk sample is readjusted and rechecked by density. As the electronics are switched on to warm up, the sample is quickly poured into the cell through the delay rod hole. The Teflon collar is slipped onto the upper rod and the rod is put into the

upper plate hole. The rod is clamped into the micrometer arm again and then the collar is tightened to the threading on the upper plate. For later runs, we also taped a Saran bag as a vapor trap to the collar on one end and to the upper part of the delay rod on the other. The Lucite box is closed, stirring is started, and the bath temperature is trimmed.

While the sample equilibrates, the electronics are tuned for the best received signal at the initial frequency (notebook 5072:80 records best tuning parameters). This entails switching to the optimum settings on the Chesapeake tuning dial, impedance matching box input and output taps, and Arenberg preamp input and output tuning slugs. The variable resistance on the impedance box and the resistances in and out on the Arenberg are adjusted by trial and error. Occasionally the Arenberg input capacitance or its tuning slugs may need attention, again by trial and error. One tries for maximum signal with a monotonic, smooth envelope. Sometimes the grease acoustical contact in one or the other transducer assembly gives out in part or in full, as evidenced by severe or total loss of received signal. Some pitfalls in the tuning procedure are noted in notebooks 5072: 127; 5090: 41 ff.

One is ready to start when the sample has equilibrated at least ½ hour with occasional stirring and the electronics are tuned. The predominant pulse frequency is

measured by zero-beating the channel A-B added signals on the CRO. The average of the bath temperature in its cycling is recorded. The velocity may be measured first, as described in Appendix I. Care is taken to keep the micrometer and also the scope delay dial moving in one direction only, for any one set of height-delay measurements. This eliminates backlash errors in the delay dial, micrometer, and the riding of the Teflon collar upon the delay rod. After the β measurements, the α data are taken, again keeping the micrometer moving in one direction on any one pass. Generally we made three passes, up-down-up, to get three independent sets of data for better statistics. The first run is alway made up, to assure that the received signal is as large as possible on the CRO screen without going off the edges. The U-100 amplitude is adjusted to make the display fit. Of course, for all α and β measurements the stirrer is off. One must be careful that the signal is stable for the α data; if it visibly alters in size over periods of about 30 sec. it may give invalid data. Causes of instability include poor thermal homogeneity in the sample, especially at high lutidine concentrations where convection is easiest to set up; and poor 'sync' adjustment of the U-100. For some overall tuning, there may also be enhanced mode conversion errors, a form of overlapping and interfering echo in the delay rods that causes oscillations to be superposed on the monotonic decrease of amplitude with

micrometer height. Since the oscillations are hard to characterize, they ruin the adaptability of the data to a linear least-squares fit. Any data run with gross disparities in micrometer intervals for succeeding db attenuation steps should be rejected and the apparatus should be retuned.

The tuning is all redone to reach the next frequency for α and β measurements, with only a nominal wait for restabilization of the electronics and with brief stirring of the sample, say 15 sec. After all four frequencies have been run, one changes the bath temperature and re-equilibrates the sample with occasional stirring for another ½ hour. One finally runs through all four isotherms--or less, if one or two of the upper isotherms is in the two-phase region at the particular composition. By this time the sample has been in the cell about 8 hours. An aliquot is taken for rechecking the composition by density, and any visual turbidity is noted, as this may signal contamination by cell corrosion or jacket-to-cell leakage. While the aliquot is thermostatting, the upper plate of the cell is removed to expose the full sample, which is rapidly transferred to a storage flask using large 50 cc. syringes without needles. Electronics, enclosure heater, and bath are all shut down. The cell is disassembled and washed with acetone and air-dried. Finally, with the pycnometer data recorded, the Tamson is shut down and the pycnometer is cleaned.

Table I. Density Calibrations and Excess Volumes of Mixing

X(lutidine)	T(C.)	ρ, g./ml.*	est. ρ_{32} / V^e, ml./mole**	est. $-(\frac{\Delta\rho}{\Delta T})_{32}$#
0.9994	31.98	0.91144	0.91142	0.00089
	33.99	0.90966	0.000	
0.0000	32.00	0.99505	0.99505	0.00032
	34.00	0.99440	0.000	
0.0300	31.96	0.99228	0.99226	0.00046
	33.98	0.99135	-0.238	
0.0600	31.98	0.98978	0.98977	0.00064
	33.44	0.98883	-0.468	
0.0663	31.98	0.98921	0.98920	0.00067
	33.24	0.98837	-0.513	
	31.97	0.98924		
0.0901	31.98	0.98729	0.98727	0.00075
	33.46	0.98618	-0.684	
0.1240	31.98	0.98496	0.98494	0.00082
	33.50	0.98372	-0.926	
0.1769	31.98	0.98113	0.98111	0.00088
	33.50	0.97980	-1.267	
0.2100	31.97	0.97853	0.97850	0.00092
	34.02	0.97664	-1.452	
0.2996	31.96	0.97113	0.97109	0.00095
	34.04	0.96916	-1.853	
0.4003	31.96	0.96215	0.96211	0.00101
	34.04	0.96014	-2.110	

* ml. = 1.000027 cc.

** linear interpolation

\# linear interpolation, units g. $ml.^{-1}$ $C.^{-1}$

Table II. Shear Viscosities

X(lutidine)	T(C.)	ρ (g./ml.)	ν^* (centistoke)	η_s (centipoise)
0.0000	24.83	0.99711	0.8963	0.8937
	32.55	0.99487	0.7598	0.7560
	34.56	0.99421	0.7299	0.7257
	39.92	0.99227	0.6591	0.6540
0.0263 **	32.52	0.99239	1.234	1.225
	33.33	0.99202	1.214	1.204
	33.73	0.99184	1.203	1.193
	34.54	0.99149	1.183	1.173
0.0545	32.40	0.98998	1.895	1.876
	33.21	0.98949	1.914	1.894
	33.60	0.98926	1.980	1.959
0.0630	32.42	0.98922	2.058	2.036
	33.21	0.98870	2.085	2.061
	33.61	0.98844	2.151	2.126
0.0710	32.40	0.98855	2.194	2.169
	33.21	0.98800	2.211	2.184
	33.61	0.98773	2.276	2.248
0.0840	32.41	0.98742	2.386	2.356
	33.22	0.98684	2.369	2.338
	33.61	0.98655	2.371	2.339
0.1032	32.40	0.98599	2.580	2.544
	33.21	0.98538	2.531	2.494
	33.61	0.98507	2.507	2.470
	34.41	0.98446	2.474	2.436
0.1265	32.40	0.98442	2.785	2.742
	33.21	0.98377	2.717	2.673
	33.60	0.98345	2.686	2.642
	34.40	0.98279	2.624	2.579
0.1544	32.40	0.98245	3.025	2.972
	33.21	0.98177	2.943	2.889
	33.61	0.98143	2.896	2.842
	34.41	0.98075	2.820	2.766

(continued on next page)

* kinematic viscosity, $\nu = \eta_s / \rho$

Table II. Shear Viscosities (continued)

X(lutidine)	T(C.)	ϱ (g./ml.)	ν^* (centistoke)	η_s (centipoise)
0.177**	32.54	0.98063	3.126	3.066
	33.34	0.97993	3.039	2.978
	33.74	0.97958	3.000	2.934
	34.54	0.97887	2.914	2.852
0.2979**	32.54	0.97071	3.340	3.242
	33.34	0.96994	3.243	3.146
	33.74	0.96956	3.173	3.076
	34.54	0.96880	3.089	2.993
0.4017**	32.54	0.96145	2.840	2.730
	33.34	0.96065	2.766	2.657
	33.74	0.96025	2.732	2.623
	34.54	0.95946	2.663	2.555
0.9901**	32.57	0.91168	0.787	0.717
	33.36	0.91097	0.780	0.711
	33.72	0.91065	0.777	0.708
	34.53	0.90992	0.768	0.699

* kinematic viscosity, $\nu = \eta_s/\varrho$

** less reliable: poorer viscometer charge volume control and mole fraction determination

.....

Shear Viscosity and Its Temperature Dependence at One Reference Temperature (33.2 C.) From Fit to Eq. (15) of Paper II

X(lutidine)	$\eta_{33.2}$	$(d \ln \eta_s / dT)_{33.2}$
0.0000	0.7460	-0.0204
0.0263 *	1.207	-0.0217
0.0545 *	1.894	+0.0167
0.0630 *	2.060	+0.0265
0.0710 *	2.184	+0.0108
0.0840 *	2.338	-0.0074
0.1032 *	2.494	-0.0236

(continued on next page)

* used second term in Eq. (15)

Table II. Shear Viscosity...Temperature Dependence... (continued)

X(lutidine)	$\eta_{33.2}$ /	$(d \ln \eta_s / dT)_{33.2}$
0.1265 *	2.674	-0.0309
0.1544	2.888	-0.0359
0.177 **		
0.2979 **	3.156	-0.0406
0.4017 **	2.670	-0.0331
0.9901 **	0.712	-0.0129

* used second term in Eq. (15)

** less reliable basic η_s data; see table above

Appendix III. Calibrations and Tests

The first important calibration is that of the pycnometer volume, which was done with distilled water at four temperatures. The experiments are recorded in notebook 5072: 27 ff., while the data are reworked in 5096:4ff. The calibration was found to be better if no temperature coefficient of the volume was included. We note here that no buoyancy corrections were applied in the weighings with stainless steel weights. Since all the solutions are in a restricted range of density and the lutidine purity is no better than 99.5%, it does not appear worthwhile to rework the weight data. Some relative calibrations of the weights used (unrecorded) indicated that the uncorrected nominal masses give an accuracy of about 0.5 mg., within the error bounds of evaporation and water pickup in making the original $\rho \leftrightarrow X$ identifications.

Lutidine purity is hard to determine quantitatively. Water content was assayed by Karl Fischer reagent several times (notebook 5072: 37 ff.; 5090: 152). It was held to 0.3 mole % for the initial $\rho \leftrightarrow X$ identifications and to 0.06 mole % for final ultrasonic measurements. Freedom from isomers and homologs was not gauged; this requires gas chromatography. Only the claim of 99+% mole purity by the supplier (supported by a reported m.p., -7 to -4 C.) can be reiterated. The distillation after drying in our laboratory

served more to draw the lutidine off the bed of drying agent than to remove homologs, which is better done by fractional crystallization, zone refining, or gas chromatography. The effectiveness of the new cell plating and sealing against contamination by cell corrosion (problems encountered: notebook 5072: 50, 98, 102 ff., 127; 5090: 114, 130 ff.) or evaporation can be weighed by the agreement of initial and final aliquot compositions in runs; also by lack of noticeable turbidity after sample runs. A final important aspect of mixture behavior over and above component purity is the establishment of our practical critical point X_c, T_c, to accurately gauge our distance from the same in any run. Our first attempts at X_c and T_c are recorded in notebook 5072: 29 ff.; a limited coexistence curve mapping is done in 5072: 74-8 to check the phase diagram published by Cox and Herington. We finally established T_c quite well at the same time that we used a platinum thermometer to calibrate our glass thermometers, check the Tamson bath stability (notebook 5090: 145 ff., esp. 148 ff.). Notebook 5096: 1 ff. reports some comments on the phase diagram and a closer determination of X_c. Our best critical parameters are X_c = 0.065 $\pm$0.001 lutidine and T_c = 33.57 C.

The accuracy and precision of our temperature measurements vary. Most viscosity, density, and ultrasonic data were taken with only calibrated glass thermometers for monitoring. The temperatures for viscosity and density are

most reliable, as the experiments were performed in the closely-controlled and homogeneous Tamson bath. Temperatures in the ultrasonic cell are regulated by a poorer bath (Sargent) and in addition there is a temperature drop in transport of the circulating water. This drop, amounting to the 0.01 C. noted earlier, was measured by a zero-corrected thermocouple in test recorded in notebook 5096: 18, and used to adjust sample cell temperature records.

The $\rho \leftrightarrow X$ identifications are actually calibrations and have no external checks. The shear viscosity data are better off, as the viscometer was calibrated with distilled water and reagent acetone (notebook 5072: 42 and 5096: 49-53-rework) using literature values for absolute water and acetone viscosities reported in the Handbook of Chemistry and Physics, edition 44, and Techniques of Organic Chemistry, ed. Weissberger, et al., respectively. The error bounds on the series of lutidine/ water mixture measurements, from differences in pressure head between calibration and run conditions, were noted according to N.B.S. Monograph no. 55 in notebook 5096: 49 ff.

In the ultrasonic experiments there are numerous possibilities for mechanical or electronic errors, either systematic or random. We recount below the numerous checks we performed, except for measurements of the principal systematic errors discussed with the data reduction schemes in Appendix IV. We might mention that these main correctible

errors are in the delay dial calibration, for velocities, and in the attenuator calibration, diffraction correction, and mode conversion, for absorption. Also in the final data reduction, the visual CRO screen reading error and the remaining systematic and random errors discussed below are lumped into an equivalent random error source.

We first consider the mechanical aspects of sound propagation. Before acoustic mode conversion in the delay rods was identified as the major source of signal drift, we looked for mechanical errors in the micrometer alignment and travel. The micrometer precision was checked with a travel indicator over short ranges (notebook 5072: 88). The effects of angular misalignment of the delay rods upon the amplitude and envelope of the received signal were checked with a goniometer replacing the micrometer (notebook 5090: 60 ff.). The resultant signal variations with angle were recorded photographically. No clear leads resulted, but it became apparent that alignment was not as critical as thought previously for either absolute signal levels or for relative change with height. The simple procedure of aligning the two delay rods before the run by use of a Lucite tube is certainly adequate. The smoothness of finishes on the delay rod faces also does not seem critical, as the lower Duralumin face deteriorated visibly without bad effects. Binding of the Teflon collar against the moving upper rod did cause signal variations, but this was care-

fully avoided during each run (notebook 5072: 129; 5090: 77). A final mechanical cause of signal variation is a variable load on the transducer housings, hence on the transducer-rod contacts. In the misalignment tests, we sometimes loaded the housing with extra weight with its collet untightened and achieved significant fractional increases in the received signal. Conceivably the pull exerted on the top housing by the RF cable could cause a smaller but still bad effect. Keeping the collet tightened eliminated the error. General accounts of signal drift errors we encountered are given in notebooks 5072: 88-90, 104 ff.; 5090: 29, 32, 35, 39 ff.

Electronic contributions to error are minimized first by using the best tuning, i. e., the simplest monotonic envelope for the RF signal. Overtones, harmonic and FM distortion in poorly-shaped pulses cause spuriously high losses (see Nozdrev, ref. 3 of App. I) and accentuate the mode conversion problems. Instability of gain at the Arenberg preamp caused repeated problems, to the point of requiring some experimental runs to be abandoned. The linearity of the Arenberg and of the two CRO channels as a unit was verified after completing the ultrasonic experiments, by dividing a variable-amplitude signal between the two circuits (notebook 5096: 41-2, 46-8). Stability of the CRO in gain and sweep was unquestionably excellent. The comparison signal amplitude is also very stable. Initially

there was a problem because its rectangular wave modulation had a slope, but this was eliminated (notebook 5090: 77) by bypassing an electronic module providing DC bias to the signal (part of the original design we inherited). The stability of the laboratory temperature probably aided that of all the electronics.

Frequency accuracy depends upon the comparison signal generator, the HP 606A. We frequently recalibrated its vernier dial against its internal beat frequency oscillator overtones. The BFO itself was checked against a Beckman counter (notebook 5096: 43-5) and found to be well within specifications. The visual beat technique for measuring received signal frequency by comparison to the reference signal worked much more simply and at least as well as the alternative, matching a whole series of peaks in the two signals displayed expanded upon the screen.

Several total calibration runs were made on benzene, with the apparatus in various stages of improvement. Benzene's α and β values are well known (ref. 7, paper II) and are taken as standards. Our apparatus and procedure seem to give good results by this check (notebook 5072: 91; 5096: 34). Our sound velocity measurements in water (notebook 5096: 35-7) indicate no dispersion with frequency, which again agrees with the literature.

Appendix IV. Ultrasonic Data Reduction and Results

We first consider the absorption data, composed of two to six sets of micrometer height (h): attenuation readings for each of 144 conditions of composition, temperature, and frequency (X,T,f). Reduction of the data to α values for each of the 144 conditions (denoted by some index k) is done in two basic steps. First, each full set of points, denoted by some double index kn and composed of N_{nk} individual points, is least-squares fit to the linear form $a_i^{kn} = \alpha_n^k h_i^{kn} + b_n^k$ (for i=1,N_{kn} in FORTRAN-style notation). Second, the various values of α_n^k of absorption computed from each of the N_k data sets are combined into a weighted average α^k, taken as our best approximation to the true absorption in the state k. In other words, the α_n^k are fit to the constant form $\alpha_n^k = \alpha^k$.

In practice, the fitting procedures are quite complicated, for two reasons. First, we must correct the raw data points a_i^{kn}; h_i^{kn} for systematic errors. Second, we must assign them realistic error bounds so that we can finally estimate the error bounds of the α^k. The following elaborations are incorporated into the reduction scheme:

-Firstly, some data sets kn recorded in the notebooks have obvious systematic errors, the presence of which was noted at the time of the experiment. Signal instability from poor tuning, from convection currents in the cell, or from faulty preamp operation is the usual culprit. These

data sets are not even used.

-Secondly, the raw attenuation readings α_i^{kn} are corrected for two systematic errors, before fitting. Errors in the micrometer readings h_i^{kn}, in the instrument or in observation are so low as to be negligible. The first systematic error is the deviation of attenuator readings on the HP 355C from actual attenuations. These actual attenuations were measured after the completion of experiments by sending the attenuator to Hewlett-Packard in Palo Alto. Calibrations at 4.5 MHz. and 13.5 MHz. are recorded in notebook 5096: 80-81. and are incorporated in the computing to translate readings to true net attenuation.

Second and more important is the correction for diffraction losses in propagation of the pulse through the liguid. A finite-area transducer does not produce a collimated column of plane waves; rather, the beam spreads over some angle and attains a warped amplitude profile. The former causes incomplete exposure of the lower transducer to the total radiated energy. The latter causes destructive interference in signals generated across the lower transducer face, hence rejection of a portion of that power impinging on the trasnducer. The shape of the sound amplitude or velocity field equivalent for two finite circular transducers is governed by ordinary hydrodynamics. R. Bass (J. Acous. Soc. Am. 30,602 (1959)) presents calculations on the theory. We had to extend these to shorter distances between

transducers, with a new expansion of the integrand in the integral representation of the loss factor. We also verified the additivity of diffraction losses to true absorption, intuitively and numerically. Details of all our calculations will be presented later in this Appendix.

The apparent diffraction loss Q depends upon the absolute delay rod spacing z, obtained from the micrometer reading through an additive constant h_o. This constant was occasionally measured for the assembled apparatus. Thus we represent the total measured attenuation (translated from the nominal attenuation setting) α_i^{kn} as

$$\begin{aligned} \alpha_i^{kn} &= A_i^{kn} + Q(z) \\ &= A_i^{kn} + Q(h_i^{kn} + h_o), \end{aligned}$$

where A is the true sample absorption plus any random errors. The actual least-squares fit is then

$$A_i^{kn} = {}_n^k h_i^{kn} + b_n^k .$$

-Thirdly, we assign estimated errors to each data point α_i^{kn}. First is a constant error σ_1 from random fractional changes in signal amplitude, in turn due to generator fluctuations or to sound-refracting convection in the cell. σ_1 is given in our original notebook work and in our computing in terms of equivalent fluctuations in CRO display height at a nominal total height of I_o (=7 cm. usually). We take σ_1 to be 0.06 cm. for our runs, which converts to 0.074 db. Second is a scope-reading error σ_2 in matching

comparison and received signals, roughly 0.15 mm. for us. Mismatch of the traces by a height σ_2 at a nominal display height of $\underline{I} = \underline{I_o}\ \underline{e}^{-a/8.686}$, where a is attenuation as usual, gives an error in attenuation δa,

$$\begin{aligned}\delta a &= \left(\frac{\partial a}{\partial I}\right)\delta I \\ &= \left(\frac{1}{8.686\ I}\right)\sigma_2 \\ &= \frac{\sigma_2}{8.686\ I_o}\ e^{a/8.686}.\end{aligned}$$

The net estimate error is

$$\sigma_i^{kn} = \frac{1}{8.686\ I_o}\left[(\sigma_1)^2 + (\sigma_2\ e^{a_i^{kn}/8.686})^2\right]^{\frac{1}{2}}.$$

This error estimate is used first to weight the data points relative to one another, for we perform the least-squares fit by minimizing the error function

$$\chi^2_{kn} = \sum_i \left(\frac{A_i^{kn} - \alpha_n^k\ h_i^{kn} - b_n^k}{\sigma_i^{kn}}\right)^2.$$

Clearly, data points at high attenuations are weighted less, as they are more error-prone. For the averaging fit of the α_n^k to α^k, the estimated error σ_{kn}^{α} in each α_n^k is compounded from the presumably independent pointwise errors σ_i^{kn},

$$(\sigma_{kn}^{\alpha})^2 = \sum_i \left(\frac{\partial \alpha_n^k}{\partial A_i^{kn}}\right)^2 (\sigma_i^{kn})^2.$$

Similarly, α^k, our best approximation to the true sample absorption, is a weighted average,

$$\alpha^k = \sum_n \frac{\alpha_n^k}{(\sigma_{kn}^\alpha)^2} \Big/ \sum \frac{1}{(\sigma_{kn}^\alpha)^2} ,$$

from minimizing

$$\chi_k^2 = \sum_n \left(\frac{\alpha_n^k - \alpha^k}{\sigma_{kn}^\alpha} \right)^2 .$$

Its error compounds as

$$(\sigma_k^\alpha)^2 = \sum_n \left(\frac{\partial \alpha^k}{\partial \alpha_n^k} \right)^2 (\sigma_{kn}^\alpha)^2$$

$$= \frac{1}{\sum_n (\sigma_{kn}^\alpha)^2} .$$

All the fits and error computations are done in a comprehensive computer program, which is flowcharted later. σ_k^α is not necessarily the final estimated error, and it is not the only information we have on error levels--we also have χ^2_k. The rescaling of errors and final confidence levels in the α^k are discussed under the sixth heading here.

-Fourthly, in both the N_k individual linear fits for the α_n^k and the final averaging for α^k, we exercise the option of deleting data points on either of two grounds. The first ground is automatic: a 3-d test is run on each data point i in turn. This means that a_i^{kn} and h_i^{kn} are tentatively deleted and a new fit made to the remaining N_{kn}-1 points. If the point i ends up more than 3 standard dev-

-iations 3 $\sigma_n^k(i)$ from the line of tentative fit, it is permanently deleted:

$$\text{Compute } R = \left| \frac{A_i^{kn} - \alpha_n^k(i) h_i^{kn} - b_n^k(i)}{\sigma_i^{kn}} \right| ;$$

$$\text{If } \begin{cases} R \geq 3, \text{ delete the point} \\ R < 3, \text{ retain it.} \end{cases}$$

More than one point may be a candidate for deletion, but the program took only the latest one; we redid several choices by hand, taking the one giving the lowest χ_k^2 (the notebook 5096 is corrected as of 7/13/71). Overriding the program choice in the case of nearly equivalent deletions calls for discretion, and is discussed in section 6, with details. If there were fewer than 4 data points to begin with, $N_{kn} < 4$, the 3-d test could not be run.

The second ground for rejection is the discretion of the user. Optional input to the computer program forces a deletion of the point i and displays the resulting α_n^k or α^k. In the former case, it does not alter the automatic inclusion of α_n^k from the automatically-selected 'best' deletion in the final averaging for α^k. If the deletion, on the basis of some observation during the experiment (recorded in the notebook), looks like a more reasonable and reliable course, the final α^k must be manually recomputed. We exercised this option several times, but did not choose to alter the automatic results. We also tried some forced deletions in the final averaging of the α_n^k and did excise a

number of runs.

-Fifthly, we tested for the presence of other systematic errors. The most likely error is a constant mismatch of the CRO displays in one direction (so it is not random). Since the received signal has a fluttering noise band at the outer edge of its envelope, we might by accident take the outer fringe of the total (noise + received signal) envelope to match the edge of the comparison envelope. Another possible error is insufficiency of the diffraction corrections. Either error changes the form of the equation our data should fit; our first guess was a quadratic,

$$A_i^{kn} = \gamma_n^k (h_i^{kn})^2 + \alpha_n^k h_i^{kn} + b_n^k.$$

Now, the reduction of the data to net error functions χ^2_{kn} is not an adequate indication of the systematic error. That is, a quadratic fit yielding a lower χ^2 than a linear fit is not necessarily preferred. F. Sculli of physics clarified this in several discussions we had (notebook 5090: 123-4; 5096: 76); least-squares fits are simply not good indicators of systematic error, except in the following sense. If the quadratic coefficient γ_n^k improves χ^2 and also ends up with an attached error σ_{kn}^{γ} sensibly smaller than itself, say $\sigma_{kn}^{\gamma} < \frac{1}{2}\gamma_n^k$, then it is probably warranted in the data representation. Conversely, inclusion of a γ_n^k which has an error $\sigma_{kn}^{\gamma} \gtrsim \gamma_n^k$ is unwarranted regardless of its effect on χ^2 and does not represent the systematic error.

The quadratic terms in our typical tests were small, but they drastically altered α_n^k and increased σ^{α}_{kn} (notebook 5096: 63). We analyzed the form of the matching error more carefully. Consider a received signal at zero attenuation with envelope height I_1 composed of the true received signal envelope I_1^o plus a constant noise band c. It is matched to the comparison signal I_o, at a micrometer reading h_o:

$$I_1 + c = I_o.$$

Now, at an apparent attenuation of n db, the received signal is actually attenuated by n_o db:

$$\begin{aligned} I_o' &= I_o e^{-n/8.686} \\ &= (I_1') + c \\ &= I_1^o e^{-n_o/8.686} + c. \end{aligned}$$

Here n_o is presumably linear with acoustical path,

$$n_o = \alpha(h_n - h_o).$$

Rearranging, we find the relation of n_o and n to be, for small c,

$$n_o \simeq n + 8.686\left(\frac{c}{I_o}\right)\left(e^{n/8.686} - 1\right) = \alpha(h_n - h_o),$$

and so a better equation for least-squares fitting the A_i^{kn} is

$$A_i + \underbrace{8.686\gamma\left(e^{A_i/8.686} - 1\right)} = \alpha h_i + b.$$

Trials of this equation showed a strong coupling of γ and α (large changes in α and large values of σ^{γ} and σ^{α}), which were recognized as coming from the A_i-like term in the underbracketed term above. This was deleted to give

$$A_i + \gamma\left[8.686(e^{A_i/8.686}-1) - A_i\right] = \alpha h_i + b.$$

Now α was not drastically altered from its linear fit value. Significantly, in all conditions $\underline{k}$, γ was small and $\sigma^{\gamma} \gg \gamma$, so we concluded there is no significant systematic error we had not corrected.

-Sixthly: Eventually, we had all our results $\{\alpha_n^k; \sigma_{kn}^{\alpha}; \chi_{kn}^2\}$ and $\{\alpha^k; \sigma_k^{\alpha}; \chi_k^2\}$. These are partly reproduced in Table II. In four runs $\underline{kn}$ we chose to reject the point deletion giving the lowest $\chi_{\underline{kn}}^2$. In three cases ($\underline{k}$=[$\underline{X}$=0.2132, $\underline{T}$=34.66, $\underline{f}$=4.5], $\underline{n}$=5; $\underline{k}$ =[0.0436,33.84,4.5],$\underline{n}$=4; and $\underline{k}$ = [0.0664,32.66,4.5],$\underline{n}$ =1) there were two deletions giving very similar χ_{kn}^2 and σ_{kn}^{α} but very different α_n^k (points 4&1, 5&1, 6&1, respectively), so we averaged them. In the fourth case ($\underline{k}$ =[0.0288,34.64,7.5],$\underline{n}$ =3), deleting point 5 gave a slightly better χ_{kn}^2 than did deleting point 4, but also a much larger σ_{kn}^{α}, so we chose the latter.

No entire run $\underline{kn}$ was rejected automatically by the 3-d test in averaging. We rejected some runs in each of 3 conditions $\underline{k}$ on extrinsic grounds. For $\underline{k}$ =(0.0722,32.66, 7.5) we eliminated runs 1-3, which were noted during experiments as having unusual signal tuning. They also gave very much different α_n^k than the last 3 runs. For the two states $\underline{k}$ =(0.0664,32.66,7.5 and 10.5) we took only the good-tuning reruns, and in the first of these we also rejected the first rerun, noted as having less reliable tuning.

The complete set of reduced data can be examined

in a computer output binder on file, containing the original output in a fully explanatory format. Deletions on discretion noted above, as well as manual selections of the best deletions over the original program's automatic choice of latest deletion, are noted in a separate standard portfolio, which also contains the raw data, program listings, condensed output (from punched cards), and table of deletions for all states.

The results are to be interpreted as follows. The relative error estimates for the data points A_i^{kn} or for whole runs α_n^k are probably accurate, for weightings in their respective fits. The absolute error levels, however, may not be. If we desired our error estimates σ_1, σ_2 to represent bounds on the true error with a confidence level of C (say, 50%), then the grand average of $\chi^2_{kn}/(N_{kn}-F) = \chi^2_{kn}/(N_{kn}-2)$, $\bar{\chi}^2$ (F =degrees of freedom in fit) should reflect this value of C. Thus $\bar{\chi}^2$ should be 1 for C =50%; 1/9 for C =95%; etc.). The specific relation is

$$C = \int_{\bar{\chi}^2}^{\infty} e^{-P^2} dP.$$

$\bar{\chi}^2$ should be adjusted to the proper level by uniformly rescaling all the errors σ_1, σ_2:

$$\left.\begin{aligned}\sigma_1 &\to Po_1\\ \sigma_2 &\to Po_2\end{aligned}\right\} \Longrightarrow \sigma_{kn} \to P\sigma_{kn} \Longrightarrow \begin{cases}\chi^2_{kn} \to P^{-2}\chi^2_{kn}\\ \chi^2_k \to P^{-2}\chi^2_k\\ \bar{\chi}^2 \to P^{-2}\bar{\chi}^2\end{cases}$$

Choose P to give proper $\bar{\chi}^2$.

This is a legitimate adjustment in the least-squares technique, as much as we can do without taking additional measurements to establish that σ_1 and σ_2 should scale differently. New error estimates change the results of the 3-d tests of course, and the whole data set should be rerun. If the new 3-d tests do not significantly alter the choice of data deletions, then the iterated $\bar{\chi}^2$ should still be near its desired value. We note that the σ's should represent 50% intervals for the 3-d test as given on p. 190; the break factor R should be adjusted for any other confidence level.

In practice, we decided that the N_k groups of data seta for the k conditions are more on an equal footing of reliability than the N_{kn} individual data sets. Thus we computed $\bar{\chi}^2_{..}$ and the tentative rescale parameter P as

$$P = (\bar{\chi}^2_{old})^{-\frac{1}{2}} = \left(\frac{1}{N}\sum_k\left[\frac{\sum_n \chi^2_{kn}}{N_k}\right]\right)^{-\frac{1}{2}}.$$

Our initial estimates of the σ's were too conservative, as our first P value was 0.30. We redid all the fits and got a more acceptable $\bar{\chi}^2$. Interestingly, the new P broken down by frequency f_k showed a systematic trend,

f, MHz.	P	f, MHz.	P
4.5	0.48	13.5	0.72
7.5	0.76		
10.5	0.52		

This probably indicates that σ_1, σ_2 are not the same for all $\underline{f}$ due to differences in envelope shape, generator stability, etc. We did a 'final' rescaling, different for each $\underline{f}$, using the computed $\underline{P(f)}$ on the previous page. We readjusted σ_k^{α} and χ_k^2, but did not redo the fits.

Finally, we did a further averaging of the new σ_k^{α} over the three isotherms $\underline{T}$ for any given $\underline{X}$ and $\underline{f}$, since α_k^k and σ_k^{α} varied little with $\underline{T}$. We obtain better statistics on σ_k^{α}. Unfortunately, one flaw remained in our data: the average $\chi_k^2/(\underline{N_k}-1)$, $\bar{\chi}_k^2$, which measures the scatter of the results α_n^k about α^k, was too large. While the data points in individual runs scattered little--the correct amount after rescaling, the results α_n^k scatter more than the errors σ_{kn} from data point scatter would indicate. Since the final errors σ_k^{α} are the most importnat, we rescaled errors once more, doubling all σ's. Then the average over $\underline{k}$ of $\bar{\chi}_k^2$ came to near unity.

In the final results in Table III, we quote $\alpha_{ex}/\underline{f}^2$, after subtracting classical shear losses $\alpha_{cl}/\underline{f}^2$ and a mode conversion correction discussed immediately below. The errors σ_k^{α} collapsed over the 2 or 3 isotherms, σ_{Xf}^{α}, indicate the bounds of the corresponding $\alpha^{XfT} = \alpha^k$. The associated confidence levels χ_{Xf}^2 are collapsed once more over $\underline{f}$ to a χ_X^2, which indicates the confidence one can have that the errors σ_{Xf}^{α} truly represent the error bounds. The χ_X^2 average to unity, of course, but the value for each $\underline{X}$ may

scatter around this. The scatter may be real, and so we do report the individual X_X^2.

Our data looked good as far as error estimates were concerned. Still, it had indications of one last systematic error, this one in frequency and not in attenuation readings. At high mole fractions of lutidine, far from the compositions showing chemical or critical relaxation, mixtures should behave as Kneser liquids with high relaxation frequencies. The frequency dependence of α/f^2 should be nil. Also, any f-dependence of α/f^2 that does develop toward lower X should consist of a monotonic decrease with increasing f. However, the four most concentrated mixtures,

$\underline{X}$ = 0.9901, 0.427, 0.3823, and to some extent, $\underline{X}$ = 0.3042, the values of $\alpha/\underline{f}^2$ at 7.5 MHz. dip lower than those at higher $\underline{f}$. Also, the values at 4.5 MHz. are notably higher than the values at 10.5 and 13.5 MHz.; the rise at 4.5 MHz. is too rapid even for strong thermal relaxation at low frequency of unknown origin.

The possible errors in $\alpha/\underline{f}^2$ at $\underline{f}$ = 4.5 and 7.5 MHz. tie in with observations during the experiments that at these same frequencies the ultrasonic pulses showed unstable shape and extra oscillations in amplitude versus height. After some searching in the acoustics literature, we finally discovered a reference to a similar phenomenon in Puls' thesis (ref. 19, paper II), called mode conversion. The sound pulse is slowed and distorted at the walls as it travels down the delay rod, forming a longer, self-interfering wavetrain. The oscillatory displacement of the delay rod face, generating sound in the liquid sample, is then not plane; not of the same amplitude and phase across the face; i.e., not of a pure vibration mode. A recent journal article (H.J. McSkimin, J. Acous. Soc. Am. 31,287(1959)) suggests breaking up the spurious modes by roughing the rod walls, as by cutting a screw thread in them (Puls). Since mode conversion (MC) causes spurious spreading and interference in the beamed sound pulse much as diffraction does, it is likely an additive attenuation. The net loss probably depends upon the total range of micrometer readings, so a

simple uniform correction depending upon $\underline{f}$ but not the value of α is not justified. However, $\alpha/\underline{f}^2$ does not vary much with $\underline{X}$ at these high concentrations of lutidine, so we will apply a uniform correction of -30 ($\times 10^{-17}$ Np. cm.$^{-1}$ sec.^{2}) to $\alpha/\underline{f}^2$ at $\underline{f}$ = 4.5 MHz., and a similar one of +8 in these units at $\underline{f}$ = 7.5 MHz. Toward lesser $\underline{X}$ this is not accurate but $\alpha/\underline{f}^2$ grows so large that a small feature in error does not qualitatively change our data or its interpretation.

Our final $\alpha/\underline{f}^2$ data for the 144 conditions of $\underline{X}$, $\underline{T}$, and $\underline{f}$ are reported in Table III, after incorporation of the MC correction and after subtraction of the classical loss $(8\pi^2\eta_s)/(3\rho\beta^3)$ listed at the side. Water data are taken from the literature, since MC problems here swamped the measurements.

Velocity

The velocity data are composed of one set of micrometer height ($\underline{h}$): signal delay ($\underline{t}$) readings for each of the conditions $\underline{k}$, except for a very few cases with two or three sets. One linear least-squares fit reduces each data set to a velocity ,

$$h_i^k = \beta^k t_i^k + c^k \ .$$

The frills in the reduction scheme parallel those for α :

(1) Some poor data sets were rejected outright and the run remade immediately during the experiments.

(2) delay time readings, from the variable sweep delay dial of the CRO, are corrected to the true delay times

according to the calibration made with a Beckman counter, as noted in Appendix III. A quadratic fit of the true delay to the dial readings was used (notebook 5096: 81). This is a very minor correction.

(3) we assign errors to each delay reading, σ_i^k. The inherent reproducibility, high accuracy, and low data scatter we noticed suggests that our main dial error is the failure to read half-divisions, so we picked $\sigma_i^k = 0.005$ turns uniformly. Each turn represented a delay of 5 μsec. usually. We obtain a confidence level function χ_k^2 and an estimated error bound σ_k for each run.

(4) we had a feature to delete data points automatically or on discretion. The 3-d tests were used uniformly, selecting the one giving the best χ_k^2, by hand if necessary. One run had an obvious error in recording of one delay reading, which we corrected manually.

(5) quadratic fits were made to test for systematic errors, and again none were found.

(6) the error information σ_k and χ_k^2 were interpreted as for κ. Our initial fits indicated a rescale of error to an almost uniform 0.1%. We think 0.3% is a more reliable estimate for all states k. Only the 4.5 MHz. values are reliable, free of the systematic error from envelope-shape change discussed in Appendix III--except that the underlined ρ's at f = 7.5 or 10.5 MHz. were done by the tedious peak-watching technique and are also reliable. The

results are given, without the trivial σ_k or χ^2_k, in Table III.

Fit Program 'Flowchart' and General Organization

A FORTRAN program was written for the IBM system 360/370 to fully process the raw data for absorption and velocity. Input is divided into groups, one for each of the 144 conditions (X,T,f). Each group is composed of first the α data, then the β data. The first card in the group is an (X,T,f) identification and remark card. An optional card before this (recognized by its format) may update the estimates of the micrometer-to-acoustical path correction h_o and of the zero-db display height I_o. Another optional format-recognized card (OFRC) before the actual absorption data updates the error estimates σ_1, σ_2; and another before the velocity data updates o for that data. The entire program is too large to list in the thesis, just as is the raw data set; both are on file in a computer binder and in a standard portfolio. The FORTRAN-style outline follows, keyed to actual statement numbers.

(final version)

```
 2 read X,T,f,title
     if OFRC, read h_o,I_o
   reread X,T,f,title
   if X=X_o go to 10
     store new X_o
     write compendium of results for old X_o
10 write title; new h_o,I_o if changed

        [α section]

   read N_k
     if N_k = 0, go to 220 (β section)
```

do 100 n = 1,N_k
read N_{kn}
if OFRC, read σ_1, σ_2
write title
read the h_i^{kn} and echo them; convert to z values for diffraction correction; assume the a_i^{kn} are in progression from 0 to $N_{kn}-1$ unless another OFRC tells us it starts from n_o
compute diffraction corrections $Q(h_i^{kn} + h_o)$ by interpolating data table cubically; first correct table to proper f
write out A_i^{kn} for inspection
compute σ^2
call for linear fit; routine called writes out all the relevant information $\alpha_n^k, \sigma_{kn}^{\alpha}$, and χ^2_{kn} and returns all for later averaging; also returns flag to denote if, and which, data point was deleted
(do optional discretionary deletions and refits)
read M_{kn} = no. of purges to be run on this one data set
call linear fit, printing same as above (do not store results)
call quadratic or other nonlinear fit
100 (call purged nonlinear fit)
write out compendium of results for linear fits for conditions k, plus averaging of same esp. for rescale parameter
call point-fit (average) of all the α_n^k; routine called prints all results α^k, σ_k^{α}, and χ_k^2
(call purged point fits)
write out compendium of results for nonlinear fits
call average of all α_n^k for nonlinear fits
(call purged fit of same)

section

read N_k (0 or 1)
if N_k= 0, go to 2 for next group of data
read N_{1k}, σ; convert latter to σ_i^k (same for all i)
read the h_i^k, t_i^k and echo them
correct t_i^k by parabolic fit
call linear fit, printing b^k, χ_k^2
(formerly, call quadratic fit)
go to 2

terminates by read error, end of data set

Diffraction Corrections

Much of this section is a rewrite or condensation of extensive information in notebook 5090: 48 ff. We give little text, so the presentation is somewhat rough, to keep its size down.

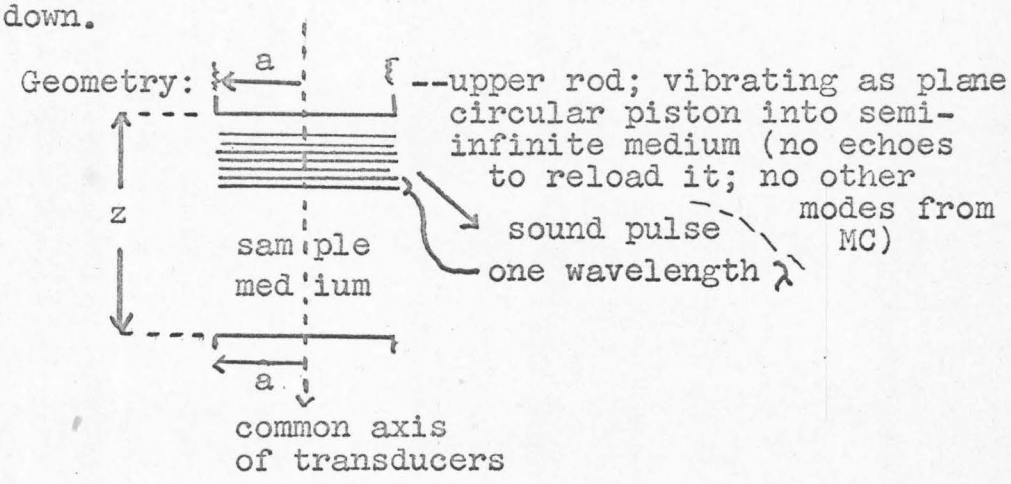

Sound pattern depends upon a/λ, z/λ, or a/λ, z. In our system a is fixed, λ ranges over 4 discrete values corresponding to the 4 frequencies, and z varies continuously from $\simeq 0.6a$ to $7a$. Compute average sound pressure on the lower rod face $\langle P \rangle_{av}$:

$$\langle P(z) \rangle_{av} = \int_0^a \frac{dr 2\pi r P(z,r)}{\pi a^2} \quad \text{, implicit function of } a/\lambda$$

$$P(z,r) = i\omega\rho_o \varphi(z,r), \quad \varphi = \text{velocity potential}$$

$$\varphi(z,r) = \beta_o a \int_o^\infty e^{-\mu z} J_o(sr) J_1(sa) \frac{ds}{\mu}$$

J_n = Bessel function of order n
β_o = sound velocity in medium
$\mu = (s^2 - k^2)^{\frac{1}{2}}$
k = propagation constant $= 2\pi/\lambda$

From A. O. Williams, Jr., J. Acous. Soc. Am. 23,1(1951), omitting many steps:

$$\langle \Psi(z) \rangle_{av} = \frac{2\mathfrak{P}_o}{a} \int_0^\infty du^{-1} e^{-sz} \frac{J_1^2(sa)}{sa}$$

and using integral representations of the Bessel functions

$$= \frac{4\mathfrak{P}_o}{\pi ik} \int_0^{\pi/2} d\theta \sin^2\theta \left[e^{-ikz} - e^{-ik(z^2+4a^2\cos^2\theta)^{\frac{1}{2}}} \right],$$

which reduces to Bass' final expression for $\langle P(z) \rangle_{av}$ by multiplying by $i\omega\rho_o$. Our interest is in the ratio $\underline{R}$ of $\langle P(z) \rangle_{av}$ to the perfect plane wave pressure $\langle P_o(z) \rangle_{av} = \rho\mathfrak{P}_o\omega e^{-ikz}/k$,

$$R = 1 - \frac{4}{\pi} \int_0^{\pi} e^{-ik\left[(z^2+4a^2\cos^2\theta)^{\frac{1}{2}} - z\right]} \sin^2\theta d\theta$$

$$\equiv 1 - I.$$

$\underline{I}$ has no closed form. Williams expands the integrand in powers of $\cos\theta$, changes variables, and gets an analytic form good for $(4ka)/(z/a)^5 \ll 2\pi$ and $(ka^4)/z^3 \ll 1$. We want to treat $z/a \gtrsim 0.6$ and $ka \approx 230\text{-}700$, while Williams' expression does not converge at the lower range of z/a.

Bass changes variables:

$$\zeta = \frac{k}{2}\left[(z^2+4a^2)^{\frac{1}{2}} - z\right]$$

$$= \left[(z^2+4a^2\cos^2\theta)^{\frac{1}{2}} - z\right] / \left[(z^2+4a^2)^{\frac{1}{2}} - z\right]$$

$$I \to \frac{2}{\pi} \int_0^1 \left[1 - \alpha(1-2u)\right] \left[\frac{1+\alpha u}{1+\alpha u - \alpha}\right]^{\frac{1}{2}} \left[\frac{1-u}{u}\right]^{\frac{1}{2}} e^{-2i\zeta u} du,$$

where for compactness $\alpha = (\zeta/ka)^2$.

Now, integrals $\underline{I}_n = \int_0^1 du e^{-2i\zeta u} u^n \left(\frac{1-u}{u}\right)^{\frac{1}{2}}$ can be expressed in terms of a few Bessel functions, as by identifying the integral with a confluent hypergeometric function

(M. Abramowitz and I. Stegun, Handbook of Mathematical Functions, N.B.S., Washington, D.C., 1964 ; p. 505). Also Bass implies

$$I_o = \frac{\pi}{2}\left[J_o(\zeta)+iJ_1(\zeta)\right]e^{-i\zeta}.$$

Using $I_n = \frac{i}{2}\frac{d}{d\zeta}I_{n-1}$ and the J_n recursion relations to reduce all Bessel functions to J_o, J_1, we find

$$I_1 = \frac{i\pi}{4\zeta} J_1 e^{-i\zeta} \quad \text{(argument of J implicitly } \zeta\text{)}$$

$$I_2 = \frac{i\pi}{8\zeta^2} e^{-i\zeta}\left[\zeta J_o-(2+i\zeta)J_1\right]$$

$$I_3 = \frac{\pi}{16\zeta^3} e^{-i\zeta}\left[(3\zeta+2i\zeta^2)J_o-(6+4i\zeta-2\zeta^2)J_1\right]$$

$$I_4 = \frac{i\pi}{32\zeta^4} e^{-i\zeta}\left[(-12\zeta-9i\zeta^2+4\zeta^3)J_o+(24+18i\zeta-11\zeta^2 -4i\zeta^3)J_1\right].$$

We still have to expand the factor in the integrand

$$f(u) = \left[\frac{1+\alpha u}{1+\alpha u-\alpha}\right]^{\frac{1}{2}}$$

in polynomial form. Bass expands about $u = 0$, but this won't converge for small z/a (large α). Instead we expanded about $u = \frac{1}{2}$ arbitrarily and gathered powers of u. Terms to u^3 adequately represented f(u) in the important range $z/a \geq 0.5$ for u in the range 0,1:

$$f(u) \simeq \sum_{n=0}^{3} \frac{f^{(n)}(\frac{1}{2})}{n!}(u-\tfrac{1}{2})^n$$

$$= A' + B'u + C'u^2 + D'u^3.$$

Total integrand:

$$g(u) = \left[1+\alpha(1-2u)\right] f(u) \simeq \sum_{n=0}^{4} c_n u^n$$

and

$$I = \frac{2}{\pi}\int_0^1 du\, g(u)\left(\frac{1-u}{u}\right)^{\frac{1}{2}} e^{-2i\zeta u}$$

$$\simeq \frac{2}{\pi}\sum_{n=0}^{4} c_n \int_0^1 du\, u^n \left(\frac{1-u}{u}\right)^{\frac{1}{2}} e^{-2i\zeta u}$$

$$= \frac{2}{\pi}\sum_{n=0}^{4} c_n I_n \,.$$

Gathering terms in ζ^n:

$$R = 1-I$$

$$= 1-2e^{-i\zeta}\left[\frac{J_0}{3}\left(-i\frac{3}{8}c_4+\left\{\frac{9}{32}c_4+\frac{3}{16}c_3\right\}\zeta+\frac{i}{8}\left\{c_4+c_3+c_2\right\}\zeta^2 + \frac{c_0}{2}\zeta^3\right)\right.$$

$$+\frac{J_1}{-4}\left(i\frac{3}{4}c_4-\left\{\frac{9}{16}c_4+\frac{3}{8}c_3\right\}\zeta-\frac{1}{32}\left\{11c_4+8c_3 +8c_2\right\}\zeta^2+\frac{1}{8}\left\{c_4+c_3+c_2+2c_1\right\}\zeta^3+\frac{i}{2}c_0\zeta^4\right)\Big]$$

where

$$c_0 = (1-\alpha)A' \;/\; c_1 = 2\alpha A'+(1-\alpha)B' \;/\; c_2 = 2\alpha B'+(1-\alpha)C'$$

$$c_3 = 2\alpha C'+(1-\alpha)D' \;/\; c_4 = 2\alpha D'$$

and

$$A' = A - \tfrac{1}{2}B + \tfrac{1}{4}C - D/8 \qquad B' = B - C + \frac{3}{4}D$$

$$C' = C - \frac{3}{2}D \qquad D' = D$$

and

$$A = b/c \qquad B = -\alpha^2/2bc^3 \qquad C = \frac{\alpha^3(4+\alpha)}{8b^3c^5}$$

$$D = \frac{\alpha^4(4+2\alpha+\alpha^2)}{8b^5c^7}$$

and

$\alpha = \gamma^2/(ka)^2$; $\gamma = \frac{k}{2}\left[(z^2+4a^2)^{\frac{1}{2}} - z\right]$; z,k,a are given in the dimensions of the problem.

The complex response ratio R is converted to an effective db loss Q,

$$|R| = e^{-Q/8.686} \rightarrow Q = 8.686 \ln|R| .$$

Q was computed for my system for a = 12.7 mm. (fixed), for four frequencies f = 4.5, 7.5, 10.5, and 13.5 MHz. (for 4 values of propagation constant k, that is), and in turn for a grid of heights z (hence for γ or α) from about 8 to 66 mm. in steps of 2 mm. (and later out to 80 mm.). Several sound velocities were tried without changing the results noticeably, so we settled on a standard β of 1570 m./sec. The FORTRAN computer program to do the work is listed in the pages stapled in notebook 5090: 52. Its input consists of: the number of classes of velocity (and absorption--explained later), and labels; number of frequencies and the f_i; a and β; the grid of z_i; absorption α; and print option parameters. It is extensively commented and easy to use. Our results in Table IV check with Bass' for larger z/a. The apparent loss factor Q was monotonic for all f in my range of z, even at very low z. This verifies that diffraction is not the cause of signal oscillation with micrometer height, and reinforces the judgment that mode conversion is the real cause.

Bass notes that non-zero absorption α can be

accommodated in the formalism by making the propagation constant $\underline{k}$ complex, $\underline{k} = 2\pi/\lambda - i\alpha$ (distinguish absorption α from $\alpha = \nu^2/(ka)^2$). The goal here is to show that $\underline{Q}$ from diffraction is additive to absorption losses for all practical purposes:

$$Q(\alpha,z) \simeq Q_0(z) + \alpha z$$

$$Q(\alpha,z) = Q_1(z) + \alpha z,$$

that is, that $\underline{Q}_1 \simeq \underline{Q}_0$. We wrote new routines to compute the Bessel functions of complex argument ν. Rather than rewrite in complex arithmetic the computing center routines which are more general than we need, we noticed that ν is large enough even at z/a as small as 0.5 (Reν ranges from 35.4 to 503 in our work) to use asymptotic expansions (Abramowitz and Stegun, p. 364):

$$J_0(z) \simeq \left(\frac{2}{\pi}\right)^{\frac{1}{2}} z^{-\frac{1}{2}} \left\{ \left(1 - \frac{9}{128z^2} + \frac{3675}{32768z^4}\right)\cos\left(z - \tfrac{1}{4}\pi\right) + \left(-\frac{1}{8z} + \frac{75}{1024z^3}\right)\sin\left(z - \tfrac{1}{4}\pi\right) \right\}$$

$$J_1(z) \simeq \left(\frac{2}{\pi}\right)^{\frac{1}{2}} z^{-\frac{1}{2}} \left\{ \left(1 + \frac{15}{128z^2} - \frac{14175}{32768z^4}\right)\cos\left(z - \tfrac{3}{4}\pi\right) + \left(\frac{3}{8z} - \frac{105}{1024z^3}\right)\sin\left(z - \tfrac{3}{4}\pi\right) \right\}$$

These expansions are used with standard complex double precision sin and cos routines, CDSIN, CDCOS.

Since cos z, sin z can be written as $\frac{1}{2}(e^{iz}+e^{-iz})$, $\frac{1}{2i}(e^{iz}-e^{-iz})$, the form of $e^{-i\nu}J_0(\nu)$ in the expression for $\underline{R}$ (hence $|\underline{R}|$, $\underline{Q}$) can be seen as dominated by the lead term $e^{-i\nu}e^{i\nu} = 1$ for any complex $\underline{z}$, if its imaginary part is

small. Thus corrections from nonadditivity of diffraction and true absorption require Im $\underline{k} = \alpha$ to approach the order of magnitude of Re $\underline{k} = 2\pi/\lambda$, which never occurs in our experiments. We proceeded with the calculations and obtained results $\underline{Q_1(z)}$ indistinguishable from $\underline{Q_0(z)}$ (additions to notebook 5090: 52). They are not reported in Table IV.

Table I. Sample of Raw Ultrasonic Data

Order of data explained in text; formats given in program listing

```
  0.1238 34.66  4.51DATA 2/25/70 BY VPG; THIS RUN STARTS TRAD'N OF BETA AT 4.5 M
HZ ONLY, NEW WAY; 5 DB READING IN 3RD RUN IS W/ POOR LIQ. CONTACT
  3
  6
 29.00 37.93 47.25 55.95 64.85 74.08   .     .     .     .     .     .     .
  6
 29.10 38.37 47.30 56.35 66.38 75.00   .     .     .     .     .     .     .
  6
 29.00 38.09 47.72 57.18 66.22 75.57   .     .     .     .     .     .     .
  1
  5  5.00D-06
 70.00 60.00 50.00 40.00 30.00
 09.00 07.72 06.44 05.16 03.89   .     .     .     .     .     .     .     .
  0.1238 34.66  7.52DATA 2/25/70 BY VPG; LAST 7.5 MHZ BETA; SIGNAL UNSTEADY, ESP
. BETWEEN 1,2 DB. IN 1ST RUN
  2
 10
 29.00 34.84 41.45 46.00 50.81 55.59 60.46 64.52 69.26 73.70   .     .     .
 10
 31.17 36.25 40.87 46.30 51.52 56.32 60.80 65.29 70.40 75.00   .     .     .
  1
  5  5.00D-06
 70.00 60.00 50.00 40.00 30.00
 09.09 07.81 06.54 05.26 04.00   .     .     .     .     .     .     .     .
  0.1238 34.66 10.53DATA 2/25/70 BY VPG

  2
 13
 29.00 31.79 34.48 37.20 39.97 43.83 45.50 48.00 51.06 53.68 56.28 58.88 62.01
 13
 31.53 34.36 36.81 39.76 42.76 45.58 48.39 51.13 54.11 56.70 59.65 62.43 65.00
  0
  0.1238 34.66 13.53DATA 2/25/70 BY VPG; SIGNAL BOUNCE  AT 5-6 DB 1ST RUN, 4-3 D
B IN 2ND RUN ; RETUNED FOR 2ND RUN
  2
 13
 29.00 30.98 32.92 34.87 35.76 37.58 39.84 41.34 43.16 45.06 47.25 49.07 51.04
 13
 29.90 32.08 33.85 36.12 37.62 39.63 41.60 43.56 45.32 47.42 49.34 51.12 53.00
  0
  0.1238 33.46 13.53DATA 2/25/70 BY VPG;

  2
 13
 29.00 30.99 32.86 34.77 36.77 38.62 40.49 42.43 44.26 46.15 48.11 49.99 51.92
 13
 30.94 33.02 34.78 36.49 38.42 40.31 42.25 44.16 46.16 48.14 50.11 52.06 54.00
  0
  0.1238 33.46 10.54DATA 2/25/70 BY VPG;

  2
 13
 29.00 31.93 34.67 37.21 40.34 43.07 46.30 49.15 51.99 54.94 57.73 60.51 63.48
 13
 30.44 33.26 36.19 38.84 41.74 44.62 47.55 50.58 53.34 56.34 59.10 61.84 65.00
  0
  0.1238 33.46  7.54DATA 2/25/70 BY VPG; 9 DB IN 3RD RUN UNUSUAL
```

```
 3
10
29.00 34.03 38.90 43.84 48.78 54.02 58.78 63.40 68.06 72.97   .     .     .
10
29.58 34.51 39.79 45.16 50.58 55.58 60.75 65.70 70.37 75.00   .     .     .
10
29.00 34.08 39.64 44.65 49.71 54.33 59.66 64.41 69.24 71.39   .     .     .
 0
 0.1238 33.46  4.52DATA 2/25/70 BY VPG

 3
 5
29.00 39.08 48.17 57.38 67.23   .     .     .     .     .     .     .     .
 5  1
36.45 46.10 55.67 64.90 74.00   .     .     .     .     .     .     .     .
 5
29.00 39.39 48.78 58.05 67.53   .     .     .     .     .     .     .     .
 1
 5  5.00D-06
70.00 60.00 50.00 40.00 30.00
09.00 07.72 06.44 05.16 03.88   .     .     .     .     .     .     .     .
 0.1238 32.66  4.52DATA 2/25/70 BY VPG; POOR T(ENCL.) CONTROL

 5
 5
29.00 39.07 49.37 59.61 69.56   .     .     .     .     .     .     .     .
 5
31.39 41.97 51.67 61.40 71.00   .     .     .     .     .     .     .     .
 5
29.00 39.53 49.58 58.45 67.74   .     .     .     .     .     .     .     .
 5
31.35 40.56 51.52 60.58 70.00   .     .     .     .     .     .     .     .
 5
29.00 38.82 47.85 57.70 67.62   .     .     .     .     .     .     .     .
 1
 5  5.00D-06
70.00 60.00 50.00 40.00 30.00
08.00 06.71 05.43 04.16 02.88   .     .     .     .     .     .     .     .
 0.1238 32.66  7.54DATA 2/25/70 BY VPG; POOR T(ENCL.) CONTROL

 2
10
29.00 34.12 39.34 44.45 49.54 54.67 60.92 64.56 69.60 74.91   .     .     .
 9  1
34.13 39.16 44.21 49.36 54.64 59.71 65.43 70.54 75.00   .     .     .     .
 0
 0.1238 32.66 10.54DATA 2/25/70 BY VPG; POOR T(ENCL.) CONTROL; BATH TEMP. READJ
. TO CORRECT DRIFT
 2
13
29.00 32.07 34.65 37.75 40.70 43.56 46.35 49.56 52.43 55.39 58.33 61.12 64.24
13
30.56 33.39 36.71 39.51 42.35 45.44 48.40 51.41 54.55 57.53 60.43 63.46 66.00
 0
 0.1238 32.66 13.54DATA 2/25/70 BY VPG; POOR T(ENCL.) CONTROL

 2
13
29.00 30.70 32.51 34.38 36.24 37.95 39.82 41.63 43.59 45.58 47.55 49.47 51.30
13
```

Table II. Sample of Initial Computed Absorptions, Velocities

Format: the headings over the columns of results are explained below. The run conditions X, T, f listed in the first three columns identify the total set of α and β data following. Absorption data come first, then α-averaging in the same format. The velocity data are of slightly different format; most noticeably, the velocity value is printed in floating point rather than integer format.

Absorption

X = mole fraction lutidine; T = temperature (C.); f = frequency (MHz.)

N = for individual runs : no. of db readings = N_{kn}
for averaging : no. of runs = N_k

$\alpha = \alpha/f^2$, in 10^{-17} Np. cm.$^{-1}$ sec.^{2}; $\sigma^{\alpha}_{\%}$ = error bound in percent ($100*\sigma^{\alpha}/\alpha$); $\chi^2 = (\chi^2/(N-F))^{\frac{1}{2}}$, N, F as in text

I = for individual runs : which point deleted by 3-d test
for average of runs : which run deleted (never occurs)

C is an indicator of type of fit done; $C = C_A C_N$

C_A= blank : linear fit or straight averaging
Q : nonlinear fit (individual runs only)

C_N= blank : initial fit, all data points used
\- : result of 3-d test; point denoted by I above has been deleted

REMARKS : under individual runs, two types occur, and only for runs with 3-d test deletions. 'Preferred' means this is the best deletion, giving lowest χ^2; 'taken auto'ly (ok)' means this is the latest deletion and was automatically chosen by the original program for averaging--but it was not the best one; this is rectified by hand later, as explained in the text.

under averages, the straight average with no deletions is the only one occurring. It is followed by the value of the average error rescale parameter P for the N_k runs in the particular average.

Velocity : exact analog of headings. Only one run is made; no averaging is done, just 3-d testing; no error rescale is computed.

X	T	F	N	C		I		REMARKS
0.1238	34.66	4.51	6	585	2.03	0	0.36	
				-585	2.03	1	0.01	TAKEN AUTO'LY (OK)
				Q 574	0.75	0	0.36	G=-0.07 EG=0.19
				Q-569	0.75	5	0.24	PREFERRED
			6	571	2.03	0	0.33	
				-574	2.22	5	0.13	PREFERRED
				Q 564	0.74	0	0.36	G=-0.05 EG=0.20
				Q-570	0.77	5	0.14	PREFERRED
			6	563	2.03	0	0.39	
				-563	2.03	7	0.14	TAKEN AUTO'LY (OK)
				Q 547	0.70	0	0.31	G=-0.11 EG=0.19
				Q-547	0.63	2	0.25	PREFERRED
				Q-544	0.70	5	0.32	TAKEN AUTO'LY (OK)
			3	573	1.21	0	0.93	AVG. ESCALE=0.32
			5	1563.5	0.25	0	0.53	
				-1560.0	0.35	5	0.13	TAKEN AUTO'LY (OK)
0.1238	34.66	7.52	10	402	0.94	0	2.50	
				-415	1.10	1	1.86	PREFERRED
				Q 347	0.31	0	1.21	G=-0.22 EG=0.06
				Q-348	0.29	3	0.79	PREFERRED
				Q-339	0.40	10	1.11	TAKEN AUTO'LY (OK)
			10	406	0.94	0	1.03	
				-406	0.94	5	1.11	TAKEN AUTO'LY (OK)
				Q 384	0.42	0	0.68	G=-0.09 EG=0.04
				Q-382	0.42	8	0.56	PREFERRED
				Q-381	0.56	10	0.69	TAKEN AUTO'LY (OK)
			2	409	0.71	0	0.0	AVG. ESCALE=1.50
			5	1569.4	0.25	0	0.76	
				-1564.8	0.35	5	0.34	TAKEN AUTO'LY (OK)
0.1238	34.66	10.53	13	376	0.66	0	1.61	
				-376	0.66	6	0.46	PREFERRED
			13	365	0.66	0	0.67	
				-364	0.73	13	0.50	PREFERRED
			2	370	0.49	0	0.0	AVG. ESCALE=0.48
0.1238	34.66	13.53	13	347	0.65	0	2.08	
				-347	0.65	6	0.53	TAKEN AUTO'LY (OK)
				Q 366	0.86	0	1.97	G= 0.05 EG=0.03
				Q-368	0.80	4	1.55	PREFERRED
				Q-365	0.88	12	2.05	TAKEN AUTO'LY (OK)
			13	326	0.65	0	0.91	
				-325	0.67	4	0.63	PREFERRED
				Q 319	0.72	0	0.85	G=-0.02 EG=0.02
				Q-318	0.69	5	0.81	PREFERRED
				Q-317	0.76	9	0.85	TAKEN AUTO'LY (OK)
			2	335	0.47	0	0.0	AVG. ESCALE=1.54
0.1238	33.46	13.53	13	328	0.65	0	0.35	
				-328	0.65	6	0.85	TAKEN AUTO'LY (OK)
			13	327	0.65	0	0.73	
				-327	0.65	4	0.25	TAKEN AUTO'LY (OK)
			2	327	0.46	0	0.0	AVG. ESCALE=0.57

X	T	F	N	C		I		REMARKS
0.1238	33.46	10.54	13	356	0.66	0	0.59	
				-356	0.67	4	0.46	PREFERRED
			13	357	0.66	0	0.35	
				-357	0.66	4	0.46	TAKEN AUTO'LY (OK)
			2	356	0.47	0	0.0	AVG. ESCALE=0.41
0.1238	33.46	7.54	10	403	0.94	0	0.63	
				-403	0.94	4	0.46	TAKEN AUTO'LY (OK)
			10	385	0.94	0	0.98	
				-381	1.09	10	0.73	PREFERRED
			10	402	0.94	0	2.29	
				-391	1.08	10	0.80	PREFERRED
			3	392	0.59	0	2.73	AVG. ESCALE=0.72
0.1238	33.46	4.52	5	550	2.68	0	0.43	
				-561	3.78	1	0.17	PREFERRED
			5	558	2.66	0	0.47	
				-569	3.75	1	0.32	PREFERRED
			5	544	2.68	0	0.65	
				-561	3.77	1	0.16	PREFERRED
			3	563	2.17	0	0.21	AVG. ESCALE=0.23
			5	1561.1	0.25	0	0.19	
				-1560.0	0.35	5	0.13	TAKEN AUTO'LY (OK)
0.1238	32.66	4.52	5	510	2.69	0	0.32	
				-503	3.82	5	0.08	PREFERRED
			5	528	2.68	0	0.61	
				-542	3.78	1	0.30	PREFERRED
				-516	3.81	5	0.43	TAKEN AUTO'LY (OK)
			5	539	2.68	0	0.99	
				-562	3.77	1	0.65	PREFERRED
			5	535	2.68	0	0.82	
				-535	2.68	1	0.17	TAKEN AUTO'LY (OK)
			5	542	2.68	0	0.26	
				-540	2.85	2	0.16	PREFERRED
			5	531	1.46	0	1.14	AVG. ESCALE=0.51
			5	1564.0	0.25	0	0.77	
				-1568.8	0.35	1	0.34	TAKEN AUTO'LY (OK)
0.1238	32.66	7.54	10	385	0.94	0	1.09	
				-387	0.96	7	0.46	PREFERRED
			9	381	1.08	0	0.58	
				-378	1.28	9	0.41	PREFERRED
			2	383	0.77	0	0.0	AVG. ESCALE=0.43
0.1238	32.66	10.54	13	350	0.66	0	0.42	
				-350	0.66	7	0.41	TAKEN AUTO'LY (OK)
			13	344	0.66	0	0.76	
				-342	0.73	13	0.48	PREFERRED
			2	345	0.49	0	0.0	AVG. ESCALE=0.45
0.1238	32.66	13.54	13	335	0.65	0	0.83	
			13	333	0.65	0	0.31	
			2	334	0.46	0	0.0	AVG. ESCALE=0.63

Table III. Final Computed Absorptions[a], After Data Purging[b]; With Error Bounds (σ^{α}_{Xf}, in percent), and Chi-Square Confidence Functions (χ^2_X) on Errors

α_{ex}/f^2, 10^{-17} Np. cm.$^{-1}$ sec.^{2}

(or, σ^{α}_{Xf}, %)

X(lutidine)	T(C.)	f(MHz.) = 4.5	7.5	10.5	13.5	α_{cl}/f^2 (χ^2_X)
0.9901	32.65	---	65	72	74	9
	33.47	---	69	76	73	9
	34.66	---	69	73	74	9
		(---)	(7.8)	(2.4)	(1.6)	(0.37)
0.427	32.68	82	91	86	87	22
	33.48	82	83	83	86	22
	34.68	94	84	84	88	21
		(5.6)	(4.7)	(1.7)	(1.5)	(0.75)
0.3823	32.66	98	108	104	107	22
	33.45	103	106	99	106	21
	34.66	107	106	102	104	21
		(5.8)	(3.7)	(1.2)	(1.1)	(0.49)
0.3042	32.66	155	152	146	137	24
	33.46	144	142	143	140	24
	34.66	152	145	141	139	23
		(2.7)	(2.7)	(0.7)	(0.7)	(1.20)
0.2132	32.64	240	222	210	208	23
	33.46	236	226	222	212	22
	34.66	247	234	218	208	21
		(2.6)	(1.4)	(0.5)	(0.8)	(0.44)
0.1772	32.64	319	292	266	252	22
	33.46	324	294	270	254	21
	34.66	340	295	271	256	20
		(1.2)	(1.5)	(0.5)	(0.7)	(0.54)
0.1238	32.66	488	373	327	315	19
	33.46	514	381	337	309	19
	34.66	526	400	352	317	18
		(1.6)	(1.0)	(0.5)	(0.7)	(1.00)

α_{ex}/f^2, 10^{-17} Np. cm.$^{-1}$ sec.^{2}

(or, σ^{α}_{Xf}, %)

X(lutidine)	f(MHz.) = T(C.)	4.5	7.5	10.5	13.5	α_{cl}/f^2 (χ^2_X)
0.0892	32.66	564	426	341	290	17
	33.48	594	459	350	301	16
	33.84	600	458	356	306	16
		(1.4)	(0.9)	(0.5)	(0.7)	1.12)
0.0722	32.66	515	445	339	267	15
	33.44	559	491	348	276	15
		(1.2)	(0.6)	(0.5)	(0.7)	(1.57)
0.0664	32.66	557	465	327	262	15
	33.45	613	498	358	285	15
		(1.2)	(0.6)	(0.5)	(0.7)	(0.66)
0.0614	32.64	486	430	304	238	14
	33.45	524	431	317	254	14
		(1.7)	(1.0)	(0.5)	(0.7)	(2.58)
0.0436	32.64	371	313	229	180	11
	33.46	406	340	241	185	11
	33.84	415	345	241	187	11
		(2.0)	(1.0)	(0.5)	(0.7)	(1.09)
0.0288	32.68	189	195	138	101	9
	33.42	202	210	141	107	9
	34.64	231	222	154	113	8
		(3.2)	(2.6)	(1.0)	(1.1)	0.65)
0.0000[c]	all	19	19	19	19	6

[a] quoted as α_{ex}/f^2, after subtracting α_{cl}/f^2 and the mode conversion correction

[b] see text on method of data-point deletion

[c] literature value, not our measurements

Final Computed Velocities, After Data Purging[a]

β, m. sec.$^{-1}$ (error bound σ_β=0.3%, all)

(values at f=4.5 MHz. and underlined values are most reliable)

X(lutidine)	f(MHz.) T(C.)	4.5	7.5	10.5	13.5
0.9901	32.65		1324.4	1336.2	1330.0
	33.47		1326.9	1324.6	1331.7
	34.66		1320.1	1324.3	1329.2
0.427	32.68	1478.6	1497.2	1495.5	1507.6
	33.48	1489.2	1498.8	1495.8	1502.6
	34.68	1489.1	1488.7	1493.9	1498.6
0.3823	32.66	1508.3	1507.8	1517.8	1520.9
	33.45	1504.2	1499.7	1508.3	1515.1
	34.66	1499.9	1500.4	1508.8	1514.0
0.3042	32.66	1540.0	1529.2	1534.2	1527.8
	33.46	1533.6	1532.9	1549.8	1527.9
	34.66	1522.4	1526.3	1527.8	1544.8
0.2132	32.64	1549.9	----	1559.7	1569.8
	33.46	1552.3	1555.0	1556.0	1574.1
	34.66	1553.3	1547.8	1548.8	1559.8
0.1772	32.64	1564.0	1566.7	1573.1	1592.1
	33.46	1567.6	1560.1	1569.1	1572.3
	34.66	1567.0	1556.9	1563.5	1581.1
0.1238	32.66	1568.8			
	33.46	1561.1			
	34.66	1560.0	1564.8		

4.5 MHz. only

X	T	β	X	T	β
0.0892	32.66	1558.8	0.0614	33.45	1562.2
	33.48	1559.9			
	33.84	1554.9	0.0436	32.64	1561.6
				33.46	1556.7
0.0722	32.66	1567.0		33.84	1557.8
	33.44	1560.6			
			0.0288	32.68	1562.2
0.0664	32.66	1565.8		33.42	1562.7
	33.45	1566.3		34.64	1560.0
0.0614	32.64	1565.2			

(continued)

β, m. sec.$^{-1}$ (error bound σ_β=0.3%, all)

(values at f=4.5 MHz. and underlined values are most reliable)

X(lutidine)	f(MHz.) T(C.)	4.5	13.5
0.0000	32.64	1516.8	1525.3
	34.66	1518.6	
benzene	32.65	1260.7	

[a]see text on method of data-point deletion

Table IV. Diffraction Corrections $Q_o(a/\lambda, z/\lambda) = Q_o(z)$ for Our System, a = 12.7 mm., β = 1570 m./sec.

(Parameters in parentheses are the more general reductions: a/λ is given next to f, z/λ next to Q itself)

z., mm. \ f, MHz. (a/λ)	Q_o in decibels			
	4.5(36.4)	7.5(60.7)	10.5(84.9)	13.5(109.2)
8	0.255 (22.9)	0.198	0.167	0.148
10	0.286 (28.7)	0.222	0.188	0.165
12	0.313 (34.4)	0.243	0.206	0.182
14	0.339 (40.1)	0.263	0.222	0.196
16	0.362 (45.8)	0.281	0.238	0.210
18	0.384 (51.6)	0.298	0.252	0.222
20	0.404 (57.3)	0.314	0.266	0.235
22	0.424 (63.1)	0.329	0.279	0.246
24	0.442 (68.8)	0.344	0.291	0.257
26	0.462 (74.5)	0.358	0.303	0.267
28	0.479 (80.2)	0.372	0.314	0.277
30	0.496 (86.0)	0.384	0.325	0.287
32	0.510 (91.7)	0.396	0.336	0.296
34	0.526 (97.4)	0.408	0.346	0.305
36	0.543 (103)	0.420	0.357	0.314
38	0.558 (109)	0.434	0.366	0.323
40	0.571 (115)	0.443	0.375	0.331
42	0.583 (120)	0.456	0.384	0.340
44	0.597 (126)	0.464	0.393	0.347
46	0.615 (132)	0.474	0.403	0.355
48	0.626 (138)	0.486 (229)	0.411	0.362
50	0.635 (143)	0.497 (239)	0.420	0.370
52	0.655 (149)	0.506 (248)	0.427	0.377
54	0.659 (155)	0.515 (258)	0.437	0.386
56	0.678 (160)	0.523 (268)	0.445	0.391
58	0.683 (166)	0.532 (277)	0.451 (388)	0.399
60	0.703 (172)	0.543 (287)	0.458 (401)	0.405
62	0.704 (178)	0.554 (296)	0.466 (415)	0.413 (533)
64	0.726 (183)	0.559 (306)	0.473 (420)	0.420 (550)
66	0.729 (189)	0.568 (315)	0.481 (441)	0.425 (568)
68	0.741 (195)	0.580 (325)	0.490 (455)	0.431 (585)
70	0.760 (201)	0.583 (334)	0.498 (468)	0.437 (602)
72	0.758 (206)	0.597 (344)	0.503 (482)	0.443 (619)
74	0.772 (212)	0.600 (354)	0.508 (495)	0.449 (636)
76	0.792 (218)	0.613 (363)	0.517 (508)	0.455 (654)
78	0.792 (224)	0.615 (373)	0.525 (522)	0.462 (671)
80	0.797 (229)	0.629 (382)	0.528 (535)	0.469 (688)

Appendix V. Details of Theoretical Interpretation of Ultrasonic Results.

Paper I developed and extended Fixman's theory for interpreting critical region sound absorption in molecular terms, beginning from a general framework of irreversible thermodynmaics. Paper II presented the ultrasonic results for our binary system, which gave clear indications of an additional absorption from thermal relaxation. It also outlined the two-part (critical + thermal) relaxation theory we developed thermodynamically to analyze our results quantitatively. Paper II finally presented our analysis, limited to the critical absorption only by fundamental theoretical obstacles. In this Appendix we give the details of our general theory and of the data interpretation, for the record as well as for any future work toward a useable total theory. First we give more details in Fixman's theory of critical absorption. Then we give details of the chemical/physical models for thermal relaxation and for solution thermodynamics. The thermodynamics could have been a unifying link between critical and thermal relaxation mechanisms, but it failed.

(A) Reduction of α_{CR}/f^2 to the molecular parameters h, l^2 or ξ, l^2:

--(1) Form of α_{CR}/f^2 from Fixman theory (equation numbers not of the form V.XX refer to our papers I or II, or

to Fixman's paper on α, ref. 5 of paper I):

$$\alpha_{CR} = \frac{\omega(\gamma_o - 1)}{2\beta C_p} \operatorname{Im} \Delta_M \qquad \text{(I.38)}$$

$$\Delta_M = \frac{\Delta}{n_1 + n_2}, \quad \Delta = \text{heat capacity/unit vol.}, \quad n_i = \text{moles/unit vol.}$$

From (I.33) and (I.34):

$$\Delta = \frac{kh}{4\pi^2}\left(T_c \frac{\partial \kappa^2}{\partial T}\right)^2 I$$

$$I = \int \frac{dk\, k^4}{(k^2+\kappa^2)(i\omega + hk^2[k^2+\kappa^2])}$$

Change variables: $x = k/\kappa$, $d = \kappa^2(h/\omega)^{\frac{1}{2}}$; (V.1)

$$I = \frac{\kappa^3}{\omega d^2} \int \frac{dx\, x^4}{(1+x^2)(-id^{-2}+x^2[1+x^2])}$$

$$= \frac{\omega^{-\frac{1}{4}}}{h^{3/4}} d^{-\frac{1}{2}} \int \sim\sim\sim \equiv \frac{\omega^{-\frac{1}{4}}}{h^{3/4}} f(d) \qquad (\alpha.12)$$

$$\Delta = \frac{kh^{\frac{1}{4}}\omega^{-\frac{1}{4}}}{4\pi^2}\left(T_c \frac{\partial \kappa^2}{\partial T}\right)^2 f(d) \qquad (\alpha.11)$$

$$\alpha_{ex}/f^2 = \frac{\omega^{-5/4}(\gamma_o - 1)k}{(n_1+n_2)2\beta C_p}\left(T_c \frac{\partial \kappa^2}{\partial T}\right)^2 h^{\frac{1}{4}} \operatorname{Im} f(d) + B(X,T,f) \equiv \mathcal{L}(d) \qquad \text{(V.2)}$$

B(X,T,f) represents TR; near X_c and at our low frequencies, its X- and f-dependence are weak, and its T-dependence is weak relative to α_{CR}/f^2; $B \simeq$ const.

We see α_{CR}/f^2 to be a function of the bulk, 'static' parameters ω, n_i, C_p, C_v, β, T_c, and also of the two microscopic parameters l^2 (since $\partial\kappa^2/\partial T = 6/l^2$) and h (d in $f(d)$ is a function of ω, l^2, and h also).

--(2) To develop a bookkeeping for fitting α_{ex}/f^2 to our data, define

$$\alpha_{ex}/f^2 = Af^{-5/4}\mathcal{L}(d) + B \qquad \text{(V.3a)}$$

$$d = C_o|T-T_c|f^{-\frac{1}{2}} \ . \qquad \text{(V.3b)}$$

Results of the fit to the data, which is a nonlinear fit in C_o, linear in A, B:

-- C_o was scanned to minimize the residual error of the linear fit. Eight data points were fit, four $\underline{f}$ at each of two T. For $C_o = 0.2$ ($\underline{f}$ in MHz., α/f^2 in 10^{-17} Np. cm.$^{-1}$ sec.^{2}), the error was minimized on a crude grid. The error was insensitive to C_o, however. There was a consistent localization of the total error in the $\underline{f} = 7.5$ MHz. points, the computed values always being lower; Eq. (V.2) gives a poor shape for α/f^2 vs. $\underline{f}$. $\mathcal{L}(d)$ was nearly constant over the $\underline{d}$-range we sampled in our 8 data points, so essentially $\alpha_{ex}/f^2 \sim f^{-5/4}$ is predicted.

--Adjustment of T_c was tried, with little result. This is as expected, since it only changes $\underline{d}$ values, to which the fit is insensitive.

--Separate fits of the four $\underline{f}$ points were tried for each of the two T; only one degree of freedom is left in both fits. Results are poor; the $\underline{B}$ term was negative for the best fits, attempting to smooth the poor shape of α_{CR}/f^2 vs. with $\underline{f}$.

--Finally, we gave $\underline{B}$ a temperature dependence, a T-coefficient of +3% deg.$^{-1}$ to -9% deg.$^{-1}$, with little effect

(C_o changes but the net error is relatively unaffected), since it does not change the problematic f-dependence of α_{ex}/f^2.

Selecting $C_o = 0.20$ MHz.$^{\frac{1}{2}}$C.$^{-1}$

$= 2.0\times10^2$ sec.$^{-\frac{1}{2}}$C.$^{-1}$,

the corresponding A, B values are

$B = 201$ ($\times10^{-17}$Np. cm.$^{-1}$sec.^{2}); very reasonable

$A = 7.0\times10^3$ ($\times10^{-17}$Np. cm.$^{-1}$sec.^{2}MHz.$^{-5/4}$)

$= 2.2\times10^{-6}$ cm.$^{-1}$sec.$^{3/4}$; about 0.1 of the value for nitrobenzene: isooctane; reasonable.

--(3) Reduce to the molecular parameters: comparing Eqs. (V.2), (V.3a), we see

$$A = \frac{(2\pi)^{-5/4}(\gamma_o-1)kh^{\frac{1}{4}}}{2\beta C_p(n_1+n_2)}\left(T_c\frac{\partial\kappa^2}{\partial T}\right)^2,$$

and comparing Eqs. (V.1), (V.3b) and using $\kappa^2 = 6|T-T_c|/l^2$,

$$C_o = (2\pi)^{-\frac{1}{2}}\frac{6\,h^{\frac{1}{2}}}{T_c l^2}.$$

Now factor all the fixed macroscopic parameters from the A, C_o expressions, leaving only powers of h, l^2:

$$A = \mathcal{A}h^{\frac{1}{4}}/l^4;\quad C_o = \mathcal{C}h^{\frac{1}{2}}/l^2$$

$$\mathcal{A} = \frac{36(2\pi)^{-5/4}(\gamma_o-1)k}{2\beta C_p(n_1+n_2)}$$

$$\mathcal{C} = (2\pi)^{-\frac{1}{2}}6/T_c.$$

Reduce the data to $C_o/\mathcal{C} = \bar{C} = h^{\frac{1}{2}}/l^2$, $A/\mathcal{A} = \bar{A} = h^{\frac{1}{4}}/l^4$, and get h, l^2 as

$$h = (\bar{C}^2/\bar{A})^{4/3},\quad l^2 = (\bar{C}/\bar{A}^2)^{1/3}$$

--(4) Evaluate $\mathcal{A}, \mathcal{C}$; need ω, k, $\gamma_o = (C_p-C_v)/C_v$,

P, $n_1+n_2 = \bar{V}^{-1}$, and T_c (take component 1 as water):

$T_c = 306.7$ K.

$\Longrightarrow \mathcal{C} = 7.80\times10^{-3}$ K^{-1}

$= 1566$ m. sec.$^{-1}$, measured

C_p, C_v--not measured independently; estimate C_p from the pure fluid values

$C_p \simeq X_1 C_p^1 + X_2 C_p^2$; C_p^2 estimated from other pyridine, heterocycle values

$= 0.935(18 \text{ cal.C.}^{-1}\text{mole}^{-1}) + 0.065(50 \text{ cal.C}^{-1}\text{mole}^{-1})$

$= 20$ cal. C.$^{-1}$ mole^{-1}

and get C_v from $C_p - C_v = T\bar{V}\theta^2/\kappa_T$, notation of paper I:

$$\theta = -(\partial\rho/\partial T)/\rho \simeq -(\Delta\rho/\Delta T)/\rho$$

For our mixture at X_c, between T = 32.65 and 34.65 C., our initial $\rho \leftrightarrow X$ data give $\rho = 0.98900, 0.98759$:

$$\theta \simeq 7.1\times10^{-4} \text{ C.}^{-1}$$

κ_T also was not measured; use $\kappa_T = \kappa_S + T\bar{V}\theta^2/C_p$

$\kappa_S = 1/\rho\beta^2$, $\rho = 0.98900\times10^3$ kg. m.$^{-3}$

$= 0.413\times10^{-9}$ nt.$^{-1}$m.^{2}

$$\bar{V} = \frac{X_1 MW_1 + X_2 MW_2}{\rho_{soln.}}$$

$$= \frac{0.065(107) + 0.935(18)}{0.989} \text{ cc. mole}^{-1}$$

$= 24.1\times10^{-6}$ m.^{3} mole^{-1}

$\kappa_T \simeq 0.458\times10^{-9}$ nt.$^{-1}$ m.^{2}

$C_p - C_v \simeq 1.94$ cal. C.$^{-1}$mole^{-1}

$\gamma_o - 1 = 0.107$

$a = 0.491\times10^{-33}$ m.^{2}molecule^{-1}sec.

$\bar{A} = A/a = 4.47\times10^{29}$ m.$^{-3}$sec.$^{-\frac{1}{2}}$molecule

$\bar{C} = C_o/C = 2.56\times10^{4}$ sec.$^{-\frac{1}{2}}$

$h = 1.66\times10^{12}$ Å^4 sec.$^{-1}$; reasonable size of pair diffusion constant

$l^2 = 50.5$ Å^2; reasonable in comparison to other systems

These values are not final; they are adjusted for Fixman's oversight, as noted in paper I.

--(4) Reduce h further, to a molecular friction constant ζ, as does Fixman (his ξ), from his Eq. (α.5):

$$h = \frac{(n_1+n_2)\bar{V}_1^2 \phi_1 kT_c}{m_1 c_2 2\pi a\zeta} \equiv \mathcal{H}/a\zeta$$

n_i in molecules/unit vol.

$\bar{V}_1$ in vol./molecule

c_2 = weight fraction of component 2 (lut.)

$\bar{V}_1 = 18.07$ cc. mole^{-1} $= 3.00\times10^{-23}$ cc. molecule^{-1}

$\phi_1 = n_1\bar{V}_1$

$$n_1 = \rho\frac{X_1}{X_1MW_1+X_2MW_2} = 0.0376 \text{ moles cc.}^{-1}$$

$\phi_1 = 0.680$

$c_2 = X_2MW_2/(X_1MW_1+X_2MW_2) = 0.708$

$\mathcal{H} = 48.8\times10^{-26}$ m.^{5}molecule^{-1} sec.$^{-2}$

$\bar{H} = h/\mathcal{H} = 3.4\times10^{-14}$ Å^{-1}sec.

$a\zeta = 1/\bar{H} = 2.94\times10^{13}$ Å sec.$^{-1}$

Now, Fixman derives $a = 3\bar{V}_2/2\pi l^2$ from the Flory-Huggins model:

$a = 1.84$ Å; very low compared to other consolutes

$\zeta = 1.6\times10^{13}$ sec.$^{-1}$; small; corrected to 0.32 in paper II, for Fixman's oversight.

(B) Derivation of Correction Factors for l, ζ from Fixman's original results, due to Fixman's oversight in the form of f(d)--faulty translation of singlet→ pair diffusion:

Fixman derived a pair diffusion equation for G(r) or its Fourier transform G_k (Eq. 40, viscosity paper), leading to our Eq. (I.33). The diffusion constant h appears in two places in the incremental heat capacity (or α, α/f^2)--as a factor in the numerator, and buried in the denominator of the integrals I or f(d). But we showed in our redevelopment that h should be replaced by h/2 in the latter place. We indicated that this requires adjustment of Fixman's l, ζ by 1.26, 0.20, respectively. We derive these factors here:

Proper form:

$$\Delta = \frac{kh'}{4n^2} \left(T_c \frac{\partial \kappa^2}{\partial T}\right)^2 I'$$

$$I' = \int \frac{dk\, k^4}{(k^2+\ ^2)(i\omega + \frac{h'}{2}k^2[k^2+\kappa^2])}$$

h' is the proper diffusion constant

Performing the change of variables

$x = k/\kappa$, $d = \kappa^2(h'/2\omega)^{\frac{1}{2}}$, similarly to before,

we get

$$I' = \frac{2}{h'}\left(\frac{h'}{2}\right)^{\frac{1}{4}} f(d) = 2^{3/4}\frac{\omega^{-\frac{1}{4}}}{h'^{3/4}} f(d),$$

with f(d) the same mathematical form as before. Thus in our forms $\alpha/f^2 = Af^{-5/4}\mathcal{Q}(d) + B$, $d = C_0 f^{-\frac{1}{2}}|T-T_c|$, we have really

$$A = 2^{3/4}\mathcal{A}(h')^{\frac{1}{4}}/(l')^4$$

$$C = \mathcal{C} 2^{-\frac{1}{2}} (h')^{\frac{1}{2}} / (1')^2$$

and

$$h' = 2^{7/3} (\bar{C}^2/\bar{A})^{4/3} = 2^{7/3} h_{old} = 5.04\, h_{old}$$

$$\Longrightarrow \zeta' = 0.20\, \zeta_{old}$$

$$1' = 2^{1/3} (\bar{C}/\bar{A}^2)^{1/6} = 2^{1/3}\, 1_{old} = 1.26\, 1_{old}.$$

(C) Proving Fixman's expression for the diffusion constant h,

$$h = \frac{kT\phi_1 \bar{V}_1^2 (n_1+n_2)}{m_1 c_2 2\pi a \zeta} \qquad (\alpha.5)$$

There are some difficulties in verifying this relation: 1) Fixman commonly does not label the variables held fixed in his partial derivatives; 2) he changes notation in transit, or makes errors in notation corrected implicitly in later papers; 3) he sometimes uses approximate equalities in derivations but quotes them as equalities. These three problems plus the spreading of his total derivation over 4 papers are great obstacles to following his line of reasoning. We have corrected some implicit assumptions of the types above in our paper I, but we still have to verify the above equation.

The diffusion equation outside the critical region (I.12) has a diffusion constant

$$D = \alpha (\partial \mu / \partial c_2) \qquad (1)$$

which is retained in the critical region (only the driving terms are altered) but written as

$$D = \frac{h\rho}{2} \kappa^2 .$$

Clearly,

$$h = \frac{2\alpha}{\rho\kappa^2}\left(\frac{\partial\mu}{\partial c_2}\right)_{P,T}$$

and from this we must derive Eq. (4.5). Let us reduce Eq. (1). First, we take, as does Fixman, c_2 to be the mass fraction of component 2. Correspondingly, μ is the difference in chemical potentials per unit concentration $\mu_2-\mu_1$. As Fixman later uses μ_1 as the chemical potential per molecule, we must convert

$$\mu = \mu_2/m_2 - \mu_1/m_1$$
$$d\mu = d\mu_2/m_2 - d\mu_1/m_1 .$$

By the Gibbs-Duhem relation, μ_1 and μ_2 are constrained to vary as

$$n_1 d\mu_1 + n_2 d\mu_2 = 0$$
$$\Longrightarrow d\mu = \frac{n_1 m_1 + n_2 m_2}{n_2 m_1 m_2}\, d\mu_1 = \frac{\rho}{n_2 m_1 m_2}\, d\mu_1 ,$$

and thus

$$D = \frac{\alpha\rho}{n_2 m_1 m_2}\left(\frac{\partial\mu_1}{\partial c_2}\right)_{P,T} .$$

-- Now, in his viscosity paper, Fixman derives a relation (Sec. A) between $\partial\mu_1/\partial\phi_2$ [or $\partial\mu_1/\partial n_2$, as easily] and the microscopic parameters $\underline{a}$ and κ^2, through the relation of osmotic pressure π and the correlation function $G_{22}(r)$:

$$\frac{\partial\pi}{\partial n_2} = kT\left[1 + n_2\int G_{22}(r)\, d\vec{r}\right]^{-1} \equiv \left(\frac{\partial P}{\partial n_2}\right)_{\mu_1,T}$$
$$= \left(\frac{\partial\mu_1}{\partial n_2}\right)_{P,T}\left(\frac{\partial P}{\partial\mu_1}\right)_{n_2,T} .$$

He uses a Maxwell relation

$$(\frac{\partial V}{\partial N_1})_{P,T,N_2} = (\frac{\partial \mu_1}{\partial P})_{T,N_1,N_2}$$

and an assumption of small compressibility of the mixture,

$$(\frac{\partial \mu_1}{\partial P})_{T,N_1,N_2} \simeq (\frac{\partial \mu_1}{\partial P})_{n_2,T} = -\bar{V}_1$$

to get

$$\frac{\partial \pi}{\partial n_2} \simeq -\frac{1}{\bar{V}_1}(\frac{\partial \mu_1}{\partial n_2})_{P,T} .$$

Now, in the critical region, according to the Ornstein-Zernike model of classical thermodynamics,

$$\int G_{22}(r)\, d\vec{r} = 4\pi a/\kappa^2$$

$$\Longrightarrow \frac{4\pi a}{\kappa^2} = -\frac{\bar{V}_1}{n_2}\left[\frac{kT}{(\partial \mu_1/\partial n_2)} + \frac{1}{\bar{V}_1}\right]. \qquad \text{(I.26)}$$

The second term in brackets is negligible relative to the first when $\partial \mu_1/\partial n_2 \to 0$, as in the critical region --unless we are trying to get the dependence of absorption on composition away from X_c (Puls' thesis, e.g.). Thus

$$\frac{\partial u_1}{\partial n_2} \simeq \frac{\bar{V}_1 kT\kappa^2}{4\pi a n_2} .$$

--We must put this in terms of $\partial \mu_1/\partial c_2$:

$$\frac{\partial \mu_1}{\partial c_2} = (\frac{\partial \mu_1}{\partial n_2})(\frac{\partial n_2}{\partial c_2})_{\bar{V}} .$$

The chain rule is justified, since c_2 (with P, T) is a complete description. We need a condition on the latter partial to reflect the P, T constancy, and we choose $d\bar{V}=0$ (low compressibility; also consistent with relation I.17

between δG and $[\delta n_2]^2$):

$$dc_2 = \left(\frac{\partial c_2}{\partial n_1}\right)_{n_2} dn_1 + \left(\frac{\partial c_2}{\partial n_2}\right)_{n_1} dn_2$$

$$c_2 = \frac{n_2 m_2}{\rho} \Rightarrow \frac{\partial c_2}{\partial n_1} = -\frac{n_2 m_1 m_2}{\rho^2}$$

$$\frac{\partial c_2}{\partial n_2} = \frac{n_1 m_1 m_2}{\rho^2}$$

$$dc_2 = \frac{m_1 m_2}{\rho^2}\left[-n_2 dn_1 + n_1 dn_2\right]$$

$$dV = \bar{V}_1 dn_1 + \bar{V}_2 dn_2 \Rightarrow dn_1 = -\frac{\bar{V}_2}{\bar{V}_1} dn_2$$

$$dc_2 = \frac{m_1 m_2}{\rho^2}\left[\frac{n_2\bar{V}_2 + n_1\bar{V}_1}{\bar{V}_1}\right] dn_2 \qquad (= 1)$$

$$\left(\frac{\partial c_2}{\partial n_2}\right)_{\bar{V}} = \frac{m_1 m_2}{\rho^2 \bar{V}_1} = \frac{m_1 c_2}{\rho \bar{V}_1 n_2}$$

Thus

$$\frac{\partial u_1}{\partial c_2} \simeq \frac{\rho \bar{V}_1 n_2}{m_1 c_2} \cdot \frac{\bar{V}_1 kT \kappa^2}{4\pi a n_2}$$

$$D = \frac{\alpha \rho^2}{n_2 m_1 m_2} \cdot \frac{\rho \bar{V}_1^2 kT \kappa^2}{m_1 c_2 4\pi a}$$

$$h = \frac{\alpha \rho \bar{V}_1^2 kT}{n_2 m_1^2 m_2 c_2 2\pi a}$$

---Fixman uses an intermolecular friction constant ζ in preference to α, converting through an ideal diffusion constant D_{id}. In Sec. VIII in his viscosity paper, he derives a rigorous relation

$$D_{id} = \frac{\alpha \rho kT}{m_1 m_2^2 n_1} \left(\frac{\partial \ln X_2}{\partial n_2}\right)_{\bar{V}} = \frac{\alpha \rho kT}{m_1 m_2^2 n_1 n_2 (n_1+n_2)\bar{V}_1}$$

and then defines

$$\zeta \equiv \frac{kT}{m_2 D_{id}}$$

$$\Longrightarrow \alpha = \frac{m_1 m_2^2 n_1 n_2 (n_1+n_2)\bar{V}_1}{\rho kT} D_{id}$$

$$= \frac{m_1 m_2 n_1 n_2 (n_1+n_2)\bar{V}_1}{\rho \zeta}$$

$$h = \frac{\rho \bar{V}_1^2 kT}{n_2 m_1^2 m_2 c_2^2 2\pi a} \cdot \frac{m_1 m_2 n_1 n_2 (n_1+n_2)\bar{V}_1}{\rho \zeta}$$

and using $n_1 \bar{V}_1 = \phi_1$, we get

$$h = \frac{\bar{V}_1^2 kT (n_1+n_2)\phi_1}{m_1 c_2^2 2\pi a \zeta} \quad , \text{ Q.E.D.}$$

(D) A Comment on Fixman's choice of the dissipative equation and its driving force: Fixman's earlier papers on general critical region thermodynamics and on ultrasonic attenuation focus on the equations of motion for the singlet and pair densities, rather than the singlet and pair concentration deviations. The latter obey a purely dissipative equation, modified from the standard non-critical diffusion equation; the choice of thermodynamic description for the entropy production and the choice of driving term are well justified. The density equations of motion, on the other hand, are mixed propagative-dissipative and encompass the

anomalous entropy production or sound absorption only for the gas-liquid critical point, and then in a non-obvious way. Fixman's first attempts to describe the liquid-liquid critical absorption failed for this reason.

(E) Estimation of the pressure-driven contribution to the critical absorption, relative to the thermal absorption: The δT term in the driven entropy fluctuation, hence in α, originated in the derivative

$$(\frac{\partial \mu^2}{\partial T})\delta T \sim (\frac{\partial^2 \mu_1}{\partial T \partial c_2})\delta T = \frac{\partial^2}{\partial T \partial c_2}(\frac{\partial G_{mix}}{\partial N_1})_{N_2},$$

where G_{mix} is the free energy change for an arbitrary mass of solution and the N_i are total numbers of moles (or molecules, if one prefers). The analogous δP-driven term is proportional, with the same constant of proportionality, to

$$\frac{\partial^3 G_{mix}}{\partial P \partial c_2 \partial N_1} = \frac{\partial}{\partial c_2}(\frac{\partial}{\partial N_1})_{N_2} \Delta V_{mix} .$$

The derivative $(\partial/\partial N_1)_{N_2}$ factors as

$$(\frac{\partial}{\partial N_1})_{N_2} = (\frac{\partial N}{\partial N_1})_{N_2}(\frac{\partial}{\partial N})_{X_2} + (\frac{\partial X_2}{\partial N_1})_{N_2}(\frac{\partial}{\partial X_2})_N$$

$$N = N_1 + N_2$$

$$= (\frac{\partial}{\partial N})_{X_2} - \frac{X_2}{N}(\frac{\partial}{\partial X_2})_N$$

and clearly $\Delta V_{mix} = N \Delta \bar{V}_{mix}$, where the bar denotes the molar quantity. Then the δP term measure becomes, for $c_2 = X_2$,

$$\frac{\partial \Delta \bar{V}_{mix}}{\partial X_2} - X_2 \frac{\partial^2 \Delta \bar{V}_{mix}}{\partial X_2^2}$$

and

$$\Delta\bar{V}_{mix} = V^E = \frac{X_1MW_1+X_2MW_2}{\rho_s} - \frac{X_1MW_1}{\rho_1} - \frac{X_2MW_2}{\rho_2}$$

$$\frac{\partial\Delta\bar{V}_{mix}}{\partial X_2} = \frac{(MW_2-MW_1)}{\rho_s} - \frac{\Delta\bar{V}_{mix}}{\rho_s}\left(\frac{\partial\rho_s}{\partial X_2}\right) - \frac{MW_2}{\rho_2} + \frac{MW_1}{\rho_1}$$

$$\rho_s{}^2\left(\frac{\partial^2\Delta\bar{V}_{mix}}{\partial X_2{}^2}\right) = -(MW_2-MW_1)\left(\frac{\partial\rho_s}{\partial X_2}\right) - \rho_s\left(\frac{\partial\Delta\bar{V}_{mix}}{\partial X_2}\right)\left(\frac{\partial\rho_s}{\partial X_2}\right)$$
$$+ \Delta\bar{V}_{mix}\left[\left(\frac{\partial\rho_s}{\partial X_2}\right)^2 - \rho_s\left(\frac{\partial^2\rho_s}{\partial X_2{}^2}\right)\right]$$

The ratio $\underline{R}$ of the pressure-induced to the temperature-induced absorption is

$$R = \frac{\left[\frac{\partial\Delta\bar{V}_{mix}}{\partial X_2} - X_2\frac{\partial^2\Delta\bar{V}_{mix}}{\partial X_2{}^2}\right]}{\left(\partial^2\mu_1/\partial T\partial X_2\right)} \cdot \frac{C_p}{TV\theta} ,$$

since for $\delta S = 0$, $\frac{C_p}{T}\delta T - V\theta\delta P = 0$.

A modified Flory-Huggins model will be used for the term $\partial^2\mu_1/\partial X_2\partial T$, in terms of mole fractions rather than volume fractions:

$$\frac{\partial\mu_1}{\partial X_2} = -\frac{R_gT}{(X_2{}^c)^2}\left[\frac{1}{X_1} - \frac{2}{X_1{}^c} + \frac{T_c}{T}\frac{X_1}{(X_1{}^c)^2}\right],$$

which is a form satisfying $\partial\mu_1/\partial X_2 = 0 = \partial^2\mu_1/\partial X_2{}^2$ at $X_2=X_2{}^c$, and $\partial^3\mu_1/\partial X_2{}^2\partial T > 0$ appropriate to a lower consolute. Then

$$\frac{\partial^2\mu_1}{\partial X_2\partial T} = -\frac{R_g}{(X_2{}^c)^2}\left[\frac{1}{X_1} - \frac{2}{X_1{}^c}\right] \rightarrow \frac{R_g}{(X_2{}^c)^2X_1{}^c} \quad \text{at } X_c .$$

Numerical evaluation (let component 1 be water), T = 33.2 C. and $X = X_c = 0.065$ lutidine:

$MW_1 = 18$ g. mole^{-1}

$MW_2 = 107$ g. mole^{-1}

$\rho_1 = 0.91035$ g. cc.$^{-1}$

$\rho_2 = 0.99467$ g. cc.$^{-1}$

$\rho_s = 0.98852$ g. cc.$^{-1}$

$$\frac{\partial \rho_s}{\partial X_2} \simeq \frac{-0.00087 \text{ g. cc.}^{-1}}{0.0100} = -0.087 \text{ g. cc.}^{-1}, \quad \text{graphically}$$

$\Delta \bar{V}_{mix} = -0.504$ cc. mole^{-1}

$R_g = 1.987$ cal. C.$^{-1}$ mole^{-1}

C_p, T, $\bar{V}$, θ have been listed in section (A).

$$\frac{\partial \Delta \bar{V}_{mix}}{\partial X_2} = -9.45 \text{ cc. mole}^{-1}$$

$$\frac{\partial^2 \Delta \bar{V}_{mix}}{\partial X_2^2} = +7.09 \text{ cc. mole}^{-1}$$

$\partial^2 \mu_1 / \partial X_2 \partial T = 503$ cal. C.$^{-1}$ mole^{-1}

$R = -0.079 = -7.9\%$

Part II: Chemical Theory of Solution Thermodynamics and of Ultrasonic Relaxation.

The thermodynamics of our lutidine: water mixtures, as of other aqueous amine or heterocycle solutions, points to strong A-B association through hydrogen-bonding. The phase behavior is affected: a lower consolute or critical mixing point is generated. The strong association equilibria also relax ultrasonically to yield a strong absorption. The latter effect has been studied by Andreae, et al.[1] with simple and not very successful models or chemical theories, and pointedly ignoring the former effect. The critical absorption phenomena have been studied only for upper consolute mixtures (with one exception), dominated by 'physical' rather than 'chemical' interactions of mixing. Our solution seems to be the first[2] calling for a careful modelling of both absorption effects in a common framework, to separate and interpret the effects which are of comparable magnitude in the critical region of interest. We have only limited guides in constructing such a theory; the chemical models of thermal relaxation are not very satisfactory as we have noted, and the models for the critical thermodynamics have been elementary physical solution theories (not beyond Flory-Huggins) used empirically, far from the more complex chemical theories. Our rather piecemeal attempts at the total theory are presented below.

Assume some model for the self-association of

water, and likewise for lutidine-water complexation:

$$A + A_{n-1} \rightleftharpoons A_n$$

$$B + A_n \rightleftharpoons BA_n \ .$$

Each equilibrium is characterized by an equilibrium constant, enthalpy change, volume change, and (for relaxation) forward rate constant. Let us denote these for the association equilibria as K_n, H_n, V_n, and k_{fn}, respectively, and with primes for the complexation equilibria. With modern computers it is possible to solve for the 'true' species concentrations given a large but finite set of equilibria with an arbitrary progression of K_n, etc. with n, and from there to compute the net thermodynamic functions of mixing and the relaxation strengths, both as functions of the macroscopic composition as perhaps measured by the mole fraction X_B. This reduces to an exercise in curve fitting with an enormous number of parameters. Our limited data on the phase diagram and on absorption do not justify such an exacting treatment, which is of limited interpretive value in any case. Our models are therefore limited to some simple progressions of the K_n, V_n, etc., such as the geometric one, $K_n = \alpha K_{n-1}$. We obtain low-order polynomial equations for the mole fractions δ_n, δ_B, and δ_{Bn} of the true species A_n, B, and BA_n, to be solved numerically for any composition X_B.

The molar free energy of mixing can be computed from the true species concentrations rather straightforwardly,

$$G_{mix} = RT\left[X_A \ln \delta_A + X_B \ln \delta_B\right] , \qquad \text{(II.10)}$$

under the assumption that the 'true' species form an ideal solution, in which case the activities of the monomers A, B equal the corresponding true mole fractions δ_A, δ_B. (A reasonable assumption to go with this is that the parameters K_n, etc. are independent of composition; this keeps things simple.) The condition for instability (immiscibility)

$$\frac{\partial^2 G_{mix}}{\partial X_A^2} < 0$$

maps the region of phase separation. The chemical term above $G_{mix} = G_{chem}$ is not sufficient to cause such a condition, but it helps it to occur and partly determines the particular mole fraction whre it occurs.

Aside from phase behavior, our model must give the correct relaxation strength Z as a function of macroscopic composition X_B. For a single general reaction

$$aA + bB + \ldots \rightleftharpoons cC + dD + \ldots$$

Herzfeld and Litovitz[3] develop a relaxation equation. Let ξ define an extent of reaction from some arbitrary initial state and let its first order disturbance (from the ultrasound) be $\delta\xi$,

$$\delta\xi = \frac{\delta n_C}{c} = \frac{\delta n_D}{d} = -\frac{\delta n_A}{a} = -\frac{\delta n_B}{b} = \ldots,$$

n_i = no. of moles of species i.

Defining the forward and backward rate constants $\tilde{k}$ and $\bar{k}$, they derive to first order (for the case $aA+bB \rightleftharpoons cC+dD$, to prevent ambiguity of expressions)

$$-\frac{d}{dt}\,\delta\xi = \bar{k}(\delta_C^o)^c(\delta_D^o)^d\left[\left\{\frac{a^2}{\delta_A}+\frac{b^2}{\delta_B}+\frac{c^2}{\delta_C}+\frac{d^2}{\delta_D}-(\Delta n)^2\right\}\delta\xi - n\,\delta\ln K\right]$$

$$\Delta n = c+d-a-b$$

$$\delta_i^o = \text{equilibrium value of } \delta_i.$$

Since $\delta \ln K = \frac{\Delta\bar{H}}{RT^2}\delta T + \frac{\Delta\bar{V}}{RT}\delta P$, we can write this as

$$-\frac{d}{dt}\,\delta\xi = \frac{1}{\tau}\left[\delta\xi - \frac{H'}{T}\delta T - V'\delta P\right],$$

the general form of irreversible thermodynamics. Here

$$1/\tau = \bar{k}(\delta_C^o)^c(\delta_D^o)^d\phi/RT$$

$$\phi = RT\left(\frac{a^2}{\delta_A}+\frac{b^2}{\delta_B}+\frac{c^2}{\delta_C}+\frac{d^2}{\delta_D}-(\Delta n)^2\right)$$

$$H' = n\Delta\bar{H}$$

$$V' = n\Delta\bar{V}$$

and the relaxation strength is as usual

$$Z = \mathrm{Im}\,K_S(\omega)$$

$$= \frac{(V'-\bar{V}\theta^\infty H')^2}{\bar{V}\phi\left[1+(H')^2/TC_p^\infty\phi\right]}\,\frac{\omega\tau}{\left[1+\omega^2\tau^2\right]} \qquad \text{(I.9)}$$

For multiple equilibria, the coupling of the reactions (one reaction's product is another's reactant, as for the pair $A+A_{n-1}\rightleftharpoons A_n$, $A+A_n\rightleftharpoons A_{n+1}$) must be removed by taking appropriate linear combinations of reactions, 'normal modes' of reaction. Eigen and deMaeyer[4] give the necessary linear algebra. The redefined equilibrium constants, volume changes, etc. can be solved for on a computer--or an analytic solution can be obtained if our choice of progression of

the elementary parameters K_n, ΔV_n, etc. is a lucky one.

The expressions for the mixing free energy and for the general relaxation strength are our mainstays in evaluating any model of the equilibria. We require three results for an acceptable model:

(1) Z, summed over the reactions and regarded as a function of the macroscopic composition, must have the correct peaking at $\underline{X}$(lutidine)$\cong$0.1, including width and height. Now, Z is hard to compute for the general case of coupled reactions. However, we do know that the principal contributor to relaxation is the complexation A-B, and not the water self-association, since pure water absorbs very little. If we assume the complexation reactions are all uncoupled, then at a frequency $f \ll 1/\tau_i$ for all τ_i such as we use,

$$\alpha/f^2 \sim \sum_n Z_n \tau_n$$

$$= \sum_n \frac{(V'-\bar{V}\theta^\infty H'_n)^2}{\bar{V}\phi_n(1+[H']_n^2/TC_p^\infty \phi_n)} \cdot \frac{1}{\bar{k}_n \delta_{Bn} \phi_n} .$$

Under the reasonable assumption that for all $\underline{n}$

$$V'_n = V'$$

$$H'_n = H',$$

and noting that the parameters $\bar{V}$, θ^∞, and TC_p^∞ are independent of $\underline{n}$, the measure of α/f^2 simplifies,

$$\alpha/f^2 \sim \sum_n \frac{1}{\bar{k}_n \delta_{Bn}(\phi_n^2 + \text{const. } \phi_n)}$$

At the end points $X_B = 0$ or 1, this can be shown to vanish

as it must; $\delta_{Bn}\phi_n \rightarrow$ finite limit, $\phi_n \rightarrow \infty$.

Practical calculations are easiest and still accurate if we model $\bar{V}, \theta^{\infty}$, and C_p^{∞} as linearly varying with composition. The progression of $\bar{k}_n$ with n must be decided upon. Two simple choices are that they are independent of n or that they follow the same progression as the K_n. Whatever the choice of progression, the sum over n in the α/f^2 measure must be done numerically. Once a reasonable shape for α/f^2 as a function of X_B has been obtained by adjusting the model parameters, it remains to check the absolute magnitude of the calculated α/f^2. While the absolute value can be changed by scaling the $\bar{k}_n$ uniformly, they cannot be adjusted such that $\tau_n \gtrsim 1/f_{max}$, where f_{max} is the upper limit of the dispersion-free frequency range--at least 13.5 MHz. in our system.

In our original calculations on all models, we used a simple and intuitive, but incorrect, measure of α/f^2, namely δ_{AB} itself for the simplest case where B associates only with monomer water A. We therefore do not report our results in this regard. Our conclusions on phase behavior are still valid. The correct measure should be computed and evaluated for our models at some later date, and the problem of reaction coupling should be attacked.

(2) The free energy of mixing must generate a critical point at the proper low mole fraction $X_B = 0.065$. Let us define $\mathcal{G} = G_{mix}/RT$ and $\mathcal{G}' = \partial\mathcal{G}/\partial X_A$, $\mathcal{G}'' = \partial^2\mathcal{G}/\partial X_A^2$.

The critical condition is $\mathcal{A}''= 0$ at some X_B. It is easy to derive that

$$\mathcal{A}''_{chem}= \frac{2}{\delta_A}\delta'_A + \frac{X_A}{\delta_A^2}\left[\delta_A\delta''_A-(\delta'_A)^2\right] - \frac{2}{\delta_B}\delta'_B + \frac{X_B}{\delta_B^2}\left[\delta_B\delta''_B-(\delta'_B)^2\right]$$

where $\delta'_A = \partial\delta_A/\partial X_A$, $\delta'_B = \partial\delta_B/\partial X_A$, etc.

It is simplest to express everything in terms of δ_A and its derivatives, using the chain rules

$$\delta'_B = (\partial\delta_B/\partial\delta_A)\delta'_A,\ \delta''_B = (\partial\delta_B/\partial\delta_A)\delta''_A.$$

Further, δ'_A, δ''_A, and $\partial\delta_B/\partial\delta_A$ are most compactly derived by implicit differentiation--of the polynomial equation for δ_A and X_A for the first two, and of the sum rule relation

$$\delta_B = 1 - \sum_n \delta_n - \sum_n \delta_{Bn} = 1 - \sum_n \delta_n - \delta_B \sum_n K'_n\delta_n$$

$$\Longrightarrow \delta_B = (1-\sum_n \delta_n)/(1-\sum_n K'_n\delta_n)$$

for $\partial\delta_B/\partial\delta_A$.

To get a phase separation, we need to add $\mathcal{A}_{phys}$, some function of composition. Now, $\mathcal{A}''_{chem}$ can bring $\mathcal{A}''$ close to zero, and certain of the models favor smallness and flatness of $\mathcal{A}''_{chem}$ at low X_B where we require it. A $\mathcal{A}_{phys}$ of the simple form $AX_A^{\,n}X_B$ can then be added, which peaks at $X_B = 3/(n+4)$. For $X_c = 0.065$ to be generated, n has to be about 50, which is very unrealistic. $\mathcal{A}_{phys}$ becomes a narrow spike. An inverse exponential such as $A\exp(a/(|X_B-X_c|+b))$ might be more realistic. Any form, however, is hard to justify on any grounds over and above the phase behavior.

Finally, we note that $\mathcal{A}_{phys}$ may alter the activity coefficients of the true species, and the equilibria must be correspondingly adjusted.

(3) The net temperature dependence of $\mathcal{A}'' = \mathcal{A}''_{chem} + \mathcal{A}''_{phys}$ must give a lower consolute point,

$$\partial \mathcal{A}''(X_B)/\partial T < 0.$$

The chemical equilibrium constants are all reduced by increased temperature, since the enthalpies of reaction are all negative. $\mathcal{A}''_{chem}$ is consequently changed. In all our models, $\mathcal{A}''_{chem}$ pulled away from zero at extreme mole fractions and bulged toward zero at intermediate X_B, as the temperature rose. To get $\partial \mathcal{A}''/\partial T < 0$ at low X_B, the major temperature dependence must be in $\mathcal{A}''_{phys}$, which is surprising and discouraging. The model for $\mathcal{A}_{phys}$ becomes more arbitrary yet more important for properties. This difficulty is our principle one, as cited in paper II.

Before ending this Appendix by listing the key equations for three chemical models, we mention that two more thermodynamic criteria could be added: accurate predictions of volume and enthalpy changes on mixing, $\Delta \bar{V}_{mix}$ and $\Delta \bar{H}_{mix}$. We do not have any data on the latter for our system, but the former is modestly informative for lutidine: water. An extra use of the volume information is in setting $\bar{V}'$ for the complexation, for use in calculating the relaxation strengths, hence $\propto / f^2$. The detailed equations for computing $\bar{V}_{mix}$ are developed as follows:

$$\Delta\bar{V}_{mix} = V^E = \bar{V}(X_B) - \bar{V}_o(X_B)$$

where

$\bar{V}_o(X_B)$ = volume per mole of monomers, unmixed

$\bar{V}(X_B)$ = volume per mole of monomers, mixed.

In turn,

$$\bar{V}_o(X_B) = X_A\bar{V}_A(0) + X_B\bar{V}_B.$$

There is an X_B-dependence of $\bar{V}_A$ because it self-associates, and even an inert diluent shifts the equilibria. Now,

$$\bar{V}_A(0) = V_t(=\text{total volume})/N_t(=\text{total no. monomers})$$

$$= \sum_k n_k\bar{V}_k / \sum_k kn_k = \sum_k \delta_k\bar{V}_k / \sum_k k\delta_k$$

$$\bar{V}_k = k\bar{V}_o + (k-1)\Delta\bar{V} \quad (\text{for } \Delta\bar{V}_n = \text{const.} = \Delta\bar{V})$$

$$\bar{V}_A(0) = \bar{V}_o + \Delta\bar{V}(1 - \sum_k \delta_k / \sum_k k\delta_k) \equiv \bar{V}_o + R_o\Delta\bar{V}.$$

Similarly, for the mixture,

$$\bar{V}(X_B) = V_t/N_t$$

$$V_t \sim \sum_k \delta_k\bar{V}_k + \delta_B\bar{V}_B + \sum_k \delta_{Bk}\bar{V}_{Bk}$$

$$\bar{V}_k = k\bar{V}_o + (k-1)\Delta\bar{V} \text{ , as before}$$

$$\bar{V}_{Bk} = k\bar{V}_o + (k-1)\Delta\bar{V} + \Delta\bar{V}'$$

$$N_t \sim \sum_k k\delta_k + \delta_B + \sum_k (k+1)\delta_{Bk} .$$

Overall, V^E has the form

$$\bar{V}_{mix} = f_1(X_B)\Delta\bar{V} + f_2(X_B)\Delta\bar{V}'.$$

$\Delta\bar{V}$ should be set from the molar volume of pure water $\bar{V}_A(0)$, leaving $\Delta\bar{V}'$ to be set from the least-squares fit of our V^E function to experiment. We take $\bar{V}_o + \Delta\bar{V}$ to represent the molar volume of ice (totally bonded water), and $\bar{V}_o + R_o\Delta\bar{V}$ to be the molar volume of water at some moderately low temperature.

Calculations of the enthalpy of mixing $\Delta\bar{H}_{mix}(X_B)$ follow the exact same outline, and use the same R_o, $f_1(X_B)$, and $f_2(X_B)$.

The chained equilibria of association cause f_1 to peak at very high X_B. For the simplest model of complexation, that of A-B monomer association only ($K'_n=0$ for $n>0$), f_2 also peaks at large X_B. However $\Delta\bar{V}_{mix}$ peaks at $X_B \simeq 0.4$, so the simple model is unphysical for at least the excess volume behavior. The other models have not been examined for their volume predictions. Getting the phase behavior, absorption, and volume/enthalpy behavior to be satisfactorily predicted by any chemical model will no doubt be very difficult, if not impossible.

Details

The algebra of the mole fraction equations is very messy and difficult to do correctly, so we present the key equations for three chemical models as a time saver for any future work on these lines.

Model I:

$$A + A_{n-1} \rightleftharpoons A_n \qquad K_n = K = \delta_n/\delta_A\delta_{n-1}$$

$$A + B \rightleftharpoons AB \qquad K' = \delta_{AB}/\delta_A\delta_B$$

$$X_A = \frac{N_A}{N_A+N_B} = \frac{\cancel{N_{tot}}(\sum_n n\delta_n+\delta_{AB})}{\cancel{N_{tot}}(\sum_n n\delta_n+2\delta_{AB}+\delta_B)}$$

$$= \frac{\delta_A[(1+K')-2KK'\delta_A+KK'(1+K)\delta_A^2]}{1+2(K'-K)\delta_A+(K-K'+K^2-4KK')\delta_A^2+2KK'(1+K)\delta_A^3},$$

$$\equiv \frac{\delta_A[a-b\delta_A+c\delta_A^2]}{1+d\delta_A+e\delta_A^2+2c\delta_A^3}$$

which reduces to the cubic form

$$(2cX_A-c)\delta_A^3+(eX_A+b)\delta_A^2+(dX_A-a)\delta_A+X_A= 0.$$

Explicit forms for the solutions to cubic equations are available, as in the Handbook of Chemistry and Physics. Generally there are three real roots δ_A obtained, only one of which satisfies the constraint that all mole fractions δ_A, δ_B, and δ_{AB} be positive.

$$\delta_B = (1-[1+K]\delta_A)/(1-K\delta_A)(1+K'\delta_A)$$

$$\partial\delta_B/\partial\delta_A = -(a + b\delta_A + c\delta_A^2)/(1-K\delta_A)(1+K'\delta_A)$$

$$\delta_A' = -(1 + d\delta_A + e\delta_A^2 + 2c\delta_A^3)/D$$

$$D = X_A(d + 2e\delta_A + 6c\delta_A^2) - a + 2b\delta_A - 3c\delta_A^2$$

$$\delta_A'' = -\frac{\delta_A'}{D}\left[2(d+2e\delta_A+6c\delta_A^2) + X_A(2e\delta_A'+12c\delta_A\delta_A') +2b\delta_A'-6c\delta_A\delta_A'\right]$$

$\mathcal{H}_{chem}$ is not very flat for this model for any moderate K, K', and δ_{AB} peaks at $X_B = 0.5$.

Model II:

$$A + A_{n-1} \rightleftharpoons A_n \qquad K_n = K$$

$$B + A_n \rightleftharpoons BA_n \qquad K_n' = K'$$

$$X_A = \frac{(1+K')\delta_A - K(1+K')\delta_A^2}{1 + (2K'-3K)\delta_A + (1+3K)(K-K')\delta_A^2 + K(1+K)(K'-K)\delta_A^3}$$

$$\equiv \frac{\delta_A[a - b\delta_A]}{1 + c\delta_A + d\delta_A^2 + e\delta_A^3},$$

cubic if $K \neq K'$, quadratic if $K = K'$.

$$\delta_B = (1-[1+K]\delta_A)/(1-[K-K']\delta_A)$$

$$\partial\delta_B/\partial\delta_A = -(a - b\delta_A)/(1 -[K-K']\delta_A)^2$$

$$\delta'_A = - (1 + c\delta_A + d\delta_A^2 + e\delta_A^3)/D$$

$$D = X_A(c + 2d\delta_A + 3e\delta_A^2) - a + 2b\delta_A$$

A reasonable model.

Model III:

$$A + A_{n-1} \rightleftharpoons A_n \qquad K_n = K$$

$$B + A_n \rightleftharpoons BA_n \qquad K'_n = K'\alpha^n$$

$$\delta_B = \frac{(1 -[1+K]\delta_A)(1 - \alpha K\delta_A)}{(1 - K\delta_A)(1 + \alpha[K'-K]\delta_A)}$$

$X_A \leftrightarrow \delta_A$ relation is quartic, unless $K = K'$, which we promptly assume:

$$\delta_B = (1 - [1+K]\delta_A)(1 - \alpha K\delta_A)/(1 - K\delta_A)$$

$$X_A = \frac{(1 + \alpha K)\delta_A - 2\alpha K(1+K)\delta_A^2 + \alpha K^2(1+K)\delta_A^3}{1 - 2K\delta_A + K(1 -\alpha + K)\delta_A^2}$$

$$\equiv (a\delta_A + b\delta_A^2 + c\delta_A^3)/(1 + d\delta_A + e\delta_A^2)$$

$$\delta'_A = -(1 + d\delta_A + e\delta_A^2)/D$$

$$D = X_A(d + 2e\delta_A) - a - 2b\delta_A - 3c\delta_A^2$$

$$\partial\delta_B/\partial\delta_A = - (a + b\delta_A + c\delta_A^2)/(1 - K\delta_A)^2$$

also a good model.

We used two more models, one the same as model III but with $K'_n = K'\alpha^{n-1}$, and one with self-association of B. The former is not noticeably different from model III, and the latter is unrealistic for our system.

References for Part II:

1. J. H. Andreae, P. D. Edmonds, and J. F. McKellar, Acustica 15,74(1965).

2. The triethylamine: water lower consolute system studied by Brown and Richardson (Phil. Mag. 4,705 1959) probably shows the same effects as our system, but it was not studied at compositions off X_c so they were not recognized.

3. K. F. Herzfeld and T. A. Litovitz, Absorption and Dispersion of Ultrasonic Waves (Academic, N. Y., 1959).

4. M. Eigen and L. de Maeyer, in Techniques of Organic Chemistry, ed. Weissberger, et al. (Wiley, N. Y., 1962), Vol. VIII, Part 2.

General Acknowledgments

I would like to thank Tony Collings and Paul Morrison of this research group for many discussions on this research, particularly for much of the organization and most of the references in the introduction on liquid state theory.

Calculations of Hartree-Fock Polarizabilities for Some Simple Atoms and Molecules, and Their Practicality*

VINCENT P. GUTSCHICK** AND VINCENT McKOY†

Arthur Amos Noyes Laboratory of Chemical Physics
California Institute of Technology
Pasadena, California 91109

Hartree-Fock electric polarizabilities have been calculated for H_2, He, Li, Be, LiH, and N_2. Perturbation theory with all the coupling terms was employed variationally for the first five, using a variety of basis sets for each. Each basis for the perturbation calculations was composed of a zero-order set, plus a first-order set (appropriate to the direction of polarization, for the molecules). The two sets are disjoint to ensure identical zero-order functions for the two molecular polarizability components and, hence, reliable anisotropy values. Nonorthogonal theory as formulated by T. P. Das and K. J. Duff [Phys. Rev. 168, 43 (1968)], assuming exact zero-order orbitals, was used for LiH. For practical reasons, the nitrogen molecule was treated by the fully self-consistent approach

---

* Contribution No.

** National Science Foundation Predoctoral Fellow, 1966-1970.

† Alfred P. Sloan Foundation Fellow.

which does not distinguish orders of perturbation. The results for all six species are in very good agreement with experiment, reflecting both a reliable choice of polarization functions and, more significantly, the basic accuracy of the Hartree-Fock method for the static charge distributions, both unperturbed and perturbed by an electric field.

I. INTRODUCTION AND THEORY

Among variational theories of molecular electronic structure, the Hartree-Fock theory has proved particularly valuable for a practical understanding of such properties as chemical binding, electric multipole moments, and x-ray scattering. It provides the most tractable method of calculating first-order properties under external or internal one-electron perturbations, either developed explicitly in orders of perturbation theory or in the fully self-consistent method. Electric polarizabilities,[1-4] and magnetic properties[5] such as spin coupling, chemical shift, and susceptibility have been treated with the theory. The accuracy and consistency of first-order properties are poorer than those of zero-order properties. Most often this is due to use of explicit approximations in solving the first-order perturbation equations, or to the inaccuracies of the zero-order molecular orbitals (MO's) which may undermine the variational principle for the second-order energy. Theoretical studies using many-body theory[6, 7] indicate that the Hartree-Fock theory itself is basically sound for static or zero-frequency properties, and we do not intend to draw further conclusions along this line. Rather, we have performed representative calculations of static electric polarizabilities for small atoms and molecules to underscore the basic soundness of perturbed Hartree-Fock theory, giving important and practical guidelines for selecting the variational basis sets for the first-order wavefunction.

Our first studies were on H_2 and the atoms He, Li, Be using a variety of simple wavefunctions constructed from Slater type orbitals (STO's). For such few-electron species, the problem is best solved by constructing explicit first-order perturbation equations for the perturbation ϕ_i^1 to the unperturbed molecular orbitals ϕ_i^0. The unperturbed electronic Hamiltonian contains one-electron terms $\underline{h_i^0}$ and two-electron terms $\underline{g_{ij}} = 1/\underline{r_{ij}}$ (in atomic units),

$$H^0 = \sum_i h_i^0 + \sum_{i<j} \sum g_{ij} \quad . \tag{1}$$

The perturbation due to an electric field $\mathcal{E}$ along the axis $\underline{k}$ is

$$H^1 = \mathcal{E} \sum h_i^1 = \mathcal{E} \sum r_{ik},$$

and the zero-order and first-order Hartree-Fock equations are respectively

$$(h^0 + \sum_j \langle \phi_j^0 | \cdot | \phi_j^0 \rangle - \epsilon_i^0) \phi_i^0 = 0 \tag{2a}$$

$$(h^0 + \sum_j \langle \phi_j^0 | \cdot | \phi_j^0 \rangle - \epsilon_i^0) \phi_i^1$$

$$+ (h^1 + \sum_j [\langle \phi_j^1 | \cdot | \phi_j^0 \rangle + \langle \phi_j^0 | \cdot | \phi_j^1 \rangle] - \epsilon_i^1) \phi_i^0 = 0, \tag{2b}$$

with the usual convention of order-by-order orthogonality,

$$\langle \phi_i^0 | \phi_j^0 \rangle = \delta_{ij} \tag{3a}$$

$$\langle \phi_i^0 | \phi_j^1 \rangle = 0. \tag{3b}$$

Here we use the shorthand notation

$$\langle a | \cdot | b \rangle c = \langle a(j) | g_{ij} | b(j) \rangle c(i) - \langle a(j) | g_{ij} | c(j) \rangle b(i). \tag{4}$$

The zero-order equation is commonly solved variationally using STO's (χ_p^0) centered on the nuclei,

$$\phi_i^0 = \sum_p c_{ip}^0 \chi_p^0. \tag{5}$$

The first-order equation may be solved variationally in a similar way. Operationally, this means making Eq. (2b) hold for all projections with the first-order basis set $\{\chi^1\}$,

$$\langle \chi_p^1 | h^0 + \sum_j \langle \phi_j^0 | \cdot | \phi_j^0 \rangle - \epsilon_i^0 | \phi_i^1 \rangle + \langle \chi_p^1 | h^1 + \sum_j [\langle \phi_j^0 | \cdot | \phi_j^1 \rangle + \langle \phi_j^1 | \cdot | \phi_j^0 \rangle - \epsilon_i^1 | \phi_i^0 \rangle = 0, \tag{6}$$

for all p and i.

Substitution of the appropriate basis expansions for the ϕ_i^1, including the explicit forms for the matrix elements ϵ_i^1, yields linear equations for the first-order coefficients c_{ip}^1. This is equivalent to minimizing the second-order energy, assuming the exactness of the zero-order solution in the total basis $\{\chi\} = \{\chi^0\} + \{\chi^1\}$,

$$\langle \chi_r | h^0 + \sum_j \langle \phi_j^0 | \cdot | \phi_j^0 \rangle - \epsilon_i^0 | \phi_i^0 \rangle = 0 \qquad (7)$$

for all r.

Given a zero-order basis $\{\chi^0\}$ and the direction or axis of polarization k, the polarization functions $\{\chi^1\}_k$ can be picked judiciously to include all important shifts in orbital amplitudes while remaining few in number. A major part of the work reported herein concerns just such choice of the basis. We have shown that the distortion of ϕ_i^0 can be adequately described by allowing each atomic orbital in the MO to distort in the electric field as a pure hydrogenic orbital would distort. For the H_2 molecule and the three atoms He, Li, Be, our work is further simplified since the polarization functions are automatically of a different symmetry from the occupied orbitals: σ_u vs. σ_g for H_2, and p vs. s for the atoms. The calculations proceed very straightforwardly to the second-order energy in the electric field ,

$$\mathcal{E}^2 E^{(2)} = \mathcal{E}^2 \sum_i \langle \phi_i^1 | h^1 | \phi_i^0 \rangle, \qquad (8a)$$

which directly measures the polarizability as

$$E^{(2)} = -\tfrac{1}{2}\alpha. \tag{8b}$$

We obtained excellent agreement with most reliable values, either experimental or theoretical. The results were markedly insensitive to the choice of zero- and first-order bases.

We were encouraged to try molecules of lower symmetry and more electrons. The first case was LiH, previously treated by Lipscomb and Stevens[1] in similar fashion. Now our simple expedient of distorting the atomic orbital basis functions as if they described hydrogenic atoms yields a first-order basis composed of functions not automatically orthogonal to the occupied orbitals by symmetry. We can Schmidt orthogonalize the χ_p^1 to the χ_q^0 before doing any perturbation calculations, but this involves much manipulation of the raw one- and two-electron integrals over basis functions. The nonorthogonal perturbation formalism of Das and Duff[8] performs instead a symmetric deorthogonalization in the matrix equations (6). They perform the deorthogonalization before separating orders of perturbation in the Hartree-Fock equations and minimizing the second-order energy with respect to the ϕ_i^1. Thus, they obtain extra terms in the first-order equation due to inexactness of the ϕ_i^0 in the augmented basis $\{\chi^0\} + \{\chi^1\}_k$: Eq. (7) is not satisfied. Most often these terms are small and can be dropped much as Das and Duff do in their final presentation. We then have at hand a formalism for computing separately the two polarizability

components $\alpha_{\underline{k}}$ ($\alpha_{\underline{zz}}$ and $\alpha_{\underline{xx}}$) in small total bases while retaining reliability of the anisotropy $\alpha_{\underline{k}} - \alpha_{\underline{\ell}}$.

Finally we tried the N_2 molecule, with its many electrons and many occupied symmetry types of orbitals. Practical zero-order bases of Gaussian type orbitals (GTO's) do not keep the ϕ_i^0-inexactness terms in the perturbation equations sufficiently small any more. Even in LiH, GTO's cause this problem. The inexactness terms are too prolific to include. The problem is avoided by shifting both zero- and first-order calculations to the common, enlarged basis $\{\chi^0\} + \{\chi^1\}_k$. The unoccupied virtual orbitals from zero-order can then act as the new χ_p^1. To once more avoid much manipulating of two-electron integrals, we abandoned the perturbation formalism in favor of the fully self-consistent approach, equivalent at low fields $\mathcal{E}$. The basic Hartree-Fock equations unseparated into orders are solved, given a finite electric field. The field is small enough such that $\phi_i \approx \phi_i^0 + \phi_i^1$ and $\underline{E} \simeq \underline{E^0} + \mathcal{E}\underline{E^{(1)}} + \mathcal{E}\underline{E^{(2)}}$ and higher orders are negligible (for N_2, $\underline{E}^{(1)} = 0$, too). Now, if one computed the two polarizability components separately, the anisotropy $\alpha_k - \alpha_\ell$ would be less reliable because the unperturbed energy is doubtlessly shifted differently in the two different total bases $\{\chi^0\} + \{\chi^1\}_k$, $\{\chi^0\} + \{\chi^1\}_\ell$. We thus prefer one large basis $\{\chi^0\} + \{\chi^1\}_k + \{\chi^1\}_\ell$ for all calculations. Fortunately, for N_2 a good zero-order basis $\{\chi^0\}$ already contains many functions which may also act as polarization functions and $\{\chi^0\}$ is not greatly enlarged by adding the nonredundant parts of $\{\chi^1\}_k$ and $\{\chi^1\}_\ell$.

Beyond the approximation of finite basis expansion for the molecular orbitals ϕ_i (in all orders), several approximations to Hartree-Fock theory have been proposed. The explicit perturbation equations (2b) are altered in these approximations to eliminate the need for all or most of the two-electron integrals over basis functions. Dalgarno[9] has discussed these methods, and the approximations have been evaluated relative to the "full theory" by Langhoff, Karplus, and Hurst.[10] While these theories save most of the effort in evaluating a first-order property, they consistently undervalue the polarizability to an unpredictable extent. We wish to test the accuracy of full Hartree-Fock theory which neglects only instantaneous correlation. We do not consider further the approximations to its perturbation formalism.

II. APPLICATIONS AND RESULTS

Many polarizability, magnetic susceptibility, and magnetic shielding calculations have been done for H_2, by all manners of perturbation theory and with all types of unperturbed wavefunctions. We focused on the simpler zero-order wavefunctions, the Coulson[11] and Ransil[12] Hartree-Fock (HF) functions and the Wang[13] valence-bond (VB) function. The Coulson and Wang wavefunctions use only one 1s atomic orbital on each center, while the Ransil function includes one 2s and one $2p_z$ in addition. In each case the wavefunction was perturbed by letting each basis function χ_p^0 assume the variational form (there is only one MO).

$$\chi_p \rightarrow \chi_p^0 + c\mathcal{E}\chi_p^1, \tag{9}$$

with c a variational constant. For the two HF wavefunctions this is equivalent to the perturbed HF formalism outlined previously,

$$\phi_i \rightarrow \phi_i^0 + \mathcal{E}\phi_i^1.$$

The analogous VB treatment involves straightforward minimization of the second-order energy.

The χ_p^1 were selected initially as solutions of the hydrogen-like atom in an electric field with χ_p^0 as the unperturbed wavefunction,

$$(-\tfrac{1}{2}\nabla^2 + \frac{Z}{r} + \frac{Z^2}{2n_p^2})\chi_p^1 + (-\zeta_p r_k - \epsilon_{pk}^1)\chi_p^0 = 0. \tag{10}$$

Here n_p is the principal quantum number of χ^0_p, ζ_p is the orbital exponent, Z is the effective nuclear charge $n_p\zeta_p$, and ϵ^1_{pk} is the first-order energy associated with the perturbation $-\mathcal{E}r_k$ along the Cartesian axis k. Thus a 1s STO in a z-directed field yields as χ^1_p a linear combination of $2p_z$ and $3p_z$ of the same ζ_p; a 2s Slater--a $2p_z$, $3p_z$, and $4p_z$ combination; a $2p_x$--a $3d_{xz}$ and $4d_{xz}$; a $2p_z$--a 1s, 2s, 3s, 4s, $3d_{3z^2-r^2}$, and $4d_{3z^2-r^2}$. All of the hydrogen molecule trials used the STO's in the χ^1_p frozen in their original linear combinations, even if, for example, only $2p_z$ and $4p_z$ were used for the 2s polarization. The molecular calculations on LiH and N_2 in contrast used Eq. (10) simply as an indication of important primitive basis functions, STO or GTO, to include in bases unconstrained by any linear combinations.

The results are in Table I. Trials A, B, and E are most relevant, as they compare three different simple wavefunctions under essentially complete polarization according to Eq. (11). They are compared to the extremely accurate polarizabilities of Kolos and Wolniewicz[14] who used a 54-term zero-order wavefunction and 34 terms in first order. Quadratic interpolation was done to the internuclear distances R used in our calculations. Sufficiently accurate experimental polarizabilities are only available at optical frequencies. The insensitivity of our results to the choice of the zero-order functions along with the first order wavefunction chosen according to Eq. (11), and their agreement with experiment, is very encouraging. Result C shows that optimization of the exponents for

polarization functions is unnecessary, and case D indicates a need for polarizing the majority of the zero-order basis.

The He, Li, and Be atoms were treated next, using Clementi's[15] unperturbed wavefunctions computed in double-zeta basis sets. An accurate He polarizability, α = 1.397 a.u., has been obtained by Johnston, et al.[16] by extrapolation of the experimental dielectric constant to zero pressure. Dutta, et al.,[17] have used many-body theory on He and found α = 1.407 a.u. Our result of 1.319 a.u. is 6.0% low relative to the experiments, the first in a trend to undervaluing the correct polarizability for atoms. The best Li polarizability was determined by Fues[18] using the Stark splitting in lithium metal; molecular beam measurements use single atoms rather than bulk metal but have been far less precise. Our Li wavefunction, which is of unrestricted Hartree-Fock form, gave a result of 167.6 a.u., 7.9% below the experimental value of 182 a.u. Beryllium atom provided our greatest success, as it has for several other calculations using Hartree-Fock theory; the computed value of 45.28 a.u. lies only 3.2% lower than the accurate many-body result of 46.77 a.u. due to Kelly.[7] No experimental results are reliable. All three atomic calculations showed negligible, usually negative contributions to α by the core orbitals, as might be expected.

The LiH molecule, as a heteronuclear species with two electronic shells, provides a somewhat better test of Hartree-Fock theory, particularly its nonorthogonal formulation discussed in the previous section. Ransil's[19] wavefunction was chosen for zero order

at the experimental internuclear distance $\underline{R} = \underline{R_e} = 3.015$ a.u. The perpendicular polarization was represented by the full set of four hydrogenic-model polarization functions χ^1_p--see Eq. (11). Standard orthogonal perturbation theory[20] could be used for $\alpha_\perp$, yielding the value 26.22 a.u. This agrees well with the most reliable theoretical estimate of 27.00 a.u. by Stevens and Lipscomb.[1] The parallel component is more difficult, requiring nonorthogonal theory. We chose to test here many of our ideas on the adequacy of polarization functions, and so we pooled all 13 primitive χ^1_p as unconstrained individual STO's, plus the two virtuals from zero-order. The complete basis yielded $\alpha_\parallel = 25.29$. Stevens and Lipscomb[1] did not compute $\alpha_\parallel$ because of the change of zero-order basis necessary to retain the orthogonal perturbation theory. Kolker and Karplus[2] have made cruder calculations, $\alpha_\parallel = 25.38$ a.u. and $\alpha_\perp = 34.42$ a.u., which are in poor agreement with ours, but at least show a negative anisotropy $\alpha_\parallel - \alpha_\perp = -9.04$ a.u.; our value is -0.93 a.u. We could conclude that the $\underline{2p}, \underline{3p}$-like orbitals from polarization of the tight $\underline{1s_{Li}}$, the $\underline{2p}$ from the $2s_{Li}$ (nearly redundant with the zero-order $\underline{2p}$), and the $\underline{2s}$ from the $\underline{2p_{Li}}$ polarization were all unimportant. This new basis $\{\chi^1\}$ yielded $\alpha_\perp = 25.04$ to confirm our judgment. Many other deletions were tried, with a nine-function set being the smallest to give a good result: the two virtuals plus the $\underline{3p}, \underline{4p}$ STO's from the $\underline{2s_{Li}}$, the $\underline{1s}, \underline{3s}, \underline{3d}$ from the $\underline{2p_{Li}}$, and the $\underline{2p}, \underline{3p}$ from the $\underline{2s_H}$ gave $\alpha_\parallel = 24.63$ a.u. In all these calculations the inner core orbital was seen to back-polarize slightly, following the trend of the atoms.

The N_2 molecule is tractable only in a Guassian basis set due to the large number of two-center, two-electron integrals required. For experience in selecting the $\{\chi_p^1\}$, we returned to the LiH molecule in a GTO basis. We attempted to reproduce the non-orthogonal perturbation theory results for STO's, choosing Gaussians contracted by Huzinaga's[21] prescription to mimic the STO's for atoms. While the zero-order energy was close, the dipole moment was poorer and the polarizability using just the two virtual orbitals was two-thirds that obtained using the STO's. This indicates poor tails for the Gaussian wavefunctions. We tried to add to the non-orthogonal perturbation theory the extra terms due to inexactness of the ϕ_i^0, but these proliferated wildly. Instead we settled for an equivalent fully-self-consistent approach discussed earlier. The polarizability is taken from the ratio of the induced dipole moment to the electric field, possibly extrapolated to zero field for greater accuracy. We did not do such extrapolations, since the larger inherent error of Hartree-Fock theory does not warrant it.

We began our LiH calculations with a very large basis of zz functions covering a full range of exponents in 1s, 2p, and 3d GTO's for Li and 1s, 2p for H. By trial and error we pared the basis to 15 functions, which yielded $\alpha_{\parallel} = 21.06$, $\alpha_{\perp} = 22.56$. The anisotropy is negative as for STO's, but absolute magnitudes are down about 15%, somewhat disturbingly. Perhaps lack of closely-spaced exponents for the Gaussians is responsible, as this disallows construction of more diffuse functions with radial nodes.

Proceeding to N_2, we built from the zero-order basis of Dunning[22] consisting of 13 contracted GTO's (22 primitives) on each nitrogen, four of the s-type, three of each p-component. The calculations were done at the experimental internuclear distance, 2.068 a.u. We added on each center a diffuse 1s (ζ = 0.0800) for z-polarization of the $2p_z$ or x-polarization of the $2p_x$; a similarly diffuse 2p (0.0800) of all three directions for x and z-polarizations of the σ orbitals; and a host of d-functions all of moderately diffuse exponent 0.200. Among the d-functions the two-center linear combination $XX_A + XX_B$ covers the x-field on π_u^x orbital; $YY_A + YY_B$ is simply the complement to the above for the σ-orbital balance; $XY_A + XY_B$ covers the x-field on π_u^y, while $YZ_A + YZ_B$ is for the z-field; XZ_A and XZ_B are used independently to represent the x-polarization of σ_g, σ_u and the z-polarization of the π_u^x orbital.

The computed $\alpha_{\parallel}$ and $\alpha_{\perp}$ are 14.97 and 9.46 a.u., respectively. It is of practical interest that it was extremely difficult to obtain convergence of the SCF procedure for the z-polarized case. Three-point extrapolation[23] by the e_k procedure for oscillating and diverging series was used, as outlined by Petersson and McKoy.[23] The comparable experimental values are $\alpha_{\parallel}$ = 16.06 and $\alpha_{\perp}$ = 9.78 a.u. obtained dynamically with Na D light.[24] Dispersion corrections may be estimated to give static polarizabilities of 15.9 and 9.7 a.u. The agreement of theory and experiment is quite remarkable. It may be partly fortuitous, due to a 5-15% underestimation of α when using a GTO basis, or to increased inaccuracy of the highly polarizable valence orbitals in systems of many electrons. One more

interesting feature of the N_2 polarization is the coupling of orbitals in pairs under the field influence. The $1\sigma_g$, $1\sigma_u$ orbitals are essentially unpolarized for both field directions. For an $\underline{x}$-field, the $2\sigma_g$ gives 11.4% of the polarizability and the $2\sigma_u$ 31.0%; the $3\sigma_g$ and $1\pi_u^x$ couple, with to latter anti-polarizing, to give another 42.4%; and the $1\pi_u^y$ yields the last 15.2%. In a $\underline{z}$-field the $2\sigma_g$ contributes 4.1%; the $2\sigma_u$-$3\sigma_g$ coupled give 26.0%; the $1\pi_u^x$ 31.1%; and the $1\pi_u^y$ 38.8%. The disparity of the last two contributions is due to a slight inequivalence in the zero-order descriptions of the two orbitals: the $\underline{xz_A}$, $\underline{xz_B}$ polarization functions also enter into the unperturbed $1\pi_u^x$.

III. CONCLUSIONS

Hartree-Fock theory for the static first-order property of polarizability appears adequate when solved exactly within a modest basis, under quite general circumstances of molecular structure and of basis set composition. The smallness of electron correlation effects has been previously displayed explicitly with many-body theory[6,7] in special cases, and the work reported here supports this conclusion more widely. Hartree-Fock may give poor electronic excitation frequencies, but at all perturbing field frequencies low relative to correlation processes for virtual or real excitations it does well for properties. The model should be useful for calculating such experimentally inaccessible properties as molecular polarizabilities in their dependence on internuclear distance, $\alpha(\underline{R})$. The variation of the polarizability of a pair of atoms as a function of distance has well-defined effects, including increased cross section for vibrational excitation in electron-molecular collisions, strong contribution to the second dielectric virial coefficient,[25] collision induced light scattering[26] and a nonlinear refractive index.[27] Of course, one must be careful in using molecular Hartree-Fock wavefunctions far from equilibrium internuclear separations $\underline{R_e}$: for molecules dissociating into fragments with unclosed shells, the Hartree-Fock wavefunction is incorrect except near $\underline{R_e}$. Multiconfiguration self-consistent field calculations can remedy this fault while increasing the computing effort; the fully self-consistent approach to polarizabilities remains viable in this framework.

ACKNOWLEDGMENTS

The authors would like to thank David Huestis, Jeffrey Hay, Robert Ladner, Woodrow Wilson, Thomas Dunning, Richard Blint, William A. Goddard, III, and Luis Kahn for help with computer programming. We had many helpful discussions on theory with Thomas Dunning and William A. Goddard, III. Tara P. Das provided much help in clarifying points about nonorthogonal perturbation theory.

REFERENCES

[1]R. M. Stevens and W. N. Lipscomb, J. Chem. Phys. 40, 2238 (1964).

[2]H. J. Kolker and M. Karplus, ibid. 39, 2011 (1963).

[3]V. G. Kaveeshar, K. T. Chung, and R. P. Hurst, Phys. Rev. 172, 35 (1968).

[4]G. P. Arrighini, M. Maestro, and R. Moccia, Chem. Phys. Letters 1, 242 (1967).

[5]H. F. Hameka, Advanced Quantum Mechanics (Addison-Wesley, Reading, Mass., 1965).

[6]T. C. Caves and M. Karplus, J. Chem. Phys. 50, 3649 (1969).

[7]H. P. Kelly, Phys. Rev. 136, B896 (1964).

[8]T. P. Das and K. J. Duff, Phys. Rev. 168, 43 (1968).

[9]A. Dalgarno, Adv. Phys. 11, 281 (1962); with J. M. McNamee, J. Chem. Phys. 35, 1517 (1961).

[10]P. W. Langhoff, M. Karplus, and R. P. Hurst, ibid. 44, 505 (1966).

[11]C. A. Coulson, Trans. Faraday Soc. 33, 1479 (1937).

[12]B. J. Ransil, J. Chem. Phys. 35, 1967 (1961).

[13]S. Wang, Phys. Rev. 31, 579 (1928).

[14]W. Kolos and L. Wolniewicz, J. Chem. Phys. 46, 142 (1967).

[15]E. Clementi, IBM Research Paper RJ-256, August 6, 1963.

[16]D. A. Johnston, C. J. Oudemans, and R. H. Cole, J. Chem. Phys. 33, 1310 (1960).

[17]N. C. Dutta, T. Ishihara, C. Matsubara, and T. P. Das, Phys. Rev. Letters 2, 8 (1969).

[18]E. Fues, Z. Phys. 82, 536 (1933).

[19]B. J. Ransil, Rev. Mod. Phys. 32, 245 (1960).

[20]R. M. Stevens, R. M. Pitzer, and W. N. Lipscomb, J. Chem. Phys. 38, 550 (1963).

[21]S. Huzinaga, ibid. 42, 1293 (1965).

[22]T. H. Dunning, ibid. 53, 2823 (1970).

[23]P. Wynn, Math. Aids Computation 54, 91 (1956); G. A. Petersson and V. McKoy, J. Chem. Phys. 46, 4362 (1967).

[24]A. A. Maryott and F. Buckley, U.S. Natl. Bur. Stds. Circular 537 (1953).

[25]See, for example, T.-K. Lim, B. Linder, and R. A. Kromhout, J. Chem. Phys. 52, 3831 (1970).

[26]J. P. McTague and G. Birnbaum, Phys. Rev. 3A, 1376 (1971).

[27]J. P. McTague, C. H. Lin, T. Gustafson, and R. Chiao, Phys. Letters 32A, 82 (1970).

TABLE I. Polarizability of H_2 for various wavefunctions.

	R	STO Bases $\{\chi^0\}$, $\{\chi^1\}$[a] for Hartree-Fock (HF) or Valence Bond (VB) Wavefunctions	$\alpha_{\parallel}$ (% error)[b]	$\alpha_{\perp}$ (% error)
(A)	1.402	$\{0\}$ = 1s (1.197) HF $\{1\}$ = 2p, 3p (1.197)	6.345 (-1.0)	4.238 (-7.5)
(B)	1.406	$\{0\}$ = 1s (1.166) VB $\{1\}$ = 2p, 3p (1.166)	6.003 (-7.1)	4.441 (-3.4)
(C)		$\{1\}$ = 2p, 3p (1.100)		4.469 (-2.8)
(D)	1.402	$\{0\}$ = 1s (1.378), 2s (1.176) 2p (1.820) HF $\{1\}$ = 2p, 3p (1.378)	6.090 (-4.9)	4.102 (-10.5)
(E)		$\{1\}$ = 2p, 3p (1.378) 2p, 4p (1.176)	6.321 (-1.3)	4.597 (+2.9)

[a] First-order bases are constrained as linear combinations by the solution of Eq. (10). See text.

[b] Error is relative to the accurate theoretical values of Ref. 14. See text. Accurate values of ($\alpha_{\parallel}$, $\alpha_{\perp}$) are (6.407, 4.584) at $\underline{R}$ = 1.402 and (6.460, 4.597) at $\underline{R}$ = 1.406. All values are atomic units (a.u.), $\underline{a_0^3}$.

Appendix I. Orbital Basis Sets and Their Method of Selection

In our perturbation calculations on H_2, He, Li, Be, and LiH using STO's, our choice of polarization functions was guided by Eq. (10) of the paper. This equation establishes the polarization function for any given pure hydrogenic function. The exact solution for z-polarization are described below. Subscripts STO and HO on orbitals mean "Slater-type orbital" and "hydrogenic orbital," respectively; the two differ in the case of nominal 2s form.

$$(A)\quad \chi^0 = (1s)_{STO} = (1s)_{HO} \quad ; n_p = 1$$

$$\chi^1 = \frac{1}{\zeta 3}\left[(2p_z)_{STO} + \sqrt{\frac{15}{8}}\ (3p_z)_{STO}\right]$$

As noted in the text, ζ is the orbital exponent of the χ^0, as well as of all STØ's in χ^1.

$$(B)\quad \chi^0 = (2s)_{STO} = \left[(1s)_{HO} - (2s)_{HO}\right]/\sqrt{3}$$

We assume that the χ^1 for the two HO components add algebraically. There is an additional problem, that $\underline{(2s)_{HO}}$ and $\underline{(2p_z)_{HO}}$ are degenerate; to solve Eq. (10) for χ^1, we must use the linear combinations $\frac{1}{\sqrt{2}}\left[\underline{(2s)_{HO}} \pm \underline{(2p_z)_{HO}}\right]$ appropriate for degenerate perturbation theory. Corresponding first-order energies are $\underline{E}^{(1)} = \mp\ \frac{3}{2\zeta}$. Then we construct $\chi^1_{\underline{2s, HO}}$ as $\frac{1}{\sqrt{2}}\left[\chi^1_{\underline{(2s+2p), HO}} + \chi^1_{\underline{(2s-2p), HO}}\right]$. The result is:

$$\chi^1 = \frac{1}{\zeta^3}\left[\left(1 - \frac{5}{2}\sqrt{3}\right)(2p_z)_{STO} + \sqrt{\frac{15}{8}}\,(3p_z)_{STO} - \frac{3}{2}\sqrt{35}\,(4p_z)_{STO}\right]$$

$$(C)\ \chi^0 = (2p_z)_{STO} = (2p_z)_{HO}$$

Following (B), we construct

$$\chi^1_{\underline{2p_z,\,HO}} \text{ as } \frac{1}{\sqrt{2}}\left[\chi^1_{\underline{(2s+2p),\,HO}} - \chi^1_{\underline{(2s-2p),\,HO}}\right],$$

with the result

$$\chi^1 = \frac{1}{4\zeta^3}\left[(1s)_{STO} - \sqrt{3}\,(2s)_{STO} - \sqrt{\frac{45}{8}}\,(3s)_{STO} + \sqrt{\frac{35}{4}}\,(4s)_{STO}\right]$$

$$- \frac{3}{4\zeta^3}\left[(3d_{3z^2-r^2})_{STO} + \sqrt{\frac{7}{2}}\,(4d_{3z^2-r^2})_{STO}\right]$$

$$(D)\ \chi^0 = (2p_x)_{STO}$$

$$\chi^1 = \frac{1}{\zeta^3}\left[\sqrt{\frac{27}{8}}\,(3d_{xz})_{STO} + \sqrt{\frac{21}{4}}\,(4d_{xz})_{STO}\right]$$

For the $\alpha_{\parallel} = \alpha_{zz}$ calculations on LiH, the constraints of the χ^1 to the above linear combinations were relaxed, and the primitive STO's occuring in the χ^1 were used as individual free basis functions.

For zero-order bases $\{\chi^0\}$ composed of GTO's, the unperturbed reference Hamiltonian for each function is no longer than that of the hydrogenic atom with its coulombic binding potential. It is instead the Hamiltonian for a harmonic oscillator. This is not realistic for the χ^0 as used, so we adopted a different technique of

selecting the χ^1 for nonorthogonal perturbation theory or fully self-consistent calculations. Basically, we referred the total GTO basis to an equivalent STO basis, constructed the corresponding (unconstrained) STO $\{\chi^1\}$, and converted the latter to GTO's. As the first step we examined the range of orbital exponents in the GTO's of any one type on one center, such as 1s on Li in the LiH case. Then we reversed Hurzinaga's (Ref. 20) prescriptions for fitting one STO with n GTO's by energy minimization. For example, Huzinaga reports that four $(1s)_{GTO}$ used to fit one $(1s)_{STO}$ range in exponents ζ_G from $0.123\ (\zeta_s)^2$ through $13.36\ (\zeta_s)^2$. In reversing Huzinaga's procedure, we identify the extreme high and low Gaussian exponents with components in expansions of the two STO's with highest and lowest exponents ζ_s. If the extreme ζ_G are g_1 (low) and g_2, respectively, the corresponding extreme ζ_s are $s_1 = \sqrt{g_1/0.123}$ and $s_2 = \sqrt{g_2/13.36}$. We then assume these two STO's polarize into the familiar STØ χ^1 above, which we reexpress in GTO's. We look at only the GTO χ^1 of extreme exponents and fill in other Gaussians in a geometric progression of exponents, usually with a ratio 3.3. Since the extreme exponents for STO χ^1 are the same as those for the STO χ^0, the conversion is simple. Thus if we are discussing only the 1s types among the GTO χ^0 and have constructed s_1 and s_2 for the corresponding STO (2p) and (3p), we need only choose the conversion of the STO (2p) and (3p) to GTO (2p)[GTO (3p) exist but are harder to use in integral routines]. Using four $(2p)_{GTO}$ to convert one $(2p)_{STO}$, the $(2p)_{GTO}$ range in exponents from $0.020\ (2s_1)^2$ to $0.734\ (2s_2)^2$.

For our fully self-consistent calculations, $\{\chi^0\}$ and $\{\chi^1\}$ combine into one large set. The zero-order basis was chosen first, and then augmented by $\{\chi^1\}$ chosen as above, deleting any χ^1 which were redundant, or nearly so, with any of the χ^0. The zero-order GTO basis for LiH was chosen in correspondence to the STO basis used by Ransil (Ref. 18), again by finding the extremes in exponent range for the corresponding GTO's and filling in with a geometric progression. This procedure has some drawbacks relative to good exponent optimization, drawbacks not remedied simply by adding a few more basis functions. Lack of closely spaced exponents is one difficulty, as it disallows generation of more diffusive atomic orbitals with radial nodes. At the high exponent end the lack of optimization incurs a penalty in zero-order energy, plus a slight unbalancing of the basis set. By trial and error we adjusted the total basis for LiH, adding and deleting functions at the extremes of the exponent range for each symmetry type and center--we even added a $\underline{(1s)}_{GTO}$ in the middle of the range to form a close-exponent pair, and we contracted the tightest $(\underline{1s})$ functions on each center into one function. These trials and their resulting α values are recounted shortly.

For N_2 we began with Dunning's zero-order basis (Ref. 21) consisting of 44 primitive GTO's contracted into 26 functions. On the basis of our experience with LiH, we added one more diffuse function of each type $(\underline{1s})$, $(\underline{2p_x})$, $(\underline{2p_y})$, $(\underline{2p_z})$ on each center. The extra $(\underline{2p})$ represent polarization of $(\underline{1s})$ types, and the extra $(\underline{1s})$ functions represent part of the χ^1 for the zero-order $(\underline{2p})$. We also

added 5 types of $\underline{(3d)_{GTO}}$ on each center to represent the rest of the χ^1 for the zero-order (2p). Careful selection of polarization functions for the zero-order (2p) forming the diffuse and very polarizable π orbitals is most important. The rationale for each type of $\underline{(3d)_{GTO}}$ is given in the paper. Four of the basic symmetry types XX, YY, ZZ, and XY occur in only one of the two possible linear combinations because the other combination does not represent the first-order polarization of any occupied molecular orbital.

Complete Specifications on Basis Sets

The second entry in each set is the type of calculation done--'OPT' for orthogonal perturbation theory, 'NOPT' for non-orthogonal perturbation theory, and 'FSCF' for fully-self-consistent-field. The H_2 bases are given in Table I in the paper and are not reproduced here.

He

α = 1.319 OPT

$\{0\}_{STO}$ = 1s (1.44608), 2s (2.86222)
E. Clementi, IBM Research Paper RJ-256, August 6, 1963.
$\{1\}_{STO}$ = 2p, 3p (1.44608, 2.86222)--constrained linear combinations in χ^1

Li

α = 167.6 OPT

$\{0\}_{STO}$ = 1s (2.43309, 4.51769) } restricted
2s (0.67142, 1.97812) } Hartree-Fock
E. Clementi, op. cit.
$\{1\}_{STO}$ = 2p (2.43309, 4.51769)
2p, 3p (0.67142, 1.97812)--constrained linear combinations in χ^1

Be

α = 45.28 OPT

$\{0\}_{STO}$ = 1s (3.3370, 5.5063)
2s (0.6040, 1.0118)
E. Clementi, op. cit.
$\{1\}_{STO}$ = 2p (3.3370, 5.5063)
2p, 3p (0.6040, 1.0118)--constrained linear combinations in χ^1

LiH (STO)

various trials
$R = 3.015$ a.u. $= R_e$

$\{0\}$ = Li: 1s (2.6909), 2s (0.7075), $2p_z$ (0.8449)
H: 1s (0.9766)
B. J. Ransil, Rev. Mod. Phys. 32, 245 (1960).

$\alpha_\perp = 26.22$ OPT $\{1\}$ = Li: $2p_x, 3p_x$ (2.6909, 0.7075), $4p_x$ (0.7075), $3d_{xz}, 4d_{xz}$ (0.8449)
H: $2p_x, 3p_x$ (0.9766)
-constrained linear combination in χ^1

19.49 OPT $\{1\}$ = as above, less Li: $3p_x$ (2.6909), H: $2p_x$ (0.9766)
-constrained linear combinations in χ^1;
constraint is probable cause of much poorer α

$\alpha_\parallel = 25.29$ NOPT $\{1\}$ = Li: $2p_z, 3p_z$ (2.6909, 0.7075), $4p_z$ (0.7075), 1s, 2s, 3s, 4s, $3d_{3z^2-r^2}, 4d_{3z^2-r^2}$ (0.8449)
H: $2p_z, 3p_z$ (0.9766)
-all unconstrained

25.04	NOPT	$\{1\}$ = $\{0\}$ + Li: $3p_z$, $4p_z$ (0.7075) 1s, 3s, 4s, 3d, 4d (0.8449) H: $2p_z$, $3p_z$ (0.9766) -deleting the redundant χ^1
25.44	NOPT	$\{1\}$ = above less 1s in χ^0; rise in α with less free variation means ϕ_i^0-inexactness terms dropped from NOPT are causing trouble
23.80	NOPT	$\{1\}$ = $\{0\}$ + Li: $3p_z$ (0.7075), 1s, 3s, 3d (0.8449) H: $2p_z$, $3p_z$ (0.9766)
23.43	NOPT	$\{1\}$ = $\{0\}$ + Li: $3p_z$ (0.7075), 3s, 3d (0.8449) H: $3p_z$ (0.9766) Best small basis
13.40	NOPT	$\{1\}$ = $\{0\}$ - just for debugging NOPT

LiH (GTO)

various trials
$R = 3.015$ a.u. $= R_e$

All calculations are FSCF; we report total Hartree-Fock energies $\underline{E_0}$, dipole moments μ_0 (both in

a.u.), and virial ratios V/T for the zero-order calculations, as partial criteria for the bases.

For comparison, the Hartree-Fock limits and exact nonrelativistic values for LiH are estimated as [P. E. Cade and W. M. Huo, J. Chem. Phys. 47, 614 (1967)]:

HF limit	'Exact'
$E_0 = -7.9873$	$E_0 = -8.0705$
$\mu_0 = 2.376$	$\mu_0 = 2.307$
	$V/T = 2.000\cdots$

$\alpha_{||} = 21.44$

$E_0 = -7.9838$

$\mu_0 = 2.3626$

$V/T = 2.00074$

Li-1s: 0.033, 0.110, 0.360, 1.20, [4.00, 13.2, 66.0, 3330.0]*

$2p_Z$: 0.0080, 0.0264, 0.0871, 0.290, 0.960, 3.20

$3d_{Z^2}$: 0.200

$3d_{X^2}, 3d_{Y^2}, 3d_{Z^2}$: 0.018, 0.060, 0.660, 2.20

H-1s: 0.080, 0.264, [0.871, 2.90, 11.6, 58.0]**

$2p_Z$: 0.018, 0.060, 0.200, 0.660

Test set - every possible useful basis function; 31 contracted GTO's from 37, or 31(37) in the notation

we will use here.

*: contracted, with coefficients 0.726440, 0.292317, 0.060146, 0.002333.

**: contracted, with coefficients 0.763697, 0.249790, 0.056681, 0.010246.

$\alpha_{||}$ = 22.78

E_0 = -7.9832

μ_0 = 2.3567

V/T = 2.00062

Li-1s: 0.033, 0.110, 0.360, 1.20, [4.00-330.0]

$2p_z$: 0.0080, 0.0264, 0.0871, 0.290, 0.960, 3.20

$3d_{z^2}$: 0.018, 0.200

$3d_{x^2}$, $3d_{y^2}$: 0.060

H-1s: 0.080, 0.0264, [0.871-58.0]

$2p_z$: 0.018, 0.200, 0.660

Supposed "best set," deleting functions from above set which contributed least polarization: 21(27)

$\alpha_{||}$ = 22.36

E_0 = -7.9835

μ_0 = 2.3568

V/T = 2.00118

Li-1s: 0.010, 0.033, 0.110, 0.360, 1.20, [4.00-330.0]

$2p_z$: 0.0264, 0.0871, 0.290, 0.960

$3d_{x^2}$, $3d_{y^2}$, $3d_{z^2}$: 0.060, 0.200, 0.660

H-1s: 0.024, 0.080, 0.264 [0.871-58.0]

$2p_z$: 0.018, 0.060, 0.200, 0.660

"Best big set" after more experience in tailoring the first GTO set: 27(33); probably best balanced in both orders.

$\alpha_{\|}$ = 21.74

E_0 = -7.9830

μ_0 = 2.3608

V/T = 2.0067

Li-1s: 0.033, 0.110, 0.360, 1.20 [4.00-330.0]

$2p_z$: 0.0871, 0.290, 0.960

$3d_{x^2}, 3d_{y^2}, 3d_{z^2}$: 0.200

H-1s: 0.024, 0.080, 0.264, [0.871-58.0]

$2p_z$: 0.060, 0.200

Cutting all minor contributors from above set: 17(23)

$\alpha_{\|}$ = 21.06

Li-1s: 0.033, 0.110, 0.200, 0.360, 1.20, [4.00-330.0]

$2p_z$: 0.0871, 0.290, 0.960

H-1s: 0.024, 0.080, 0.264, [0.871-58.0]

$2p_z$: 0.200

Simplest "adequate" basis for $\alpha_{\|}$: 14(20)

$\alpha_\perp = 22.56$

Li-1s: 0.033, 0.110, 0.200, 0.360, 1.20, [4.00-330.0]

$2p_z$: 0.290, 0.960

$2p_x$: 0.0871, 0.290

H-1s: 0.024, 0.080, 0.264, [0.871-58.0]

$2p_z$: 0.200

$2p_x$: 0.080, 0.200

Simplest "adequate" basis for $\alpha_\perp$: 17(23); it is obvious how to combine this with the above set to get the best total basis - which we did not waste time doing, instead proceeding to N_2.

N_2 GTO

$\underline{R} = 2.068$ a.u. $= \underline{R_e}$

Zero-order basis functions from Dunning's N_2 wavefunction (Ref. 22) are unmarked. Polarization functions we added are starred. Basis functions occurring free on each center are denoted as $(\ )_{\underline{A}}$, $(\ )_{\underline{B}}$; those occurring on both centers but constrained to only one of the two linear combinations are denoted as $(\ )_{\underline{A}} \pm (\ )_{\underline{B}}$. Total basis is 40(66) GTO's.

$\alpha_{\parallel} = 14.97$

$\alpha_{\perp} = 9.464$

$E_0 = -108.89926$‡

$V/T = 2.00054$

		coefficients (from Dunning)
$1s_A, 1s_B$	5909.4399	0.0020033
	887.4510	0.0153045
	204.7490	0.0742662
	59.8376	0.2532725
	19.9981	0.6003592
	2.6860	0.2450225
	7.1927	
	0.7000	
	0.2133	
	0.0800*	
$2p_{x_A}, 2p_{x_B}, 2p_{y_A}, 2p_{y_B}, 2p_{z_A}, 2p_{z_B}$	26.7860	0.0267996
	5.9563	0.1708759
	1.7074	0.5726499
	0.5314	
	0.1654	
	0.0800*	
3d: $XX_A + XX_B$	0.200*	
$YY_A + YY_B$	0.200*	
$XY_A + XY_B$	0.200*	
XZ_A	0.200*	
XZ_B	0.200*	
$YZ_A + YZ_B$	0.200*	

†Originally, the 2p function of exponent 0.5314 was included in a four-way contraction. We split if off for polarization freedom.

‡Compare to Dunning's zero-order values, E_0 = -108.8877.

Appendix II. Extended Comments on the Derivation and Use of Nonorthogonal (Hartree-Fock) Perturbation Theory

We mentioned in the paper that the nonorthogonal perturbation theory (NOPT) as given by Das and Duff eventually caused us problems. Their formalism uses the approximation that the zero-order Hartree-Fock equation

$$(h^0 - \epsilon_i^0)u_i^0 = 0 \tag{A}$$

is exactly satisfied: in projecting with any function χ_p^1 we obtain zero

$$\langle \chi_p^1 | h^0 - \epsilon_i^0 | u_i^0 \rangle = 0 \tag{B}$$

Actually, if the basis $\{\chi^1\}$ contains any functions not in $\{\chi^0\}$, then Eq. (B) is not true. We recount here our findings in trying to derive the most exact NOPT equations and to use them.

There are two basic expressions which any NOPT formalism must yield. First and more important is the first-order Hartree-Fock equation satisfied by the nonorthogonal (in first order) orbitals. Expansion of the first-order orbitals $\underline{u_i^1}$ in the first-order basis $\{\chi_p^1\}$

$$u_i^1 = \sum c_{ip}^1 \chi_p^1, \tag{C}$$

and projections of the first-order equation with each χ_p^1 in turn

yield linear equations for the c^1_{ip}. The second expression needed from NOPT is that for the second-order energy $E^{(2)}$ of the total determinantal Hartree-Fock wavefunction--simplified by use of the first-order differential equation (1.d.e.) to a form involving only matrix elements of the perturbation operator h^1 (in orthogonal Hartree-Fock [OHF] the expression is simply

$$E^{(2)} = \sum_i \langle u^0_i | h^1 | u^1_i \rangle). \tag{D}$$

The general route to the 1.d.e. of NOPT is to construct the total energy $\langle E \rangle$ for the wavefunction through second order (in any one orbital consider only terms through first order in non-orthogonality); perform the variation of the energy with respect to u^1_i, $\delta E/\delta u^1_i$, and select the first-order part; and finally simplify as much as possible with use of the zero-order differential equation (0.d.e.)--preferably only in its exact form

$$\langle u^0_j | h^0 - \epsilon^0_i | u^0_i \rangle = 0 \tag{E}$$

and not assuming additionally the validity of Eq. (B). For practical calculations the 1.d.e. is converted to linear equations for the u^1_i expansion coefficients in the basis $\{\chi^1\}$. Before any numerical work, it is valuable to check the linear equations at least for symmetry: the linear equations from the 1.d.e. have the form

$$F_{ip;jq}\, c_{jq} = I_{ip} \tag{F}$$

where the (ip)-th equation comes from the variation $\delta E/\delta u_i^1 = 0$ projected with χ_p^1. We require

$$F_{ip;jq} = F_{jq;ip} \tag{G}$$

since

$$F_{ip;jq} = \frac{\partial}{\partial c_{jq}} \left(\frac{\partial E}{\partial c_{ip}} \right) = \frac{\partial^2 E}{\partial c_{jq} c_{ip}} \tag{H}$$

and

$$F_{jq;ip} = \frac{\partial^2 E}{\partial c_{ip} \partial c_{jq}} \tag{I}$$

and the order of derivatives cannot matter because the energy E is analytic in the coefficients (particularly because the coefficients contain the electric field strength).

Das and Duff follow the three-part route described above. Their Eq. (7) is the Hartree-Fock expectation value of the energy, through second-order. Their Eq. (10) is the result of the variation $\partial E/\partial u_i$ after using the 0.d.e. [in the extended, approximate sense of Eq. (B)] to simplify it. It is still of mixed orders, zero through two, but the first-order terms are at their simplest. Thus they have done the last two steps at once in going from their Eq. (7) to Eq. (10). Finally, they explicitly select the first-order part of their Eq. (10), displaying the zero- and first-order parts of the one-electron operator, h^0 and h^1, explicitly also; the result is Eq. (14).

Our attempts to use NOPT as given by Das and Duff (DD) began with a derivation of the form appropriate to doubly-occupied molecular orbitals. We worked from the OHF equations (12) adapted to double occupancy by the simple expedient of interpreting the operation $\langle a|\cdot|b\rangle c$ as

$$2\langle a(1)|g_{12}|b(1)\rangle c(2) - \langle a(1)|g_{12}|c(1)\rangle b(2) \qquad (J)$$

rather than as in Appendix I. After symmetric deorthogonalization of the orthogonal orbitals $\bar{u}_i$ as

$$\bar{u}_i = u_i - \tfrac{1}{2}\sum_{k\neq i}\langle u_k|u_i\rangle u_k, \qquad (K)$$

we obtained a first-order equation not in entire analogy to Eq. (14), but by using the assumption of Eq. (A) three times we completed the analogy. The lack of rigor for Eq. (14) or its double-occupancy analog was somewhat disturbing but initially felt to be of the same or lesser order than the inherent error in finite-basis expansion of orbitals.

Our second step was checking the symmetry of the linear equations derived from our analog of Eq. (14), that is, the satisfaction of Eq. (G). We found an asymmetry, though it could be removed by removing a summation restriction $k \neq j$ appearing in Eq. (14) or its analog. After correspondence with both Das and Duff, we confirmed our interpretation of some ambiguous terms in Eq. (14) and resolved our original problem as one of convention.

To eliminate possible ambiguity in the deorthogonalization prescription, Eq. (K) or their Eq. (11), the restriction

$$\langle u_i^1 | u_i^0 \rangle = 0 \qquad \text{(L)}$$

was entered. This auxiliary condition must be incorporated into the linear equations (F) for the c_{ip}^1 as extra equations [and then (G) need not hold], or it can be incorporated after the solution. That is, the orbitals u_i^1 and

$$u_i^1 = u_i^1 - \langle u_i^1 | u_i^0 \rangle u_i^0$$

satisfy the same 1.d.e. Thus in principle we could drop the summation restriction as we had planned (the added term vanishes anyway).

We derived the expression for $E^{(2)}$ at this time, both by deorthogonalizing the total Hartree-Fock energy and projecting second-order terms, and by direct deorthogonalization of the simplified $E^{(2)}$. Both times we found the result

$$E^{(2)} = \sum_i \{\langle u_i^0 | h^1 | u_i^1 \rangle - \sum_{j \neq i} \langle u_i | u_j \rangle' \langle u_i^0 | h^1 | u_j^0 \rangle\}, \qquad \text{(M)}$$

where

$$\langle u_i | u_j \rangle' = \langle u_i^1 | u_j^0 \rangle + \langle u_i^0 | u_j^1 \rangle,$$

and the restriction $j \neq i$ applies when $\langle u_i^0 | u_i^1 \rangle = 0$ is forced. As a check, we programmed OHF PT to compare to NOPT using the

unoccupied virtual orbitals as the $\{\chi^1\}$. We also verified that Eq. (14) correctly reduces to OHF PT.

As we noted in the paper, our initial numerical results showed much instability in the calculated second-order energy with regard to basis changes. Some instability was probably due to using Eq. (M) with the restriction $i \neq j$ intact, but some remained after removing the restriction. Apparently the use of assumption (A) was responsible.

Quite a while later, we attempted a derivation of the most correct 1.d.e. We deorthogonalized the OHF equations with the extra $k = i$ term in the deorthogonalization. We found that the 0.d.e. is used in both stages of Das and Duff's derivation, going from Eq. (7) → Eq. (10) and from Eq. (10) → Eq. (14). In our more correct analog to Eq. (14), derived without use of the 0.d.e. and also allowing $\langle u_i^0 | u_i^1 \rangle \neq 0$, we found the linear equations it gave were not symmetric. Yet the use of the 0.d.e. to derive Das and Duff's Eq. (14) valid for $\langle u_i^0 | u_i^1 \rangle \neq 0$ did yield symmetric linear equations. The symmetry should be unaffected by use of the 0.d.e. This paradox is yet unresolved, after much rechecking of algebra.

Starting afresh, we took Eq. (7) (which we assumed was accurate) and projected $E^{(2)}$ explicitly from it. We then performed the variation $\delta E^{(2)}/\delta u_i = 0$ to get the 1.d.e. Some summation restrictions had to be cleared up and then we obtained symmetric linear equations. However, the numerical results were unstable

as before. A check of Eq. (7) was initiated, deriving the expectation of the energy E through second order by directly calculating the contributions of each permutation operator in the matrix elements $\langle\psi|\underline{H}|A\psi\rangle$, $\langle\psi|\underline{A}\psi\rangle$ where ψ is the unsymmetrized straight product of HF orbitals, $\underline{A}$ is the familiar antisymmetrizer composed of a sum of signed $\underline{n}$-electron permutations, and $\underline{H}$ is the total $\underline{N}$-electron Hamiltonian. The 1.d.e. we derived by variation contained new terms and, unfortunately, did not reduce to Eq. (14) under the assumptions of Eqs. (A) and (L) [yet Eq. (14) is known to be the valid deorthogonalized form of the OHF equations under these assumptions, as we showed before].

In sum, our problems are twofold: the inability to verify Eq. (7) for the total energy either (1) by reference to the more basic form $\underline{E} = \langle\psi|\underline{H}|A\psi\rangle/\langle\psi|\underline{A}\psi\rangle$ or (2) by exact reduction of Eq. (7) to a symmetric, stable set of linear equations. Amplifying the latter problem, we note that avoiding use of the 0.d.e. should preserve the variational principle for $\underline{E^{(2)}}$ with respect to the basis $\{\chi^1\}$, independent of any errors in (A) from finitude of the basis expansion. That is, the numerical results should be stable and $E^{(2)}$ monotonic with addition of χ^1 functions.

Soon after encountering all these difficulties, we abandoned NOPT for the equivalent FSCF approach, achieving acceptable results for both LiH and N_2. The proper NOPT equations still elude us, but we feel they are not as useful or reliable as FSCF, contrary to our original estimations. We now cover the exact

utilities of OPT, NOPT, and FSCF approaches to sustain this last claim.

Given a zero-order basis $\{\chi^0\}$, the best bases $\{\chi^1\}_x$ and $\{\chi^1\}_z$ for the two directions of polarization are well-defined in our scheme. The two straightforward ways of proceeding to calculate $\underline{E^{(2)}}$ and α are OPT and FSCF. In both we combine all three bases into one large basis, eliminating redundant functions, and obtain a set about twice as large as $\{\chi^0\}$ for small molecules, or perhaps 1.5 times as large for big molecules (N_2). Of course, we combined both $\{\chi^1\}$ at once to avoid unbalancing the two calculations, $\alpha_{\underline{xx}}$ and $\alpha_{\underline{zz}}$, and lowering the anisotropy accuracy thereby. The two-electron integral computation time is 16 down to 5 times that for $\{\chi^0\}$, depending on molecular complexity. OPT and FSCF give equivalent results in this total basis. [While FSCF is more readily adapted from existing SCF programs, OPT can be faster in the actual 1.d.e. solution if we borrow the complicated integral-handling from SCF programs.] The nonstraightforward procedure is NOPT, requiring two separate basis set mergers, $\{\chi^0\} + \{\chi^1\}_x$ and $\{\chi^0\} + \{\chi^1\}_z$, again eliminating redundant functions. The merged sets are roughly 1.6-1.35 times as large as $\{\chi^0\}$ [small and large molecule limits], and require total two-electron integral times range from 13-6.6 times that for $\{\chi^0\}$. The total calculation time for NOPT is only trivially smaller than that for OPT or FSCF--yet NOPT is so much harder to obtain in correct form, and in addition its α calculations do not give the

zero-order MO determination the benefit of using the diffuse polarization functions to increase the accuracy (of the zero-order MO's, hence also of α itself).

Introduction

Utility of Vibrational Energy Transfer Studies in Chemistry

The problem of molecular vibrational or rotational excitation in binary collisions is well studied, perhaps overly so in some respects. Many different kinds of experiments in thermal, hot-atom, or molecular beam systems are aimed at extracting vibrational (or less often, rotational) excitation cross-sections or relaxation times, especially for the lower energy levels which are easiest to distinguish individually. In addition there have been many calculations on simplified models of the colliding molecules, quantum and classical, exact and approximate. We present such a model calculation for the H_2-H_2 system in a paper following this introduction.

The understanding of vibrational relaxation in particular is important for chemistry. It is deeply involved in collisional activation[1] in gas reactions, and it is also of interest for other bulk processes: ultrasonic absorption and other transport (see the introduction to part I of this thesis); optical fluorescence[2] (including the existence of competing radiationless decay[3] in large molecules), and molecular laser operation[4]; and some esoteric astrophysical processes[5], such as comet tails and nebular radio emission. As chemists, we concentrate on its importance in the theoretical understanding of chemical reactions.

A chemical description of a bulk system in terms

of singlet distribution functions (concentrations) for distinct molecular species is presumable accurate for thermodynamic, transport, electromagnetic, and other macroscopic properties. (The neglected 'physical' interactions of molecules cause severe problems in dense phases, of course--see the introduction to part I of this thesis, especially section G on associated liquids.) With this presumed to be true, the change of system properties (including heat, work) with time is ascribed to changes in concentration of chemical species[6] through reactions.

In any complex kinetic system in bulk matter, it is reasonable to assume we can decompose the rates of change of species concentrations and corresponding bulk properties into elementary steps or reactions. Each elementary reaction is taken as a simple rate process described by a rate law, with the rate constant dependent on temperature, pressure, and other conditions (and only weakly on chemical composition). Of course for nonthermal systems this is a more questionable analysis and a direct appeal should be made to time-dependent molecular distribution functions or other essentially complete many-body descriptions--and even in fast-reacting thermal systems the local and transient disturbances from local thermodynamic equilibrium require corrections to the forms of empirical rate law expressions[7]. To continue, this principle of decomposability into elementary reactions is the foundation of all chemical kinetics.

Let us consider the molecular dynamics and some of the statistical-mechanical nature of the binary collisions in the various kinds of elementary reactions, particularly regarding the role of vibrational energy. For brevity we must moit discussion of the often fascinating coupling[8] of elementary steps into total reacting systems, involving staging, competition, branching, and elegant derivative phenomena such as feedback loops common in biochemistry[9].

All types of elementary reactions are presumably governed by the same general laws of quantum mechanics and statistical mechanics. However, a real understanding demands detailed (and necessarily approximate or modeled) theoretical frameworks and experimental techniques, very much dependent on the specific type of reaction. After all, chemical reactions range from ionic solid reactions through aqueous acid-base reactions and electrochemistry to free-radical gas phase reactions. Reactions may be classified by MOLECULARITY: unimolecular, bimolecular, (rarer) termolecular and higher. In the interest of unity, we may claim that unimolecular reactions are a limiting case of bimolecular ones, with a metastable, unarranged product in the reactive region of molecular configuration,or arrangement channel. Similarly, termolecular recombinations are viewed as the inverse of bimolecular dissociation, which is reaction into a new arrangement channel above an energetic threshhold. REARRANGEMENT TYPE is another division scheme on the basis

of the exact manner of particle regrouping: exchange (atom or group), abstraction, simple charge transfer; recombination/dissociation (for termolecular only). The ELECTRONIC FORM OF REACTANTS, whether ionic, neutral, or free radical, influences the gross nature of the intermolecular interaction potential. The manner of ENERGIZATION or initiation determines the relative involvment of the various molecular degrees of freedom (d.o.f.) and the statistics governing energy transfer among them both temporally and spatially: thermal--all d.o.f.; photochemical or (particle-)radiative = hot-atom--variable balance of translation, vibration, chiefly; shock wave--translation initially; molecular beam (non-bulk)--any desired d.o.f. or combination, in principle. The THERMODYNAMIC STATE or STATE OF AGGREGATION is a chief determinant of the statistics of energy and mass redistribution in <u>successive</u> collisions: dilute gas, dense fluid, solid; pure, diluted by inert species, solvated; homophase or heterophase situation of reaction partners. Changes of phase from reactants to products (e.g., precipitation, gas evolution) affect the kinetics on the hydrodynamic time scale (much longer). Catalysis is challenging to describe theoretically, as it involves a special aggregation or three-body-level molecular distribution, often heterophase. The MODE OF PROPAGATION is rather like a subset of rearrangement type: chain, branched, nonchain; polymerizing or not. Special aspects of propagation such as caging[10] in

liquids could be added here, or under the thermodynamics; caging is a result of significant structure in the two-body molecular distribution functions and their time-evolution. THERMODYNAMIC CONSTRAINTS in the bulk (adiabatic, isochoric, or isobaric maintenance; openness to mass exchange; hydrodynamic conditions of flow or mixing; and phase change during reaction) give convenient further divisions but are not essential either empirically or microscopically. Such constraints are merely boundary conditions on the differential equations of species, momentum, and energy balances already fixed by the basic rate laws.

The eventual goal of experimental or theoretical reaction studies is extraction or calculation of the rate law, including its dependence on temperature, pressure, etc. and also its dependence on a few basic features of the molecules. More detailed information is possible, especially theoretically (which may be viewed as a more fundamental approach to the temperature dependence, etc.): rate constants in rate laws are simple thermal (Boltzmann) averages of more basic reactive cross-sections[11]. If the relative translational energy $\underline{E}$ of the reactants in a given encounter is a valid total delineation for the collision (other d.o.f. are presumed to have a Boltzmann population of their energy levels at some temperature low compared to the equivalent translational temperature--often true for the important range of translational energy), then a cross-section $\sigma(\underline{E})$ is

a more detailed result[11]. For complete state resolution in reactants and products of all d.o.f. energy levels, the result is o(n,m), where n, m denote the complete set of quantum numbers for the reactants, products. More quantum-mechanically correct is the S-matrix S(n,m) $o = S^2$, for proper compounding of multi-stage processes of activation.

The problem we address in our vibrational excitation studies is, How does vibrational energy storage and transfer affect the equilibria and rates for each type of reaction above? There is sketchy knowledge for limited types of reactions. Unimolecular decomposition rates of gases are apparently well-explained[12] by the accumulation of large amounts of vibrational energy in all the molecular bonds through hard collisions. The actual decomposition occurs when by chance most of the quanta localize in one bond and break it. The theory has seen many successive refinements. Simple gas-phase abstraction reactions, such as K + HCl-- KCl + H, are also undergoing much study[13]. Polanyi[14] in particular has sought the effects of very general features in the potential energy surface (on which the reactants and products move; see later) on the effectiveness of reactant vibrational energy in causing reaction, or conversely, on the degree of vibrational excitation in the products. Some qualitative knowledge has been gained in this regard about attractivenss or repulsiveness of entrance and exit channels, presence of net energetic barriers either

direction (endo- or exo-thermicity of reaction), and entrance or exit location of additional, local energetic barriers or wells. Finally, vibrational energy flow is readily followed in systems fitting the stochastic[15] (strong collision, totally diabatic) or transition-state[16] (completely adiabatic) models, which apply in rare limiting cases but then among almost all classes of reaction. In the stochastic model all energy in the reactants (and products, as well) is equivalent. In transition-state theory, the change of vibrational quantization from reactant to intermediate and on to product transfers definite amounts of energy to other degrees of freedom, to retain adiabaticity in every d.o.f.

Most reactions fall outside the scope of the reaction classes and theoretical models above, and require more detailed analysis and calculations in order to understand the absolute rates and their dependence on thermodynamic conditions and molecular structure. Beginning with the surer knowledge of the statics--of the vibrational level spacing/density in all the important reactant configurations, we must develop the dynamics: the coupling of the vibrational d.o.f. to other d.o.f. in collisions, and how collisions compound statistically in succession. Some averaging procedure for the d.o.f. not directly involved in reaction must also be developed. Theoretical studies are generally of two types: (1) a' priori models of the molecular

dynamics, proceeding from many cross-section calculations over representative energy ranges and partner orientations (classically--over translational and internal states, quantum-mechanically) to a final macroscopic rate constant; (2) fitting experimental rate constants to a parametric form of the cross-section as $\sigma(\underline{E})$ [11], assuming a model in which $\underline{E}$ = relative translational energy is all that matters. The latter is a more recent approach. The former is more basic and even underpins the latter, and thus we concentrate on it.

Let us consider the general approach to the theory of reactions through collision dynamics (scattering theory), particularly for 'clean' gas-phase bimolecular reactions. A model is selected for the division of the internal molecular d.o.f., and the reaction coordinates identified along with the proper division of configuration space into reactants, products, and interaction region. One then assumes a potential energy surface (PES) for the total molecular motion (from molecular quantum mechanics calculations generally--fraught with its own great difficulties[5,17]) and projects it onto the reaction coordinates as a cut in the hyperspace of total motion; the potential variation in the remaining d.o.f. coordinates is developed as some basis expansion, usually. One might also assume directly the form of the PES projection on the reaction coordinate and main d.o.f., commonly a Lennard-Jones analytic form in some key interatomic coordinate. The Hamiltonian for the equations of motion must

be simplified to involve only the reaction coordinate and a few important d.o.f.; other d.o.f. are neglected, or rarely, averaged analytically or approximately. In the d.o.f. remaining explicitly, one then distinguishes the 'channels' or net quantum states of motion, as by relative kinetic energy E, total angular momentum J, vibrational quantum numbers n_i --often neglecting subdivision into rotational states. The blocks of channels which are coupled by the potential are identified. For example, channels of different total J do not couple; the total wavefunction or classical phase-space distribution breaks into a sum over various J-components, called partial waves in quantum mechanics[18]. The differential equations(d.e.) of motion are solved for the whole relevant range of initial conditions (initial channels) with proper scattering boundary conditions imposed[19,20]. Either quantum or classical (or semiclassical) equations can be assumed, and then solved by essentially exact or else approximate (perturbation, variation) methods.

In the quantum treatments of the related inelastic but nonreactive scattering, one invariably performs a channel expansion of the total wavefunction for the motion (in a stationary state representation). Extra channels are included which are not energetically accessible at long times ('virtuals'; their involvement in motion generates some uniquely quantum phenomena--tunneling[21] through classical barriers; and resonances[22] which are rapid changes, with

initial energy, of the exit channel distribution, from rapid alteration in quantum interference effects). The total Schrodinger d.e. factors into coupled d.e.'s for the channels. Solution methods for the CC equations vary widely[23] in approach and in adaptability to different probelms. Returning to reactive scattering, we encounter difficulties in channel expansions because the channels of one arrangement channel are a complete set, yet boundary conditions in the other arrangement channels (products, e.g.) cannot be formulated in terms of them. Physicists[29] attacked this problem first; now there are numerous ways around the problem in a practical sense[20].

Finally the solutions for motion under 'pure' initial conditions are converted to S-matrix elements or scattering cross-sections σ, and then averaged over the (thermal, Boltzmann) statistical distribution in initial channels. Statistical mechanical and quantum corrections for interference among channels or temporally enter here--e.g., corrections for generation of nonequilibrium fluid structure (hence collision statistics) by temporal heating[7] in fast reactions; or corrections for multiple collisions during 'activation' in dense fluids.

We have outlined above an essentially complete, detailed theory. It rarely gets tested in total by actual numerical calculations even without thermal averaging, for realistic systems. Only one total calculation[30] has been

done, in the simplest system H + H_2 -- H_2 + H for a few initial kinetic energies. The more practical and valuable use of the theory involves only parts of it at a time, with further simplifications of the equations of motion through models for the coupled molecular motions--even to very crude models such as stripping and harpooning[31], ignoring the detailed internal motions and postulating abrupt shifts in the PES, and using simple gas kinetic theory for total collision (reactive and non-reactive) cross-sections. With sufficient work on models of all degrees of rigor we should hope to develop a manageably small set of concepts to analyze any reaction rate and/or its component cross-sections--or partial aspects of same, such as the effect of simultaneous rotational transitions[32] on vibrational transition cross-sections. An exploding volume of kinetic data and other experimental data (ultrasonic relaxation, laser operation, etc., as noted earlier) is awaiting understanding through correlation with a few basic molecular parameters by use of the theory.

References

1. B. Stevens, Collisional Activation in Gases (Pergamon, Oxford, 1967).

2. See, for example, the review by R. G. Gordon, W. Klemperer, and J. I. Steinfeld, Ann. Rev. Phys. Chem. 19, 215(1968).

3. B. R. Henry and M. Kasha, ibid. 19,161(1968).

4. See refs. 143-149 in review, ref. 2 above; and ref. 116 in the introduction to part I of this thesis.

5. M. Krauss, in Proceedings of the Conference on Potential Energy Surfaces in Chemistry, ed. W. A. Lester, Jr., IBM Publ. RA-18, Jan. 14, 1971, p.6.

6. S. Golden, Quantum Statistical Foundations of Chemical Kinetics (Oxford, 1969).

7. See, for example, W. G. Valance and E. W. Schlag, J. Chem. Phys. 45,4280(1966); N. S. Snider and J. Ross, ibid. 44,1087(1966); R. Kapral, S. Hudson, and J. Ross, ibid. 53,4387(1970); B. Shizgal and M. Karplus, ibid. 52,4262(1970).

8. K. J. Laidler, Chemical Kinetics (McGraw-Hill, N. Y., 1965), Chs. 7,8; S. W. Benson, The Foundations of Chemical Kinetics (McGraw-Hill, N. Y., 1960), Chs. 10, 11.

9. A. L. Lehninger, Biochemistry (Worth, N. Y., 1970), Ch. 8; J. Paul, Cell Biology (Stanford U. Press, Stanford, Calif., 1964), Ch. 7; M. Calvin, Chemical Evolution (Oxford, 1969), Ch. 8.

10. J. Franck and E. Rabinovitch, Trans. Far. Soc. 30,120 (1934); Laidler, op. cit.; Benson, op. cit. ; and many recent references for particular systems.

11. L. A. Melton and R. G. Gordon, J. Chem. Phys. 51,5449 (1969); A. Kuppermann and J. M. White, ibid. 44,4352 (1966); with D. R. Davis and J. A. Betts, to be publ.; A. Kuppermann, J. Stevenson, and P. O'Keefe, Disc. Far. Soc. 44,46(1967).

12. N. B. Slater, Theory of Unimolecular Reactions (Cornell U. Press, Ithaca, N. Y., 1959); and references cited therein; Benson, op. cit.; F. H. Mies, J. Chem. Phys. 51,798(1969); C. W. Larson and B. S. Rabinovitch,

ibid. 51,2293(1969).

13. N. S. Snider, ibid. 51,4075(1969); S. F. Fischer. G. L. Hofacker, and R. Seiler, ibid. 51,3951(1969); D. G. Truhlar and A. Kuppermann, ibid. 52,384(1970); K. T. Tang and M. Karplus, ibid. 49,1676(1968); L. M. Raff, L. B. Sims, D. L. Thompson, and R. N. Porter, ibid. 53,1606(1970); L. L. Poulsen, ibid. 53,1987(1970).

14. J. C. Polanyi, IBM Publ. RA-18, Jan. 14, 1971; and references cited therein.

15. P. Pechukas, J. C. Light, and C. Rankin, ibid. 44,794 (1966), and work cited therein; D. G. Truhlar, ibid. 51,4617(1969); K. Morokuma, B. C. Eu, and M. Karplus, ibid. 51,5193(1969); W. H. Miller, ibid. 52,543(1970).

16. D. L. Bunker, Theory of Elementary Gas Reaction Rates (Pergamon, Oxford, 1966); H. S. Johnston, Gas Phase Reaction Rate Theory (Ronald, N. Y.,1966); D. G. Truhlar, J. Chem. Phys. 53,2041(1970), and references therein; Benson, op. cit.; Laidler, op. cit.

17. A. C. Wahl, IBM Publ. RA-18, Jan. 14, 1971, p. 83; A. D. McLean, ibid., 87.

18. See, for example, N. F. Mott and H. S. W. Massey, The Theory of Atomic Collisions (Oxford, 1965).

19. See our paper following this introduction,for inelastic nonreactive scattering.

20. For reactive scattering. K. T. Tang, B. Kleinman, and M. Karplus, J. Chem. Phys. 50,1119(1969); D. J. Diestler, ibid. 50,4746(1969); T. G. Efimenko, B. N. Zakhariev, and V. P. Zhigunov, Ann. Phys. 47,275(1968); C. C. Rankin and J. C. Light, J. Chem. Phys. 51,1701 (1969); R. A. Marcus, ibid. 49,2610,2617(1968); W. H. Miller, ibid. 50,407(1960).

21. Bunker, op. cit., §2.4.

22. R. D. Levine, B. R. Johnson, J. T. Muckerman, and R. B. Phys. 49,56(1968).

23. The Born, distorted wave, and perturbed stationary state methods (18) are very approximate reductions of the channel coupling; the largely uncoupled CC equations resulting are then numerically integrated by a simple technique. For numerical integration of the full CC equations, the straightforward techniques such as the pointwise Runge-Kutta-Gill have been

superceded by others. Very promising aomng these is Gordon's (24) new piecewise integration in large steps, using a two-function basis expansion in each interval. There is also the invariant imbedding (25) transformation of the CC equations through the integral equation form (with the scattering boundary conditions thus built in) to an alternative set of coupled d.e.'s for the S-matrix elements directly--to be integrated numerically (however, they are nonlinear). A recent Fredholm technique(26) solves the integral equation for the S-matrix directly in a basis expansion extended to the translational coordinate --its chief advantage lies in the ability to treat exchange potentials and other ordinarily paralyzing complications. Another direct integral equation solution has been given by Sams and Kouri (27). Most recently there has been a similar direct solution for the scattering matrix, based upon a parametric reduction (28) of the scattering and potential matrices.

24. R. G. Gordon, J. Chem. Phys. 51,14(1969).

25. D. Secrest and B. R. Johnson, ibid. 45,4556(1966); M. E. Riley and A. Kuppermann, Chem. Phys. Lett. 1,537 (1968).

26. W. P. Reinhardt and A. Szabo, to be publ.

27. W. N. Same and D. J. Kouri, J. Chem. Phys. 51,4809 (1969).

28. H. A. Rabitz, ibid. 55,407(1971).

29. E. Gerjuoy, Ann. Phys. 5,58(1958); see also T.-Y. Wu and T. Ohmura, Quantum Theory of Scattering (Prentice-Hall, Englewood Cliffs, N. J., 1962), §M; the essentially final formal solution was given by L. D. Faddeev, Soviet Phys.-JETP 12,1014(1961).

30. G. Wolken, M. Karplus, and R. G. Gordon, to be publ.

31. D. R. Herschbach, Adv. Chem. Phys. 10,319(1966); with J. H. Birely, J. Chem. Phys. 44,1690(1966); R. E. Minturn, S. Datz, and R. L. Becker, ibid. 44,1149 (1966).

32. K. Takayanagi, Prog. Theor. Phys. 25,S1(1963); J. D. Kelley, 159th Natl. Meeting, Amer. Chem. Soc., L. A., Calif. (1971).

Reprinted from THE JOURNAL OF CHEMICAL PHYSICS, Vol. 52, No. 9, 4807–4817, 1 May 1970
Printed in U. S. A.

Calculation of Transition Probabilities for Collinear Atom–Diatom and Diatom–Diatom Collisions with Lennard-Jones Interaction

VINCENT P. GUTSCHICK* AND VINCENT MCKOY
Arthur Amos Noyes Laboratory of Chemical Physics, California Institute of Technology,† Pasadena, California 91109
AND
DENNIS J. DIESTLER
Department of Chemistry, University of Missouri,‡ St. Louis, Missouri 63121
(Received 10 March 1969)

Numerical integration of the close coupled scattering equations is performed to obtain vibrational transition probabilities for three models of the electronically adiabatic H_2–H_2 collision. All three models use a Lennard-Jones interaction potential between the nearest atoms in the collision partners. The results are analyzed for some insight into the vibrational excitation process, including the effects of anharmonicities in the molecular vibration and of the internal structure (or lack of it) in one of the molecules. Conclusions are drawn on the value of similar model calculations. Among them is the conclusion that the replacement of earlier and simpler models of the interaction potential by the Lennard-Jones potential adds very little realism for all the complication it introduces.

INTRODUCTION

There is current interest in quantum-mechanical treatments of molecular collisions involving excitation of internal degrees of freedom and possibly reaction. The collision systems pose a multichannel scattering problem, commonly solved by the coupled channels (CC) method. The CC equations are coupled differen-

tial equations derived as follows for a nonreactive system: consider a system composed of two asymptotically isolated parts described by internal coordinates $\mathbf{r}_1$, $\mathbf{r}_2$. Let the relative coordinate be given by R. Into the Schrödinger equation,

$$[T(\mathrm{R})+H^0(\mathbf{r}_1,\mathbf{r}_2)+V_I(\mathbf{r}_1,\mathbf{r}_2,\mathrm{R})-E]\psi(\mathbf{r}_1,\mathbf{r}_2,\mathrm{R})=0 \tag{1}$$

(where T is the operator for kinetic energy of relative motion), substitute the state or channel expansion

$$\psi(\mathbf{r}_1,\mathbf{r}_2,\mathrm{R})=\sum_n f_n(\mathrm{R})\phi_n(\mathbf{r}_1,\mathbf{r}_2), \tag{2}$$

where $\{\phi_n\}$ is a complete orthonormal set of the eigenfunctions of H_0,

$$H^0\phi_n=\epsilon_n\phi_n. \tag{3}$$

Left multiplication of Eq. (1) by ϕ_m^* and integration over the coordinates $\mathbf{r}_1$, $\mathbf{r}_2$ yields the CC equations

$$(-T(\mathrm{R})+E-\epsilon_m)f_m(\mathrm{R})=\sum_n V_{mn}(\mathrm{R})f_n(\mathrm{R}), \tag{4}$$

where

$$V_{mn}(\mathrm{R})=\langle\phi_m(\mathbf{r}_1,\mathbf{r}_2)\mid V_I(\mathbf{r}_1,\mathbf{r}_2,\mathrm{R})\mid\phi_n(\mathbf{r}_1,\mathbf{r}_2)\rangle. \tag{5}$$

These equations are solved subject to boundary conditions, generally that asymptotically ($\mid\mathrm{R}\mid\rightarrow\infty$) the relative motion becomes free, i.e.,

$$f_n(\mathrm{R})\sim\exp(i\mathbf{k}_n\cdot\mathrm{R})+\text{scattered waves}. \tag{6}$$

The form of the scattered waves depends upon the dimensionality of the system. The ratio of scattered to incident flux, with flux defined by

$$\mathbf{j}_n(\mathrm{R})=(\hbar/2\mathrm{m})\ \mathrm{Im}(f_n^*\nabla f_n), \tag{7}$$

is the transition probability (one dimension) or cross section (two or three dimensions). As closed-form analytical solutions of Eqs. (4) are not ordinarily obtainable, several techniques have been developed for their accurate numerical integration.[1-5] We developed our own technique of integration using Dirichlet boundary conditions and simple one-step Euler integration. This was the fastest technique available to us at the time of our calculations, though it is now superseded by the reference solution methods of Refs. 4 and 5. The parameters controlling the accuracy of the integration—step size, end points of the integration in the coordinate R, the number of channels included in the expansion Eq. (2), and the accuracy of the numerical integration for the potential matrix elements $V_{mn}(\mathrm{R})$ in Eq. (4)—were chosen such that each individual transition probability was converged to within 1% of its "true" value and detailed balance error, as measured by the quantity

$$e_{mn}=[(P_{mn}-P_{nm})/P_{mn}]\times 100\%, \tag{8}$$

was limited to 0.1%–0.4%, allowing us to report only one probability of each equivalent pair P_{mn}, P_{nm}.

In the first section of this paper, we define the coordinates for the one-dimensional or collinear atom–diatom and diatom–diatom collisions with vibrational excitation. We then specify numerical values of parameters used to define the three models of the H_2–H_2 collision. Two of these models are atom–diatom type, one of which takes the potential for the diatom vibration as the harmonic potential, the other as the Morse potential. The third model is the diatom–diatom type, with each diatom being a harmonic vibrator. Masses of the atoms and diatoms are chosen such that all three models are appropriate for the H_2–H_2 collision—this requires the atom mass to equal the total mass of the diatom. Finally, a Lennard-Jones interaction potential is assumed to operate between the nearest atoms in the collision partners. This is a more realistic choice than the more common one of an exponential potential, at least at low collision energies. In Sec. II we present the numerical results for the transition probabilities. We contrast the physical behavior of the models for qualitative insight into the effects of vibrational anharmonicity and internal structure in the collision partners, and comment briefly on related semiclassical and classical calculations. Finally, we conclude that the simpler exponential interaction potential is preferable to the Lennard-Jones potential because it reproduces transition probabilities for the latter very accurately while requiring far less computing time.

I. NATURE OF THE THREE MODEL CALCULATIONS

A. The Atom–Diatom Collision in One Dimension

The original coordinates for this system are simply the positions x_1, x_2, x_3 of the three masses m_1, m_2, m_3, with m_1-m_2 comprising the bound or diatomic system. The operator for the Hamiltonian minus the energy eigenvalue is

$$H-E=-\frac{\hbar^2}{2m_1}\frac{\partial^2}{\partial x_1^2}-\frac{\hbar^2}{2m^2}\frac{\partial^2}{\partial x_2^2}-\frac{\hbar^2}{2m_3}\frac{\partial^2}{\partial x_3^2}+V_{12}'(x_2-x_1)+V_I'(x_3-x_2)-E. \tag{9}$$

The interaction potential $V_I'(x_1-x_3)$ has been neglected. We show in the Appendix that several consecutive transformations of coordinates can be performed which (1) put the system into the form of an "atom" colliding with another, oscillating atom bound to an equilibrium position—a two-body problem; see Fig. 1—and (2) reduce all coordinates, masses, and potential parameters to a smaller number of dimensionless quantities. The operator $H-E$ in new units and coordinates is

$$H-E=-1/2\mu(\partial^2/\partial x^2)-\tfrac{1}{2}(\partial^2/\partial y^2)+V_{12}(y)+V_I(x-y)-E, \tag{10}$$

where the energy E is exclusive of center-of-mass mo-

tion and is measured in units of $\hbar\omega$, twice the ground-state vibrational energy of the oscillator m_1-m_2. The set of parameters for the collision reduces to E, μ, and the parameters of the two potentials.

Next we make the channel expansion, Eq. (2). The function $\phi_n(y)$ representing bound states of the oscillator are solutions of the eigenvalue equation

$$[-\tfrac{1}{2}(\partial^2/\partial y^2)+V_{12}(y)-\epsilon_n]\phi_n(y)=0. \quad (11)$$

Again, the energies ϵ_n are measured in units of twice the ground-state oscillator energy, so that for the ground state, $\epsilon_1=\frac{1}{2}$. Two models for the oscillator have been used in our calculations: (1) the harmonic oscillator, for which

$$V_{12}(y)=\tfrac{1}{2}y^2,$$
$$\epsilon_n=n-\tfrac{1}{2}, \qquad n=1, 2, 3, \cdots,$$
$$\phi_n(y)=[2^{n-1}(n-1)!]^{-1/2}H_{n-1}(y)\exp(-y^2/2), \quad (12)$$

where H_n is the Hermite polynomial, and (2) the Morse oscillator, for which

$$V_{12}(y)=D_e(e^{-2\beta y}-e^{-\beta y}),$$
$$\epsilon_n=[2(2D_e)^{1/2}/\beta](n-\tfrac{1}{2})-\tfrac{1}{2}\beta^2(n-\tfrac{1}{2})^2,$$
$$\phi_n(y)=N_n\exp(-de^{-\beta y})(2de^{-\beta y})^{(k-2n+1)/2} \times L_{k-n}^{k-2n+1}(2de^{-\beta y}), \quad (13)$$

with

$$d=(2D_e)^{1/2}/\beta,$$
$$k=2d,$$
$$N_n=\text{normalization constant}, \quad (13')$$

and where $L_{a+n}^{n}(x)$ is a generalized Laguerre polynomial. The quantity D_e is the depth of the potential well, and β is an anharmonicity parameter. The Morse oscillator has a finite number of bound states, up to $n_{\max}=k$. The CC equations for both models have the form

$$(d^2/dx^2+k_n^2)f_n(x)=2\mu\sum_{m=1}^{n_{\text{tot}}}V_{nm}(x)f_m(x), \quad (14)$$

with

$$k_n^2=2\mu(E-\epsilon_n),$$
$$V_{nm}(x)=\langle\phi_n(y)\mid V_I(x-y)\mid\phi_m(y)\rangle$$
$$=\int_{-\infty}^{\infty}dy\phi_n(y)V_I(x-y)\phi_m(y),$$

$n_{\text{tot}}=$ number of states retained in the channel expansion. (14′)

Our choice of the interaction potential $V_I(x-y)$ is the Lennard-Jones potential with its singularity at $x-y=0$ replaced by a finite step.

$$V_I(x-y)=4\epsilon\{[\sigma/(x-y)]^{12}-[\sigma/(x-y)]^6\}, \quad x-y\geq b$$
$$=V_I(b), \quad x-y<b, \quad (15)$$

although another choice, the exponential potential,

$$V_I(x-y)=C\exp[-\alpha(x-y)] \quad (16)$$

was used to check our method by duplicating some calculations of Secrest and Johnson.[3]

As a shorthand notation for the two models let us use HOLJ for the harmonic oscillator hit by an atom interacting with it by a Lennard-Jones potential, and MOLJ for the Morse oscillator and the same Lennard-Jones interaction (and HOEXP for the harmonic oscillator and the exponential potential). In all of these calculations, the parameters μ, ϵ, σ (and also D_e, β for the MOLJ case) were chosen to represent the collision of two hydrogen molecules, one of which has its vibrational degree of freedom frozen out. The dimensionless values of the parameters are then

$$\mu=0.5,$$
$$\epsilon=5.707\times10^{-3},$$
$$\sigma=46.71,$$
$$D_e=8.3255,$$
$$\beta=0.24886, \quad (17)$$

as converted from dimensioned quantities quoted in Bhatia[6a] and Herzberg[6b] and Herzfeld and Litovitz.[6c] A slight adjustment of β from a calculated value of 0.24840 was made to obtain the proper value of $\epsilon_1=0.5$ for the ground vibrational level. The values of D_e and β allow 16 bound levels for the Morse oscillator.

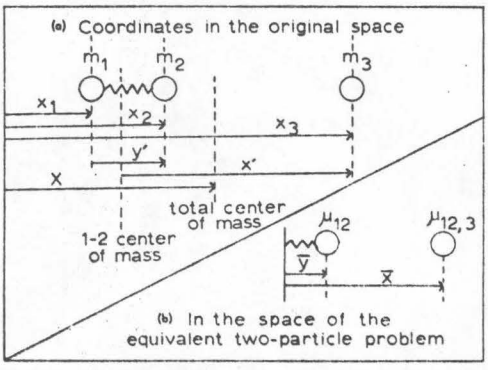

FIG. 1. The original (a) and transformed (b) coordinates for the atom–diatom collision in one dimension.

B. The Diatom–Diatom Collision in One Dimension

The original coordinates for this system are the positions x_i $(i=1, 2, 3, 4)$ of the four masses m_i, with m_1-m_2 and m_3-m_4 forming the two bound diatomic systems. Assuming the dominant nonbound interaction

TABLE I. Selection of channels to include in diatom–diatom problem. Maximum excitation of each diatom is to second vibrational level $n_i=2$.[a]

Method (1)—form all possible product states (n_1, n_2) with n_1, n_2 independently ranging from 1 to 4				Method (2)—add the restriction $n_1+n_2\leq 4$	
Channel no.[b]	(n_1, n_2)	Channel no.	(n_1, n_2)	Channel no.[b]	(n_1, n_2)
1	1, 1	9	3, 1	1	1, 1
2	1, 2	10	3, 2	2	1, 2
3	1, 3	11	3, 3	3	2, 1
4	1, 4	12	3, 4	4	1, 3
5	2, 1	13	4, 1	5	2, 2
6	2, 2	14	4, 2	6	3, 1
7	2, 3	15	4, 3	7	1, 4
8	2, 4	16	4, 4	8	2, 3
				9	3, 2
				10	4, 1

[a] Values of n_i to 4 should be included on the basis of atom–diatom model results.

[b] In each selection scheme the open channels are in bold face.

V_I to be between particles 2 and 3, one has

$$H-E=\sum_{i=1}^{4}-(\hbar^2/2m_i)(\partial^2/\partial x_i^2)+V_{12}'(x_1-x_2)+V_{34}'(x_3-x_4)+V_I'(x_2-x_3)-E. \quad (18)$$

In the Appendix we show that successive coordinate transformations, analogous to those used to reduce the atom–diatom problem, put the system into the form of a diatom oscillator hitting a bound oscillating "atom." The system parameters are also made dimensionless. The operator $H-E$ in the transformed coordinates is

$$H-E=-(1/2\mu)(\partial^2/\partial x^2)-\tfrac{1}{2}(\partial^2/\partial y_1^2)-\tfrac{1}{2}(\partial^2/\partial y_2^2)+V_{12}(y_1)+V_{34}(y_2)+V_I(x-y_1-y_2)-E \quad (19)$$

for a system of two *identical* diatoms; the general form is given in the Appendix. Again, E is the energy, exclusive of center-of-mass motion, in units of twice the ground vibrational energy of either oscillator. The set of parameters remains E, μ, and the parameters of the potentials, as in Sec. I.A. The diatom–diatom collision can be made physically equivalent to the atom–diatom collision, so that comparisons of analogous transition probabilities will illustrate the effect of an internal degree of freedom in the incident "particle." In addition, "resonant" energy transfer involving interchange of vibrational quanta between the diatoms with no conversion of translational energy exists for the diatom–diatom case.

The channel expansion of Eq. (2) takes the form

$$\psi(x, y_1, y_2)=\sum_n f_n(x)\phi_{n1}(y_1)\phi_{n2}(y_2), \quad (20)$$

where the ϕ_{n1}, ϕ_{n2} are solutions of eigenvalue equations of the form (10). In our calculations, both diatom oscillators are modeled as harmonic oscillators and the interaction potential is the Lennard-Jones potential; this model is denoted by the shorthand HOHOLJ. System parameters exclusive of the energy E are

$$\mu=0.5,$$
$$\epsilon=5.707\times 10^{-3},$$
$$\sigma=46.71. \quad (21)$$

Test calculations on a model with the exponential potential successfully duplicated the results of Riley.[1]

The CC equations have the general form

$$(\partial^2/\partial x^2+k_n^2)f_n(x)=2\mu\sum_m V_{nm}(x)f_m(x), \quad (22)$$

where

$$k_n^2=2\mu(E-\epsilon_{n1}-\epsilon_{n2}),$$

$$V_{nm}(x)=\langle\phi_{n1}(y_1)\phi_{n2}(y_2)\mid V_I(x-y_1-y_2\mid\phi_{m1}(y_1)\phi_{m2}(y_2)\rangle.$$

The ordering of states in the expansion (20) becomes significant when we truncate the expansion. Two ways to order or include channels suggest themselves: (1) retain a certain number of states for each oscillator, yielding the correspondence between n and $(n1, n2)$ given in the left-hand columns of Table I, or (2) retain product states $(n1, n2)$ up to a certain energy level $\epsilon_{n1}+\epsilon_{n2}$, yielding the correspondence of n and $(n1, n2)$ given in the right-hand columns of Table I. The second approach places all open channels together at the beginning of the numbering scheme, and makes for a smaller set of coupled equations for similar accuracy; that is, the states $(n1, n2)$ where both $n1$ and $n2$ are high virtual states will be relatively unimportant. The second approach will be used in our HOHOLJ calculations.

Note the occurrence of equivalent channels $(n1, n2)\leftrightarrow(n2, n1)$. These channels are physically distinct; a transition from one to the other involves no conversion of translational into vibrational energy—it is a *resonant* energy transfer.

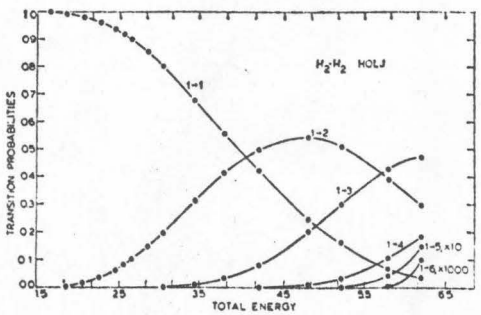

FIG. 2. Energy dependence of the transition probabilities $P(1\to n)$ from the ground state in the atom–diatom problem, HOLJ model.

TABLE II. Calculated transition probabilities for HOLJ model. Numbers in parentheses are negative powers of 10 multiplying result.[a]

	E[b]					
$P_{n\to m}$	1.55	1.65	1.85	2.05	2.25	
1→1	0.9999	0.9992	0.9946	0.9835	0.964	
1→2	0.121(3)	0.792(3)	0.538(2)	0.165(1)	0.357(1)	
2→2	0.9999	0.9992	0.9946	0.9835	0.964	

	E					
$P_{n\to m}$	2.45	2.55	2.65	2.85	3.05	3.45
1→1	0.936	0.918	0.898	0.852	0.799	0.674
1→2	0.638(1)	0.815(1)	0.101	0.147	0.199	0.314
1→3		0.506(5)	0.411(4)	0.406(3)	0.170(2)	0.109(1)
2→2	0.936	0.918	0.897	0.843	0.771	0.580
2→3		0.235(3)	0.152(2)	0.100(1)	0.296(1)	0.105
3→3		0.99976	0.9984	0.990	0.969	0.884

	E					
$P_{n\to m}$	3.80	4.20	4.80	5.20	5.80	6.20
1→1	0.555	0.420	0.245	0.157	0.687(1)	0.351(1)
1→2	0.412	0.498	0.543	0.510	0.394	0.296
1→3	0.323(1)	0.799(1)	0.201	0.300	0.427	0.470
1→4	0.421(4)	0.855(3)	0.106(1)	0.322(1)	0.105	0.183
1→5			0.107(4)	0.264(3)	0.422(2)	0.149(1)
1→6					0.350(5)	0.100(3)
2→2	0.384	0.179	0.104(1)	0.222(1)	0.175	0.299
2→3	0.202	0.313	0.383	0.328	0.148	0.416(1)
2→4	0.640(3)	0.870(2)	0.631(1)	0.136	0.258	0.297
2→5			0.123(3)	0.228(2)	0.241(1)	0.644(1)
2→6					0.341(4)	0.773(3)
3→3	0.755	0.536	0.177	0.313(1)	0.387(1)	0.134
3→4	0.982(2)	0.698(1)	0.238	0.326	0.297	0.180
3→5			0.108(2)	0.137(1)	0.878(1)	0.170
3→6					0.233(3)	0.401(2)
4→4	0.989	0.921	0.676	0.421	0.805(1)	0.364(2)
4→5			0.124(1)	0.834(1)	0.256	0.317
4→6					0.156(2)	0.186(1)
5→5			0.986	0.900	0.612	0.338
5→6					0.146(1)	0.945(1)
6→6					0.9835	0.882

[a] Calculated values of P_{nm} and P_{mn} were always well within 1% of each other. To avoid redundancy, only the former are given.

[b] Energy units are $\hbar\omega$, twice the ground-state vibrational energy of the diatom.

II. RESULTS OF MODEL CALCULATIONS

Tables II–IV present our calculated transition probabilities for the HOLJ, MOLJ, and HOHOLJ models. The total error in these results is in the range of 1% or less. The behavior of selected probabilities P_{mn} as functions of energy is illustrated in Figs. 2-6. The clearest feature for both atom–diatom models HOLJ and MOLJ, which cover significant energy ranges, is the oscillation of the P_{mn}. For instance, the elastic transition probability P_{22} in the HOLJ model decreases steadily until it reaches a deep minimum near $E=4.9$; then, despite the opening of an additional *in*elastic channel at $E=4.5$, P_{22} begins to rise rapidly. This is "caused" by the

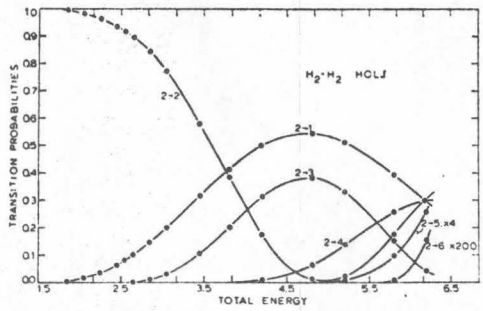

FIG. 3. Energy dependence of the transition probabilities $P(2\rightarrow n)$ from the first excited state in the atom–diatom problem, HOLJ model.

downward turns in probabilities P_{21} and P_{23}. We see a similar behavior in transitions from initial states 1 and 3, P_{1n} and P_{3n}. Comparing transitions according to their initial state, we note that the coupled oscillations in probabilities set in at a lower value of initial kinetic energy $E-\epsilon_n$, the higher the initial state n.

This oscillatory behavior has been found in similar atom–diatom model systems by previous workers. Shuler and Zwanzig[7] found sharp-peaked oscillations for all transitions in their exact but specialized quantum-mechanical treatment of the harmonic diatom and the hard-sphere interaction potential,

$$V_I(x-y)=0, \qquad x-y>0.$$
$$\infty, \qquad x-y=0. \tag{23}$$

The exact result of Secrest and Johnson[3] for several HOEXP models show maxima in inelastic probabilities. The exact semiclassical results of Rapp and Sharp[8] for a HOEXP-like model show regular oscillations. The oscillations in our results and the results quoted above are real, although there have been many approximate calculations in which the use of low-order perturbation theory or the artificial exclusion of most of the channels in expansion (2) has led to a spurious effect.

A major part of the analysis of our results is the

TABLE III. Calculated transition probabilities for MOLJ model.[a]

	E[b]			
$P_{n\rightarrow m}$	1.55	1.90	2.30	2.75
1→1	0.99983	0.9958	0.980	0.939
1→2	0.165(3)	0.417(2)	0.198(1)	0.604(1)
1→3				0.129(3)
2→2	0.99983	0.9958	0.980	0.931
2→3				0.819(2)
3→3				0.9917
	E			
$P_{n\rightarrow m}$	3.40	4.15	4.45	4.85
1→1	0.854	0.724	0.662	0.582
1→2	0.142	0.255	0.302	0.354
1→3	0.314(2)	0.204(1)	0.345(1)	0.602(1)
1→4	0.159(5)	0.306(3)	0.977(3)	0.320(2)
1→5		0.138(6)	0.317(5)	0.394(4)
1→6				0.198(7)
2→2	0.780	0.508	0.391	0.249
2→3	0.779(1)	0.229	0.287	0.347
2→4	0.868(4)	0.809(2)	0.198(1)	0.475(1)
2→5		0.623(5)	0.111(3)	0.104(2)
2→6				0.764(6)
3→3	0.915	0.643	0.493	0.296
3→4	0.412(2)	0.108	0.182	0.281
3→5		0.182(3)	0.230(2)	0.145(1)
3→6				0.180(4)
4→4	0.9958	0.878	0.756	0.531
4→5		0.598(2)	0.407(1)	0.137
4→6				0.371(3)
5→5		0.9938	0.957	0.838
5→6				0.919(2)
6→6				0.9904

[a] Calculated values of P_{nm} and P_{mn} were always well within 1% of each other. To avoid redundancy, only the former are given.

[b] Energy units are $\hbar\omega$, twice the ground-state vibrational energy of the diatom.

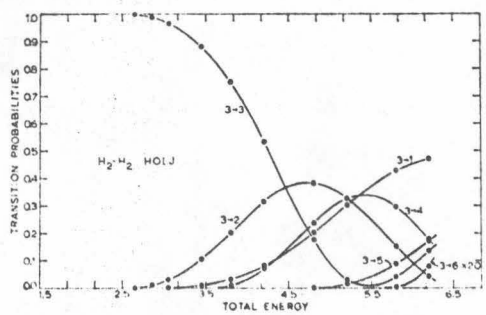

FIG. 4. Energy dependence of the transition probabilities $P(3\rightarrow n)$ from the second excited state in the atom–diatom problem, HOLJ model.

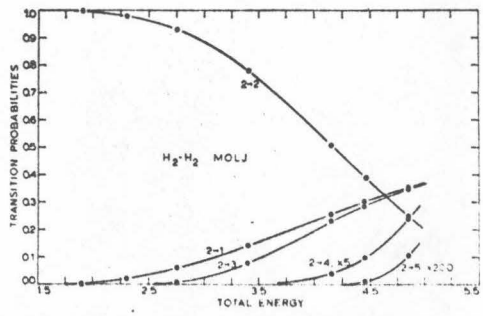

FIG. 5. Energy dependence of the transition probabilities $P(2\rightarrow n)$ from the first excited state in the atom–diatom problem, MOLJ model.

TABLE IV. Calculated transition probabilities for HOHOLJ model.[a]

$P_{n\to m}$	E[b] 2.05	2.15	2.35	2.55	2.75	2.95
11→11[c]	0.99990	0.99934	0.9956	0.987	0.972	0.951
11→12	0.508(4)	0.329(3)	0.219(2)	0.656(2)	0.140(1)	0.245(1)
12→12	0.9929	0.980	0.950	0.914	0.872	0.825
12→21	0.707(2)	0.194(1)	0.474(1)	0.789(1)	0.114	0.150

$P_{n\to m}$	E 3.08	3.15	3.35	3.55
11→11	0.934	0.923	0.890	0.853
11→12	0.328(1)	0.382(1)	0.547(1)	0.731(1)
11→13	0.183(5)	0.680(5)	0.648(4)	0.261(3)
11→22	0.366(5)	0.136(4)	0.130(3)	0.523(3)
12→12	0.792	0.773	0.714	0.650
12→21	0.175	0.188	0.224	0.258
12→13	0.192(3)	0.603(3)	0.381(2)	0.108(1)
12→22	0.104(3)	0.329(3)	0.214(2)	0.627(2)
12→31	0.143(4)	0.548(4)	0.524(3)	0.204(2)
13→13	0.980	0.963	0.909	0.846
13→22	0.200(1)	0.360(1)	0.848(1)	0.136
13→31	0.110(3)	0.352(3)	0.203(2)	0.556(2)
22→22	0.960	0.927	0.826	0.715

[a] Calculated values of $P(n1, n2)\to(n1', n2')$ that should be equal among themselves by time-reversal invariance or symmetry were negligibly different. Only one member is given to avoid redundancy.

[b] Energy units are $\hbar\omega_{12}=\hbar\omega_{34}=\hbar\omega$, twice the ground-state vibrational energy of either diatom.

[c] The transition $(n1, n2)\to(n1', n2')$ is abbreviated to $n1n2\to n1'n2'$.

comparison and contrast of the three models for the H_2–H_2 collision. Suitable quantities for comparison include analogous transition probabilities (as 1→2 HOLJ, 1→2 MOLJ, 11→12⊕11→21 HOHOLJ), net energy transfer from analogous initial states, and relative strengths of multiquantum jumps. Contrasts of HOLJ and MOLJ models will tell us something about the effects of anharmonicity, and contrasts of HOLJ and HOHOLJ will help reveal the effect of internal structure in the incident particle. At the same time, examinations of models individually show the basic energy behavior of the probabilities and other properties that are as instructive as the obvious contrasts between models. Specific items we can study, both within and between models, include comparisons of (1) all transi-

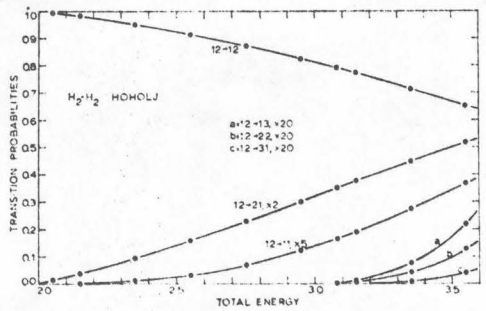

FIG. 6. Energy dependence of the transition probabilities $P(12\to mn)$ in the diatom-diatom problem, HOHOLJ model. The initial state 1-2 has one of the diatoms in its ground state, the other in its first excited state.

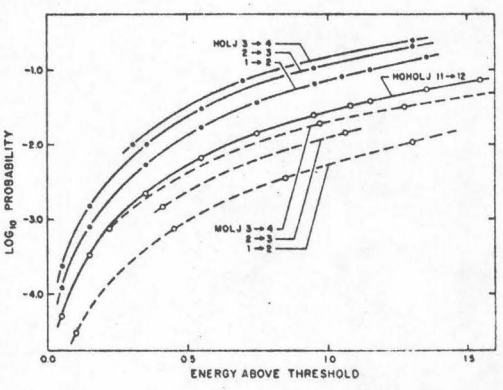

FIG. 7. Demonstration of very similar energy dependence for one-quantum jumps in all three models of the H_2–H_2 collision, HOLJ, MOLJ, HOHOLJ. The curves of $\log_{10}$(probability) have been biased by −0.75 in the MOLJ cases for clarity.

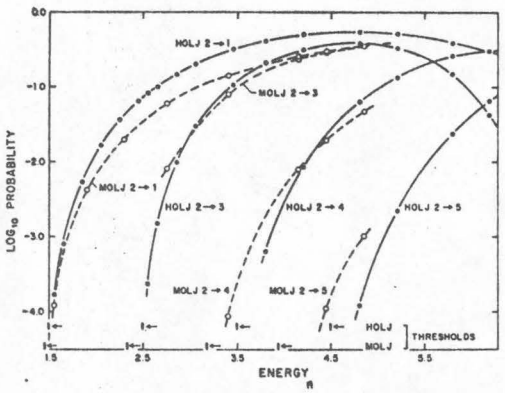

FIG. 8. Comparison of all transition probabilities $P(2\rightarrow n)$ from the first excited state. The two atom–diatom models HOLJ and MOLJ are both represented.

tions of a given type, such as one-quantum jumps $P_{n,n+1}$, for various initial states n, (2) all transitions P_{nm} from a given initial state n, (3) net energy transfer (translational to vibrational) from each state n, defined for the atom–diatom models as

$$\langle \Delta E_n \rangle = \sum_m{}' P_{nm}(\epsilon_m - \epsilon_n), \tag{24}$$

where the ϵ_i are the energy eigenvalues for the diatom vibration. The diatom–diatom model has several types of energy transfer that will be defined later.

Figure 7 presents a logarithmic plot of several one-quantum jump probabilities for each of the three models. The abscissa in each case is energy above threshold $E_{ex}=E-\epsilon_{n+1}$, rather than initial kinetic energy. The striking fact brought out by the logarithmic plot is that all the $P_{n,n+1}$ for a given model behave much like

$$P_{n,n+1}(E) = \text{Const}_n f(E_{ex}), \tag{25}$$

with $f(_{ex})$ the same for all n. Further, $f(E)$ is very similar for the HOLJ and HOHOLJ models, while $\log f(E)$ for MOLJ has a smaller slope at the lowest energies. Pursuing this point of similarity, we turn to the actual magnitudes of probabilities at low energy. For the analogous transitions $11\rightarrow 12 \oplus 11\rightarrow 21$ HOHOLJ and $1\rightarrow 2$ HOLJ, we find

$$(P_{11\rightarrow 12}+P_{11\rightarrow 21})_{\text{HOHOLJ}}/(P_{12})_{\text{HOLJ}} \approx 0.8 \tag{26}$$

at low energy. Not only do these transitions have similar $f(E)$ or "slopes," but their magnitudes are close, being reduced for the HOHOLJ case by the extra adiabaticity or softness introduced into the collision process by the extra internal degree of freedom. That the change from HOLJ to HOHOLJ is principally the addition of a very modest amount of adiabaticity is supported by comparing the $11\rightarrow 12$ and $21\rightarrow 22$ HOHOLJ probabilities. The two values are extremely close at low energies, indicating again that the initial state of our extra internal degree of freedom has little effect of itself on transition probabilities—which would not be true if the extra degree of freedom coupled strongly to translation. However, it does couple strongly to the vibration of the other diatom, giving rise to highly favored resonant energy transfers of the type $12\rightarrow 21$. The latter transitions may be of independent interest, but they do not drain much probability from other transitions at modest energies.

Proceeding to the HOLJ–MOLJ comparison, we find the ratio $(P_{12})_{\text{MOLJ}}/(P_{12})_{\text{HOLJ}}$ is quite small—around 0.3–0.4. This is readily explained by the lower coupling between adjacent states of the anharmonic oscillator (compared to that for a harmonic oscillator) induced by a potential that is essentially linear in the oscillator coordinate. This near linearity in the coordinate y holds near the classical turning point x_t, where $V_I(x_t-\langle y\rangle)=E-\epsilon_n$, for our Lennard-Jones potential—and it is the region of x_t that is most important. The problem of why MOLJ one-quantum jumps have a different "slope" at low energies than HOLJ jumps cannot be commented on with our calculations limited to so few energies.

Figure 8 presents a comparison of the second type, among all transitions from initial state 2 (P_{21}, P_{23}, P_{24}, P_{25}) for both atom–diatom models. It is also a logarithmic plot, and the abcissa is appropriately the total energy E. A clear feature is that the horizontal or energy gaps between adjacent curves $2\rightarrow n$, $2\rightarrow n+1$ are widening as n increases. That is, in either of the two models, the higher the quantum jump, the more slowly the probability grows. The explanation is again in the essential linearity of the interaction potential at the classical turning point; the first-order coupling of a final state to the initial state is a very strongly decreasing function of the number of quantum jumps in the transition. This argument does not hold as well for the anharmonic MOLJ model, and so the energy intervals between the various curves do not widen as

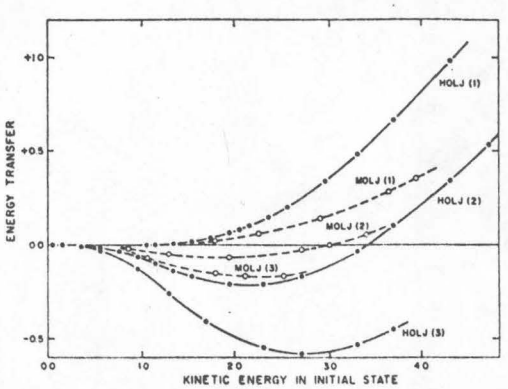

FIG. 9. Atom–diatom collision: net transfer of energy from translation to diatom vibration as a function of the initial state (n) and of the kinetic energy in the initial state. Both HOLJ and MOLJ models are represented.

rapidly here, even after we discount the decreasing intervals between thresholds.

We have no HOHOLJ results for transitions higher than two-quantum jumps, and these only from the ground state. Yet the HOHOLJ model has a greater variety of transition types or processes than the atom–diatom models. Finding the relative magnitudes of the different processes is a worthwhile task. The processes we distinguish, and examples of each, are:

E—Elastic: 11→11, 12→12

R—Resonant: no net quantum jump in the pair of diatoms, i.e., opposite jumps in each diatom: 12→21, 22→13

SR—Semiresonant: opposite jumps of different order in each diatom: 12→31

NR—Nonresonant:

(a) One-quantum jump: 11→12, 22→12

(b) Two-quantum jump: 11→13

(c) Double one-quantum jump: 11→22

The HOHOLJ results at the modest energy $E=3.55$ show that the strengths of processes generally follow the order

$$\text{E}>\text{R}>\text{NR(a)}>\text{SR}>\cdots, \qquad (27)$$

reflecting the weakness of translational–vibrational coupling compared to vibrational–vibrational (V–V) coupling. There are V–V processes that are weak, as the 13→31 transition involving concerted two-quantum jumps that are approximately forbidden in first order.

Our final study is of energy transfer. Figure 9 plots $\langle\Delta E_n\rangle$ for both atom–diatom models from initial states 1, 2, and 3 as functions of initial kinetic energy. MOLJ has about 40% the energy transfer efficiency of HOLJ, from the initial states 1 or 2. The energy transfer in state 2 reaches a node at lower energy for MOLJ than HOLJ, reflecting the earlier opening up of new channels for MOLJ. The disparity in form for HOLJ and MOLJ energy transfer appears to be very pronounced for high initial states.

To define the measure of energy transfer for diatom–diatom collisions, we must denote the subsystems or degrees of freedom between which the transfer occurs. These subsystems are translation or "tr," diatom 1–2 or "d" (playing the same role as the diatom in atom–diatom collisions), and diatom 3–4 or "a" (playing the same role as the atom). The energy transfers most directly comparable to the atom–diatom results are tr→a+d≡tr→all, tr→d (not equal in general to tr→a; "d" and "a" may be initially in different states, making for distinguishability in this otherwise symmetric system), and tr+a→d≡all→d. Figure 10 presents these three $\langle\Delta E\rangle$ functions for HOHOLJ in initial states 11, 12, and 13, plotted as functions of initial kinetic energy. ΔE(tr→d) is very nearly identical for states 11 and 12 for comparable distances above their respective thresholds, corresponding to our finding that the state of a does not much affect the coupling of d to tr. There is

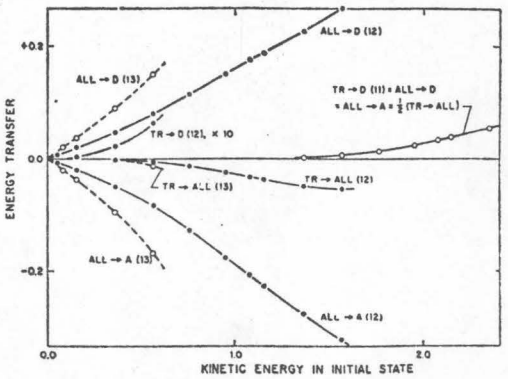

FIG. 10. Diatom–diatom collision, HOHOLJ model: net transfer of energy between the various degrees of freedom (e.g., TR = translation; see text for symbol meaning), as a function of initial state (n_1n_2) and of the kinetic energy in the initial state.

also the expected trend, that ΔE(all→d) increases strongly as the state of "a" is raised. As there is nothing surprising within Fig. 10, we proceed to compare HOHOLJ with HOLJ via their ratio $\Delta E(\text{tr}\rightarrow\text{all})/\Delta E$ for analogous initial states. For HOHOLJ state 11 and HOLJ state 1, the ratio is around 0.8, reflecting the extra adiabaticity of the diatom–diatom case. For HOHOLJ state 21 and HOLJ state 2, the ratio is about 0.4, probably due to the drain of the resonant process 12→21. The same ratio occurs in the comparison HOHOLJ 31↔HOLJ 3 and in the weaker comparison HOHOLJ 22↔HOLJ 3.

We may draw a number of conclusions from our results, particularly regarding the value of similar model calculations on intermolecular energy transfer. Despite the limitations of our models—one-dimensionality, a restricted and modeled interaction potential, and the simplicity of the models of the diatoms—we have extracted a number of physical insights into the collision of two fairly stiff diatoms, if not into the actual H_2–H_2 collision. The effects of anharmonicity and of internal degrees of freedom, and the relative magnitudes of different processes are among the insights. Certainly, calculations on a wider sampling of collision partners within the same general modeling scheme can be recommended as a practical and valuable project; the computing times are moderate. We are also able to suggest some precautions and some simplifications in modeling a collision system. First, the introduction of all the internal degrees of freedom of the collision partners is not as necessary for reasonably accurate calculations as a fair degree of anharmonicity in the vibrations. Neither complication can really be ignored and semiempirical corrections based on careful studies of additional systems are probably desirable. Secondly, the choice of analytic form for the interaction potential is not nearly as important as the careful estimation of the parameters for the chosen form. To support this claim

we turn to some results of A. Wagner of this laboratory. In entirely similar calculations he employed HOEXP and HOHOEXP models for the H_2–H_2 system with the EXP (exponential) potential parameter α carefully fitted by various least-squares techniques to the Lennard-Jones parameters σ, ϵ. His calculations duplicated ours within several percent for all but the highest quantum jumps at the highest energies, where one probability might be off as much as a factor of 2. Let us consider that neither LJ nor EXP potentials are terribly realistic, and that the change in probabilities in switching from one to the other is less than the change produced by a very minor shift in the parameters of either one. We see no reason to retain the LJ potential with its attendant great increase in complexity and computing time,[9] at least in treating systems such as ours where the energy quanta exchanged in collision are considerably larger than the small attractive well in the LJ potential. If one *must* use a potential that has an appreciable attractive portion, as a chemical "well," or if one must do accurate calculations, his best choice of potential is one tabulated numerically. If one is satisfied with as simple a potential as the exponential, he should choose his parameters very carefully. A much-needed study is the development of simple but more adequate model intermolecular potentials, particularly for three-dimensional systems.

ACKNOWLEDGMENTS

One of us (D. D.) wishes to thank the California Institute of Technology for its hospitality. We would like to thank A. Wagner, N. W. Winter, and D. G. Truhlar of the California Institute of Technology for helpful discussions. We are particularly grateful to Merle E. Riley, presently at the Harvard College Observatory, for a thorough and helpful criticism of the manuscript and for other suggestions.

APPENDIX

Transformation to Dimensionless Coordinates for the Atom–Diatom Problem

Figure 1(a) shows the original coordinate system. The first step is to separate the center of mass motion in Eq. (9), by defining new coordinates

$$X=(m_1x_1+m_2x_2+m_3x_3)/M, \qquad M=m_1+m_2+m_3$$

$=$ coordinate of center of mass of entire system.

$$x'=x_3-(m_1x_1+m_2x_2)/m, \qquad m=m_1+m_2$$

$=$ distance between particle 3 and center of mass of system 1–2,

$$y'=x_2-x_1, \tag{A1}$$

and corresponding masses

$$M\rightarrow X,$$
$$\mu_{12,3}=mm_3/M\rightarrow x'$$
$$\mu_{12}=m_1m_2/m\rightarrow y'. \tag{A2}$$

The new form of the operator $H-E$ is

$$-\frac{\hbar^2}{2M}\frac{\partial^2}{\partial X^2}-\frac{\hbar^2}{2\mu_{12,3}}\frac{\partial^2}{\partial x'^2}-\frac{\hbar^2}{2\mu_{12}}\frac{\partial^2}{\partial y'^2}$$
$$+V_{12}(y')+V_I[x'-(m_1/m)y']-E. \tag{A3}$$

Now remove the center-of-mass motion; write

$$E=E_{\rm tr}+E_{\rm vib}$$
$$=E_{\rm tr}^{\rm cm}+E_{\rm tr}^{\rm rel}+E_{\rm vib}, \tag{A4}$$

and remove the operator

$$-(\hbar^2/2m)(\partial^2/\partial X^2)-E_{\rm tr}^{\rm cm}=0 \quad \text{(for eigenstates)}. \tag{A5}$$

Next, place x' and y' on an equal footing by defining

$$x'=(m_1/m)(\bar{x}+y_0'), \quad \text{or} \quad \bar{x}=(m/m_1)x'-y_0',$$
$$y'=\bar{y}+y_0', \quad \text{or} \quad \bar{y}=y'-y_0', \tag{A6}$$

where y_0' is the equilibrium value of y'. The corresponding masses are

$$\bar{\mu}=(m_1^2/m^2)\mu_{12,3}=m_1^2m_3/mM\rightarrow\bar{x},$$
$$\mu_{12}\rightarrow\bar{y}, \tag{A7}$$

and the operator $H-E$ becomes

$$-\frac{\hbar^2}{2\bar{\mu}}\frac{\partial^2}{\partial\bar{x}^2}-\frac{\hbar^2}{2\mu_{12}}\frac{\partial^2}{\partial\bar{y}^2}+\bar{V}_{12}(\bar{y})+\bar{V}_I(\bar{x}-\bar{y})-\bar{E}, \tag{A8}$$

where

$$\bar{V}_{12}(\bar{y})=V_{12}(\bar{y}+\bar{y}_0'),$$
$$\bar{V}_I(\bar{x}-\bar{y})=V_I[(m_1/m)(\bar{x}-\bar{y})],$$
$$\bar{E}=E-E_{\rm tr}^{\rm cm}. \tag{A9}$$

Lastly, divide the whole of Eq. (A8) by $\hbar\omega=$ twice the ground-state vibrational energy of the 1–2 system, and absorb the factors $\hbar^2/2\mu_i$ into the derivative terms. Define

$$x=(\mu_{12}\omega/\hbar)^{1/2}\bar{x},$$
$$y=(\mu_{12}\omega/\hbar)^{1/2}\bar{y},$$
$$\mu=\bar{\mu}/\mu_{12}=m_1m_3/Mm_2,$$
$$E_r=\bar{E}/\hbar\omega \tag{A10}$$

to obtain Eq. (10)

$$-(1/2\mu)(\partial^2/\partial x^2)-\tfrac{1}{2}(\partial^2/\partial y^2)+V_{12}'(y)+V_I'(x-y)-E_r,$$

where

$$V_{12}'(y)=\frac{\bar{V}_{12}[(\hbar/\mu_{12}\omega)^{1/2}y]}{\hbar\omega}=\frac{V_{12}[(\hbar/\mu_{12}\omega)^{1/2}y+y_0']}{\hbar\omega},$$

$$V_I'(x-y)=\frac{\bar{V}_I[(\hbar/\mu_{12}\omega)^{1/2}(x-y)]}{\hbar\omega}=\frac{V_I[(m/m_1)(\hbar/\mu_{12}\omega)^{1/2}(x-y)]}{\hbar\omega}. \quad \text{(A11)}$$

The transformations in (A11) will change all parameters of the original potentials into dimensionless quantities, and in some cases reduce the number of parameters in V_{12} by one.

Transformation to Dimensionless Coordinates for the Dia'om-Diatom Problem

We separate the center-of-mass motion from Eq. (18) by defining the coordinates and corresponding masses

$$X=\sum^{4} m_i x_i/M, \qquad M=m_1+m_2+m_3+m_4,$$

$$y_{12}'=x_2-x_1, \qquad \mu_{12}=m_1m_2/m_{12} \qquad (m_{ij}=m_i+m_j),$$

$$y_{34}'=x_4-x_3, \qquad \mu_{34}=m_3m_4/m_{34},$$

$$x'=(m_3x_3+m_4x_4)/m_{34}-(m_1x_1+m_2x_2)/m_{12}, \qquad \mu_{12,34}=m_{12}m_{34}/M$$

$=$ distance between the centers of mass of systems 1-2 and 3-4. (A12)

The operator $H-E$, dropping the operator (A5), is

$$-\frac{\hbar^2}{2\mu_{12}}\frac{\partial^2}{\partial y_{12}'^2}-\frac{\hbar^2}{2\mu_{34}}\frac{\partial^2}{\partial y_{34}'^2}-\frac{\hbar^2}{2\mu_{12,34}}\frac{\partial^2}{\partial x'^2}+V_{12}(y_{12}')+V_{34}(y_{34}')+V_I\left(x'-\frac{m_1}{m_{12}}y_{12}'-\frac{m_4}{m_{34}}y_{34}'\right)-E. \quad \text{(A13)}$$

Next put x' and y_{12}' on the same footing, by defining new coordinates and masses,

$$\bar{x}=(m_{12}/m_1)x'-y_{12}^0-\bar{\gamma}y_{34}^0, \qquad \bar{\mu}_{12,34}=(m_1^2/m_{12}^2)\mu_{12,34},$$

$$\bar{\gamma}=m_{12}m_4/m_1m_{34},$$

$$\bar{y}_{12}=y_{12}'-y_{12}^0, \qquad \mu_{12},$$

$$\bar{y}_{34}=y_{34}'-y_{34}^0, \qquad \mu_{34}. \quad \text{(A14)}$$

The potential terms in $H-E$ become

$$\bar{V}_{12}(\bar{y}_{12})+\bar{V}_{34}(\bar{y}_{34})+\bar{V}_I(\bar{x}-\bar{y}_{12}-\gamma\bar{y}_{34})=V_{12}(\bar{y}_{12}+y_{12}^0)+V_{34}(\bar{y}_{34}+y_{34}^0)+V_I[(m_1/m_{12})(\bar{x}-\bar{y}-\bar{\gamma}\bar{y}_{34})]. \quad \text{(A15)}$$

The operator is finally made dimensionless by dividing by $\hbar\omega_{12}$ and absorbing dimensional factors into the second differential operators. Define

$$x=(\mu_{12}\omega_{12}/\hbar)^{1/2}\bar{x},$$

$$y_{12}=(\mu_{12}\omega_{12}/\hbar)^{1/2}\bar{y}_{12},$$

$$y_{34}=(\mu_{34}\omega_{34}/\hbar)^{1/2}\bar{y}_{34},$$

$$\bar{\mu}=\mu_{12,34}'/\mu_{12}=m_1m_{34}/Mm_2,$$

$$\gamma=(m_2/m_3)(\mu_{34}\omega_{12}/\mu_{12}\omega_{34})^{1/2} \quad \text{(A16)}$$

to obtain the generalization of Eq. (19),

$$H-E=-(1/2\mu)(\partial^2/\partial x^2)-\tfrac{1}{2}(\partial^2/\partial y_{12}^2)-(\omega_{34}/\omega_{12})(\partial^2/\partial y_{34}^2)+V_{12}'(y_{12})+V_{34}'(y_{34})+V_I'(x-y_{12}-\gamma y_{34}). \quad \text{(A17)}$$

The potentials are related to their original forms by

$$V_{12}'(y_{12})=V_{12}[(\hbar/\mu_{12}\omega_{12})^{1/2}y_{12}+y_{12}^0]/\hbar\omega_{12},$$

$$V_{34}'(y_{34})=V_{34}[(\hbar/\mu_{34}\omega_{34})^{1/2}y_{34}+y_{34}^0]/\hbar\omega_{12},$$

$$V_I'(x-y_{12}-\gamma y_{34})=V_I[(m_1/m_{12})(\hbar/\mu_{12}\omega_{12})^{1/2}(x-y_{12}-\gamma y_{34})]/\hbar\omega_{12}. \quad \text{(A18)}$$

* National Science Foundation Predoctoral Fellow, 1966-1969.

† Contribution No. 3909.

‡ Presently at the Department of Chemistry, Purdue University, Lafayette, Ind. 47907.

[1] M. E. Riley, thesis, California Institute of Technology, 1968 (unpublished); M. E. Riley and A. Kuppermann, Chem. Phys. Letters 1, 537 (1968).

[2] S-K Chan, J. C. Light, and J. Lin, J. Chem. Phys. 49, 86 (1968).

[3] D. Secrest and B. R. Johnson, J. Chem. Phys. 45, 4556 (1966). For earlier work in multichannel invariant imbedding consult F. Calogero, *Variable Phase Approach to Potential Scattering* (Academic Press Inc., New York, 1967), Chap. 19.

[4] R. Gordon, J. Chem. Phys. 51, 4 (1969).

[5] A. Cheung and D. Wilson, J. Chem. Phys. 51, 4733 (1969).

[6] (a) A. B. Bhatia, *Ultrasonic Absorption* (Oxford University Press, 1967), for values of ϵ and σ; (b) G. Herzberg, *Spectra of Diatomic Molecules* (D. Van Nostrand, Co., Inc., Princeton, N.J., 1939), for values of D_e and β; (c) K. F. Herzfeld and T. A. Litovitz, *Absorption and Dispersion of Ultrasonic Waves* (Academic Press Inc., New York, 1959).

[7] K. E. Shuler and R. Zwanzig, J. Chem. Phys. 33, 1778 (1960).

[8] D. Rapp and T. E. Sharp, J. Chem. Phys. 38, 2641 (1963).

[9] In HOLJ computations, 90%-95% of the net computing time was spent in calculating the potential matrix elements $V_{mn}(x)$ and only 5%-10% on actual solution of the CC equations. In HOEXP calculations, only about 1%-2% of the time was spent computing potential matrix elements. Similar percentage figures would hold even for the CC integration techniques of Refs. 4 and 5.

Appendix. Our CC Integration Technique

At the time of our calculations, there were essentially two possible numerical integration techniques. First was straightforward numerical integration in the coordinate $\underline{x}$, statring from some $\underline{x_o}$ where $\Psi(\underline{x},\underline{y}) \simeq 0$. A standard integrator such as Runge-Kutta-Gill is used. A number $\underline{n_s}$ of linearly-independent solutions, $\underline{n_s} \geq \underline{n_{op}}$ ($\underline{n_{op}}$ = number of open channels) is required, each of the form

$$\psi_k = \sum_{n=1}^{n_{tot}} f_n^{(k)}(x)\phi_n(y). \qquad (1)$$

These solutions are begun with the proper physical boundary condition (b.c.) that $\underline{f_n^{(k)}(x_o)} = 0$ but do not obey the proper scattering boundary conditions for pure states in the potential-free region $x \to \infty$. These conditions are that right-incident waves exist in only one channel $\underline{n}$, with scattered waves in all channels:

$$\psi^I(x,y) = \sum_{n=1}^{n_{tot}} F_n^{(I)}(x)\phi_n(y)$$

$$F_n^{(I)}(x) \underset{x\to\infty}{\to} \delta_{nI}e^{-ik_nx} + A_n{}_I e^{+ik_nx} .$$

Only an integral equation can build in these conditions (and such a technique was developed about the same time by M.E. Riley; see ref. 25 of the introduction). Our $\underline{n_s}$ independent solutions behave asymptotically as

$$f_n^{(k)}(x) \to B_n^k e^{-ik_nx} + A_n^k e^{+ik_nx} . \qquad (2)$$

They must be linearly combined to meet the scattering b.c.,

$$F_n^{(I)}(x) = \sum_{k=1}^{n_s} c_k^{(I)} f_n^{(k)}(x).$$

The n_s straightforward integrations with independent starting b.c., such as

$$\frac{d}{dx} f_n^{(k)}(x) = \delta_{nk} , \qquad (3)$$

must be dressed up to be practical. As the solutions are propagated from x_o to some x_f essentially in the potential-free region, the virtual channels with their exploding components

$$f_n^{(k)} \rightarrow B_n^k e^{+|k_n| x} + A_n^k e^{-|k_n| x}$$

dominate the couplings of all the other $f_n^{(k)}$ and cause practical linear dependence in the solutions. Periodic reorthogonalization, as in the DRILL method developed by M. E. Riley (Ph.D. thesis, Caltech, 1968) is the easiest solution.

The second technique was the recently-developed total finite-difference (FD) method (D. J. Diestler and V. McKoy, J. Chem. Phys. 48,2941(1968)). It is an extension of sorts of the previous method which discretizes one coordinate, x, to effect a numerical solution. FD discretizes both x and y to obtain matrix equations for the wavefunction at the mseh points (x_i, y_i). It does not have linear dependence problems for reasons much the same as in our final method discussed shortly. However, it is very time-consuming for most physical problems with large ranges of x, y to be

covered. It is more useful for small regions of strong coupling and especially for the interaction region of reactive scattering (Diestler and McKoy, ibid. 48,2951(1968)) where we do not wish to commit ourselves to a channel expansion in one or the other arrangement channel. In our type of problem, however, we should make use of our knowledge of the uncoupled y-motion--i.e., of the $\phi_n(y)$; we require fewer $\phi_n(y)$ than mesh points in y to cover the y-space. Thus we converted FD to the CC equations and achieved the fastest method to date, which we called finite-difference-matrix (FDM). Consider how we would solve Eq. (14) of the text numerically: discretize it in x as (suppress the index k for now)

$$(\frac{1}{h^2}\delta_o^2 + k_n^2)f_n(x) = 2\mu\sum_m V_{nm}(x)f_m(x),$$

where the difference operation δ_o^2 is

$$\delta_o^2 f_n(x) = f_n(x+h) - 2f_n(x) + f_n(x-h)$$

and h is clearly the mesh spacing in x. Rewrite this as

$$\left[-\frac{2}{h^2} + k_n^2 - 2\mu V_{nn}(x)\right] f_n(x) + \frac{1}{h^2} f_n(x+h)$$

$$+ \frac{1}{h^2} f_n(x-h) - 2\mu\sum_{m\neq n} V_{nm}(x)f_m(x) = 0. \qquad (4)$$

To get one of the linearly-independent solutions $\{f_n^{(k)}(x)\}$, values of the $f_n^{(k)}(x)$ must be specified at two points x_1, x_2. Note that the choice $x_1 = x_o$, $x_2 = x_o + h$ nearly corresponds to the b.c. (3) for the old method of solution. A more appropriate choice of x_1, x_2 would be x_o

and x_f, as for example,

$$f_n^{(k)}(x_o) = 0 \quad ; \quad f_n^{(k)}(x_f) = \delta_{nk}.$$

Three considerations dictate this choice of x_1, x_2. The first is simply that the above equations fulfill the true b.c. at $x = x_o$. The second is that the second of the equations is an ideal form for constructing solutions close to true scattering solutions at x_f; exploding exponential solutions

$$B_n^k e^{+|k_n|x}$$

in virtual channels are forced to die out at $x = x_f$ in the first n_{op} independent solutions. Practical calculations on HOLJ and MOLJ verified that only n_{op} independent solutions need be generated and linearly combined, rather than n_{tot}. The third consideration is that our b.c. allow us to write the discretized CC equations in a matrix form. Write the entire set of $f_n^{(k)}(x_i)$ for all n and i as a single column vector $\underset{\sim}{X}^{(k)}$ whose elements are

$$\left(\underset{\sim}{X}^{(k)}\right)_j = f_n^{(k)}(x_i) \tag{5}$$

where

$$j = (i-1)n_{tot} + n$$

$$x_i \in [x_1, x_{f-1}] .$$

Eqs. (4) can be written in the matrix form

$$\underset{\sim}{A}\ \underset{\sim}{X}^{(k)} = \underset{\sim}{b}^{(k)}$$

where

$$(\underset{\approx}{A})_{jj} = -\frac{2}{h^2} + k_n^2 - 2\mu V_{nn}(x_i) \qquad (6)$$

$$(\underset{\approx}{A})_{jk} = \frac{1}{h^2}, \quad k = j \pm n_{tot}$$

$$(\underset{\approx}{A})_{jk} = -2\mu V_{nm}(x_i), \quad k = (i-1)n_{tot} + m$$

$$m \leq n_{tot}$$

$$(b)_j = 0, \quad j < (f-i)\, n_{tot}$$

$$(b)_j = \delta_{nk}, \quad j \geq (f-i)\, n_{tot} \ .$$

The matrix $\underset{\approx}{A}$ is seen to be banded with a half-bandwidth of $n_{tot}+1$ (note the relation of Eqs. (5), (6) to the original FD method). A very rapid and accurate routine has been coded (for the IBM 7094 originally, on which all our calculations were performed) by McCormack and Hebert (C. McCormack and K. Hebert, "Solutions of Linear Equations with Digital Computers", Technical Report, Engineering Division, California Institute of Technology, 1965, unpublished) for solving equations of the above form using a Gauss triangularization and elimination technique. Both core and disk storage are used, allowing large solution vectors (up to 16,000 elements). Our initial calculations proved to be of the same order of practicality as DRILL calculations.

For reduction of our primitive solutions to the proper pure scattering states by linear combination, see the first reference to Diestler and McKoy. In any event, given the final 'reflection coefficients" A_n^I for the true

scattering states, the probabilities of transitions P_{mn} from state m to n are calculated simply as

$$P_{In} = \frac{k_n}{k_I} |A_n^I|^2.$$

This formula follows directly from the definition of probabilities as ratios of incoming currents in I and outgoing currents in n.

a. Some Problems in Numerical Technique

Given an atom-diatom collision system, the parameters E, μ, and the parameters of the potentials V_{12}, V_I (henceforth called system parameters) are fixed. Several solution-method parameters remain to be chosen. The most obvious is n_{tot}, the number of channels retained in the expansion (1). Practical calculations carried out at energies E such that 2, 3, 4, 5, and 6 channels are open indicated that values n_{tot} = 4, 5-6, 7, 9, and 10, respectively, suffice to give transition probabilities converged to within one percent. These values are appropriate to the HOLJ and MOLJ models and should not be taken as general guides (the optimal number depends upon the degree of diabaticity in the collision and the relative spacing of the upper levels of vibration). A second parameter is the step size h in the difference equations. Experience indicated that a good choice is $h = 0.15/k_1$, where k_1 is the wavenumber of channel 1. The error introduced by keeping h this coarse, when compounded with the channel-truncation error, yielded a net error of less than one percent (relative) in the P_{In}. The

use of several coarser values of h with subsequent extrapolation (as in Diestler and McKoy) is more time-consuming for the same accuracy, and a like criticism applies to use of a coarser h with higher-order difference approximations to the CC d.e.'s.

A further set of parameters is the pair of limits x_o, x_f. The Lennard-Jones potential is singular at $x-y = 0$ but may be cut off at some b and set to a constant value for $x-y \leq b$. A good scheme is to cut off V_I when it reaches a magnitude of ten times the maximum kinetic energy (and is thus impenetrable to the particle even quantum-mechanically)

$$V_I \rightarrow 10\ (E-\epsilon_1)$$
$$=10\ (E-0.5).$$

A complementary choice of x_o is $x_o \simeq b - 3$. The value of x_f is strictly equal to infinity, since the Lennard-Jones potential is of infinite range. However, the CC equations effectively decouple to give free plane-wave $f_n(x)$ as of Eq. (2) when V_I drops to some small value. Decoupling occurs later (at larger x_f, smaller V_I) as the energy E approaches a threshhold of a channel from above, so the choice of x_f will depend upon the smallest wavenumber k_m in the problem at hand. To illustrate, two choices are

$$V_I(x_f) \approx 2.5 \times 10^{-6} \text{ when } k_m^2 \approx 0.05$$
$$V_I(x_f) \approx 2.0 \times 10^{-4} \text{ when } k_m^2 \gtrsim 0.35.$$

A final parameter is n_s, the number of linearly-independent solutions to be generated. This was set to n_{op} in all our

calculations for reasons noted earlier.

Regarding accuracy of the solutions $\underset{\sim}{X}^{(k)}$, there are two considerations in addition to the choices of parameters above. The first is the accuracy attainable in solution of the FDM equations (6) by Gauss' method. Tests were made using the feature of the routine which allows iterative improvement of the solutions. Basically, only small and uniform changes in the phases of the $f_n^{(k)}$ were noted in improved solutions, even for lengthy solution vectors near channel threshholds. This reveals an advantage of FDM, in that significant errors do not 'propagate'. The second consideration is the accuracy in evaluating matrix elements $V_{mn}(x)$ for the HOLJ and MOLJ models studied. Analytic forms do not exist and numerical quadrature must be used. Extensive trials showed that for the HOLJ case, where the oscillator eigenfunctions $\phi_n(y)$ are spatially compact, a twenty-point Hermite quadrature in y gave good results. For the MOLJ case, the eigenfunctions for higher n become quite diffuse, making something like our 181-point trapezoidal quadrature necessary. at least for $x < \sigma$ (the Lennard-Jones parameter). To save computer execution time, a series expansion of $V_I(x-y)$ in powers of $y-y_o$ (y_o is roughly the average location of the maxima in $\phi_n(y)$) was used for $x-y_o \geq \sigma$, yielding $V_{lm}(x)$ as a sum over moment integrals.

b. Similar Considerations for Diatom-Diatom Cases

For these cases, as noted in the text the CC

equations have exactly the same form as Eq. (14) of the text but the channel index $\underline{n}$ is really a double index $\underline{n_1 n_2}$ denoting the states of vibration in both collision partners. The total number of channels rises, and exactly which double channels are to be retained is a little tricky--the choice is discussed in the text and in Table I there.

The discussion of section (a) on b.c. applied to the primitive solutions $\{\underline{f_n^{(k)}(x)}\}$ and the final physical solutions $\{\underline{F_n^{(I)}(x)}\}$ also holds for the diatom-diatom case. The primitive b.c. were slightly modified, however, to read

$$f_n^{(k)}(x_f) = \begin{cases} 0, & n \neq k,\ n > n_{op} \\ 0.1, & n \neq k,\ n \leq n_{op} \\ 1.0, & n = k\ . \end{cases}$$

We found a slight improvement in accuracy near threshholds over the original b.c. One problem peculiar to the case of identical diatoms and to the necessary b.c. is that the matrix $\underline{A}$ in the diatom-diatom analog of Eq. (6) is nearly singular due to the presence of equivalent channels $(\underline{n1, n2}) \leftrightarrow (\underline{n2,n1})$. These channels are physically distinct; a transition from one to the other involves no conversion of translational into vibrational energy--it is a resonant transfer. However, their respective coupled equations differ mathematically only due to b.c. on the $\underline{f_m^{(k)}(x)}$. They would otherwise be related by a single permutation of terms on the right-hand side of Eq. (6). Without going into more

detail, we note that the $f_n^{(k)}(x)$ for equivalent channels n and n' become very similar for all but two values of the superscript k, and identical whenever k corresponds to a channel ($n3$, $n3$). The implications of this behavior for the FDM method of solution by Gauss' algorithm are that each initial solution vector $\underline{X}^{(k)}$ is accurate, but attempts to iteratively improve the solution lead to divergences. No practical problems were caused by this difficulty.

The solution method parameters h, x_o, x_f, and n_s are chosen by the criteria outlined in section (a). The goal of our calculations on the HOHOLJ model is to have probabilities P_{mn} of relative accuracy one percent. The choice of adjustable parameters given above can assure this goal for the energy range encountered, if the matrix elements $V_{nm}(x)$ are calculated with sufficient accuracy (perhaps 1 part in 10^4). These matrix elements require a two-dimensional numerical quadrature in the variables y_1, y_2. Each dimension was treated by twenty-point Hermite quadrature, as for the atom-diatom case. To cut down on computer execution time, the $V_{nm}(x)$ were tabulated on magnetic tape at a modest grid spacing $x = 0.20$, and each calculation of the solution vectors at a given energy used matrix elements interpolated cubically from this tabulation. The error added into the P_{mn} by interpolation error was about 0.01%.

c. Miscellany: Timings, Refinements, Relation to 3-D Scattering

Precise timings for calculations by our method are only of academic interest, while the order of magnitude and dependence on energy E (or equivalently, on n_{tot}) and on the complexity of the model are more generally significant. First, we note some typical compute times on an IBM 7094 (roughly the same speed as the new IBM 370/155). For the HOLJ model used here, the times are:

E	n_{tot}	t(sec.)
2.45	4	53
3.05	6	112
6.20	10	438

and for HOHOEXP (similar to HOHOLJ but using only trivial time for computing $V_{nm}(x)$ relative to actual Gauss solution; better indicator of the integrator per se):

2.46	9	127 .

Gordon's new integrator (ref. 24 of introduction) should cut these times by an average factor of about 20. Thus calculations with 40-50 channels are even feasible at the extreme, since all integrators' times increase roughly as n_{tot}^3. This is nothing to lament, really, since the detailed S-matrix for a large number of channels is not very meaningful for an understanding of collision processes--for the same reason that in statistical mechanics the trajectories of 10^{23} particles in a bulk system aren't meaningful: both are

filled with irrelevant detail, irrelevant for the aim of correlating molecular structure with properties. A further argument against large model problems is the rising proportion of computing effort going into computing just the V_{nm} matrix elements; for HOLJ these take about 50-70% of the total compute time, while for HOHOLJ they consume fully 95%.

Before closing, we should like to mention two possible refinements to the scattering solutions; the second is of interest even for newer CC integrators. First, analogous to the use of higher-order predictor-corrector formulae in the straightforward CC integrators such as DRILL, the actual numerical integration scheme in FDM can be improved. An obvious action is switching to a five-point difference formula in discretization, possibly a Numerov formula. At the endpoints x_o, x_f, of course, we shall have to revert to the 3-point formula. We did not try this, as our total computing effort was modest as the method stood--and we may not even gain by increasing the mesh size h but doubling the matrix bandwidth to $2\, n_{tot} + 1$. Besides, Gordon's integrator has superceded all simple integrators.

The second refinement tested was a shortening of the distance in x, $x_f - x_o$, over which we propagate the solutions $f_n^{(k)}(x)$ before assuming they have attained their essential potential-free plane-wave form and proceeding to analyze them for the A_n^k, B_n^k and hence the transition probabilities. The common experience of investigators in

molecular scattering theory is that V_I must be down to the general magnitude of 10^{-4} energy (oscillator) units for the analysis and probabilities to be stable (to variations in the analysis point x_f, that is). We felt that the strong diabatic (transition-causing) couplings of channels might be completed (especially in systems with 'soft' interactions V_I) much earlier, say at x_d where $V_I \approx 0.1$. Analysis at x_d in an adiabatic basis for this x might be successful. This adiabatic basis of oscillator functions is parametric in x_d, i.e., it is $\phi_n(y|x_d)$, and each function is a solution of the equation

$$\left[-\tfrac{1}{2}\frac{d^2}{dy^2} + V_{12}(y) + V_I(x_d-y) - \bar{\epsilon}_n(x_d)\right]\phi_n(y|x_d) = 0.$$

This basis of 'perturbed stationary states' must be solved for numerically in general, and definitely when V_I is a Lennard-Jones potential. To be brief, this analysis failed, for our HOLJ H_2-H_2 model at least. Perhaps diabatic coupling is strong even to low V_I for the harder potentials.

In closing, we should like to mention one point of interpretation of the one-dimensional (1-D) or collinear solutions: the wavefunction in our 1-D model is also the S-wave portion of the partial-wave expansion of the 3-D wavefunction, for a 'breathing sphere' (a collision system where there is no diatom-orientation- or angle-dependence in the interaction potential; implies a perfect but compressible sphere):

$$\Psi^I_{3D}(x,y) = \sum_n \left\{ \delta_{nI} e^{ik_I z} + g_n(\theta) e^{ik_n r}/r \right\} \phi_n(y)$$

$$\left(H = -\frac{h^2}{2\mu}\nabla^2 + H^o(y) + V_I(r-y) \right)$$

$$= \sum_n \left[\frac{1}{r} \sum_l u^n_l(r) P_l(\cos\theta) \right] \phi_n(y),$$

where $u^n_l(r)$ satisfies

$$\left[\frac{d^2}{dr^2} - \frac{l(l+1)}{r^2} + k_n^2 \right] u^n_l(r) = 2\mu \sum_m V_{nm}(r) u^m_l(r).$$

Clearly for $l = 0$ (S-wave) this is our collinear collision equation of motion. What does this imply for the relation of the 1-D transition probabilities (pure numbers) to 3-D transition cross-sections (areas)? Now, the 3-D scattering amplitude $g_n(\theta)$ has the form

$$g_n(\theta) = \frac{1}{2ik} \sum_l (2l+1)(-1)^{l+1} (A^I_{n,l} - (-1)^l \delta_{nI}) P_l(\cos\theta)$$

where the $A^I_{n,l}$ are the simple generalization for the l-waves of the A^I_n of our S-wave. The 3-D differential cross-section is $\sigma_{In}(\theta) = \left| g^I_n(\theta) \right|^2$, and the total cross-section Q^{In}_{tot} integrated over angles θ is simply

$$Q^{In}_{tot} = \frac{\pi}{k_I^2} \sum_l (2l+1)(A^I_{n,l} - (-1)^l \delta_{nI})^2.$$

For $n \neq I$ and for S-wave scattering dominating, the total cross-section simplifies to

$$Q^{In}_{tot} \simeq \frac{\pi}{k_I^2} \left| A^I_{n,o} \right|^2 = \frac{\pi k_n}{k_I^3} P_{In}.$$

This is the result we seek; note that Q is an area, rightly.